



**London
South Bank
University**

EST 1892

Investigation of Wax Depositional Behaviour in Straight and Curved Pipes– Experiments and Simulation

By

Nura Makwashi

<https://orcid.org/0000-0003-3673-3196>

A thesis submitted in partial fulfilment of the requirements for the award
of the Degree of Doctor of Philosophy in
Chemical Process and Energy Engineering

School of Engineering
London South Bank University

January 2020

© Copyright to London South Bank University (LSBU)

Dedication

This thesis is dedicated to the lovely memory of my late parent “Hon. Makwashi Abubakar and Mrs Fatima (Tumba) Makwashi”, your words of inspiration and encouragement in the pursuit of excellence, still remain on. Also, to my late wife Shema’u Badamasi may you continue to rest in perfect peace and my lovely wife Zainab and children Abdur-Rahman and Fatima, you are my most treasured!!!

Declaration of Authorship

I, Makwashi Nura, declare that this thesis and the work presented in it are my own and is expressed in my own words with fabulous support of my supervisory team. The work is the original contribution submitted for examination in consideration of the award of a degree of Doctor of Philosophy in Chemical Process and Energy Engineering. The thesis has not been submitted for any other degree or professional qualification and does not breach copyright law. Any uses of other authors e.g. ideas, equations, figures, text, tables, and programs are properly cited and acknowledged.

Aknowledgements

First of all, I would like to thank the Almighty Allah for giving me the opportunity, strength, and endurance to finish my PhD. The journey would not have been feasible without the tremendous support of my family, supervisors, colleagues and friends.

I want to express my sincere gratitude to my supervisory team; Dr Donglin Zhao (director of studies), Dr Pedro Diaz and Dr Abdelhamid Fenghour for their guidance, support, professionalism and supervision during this work. Special thanks to Dr Zhao whose confidence and outlook inspired me during a trying time within the study period, your off-work support has been invaluable. I must emphasise that working under your supervision was such an honour.

My sincere thanks to the technical staff of chemical engineering lab (Mr Charles Coster and Mr William Cheung), electrical electronics lab (Mr Zahir Mehdi) and Mechanical Engineering workshop (Mr Nick Duggan) for the guidance in the flow rig setups, sensors testing and construction of the pipelines. I would also like to thank my Dr Abdulkadir Mukhatar (Head of Department, Chemical Engineering FUT Minna, Nigeria), Dr Tarik Saif (Project Management Consultant at Atkins Energy & High Speed), Prof. Asa Barber (Dean LSBU), Dr Fatemeh Jahanzad, Dr Sandra Dudley, Ms Nicole Auguste for their tremendous support throughout my research. Special thanks to London Doctoral Academy team who have developed my research skills and push my research towards better opportunities.

The financial support received from the Nigerian Government through the Petroleum Technology Development Fund is highly appreciated. The experiences gained as a freelancer staff from BBC Hausa Service and the LSBU is well cherished and will never be forgotten. I want to thank my PhD colleagues from whom I have learnt and enjoyed my PhD journey, including Dr Hurso Adam, Dr Ganiyu Sikiru, Dr Kwame Sarkodie, Dr Victor Onyenkeadi, and Dr Yusuf (Kano). Finally, I would like to express my sincere gratitude to Gen Aliyu Gusau, Sheik Abdurrazaq Ibrahim (Amir NMFUK), Auntie Fatima Abdulsalam, Auntie Hafsat (Abuja), Saleem Ishaq and Auntie Murjanatu and Shakeer family (London), my entire family members, and friends who have been inspirational during the whole PhD programme.

Abstract

Deposition wax is one of the chronic flow assurance problems that continue to attract attention in the oil and gas field, particularly as the hydrocarbon explorations and productions in recent years move into a colder environment. The accumulation of the wax deposit in the pipeline reduced or interrupted the production, and in the worst-case completely clogged the pipeline, resulting in equipment failure or field abandonment. Although significant progress has been made in mitigating the problem, many questions about the full understanding of the factors and the physical process mechanisms of deposition remain unanswered. Predominant researches are being conducted in straight pipes. The impact of pipe curvatures such as pipe bends, elbows, and inclinations (found in production and transportation systems) on the increased severity of the deposition is not well studied, only very limited studies being reported. In this thesis, the deposition of wax was studied in a single-phase flow using a novel laboratory-scale flow loop accommodating three different pipes configurations: a straight pipe and curved pipes with 45° and 90° bends.

Series of experiments were carried out using a crude blend with and without chemical inhibitor at different flow rates – under laminar (Q_{oil} ; 3, 5, 7 l/min) and turbulent flow (Q_{oil} ; 9, 11 l/min) conditions and at different ambient cooling temperatures of 10, 15, 25 °C ($T_{cool} \leq$ pour point temperature of the oil) and 30, 35, 40 °C ($T_{cool} \geq$ WAT of oil). The experimental period was varied from 2, 4, 6, 8 hours. Prior to the flow loop studies, three different waxy crude oil samples and four commercial wax inhibitors are screened and characterised through different standard techniques. The wax content of crude oil samples A, B, and C was found to be 12.05, 20.05, and 14wt%, n-paraffin distributions ranges from C15-C74, WAT and pour point varies from 28 to 30°C and 19.5 to 25.5°C respectively. Similarly, SARA (saturated/aromatic/resin/asphalte) fractions, wax appearance temperature, viscosity, pour point, and the colloidal instability index of the samples was obtained. A new wax inhibitor was developed by blending different fractions of commercial inhibitors improved the performance and transformed the needle-like or rod-like crystals structure of the oil samples into an agglomerate with small particles dispersed in the oil matrix.

The flow loop studies showed that the rate of wax deposition without inhibitor is significantly higher in curved pipes than in the straight pipe. In horizontal flow study – the test section with 90° bends pipes produces the highest wax deposition rate compared to the straight pipe test section and a test section with 45° bends pipes. For instance, under a low case scenario (i.e. at $T_{cool}, 15^{\circ}C$ and $Q_{oil}, 5$ l/min), around 22% of the wax deposition rate was seen in straight pipe test section after 2 hours compared to 36% and 43.5% of the wax deposition rate in test sections with 45° bend pipes and 90° bend pipes sections. This implies at the same conditions where the system experienced 0% wax deposition in the straight pipe it underwent 14% and 19% deposition, respectively, for the pipe with 45° and 90° bends. However, the severity of wax deposition in curved pipes simultaneous decreases with increasing coolant temperature and flow turbulence and vice versa. On the other hand, increase in elevation of the pipes, however, led to a more wax deposition; higher percentage of wax deposit was observed in 45-degree compared to 90-degree curved pipe. Therefore, contrary to some theory established in the literature, this research concluded that gravity settling mechanism plays a role in the deposition process alongside with other mechanisms.

The study with the new blended inhibitor produced a significant reduction of wax deposition. At 1500-ppm and at a cooling temperature of 15°C, around 80% of the wax deposition problem could be reduced under a turbulent flow regime. At the same flow rate but at a relatively higher temperature of 25°C (i.e. pour point temperature), 100% wax prevention was reached even at a lower concentration (500-ppm). Whereas, in the laminar flow regime (e.g. 7 l/min), 100% wax deposition prevention could only be achieved at the higher concentrations of 1000 and 1500-ppm at 30°C. On the other hand, the experimental results under different conditions were simulated with OLGA software. The predicted results are in good agreement with the experimental data, particularly in the straight pipe.

Base on the flow loop design, a new correlation using pressure drop a relationship was developed for quantification of wax deposit thickness in curved pipes. Generally, the established model relates wax deposit thicknesses, with a bend angle of the pipes and pressure drop due to the wax build-up with reasonable agreements to the published data, especially at steady-state conditions.

Table of Contents

DEDICATION.....	I
DECLARATION OF AUTHORSHIP	III
ACKNOWLEDGEMENTS.....	IV
ABSTRACT.....	V
TABLE OF CONTENTS	VII
LIST OF FIGURES.....	XI
LIST OF TABLES.....	XVI
LIST OF NOMENCLATURE	XVII
CHAPTER 1.....	1
INTRODUCTION AND RESEARCH AIM AND OBJECTIVES	1
1.1 INTRODUCTION	1
1.2 WAXES DEPOSITION CHALLENGES AND TREATMENT.....	2
1.3 MOTIVATION FOR WORK	6
1.4 RESEARCH AIM AND OBJECTIVES	8
1.5 ACHIEVEMENT	9
1.6 PUBLICATIONS (CONFERENCES AND JOURNALS)	10
1.7 THESIS STRUCTURE	11
CHAPTER 2.....	13
LITERATURE REVIEW	13
2.1 INTRODUCTION	13
2.2 FLOW ASSURANCE.....	13
2.3 FLOW ASSURANCE CHALLENGES.....	13
2.3.1 GAS HYDRATES.....	14
2.3.2 ASPHALTENES.....	16
2.4 PARAFFIN WAXES	18
2.4.1 WAXY CRUDE OIL PROPERTIES.....	19
2.4.2 PRECIPITATION OF WAX CRYSTAL.....	20
2.4.2.1 NUCLEATION.....	20
2.4.2.2 CRYSTAL GROWTH.....	21
2.4.3 DEPOSITION OF SOLID WAXES	21
2.4.4 MECHANISMS OF WAX DEPOSITION	24
2.4.4.1 MOLECULAR DIFFUSION.....	25
2.4.4.2 SHEAR DISPERSION	28
2.4.4.3 BROWNIAN DIFFUSION	30
2.4.4.4 GRAVITY SETTLING	31
2.4.4.5 SHEAR STRIPPING	32
2.4.5 FACTORS LEADING TO WAX PRECIPITATION AND DEPOSITION.....	32
2.4.5.1 EFFECT OF TEMPERATURE.....	33
2.4.5.2 EFFECT OF COMPOSITION.....	33
2.4.5.3 EFFECT OF FLOW RATE AND SHEAR RATE	34

2.4.5.4	EFFECT OF PRESSURE	35
2.4.5.5	EFFECT OF PIPE SURFACE PROPERTIES	35
2.4.5.6	EFFECT OF DEPOSITION TIME AND AGING.....	36
2.4.6	PARAFFIN WAX MANAGEMENT.....	37
2.4.6.1	MECHANICAL METHOD	37
2.4.6.2	THERMAL METHOD	38
2.4.6.3	CHEMICAL METHOD.....	39
2.4.6.4	INTERACTION MECHANISMS BETWEEN CHEMICAL INHIBITORS AND WAX CRYSTALS	41
2.4.7	WAX DEPOSITION SIMULATION	43
2.4.7.1	RRR MODEL.....	44
2.4.7.2	MATZAIN MODEL	44
2.4.7.3	HEAT ANALOGY	44
2.5	FLUID FLOW THROUGH PIPE CURVATURE.....	45
2.5.1	FLUID FLOW THROUGH A STRAIGHT PIPE – SINGLE-PHASE.....	45
2.5.2	FLUID FLOW THROUGH A CURVED PIPE – SINGLE-PHASE	47
2.6	ORIGINAL CONTRIBUTION TO KNOWLEDGE.....	48
CHAPTER 3.....		52
EXPERIMENTAL METHODS AND ANALYTICAL TECHNIQUES		52
3.1	INTRODUCTION	52
3.2	CRUDE OIL SAMPLE SELECTION.....	53
3.2.1	SYNTHETIC CRUDE OIL.....	54
3.3	CRUDE OIL CHARACTERIZATION	55
3.3.1	SPECIFIC GRAVITY AND API	56
3.3.2	WAX CONTENT ANALYSIS.....	56
3.3.3	POUR POINT OF CRUDE OIL.....	57
3.3.4	RHEOLOGICAL PROPERTIES	58
3.3.5	CRYSTALS MORPHOLOGY OF WAXY CRUDE OIL.....	59
3.3.6	SARA ANALYSIS	60
3.3.7	COLLOIDAL INSTABILITY INDEX (CII)	62
3.3.8	N- PARAFFIN DISTRIBUTION OF CRUDE OIL SAMPLES	63
3.3.8.1	SAMPLE PREPARATION:	64
3.4	ANALYSIS OF WAX INHIBITORS EFFICIENCY	65
3.5	PIPELINE FLOW RIG DESIGN	67
3.5.1	FLOW RIG COMPONENTS.....	71
3.5.1.1	TEST SECTIONS.....	71
3.5.1.2	CRUDE OIL RESERVOIR.....	72
3.5.1.3	CONDENSER	72
3.5.1.4	CRUDE OIL PUMP	72
3.5.1.5	FREQUENCY INVERTER	72
3.5.1.6	FLOW METER	73
3.5.1.7	HOT WATER BATH	73
3.5.1.8	CIRCULATING CHILLER	73
3.5.1.9	PRESSURE SENSOR.....	74
3.5.1.10	THERMOCOUPLES.....	75
3.5.1.11	BORESCOPE INSPECTION	76
3.6	DEPOSITION TESTING PROCEDURE.....	77

3.7	EXPERIMENTAL TEST MATRICES	79
3.8	QUANTIFICATION OF DEPOSIT WAX THICKNESS	81
3.8.1	PRESSURE DROP METHOD	82
3.8.2	WEIGHT-BALANCE AND VOLUME CORRELATION METHOD.....	85
3.8.3	ENERGY-BALANCE METHOD.....	87
3.8.4	WET FILM-THICKNESS GAUGE.....	89
3.9	OLGA: MULTIPHASE FLOW SIMULATOR	90
3.9.1	CRUDE OIL PROPERTIES FOR WAX TABLE AND PVT TABLE FILES.....	91
3.9.2	WAX DEPOSITION SIMULATION AND SENSITIVITY ANALYSIS.....	92
CHAPTER 4.....		94
ANALYSIS OF CRUDE OIL CHARACTERISTICS AND EFFECT OF INHIBITOR ON RHEOLOGICAL PROPERTIES		94
4.1	INTRODUCTION	94
4.2	ANALYSIS OF API GRAVITY, DENSITY AND SPECIFIC GRAVITY	96
4.3	STUDY OF WAX CONTENT	96
4.4	ANALYSIS OF SARA FRACTION	97
4.4.1	ANALYSIS OF COLLOIDAL INSTABILITY INDEX (CII).....	99
4.5	RHEOLOGICAL BEHAVIOUR OF CRUDE OIL SAMPLES AND WAX INHIBITORS	100
4.5.1	EFFECT OF TEMPERATURE AND SHEAR RATE ON VISCOSITY, WAT AND POUR POINT.....	101
4.5.2	MEASUREMENT OF YIELD STRESS.....	106
4.5.3	EFFECT OF WAX INHIBITORS ON CRUDE OIL RHEOLOGICAL PROPERTIES	107
4.5.3.1	VISCOSITY, WAX APPEARANCE TEMPERATURE AND POUR POINT BEHAVIOURS	109
4.5.3.2	STUDY OF BLENDED WAX CHEMICALS INHIBITOR ON OIL RHEOLOGY	111
4.6	MICROSCOPIC ANALYSIS OF CRUDE OIL	112
4.7	N-PARAFFIN DISTRIBUTION OF CRUDE OIL SAMPLE.....	114
4.7.1	WHOLE OIL AND TOPPED OIL CHROMATOGRAPH.....	115
4.7.2	MERGING THE 'WHOLE' AND 'TOPPED' DATA.....	117
CHAPTER 5.....		121
ANALYSIS OF WAX DEPOSITION IN PIPELINE FLOW RIG.....		121
5.1	INTRODUCTION	121
5.2	PRESSURE AND TEMPERATURE RESPONSE FROM THE FLOW RIG	122
5.3	WAX DEPOSITION ANALYSIS IN STRAIGHT PIPE	124
5.3.1	EFFECT OF TEMPERATURE GRADIENT ON WAX DEPOSITION	125
5.3.2	INFLUENCE OF CRUDE OIL FLOW RATE	130
5.3.3	ERROR ANALYSIS IN DEPOSIT THICKNESS MEASUREMENT.....	133
5.3.4	DEPOSIT THICKNESS VARIATION WITH TIME.....	136
5.4	WAX DEPOSITION ANALYSIS IN CURVED PIPES	138
5.4.1	NEW MODEL FOR DEPOSIT THICKNESS QUANTIFICATION IN A BEND PIPE.....	139
5.4.2	STUDY OF THE EFFECT OF THE MAIN CONTROL PARAMETERS ON WAX DEPOSITION IN CURVED PIPES.....	145
CHAPTER 6.....		155
EFFECT OF BLENDED WAX INHIBITOR ON WAX DEPOSITION.....		155
6.1	INTRODUCTION	155
6.2	EFFECT OF THE INHIBITOR AT VARIED TEMPERATURE – STRAIGHT PIPE SECTION	156
6.3	EFFECT OF THE INHIBITOR AT VARIED FLOW RATE– STRAIGHT PIPE SECTION	162
6.4	STUDY OF THE INHIBITOR IN FLOW RIG WITH BEND PIPES SECTIONS.....	164

CHAPTER 7.....	170
SIMULATION OF WAX DEPOSITION.....	170
7.1 INTRODUCTION	170
7.2 ANALYSIS OF FLUID CHARACTERISTICS AND WAT	170
7.2.1 ANALYSIS OF WAT AND WAX PRECIPITATION	171
7.2.2 DISTRIBUTION OF SCN AND PHASE ENVELOP OF THE CRUDE OIL.....	173
7.3 WAX DEPOSITION SIMULATION USING OLGA	175
7.3.1 MODEL SELECTION FOR WAX SIMULATION.....	176
7.3.2 EFFECT OF WAX POROSITY.....	178
7.3.3 BASE CASE: SIMULATION STUDY.....	180
7.3.4 COMPARISON OF WAX SIMULATIONS WITH EXPERIMENT: STRAIGHT PIPELINE.....	183
7.3.5 SIMULATION STUDY IN THE STRAIGHT PIPE WITH ELEVATION	186
CHAPTER 8.....	190
8.1 CONCLUSIONS	ERROR! BOOKMARK NOT DEFINED.
8.2 RECOMMENDATION FOR FUTURE WORKS	193
REFERENCES	195
APPENDICES.....	216

List of Figures

Figure 1-1: Sample wax pig out of platform C in the North Sea (Labes-Carrier <i>et al.</i> , 2002)	3
Figure 2-1: Typical flow assurance problems at a different stage of production (Serintel, 2017).....	14
Figure 2-2: Typical conceptual hydrates formation, agglomeration and plugging in multiphase flow system (Sum, 2013).....	15
Figure 2-3: Appearance of asphaltene samples from crude oil. (a) A laboratory sample of n-heptane asphaltenes (Time, 2011) (b) Crude oil pipeline blocked by asphaltene and waxes (Headen <i>et al.</i> , 2007)	17
Figure 2-4: Paraffin waxes molecular structure (Hasbullah, 2011)	19
Figure 2-5: (a) Network of interlocking wax crystal by cross-polarized microscopic (b) a schematic of the “house-of-card” configuration of wax particles (Paso <i>et al.</i> , 2005; Zheng, 2017)	22
Figure 2-6: Wax deposition occurs when the inner wall temperature is below the wax appearance temperature (Lee, 2008)	23
Figure 2-7: Process of deposition of crystal wax (Siljuberg, 2012).....	24
Figure 2-8: Schematic of molecular diffusion as the wax deposition mechanism (Huang <i>et al.</i> , 2015).....	26
Figure 2-9: (a) Wax particle located in shear flow (Adapted from Siljuberg, 2012). (b) Potential streamlines around a rotating particle in shear flow (Zhu <i>et al.</i> , 2008).....	29
Figure 2-10: Hot Water Circulation (a) Wet insulated Hot Water Pipe (b) Hot Water Bundle (Leandro <i>et al.</i> , 2013; Ansart <i>et al.</i> , 2014).....	38
Figure 2-11: Electrically Trace Heated Pipe-in-Pipe ETH-PiP Structure (Ansart <i>et al.</i> , 2014).....	39
Figure 2-12: Interaction mechanism between wax crystals modifier with wax crystals (Adapted from Allen and Roberts, 1978, cited in Sousa <i>et al.</i> , 2019 and Al-yaari, 2011).	43
Figure 2-13: Schematic of a straight pipe with fully developed velocity profiles in laminar and turbulent flow regimes (adapted from UIO, 2004).....	46
Figure 3-1: Sequential workflow for wax deposition experimental study. Highlights the overall stages and some of the most appropriate techniques and parameters obtained: before, during and at the end of the experiment flow study.	53
Figure 3-2: Wax sample: (a) Solid wax measured with weight balance (b) Set-up for mixing dead crude oil with solid wax at a constant temperature.	55
Figure 3-3: Vacuum filtration set-up with Buchner funnel and flask for filtration of wax content from (A) crude oil sample B and (B) crude oil sample A and C after 24 hr cooling at -20°C	57
Figure 3-4: Bohlin Gemini II Rheometer for measurement of WAT, PPT and viscosity at specific shear and different temperature.	58
Figure 3-5: A snapshot of viscometric data from Bohlin II rheometer at varied cooling temperature (50 – 0°C), constant shear rate (120 /s).....	59
Figure 3-6: Carl Zeiss Axiovert S100 inverted optical microscope for the study of waxes crystals morphology in crude oil undoped and doped with a chemical inhibitor	60
Figure 3-7: Flow chart adapted for crude oil sample fractionation (Zeng <i>et al.</i> , 2012).....	61
Figure 3-8: Open column chromatography set-up used for SARA analysis of a crude sample	62
Figure 3-9: Agilent 6890 gas chromatograph (Picture was taken from Plymouth University)	64

Figure 3-10: Wax deposition flow rig facility designed with Straight Pipe and 45° Bend Pipeline. Where; FM: flow meter, P1 and P2: inlet and outlet pressure of the test section, T1 and T4: inlet and outlet oil temperature, T3 and T2: the inlet and outlet coolant (water-glycol mixture) temperature.	69
Figure 3-11: Schematic: (a) Design Parameters of Bend Pipeline Test Section with two 45-degree bends. (b) adapted from Idelchik (1986).....	69
Figure 3-12: Wax deposition flow rig facility designed with Straight and 90° Bend Pipeline. Where; FM: flow meter, P1 and P2: inlet and outlet pressure of the test section, T1 and T4: inlet and outlet oil temperature, T3 and T2: the inlet and outlet coolant (water-glycol mixture) temperature	70
Figure 3-13: Parameters of the Pipeline test section with 90° bends (L = 1000 mm), with two bulkheads connected.....	70
Figure 3-14: Flow rig set-up with straight pipe test section consists of; 1– Computer with the Software. 2– Pressure PicoScope. 3– Thermocouples Data Logger. 4&9– Inlet & Outlet Pressure Sensors. 5&8– Inlet & Outlet Control Valves. 6&7– Inlet & Outlet Oil Thermocouples. 10– Removable Jacked Straight Pipe Test Section. 12&11– Inlet and Outlet Coolant Fluid with Thermocouples attached. 13– Oil Pump. 14– Oil Flow out of the Pump. 15– Oil Flow into the Pump. 16– Hot Water Bath. 17– Oil Reservoir. 18– Condenser Tube. 19– Ice/Cold Water Bath for Condenser. 20– Oil Pump Frequency Inverter. 21– Chiller Programmable Temperature Controller. 22– Coolant Pump connected to the Test Section. 21– Circulating Chiller.	74
Figure 3-15: Flow rig set-up with bend pipe in an open cooling tank consists of; 1– Programmable Temperature Controller. 2– Circulating Chiller. 3– Water Pump connected to Fine Tube Heat Exchanger. 4– Flow Meter. 5&10– Inlet & Outlet Pressure Sensors. 6&9– Inlet & Outlet Control Valves. 7&8– Inlet & Outlet Oil Thermocouples. 11– Cooling Water Tank. 12– Fine Tube Heat Exchanger. 13– 45-degree bend pipe at zero elevation. 14&15– Water and Pipe Thermocouples. 16– Mechanical Overhead Stirrer. 17– Water Thermometer. 18– Oil Pump. 19– Hot Water Bath. 20– Condenser Tube. 21– Oil Reservoir. 22– Ice/Cold Water Bath for Condenser. 23– Oil Pump Frequency Inverter. 24– Detached Straight Pipe-in-Pipe Test Section. 25– Thermocouples Data	76
Figure 3-16: A Segment of Pipe-in-Pipe Cross Section with different Parameters (adapted from Sarica and Volk, 2004): The crude oil flow in the inner section of the pipe whereas, the mixture of water and glycol (coolant) flow in the shell section of the jacked pipe. ...	82
Figure 3-17: (a) Dip-type wet film thickness gauge scaled from 50 – 1200 μm (https://www.elcometer.com). (b) Constructed dip-type wet film thickness gauge scaled from 650 – 1200 μm attached with a long handle. (c) Constructed gauge scaled from 50 – 600 μm with measured deposit thickness from the test section.	90
Figure 3-18: Single flow path diagram in the OLGA software with closed inlet node where the source is located and the heat transfer source around the flow line and a pressure outlet node.	93
Figure 4-1: Correlation between the API, density, and wax content of three crude oil samples.....	96
Figure 4-2: SARA fraction of crude oil sample and colloidal instability index (CII).	98
Figure 4-3: Samples of Saturate, Aromatics and Resins fraction obtained from crude oil sample A, B and C.....	99
Figure 4-4: Evaluation of crude oil samples stability of using Yen’s model.....	100
Figure 4-5: Effect of shear rate on viscosity and wax appearance temperature at different temperatures. Top left: Sample A crude oil. Top right: Sample B. Bottom: Sample C..	102
Figure 4-6: Influence of shear rate on crude oil viscosity at three different temperature (5, 25, 35°C) using samples A (top left), B (top right) and C (at the bottom).....	103
Figure 4-7: Rheological behaviour of crude oil sample A, B and C at a shear rate of 120 (1/s) and different temperature	105

Figure 4-8: The relationship between shear stress and the shear rate at different temperature	107
Figure 4-9: Rheological behaviour of sample B crude mixed with different inhibitor at a constant shear rate of 120 1/s and varied concentration (500, 1000 and 1500ppm). Top left: W2001. Top right: W2003. Bottom left: W2004. Bottom right: W2005 inhibitor.....	109
Figure 4-10: Effect of chemical inhibitors on (a) viscosity at 5°C and shear rate of 120 1/s and (b) pour point at a shear rate of 120 1/s at varied cooling temperature (0 – 50°C).....	110
Figure 4-11: Performance of different inhibitors. Left results: Rheological behaviour of four commercial inhibitors compared to other blends inhibitors. Righ: Effect of four commercial inhibitors and blend ‘A’ inhibitor on WAT and pour point.	112
Figure 4-12: Evaluation of macroscopic morphology of crude oil samples (A, B and C) mixed with blended A wax inhibitor (A*, B* and C*) Wax Crystals Morphology with.....	113
Figure 4-13: Chromatographs of different solvents. Top Left: The solvent blank (cyclohexane). Top Right: A standard consist of some even carbon number from C10 to C60. Bottom Left: A typical chromatograph of Polywax 655 external standard.	115
Figure 4-14: Chromatogram of crude oil sample A. Left: Whole oil chromatogram. Right: Topped oil chromatogram	116
Figure 4-15: Chromatogram of crude oil sample B. Left chromatogram: Whole oil chromatogram. Right chromatogram: Topped oil chromatogram.....	117
Figure 4-16: Correlation chart for waxy crude oil sample A	118
Figure 4-17: Correlation chart for waxy crude oil sample B	118
Figure 4-18: n-Paraffin distribution of waxy crude oil samples A and B	119
Figure 5-1: Pressure and temperature sensors responses. <i>Qoil</i> , 7 l/min prior to the wax deposition. (a)– Voltage (Pressure) reading at $\Delta Pt = 0$ i.e. the pressure drop is zero, and at $\Delta Pt = 26$ pressure measurement after 26 minutes of the test. (b)– Temperature correlation after 26 minutes of the test	124
Figure 5-2: Effect of varied cooling temperature (15, 20, 25, 30, 35 and 40°C) on wax deposition at constant crude oil temperature (45°C) and experimental time of 2 hrs. (a) – Experiment at a constant oil flow rate of 5 l/min (laminar flow). (b) – Experiment at a constant oil flow rate of 9 l/min (turbulent flow).	127
Figure 5-3: Effect of varied crude oil flow rate; 2, 3, 4 and 5 l/min (laminar regime) and 7, 9 and 11 l/min (turbulent flow) on wax deposit thickness: (a) – cooling at 15°C (below pour point). (b)– cooling at 30°C (at wax appearance temperature)	131
Figure 5-4: Effect of varied flow rate on weight and volume of the deposited wax. (a)- at a constant cooling temperature of 15°C. (b)- at a constant cooling temperature of 30°C.	133
Figure 5-5: Parity plot validation of deposit thickness (δw) obtained from weight–balance (reference data) and pressure drop method with volume correlation method and heat transfer methods. (a)– Thickness at <i>Qoil</i> = 5 l/min and <i>Tcoolant</i> = 15, 25, 30, and 35°C. (b)– Thickness at <i>Qoil</i> = 9 l/min and <i>Tcoolant</i> = 15, 25, 30, and 35°C.	135
Figure 5-6: Parity plot, validation of experimental deposit thickness (δw) obtained from weight–balance (reference data) and pressure drop method with volume correlation method and heat transfer methods. (a)– Thickness at <i>constant Tcoolant</i> = 15°C and <i>Qoil</i> = 2, 3, 5,7, 9 and 11 l/min. (b)– Thickness at <i>constant Tcoolant</i> = 30°C and <i>Qoil</i> = 2, 3, 5,7, 9 and 11 l/min.	136
Figure 5-7: Sample of wax pigging operation inside the jacked test section obtained in the laboratory.	136
Figure 5-8: The effect of different experimental time on the wax deposition measured in thickness as a function of different cooling temperature. (a)– at laminar flow regime (5 l/min). (a)– at turbulent flow regime (9 l/min).	137

- Figure 5-9: Typical velocity profiles with a separated flow in pipe bend: (a) Longitudinal and rectangular cross-section around the 90° bends (Adapted from Idelchik, 1986), (b) Bend parameters 141
- Figure 5-10: Parity plot– comparison of the new model with the existing correlation weight–balance (reference data). Left– Thickness at constant T_{coolant} = 15°C and Q_{oil} = 5,7, 9 and 11 l/min. Right– Thickness at constant T_{coolant} = 30°C and Q_{oil} = 5,7, 9 and 11 l/min. 144
- Figure 5-11: Effect of varied cooling temperature under different flow rates on wax thickness in 45° bend pipe test-section: Left – Horizontal flow experiment. Right – Inclined flow experiment. 146
- Figure 5-12: Effect of varied cooling temperature under different flow on wax thickness in 90° bend pipe test-section: Left – Horizontal experiment. Right – Inclined experiment. 147
- Figure 5-13: A comparison between deposit thickness in the straight pipe (horizontal flow) with 45° bend pipe section (the top Figures) and 90° bend pipe section (the bottom Figures) in horizontal and inclined flow. Left– cooling at 15°C (below pour point). Right– cooling at 30°C (above pour point). 149
- Figure 5-14: Comparison of the severity of wax deposition in 45° and 90° curved pipe in horizontal and inclined flow at a different oil flow rate. Left– cooling at 15°C. Right– cooling at 30°C. 151
- Figure 5-15: Relative percentage severity of wax deposition for three-curvature pipes (i.e. 0, 45 and 90-degree bend pipes) under horizontal flow. Top Left and Right: at 5 and 7 l/min and at constant cooling at 15°C. Bottom Left and Right: at 9 and 11 l/min and a constant cooling at 15°C. 153
- Figure 5-16: Cross-sectional view of the deposit thickness on the pipe wall: A – wax deposit after 45° bends in inclined flow, B – wax deposit at 2l/min and 10°C, C – Empty pipe and D – Various waxing problem in straight and curved pipe. 154
- Figure 6-1: Effect of varied cooling temperature on wax deposit thickness in straight pipeline test section at (a) laminar flow (5 l/min) and (b) turbulent flow (11 l/min) 158
- Figure 6-2: Combined effect of varied flow rate, cooling temperature and inhibitor concentration on wax deposition (in mass) – through Straight Pipeline Test Section.: (a) at T_{cool}= 15°C, (b) at T_{cool}= 25°C, and (c) at T_{cool}= 30°C 159
- Figure 6-3: The percentage efficiency of blended wax inhibitor at a different flow rate in a straight pipe section (a) at 15°C cooling temperature (below pour point). (b) at 25°C cooling temperature (at pour point). (c) at 30°C cooling temperature (at WAT). 161
- Figure 6-4: Effect of variation of flow rate, and inhibitor concentration on Wax Deposit Thickness at (a) T_{cool}= 15°C, (b) T_{cool}= 25°C, and (c) T_{cool}= 30°C through Horizontal Straight Pipeline Test Section 163
- Figure 6-5: Effect of varied flow rate and inhibitor concentration on wax deposit thickness–through horizontal 45° bend pipe section at (a) T_{cool}= 15°C (b) T_{cool}= 25°C and (c) T_{cool}= 30°C. 166
- Figure 6-6: Effect of varied flow rate and inhibitor concentration on wax deposit thickness–through inclined 45° bend pipe section at (a) T_{cool}= 15°C (b) T_{cool}= 25°C and (c) T_{cool}= 30°C. 167
- Figure 6-7: Combined effect of varied flow rate, cooling temperature and inhibitor concentration on the mass of the wax deposit (in grams) through horizontal 45° bend pipe test section: (a) at T_{cool}= 15°C, (b) at T_{cool}= 25°C, and (c) at T_{cool}= 30°C. 169
- Figure 7-1: Wax precipitation curve from Coutinho thermodynamic model at different pressure and temperature..... 173
- Figure 7-2: Single carbon number (SCN) distribution of the sample B crude oil predicted by Coutinho model matches the experimental data 174

Figure 7-3: Phase envelope of sample B crude oil. The red line represents the wax extraction curve and the blue region represents are envelops for two-phase (oil-gas).....	175
Figure 7-4: Trend plot comparison of wax thickness predicted using RRR, Matzain and Heat analogy models at a constant flow rate of 5 l/min, 80% wax porosity and cooling at 25°C.	178
Figure 7-5: Effect of wax porosity on wax thickness predicted using Matzain model at a constant flow rate of 5 l/min and $T_{cooling} = 25^{\circ}\text{C}$	180
Figure 7-6: Wax deposition profile for the straight flow line section at a constant flow rate of 5 l/min, the cooling temperature at 25°C, and simulation period 4 hr.....	181
Figure 7-7: Trend plots for wax deposition in the straight flow line section at a constant cooling temperature of 25°C and 80% porosity. (a) Deposition at a constant flow rate of 5 l/hr for 2hrs simulation. (b) Deposition at two different flow rate of 5 and 9 l/min and.....	183
Figure 7-8: Comparison of deposit thickness as a function of different cooling temperature (15, 25, and 30°C) and 8 hrs testing between the experimental and simulation studies at constant $Q_{oil} = 5$ l/min, $T_{oil} = 45^{\circ}\text{C}$ and wax porosity (0.8) in a straight pipeline section.	185
Figure 7-9: Comparison of deposit thickness as a function of different cooling temperature (T_c) and time between the experimental and simulation studies at constant $Q_{oil} = 9$ l/min, $T_{oil} = 45^{\circ}\text{C}$ and wax porosity (0.8) in a straight pipeline section.	186
Figure 7-10: Deposit thickness as a function of different cooling temperature (T_c) and time between the experimental and simulation study at constant $Q_{oil} = 5$ l/min, $T_{oil} = 45^{\circ}\text{C}$ and wax porosity (0.8) in a pipeline section with elevation.....	188
Figure 7-11: Deposit thickness as a function of different cooling temperature (T_c) and time between the experimental and simulation study at constant $Q_{oil} = 9$ l/min, $T_{oil} = 45^{\circ}\text{C}$ and wax porosity (0.8) in a pipeline section with elevation.....	189
Figure A1: Photo of the four commercial wax inhibitors supplied by Roemex oil company	218
Figure A 2: Total ion chromatographs of solvent blank (top) and WHOLE oil samples A (middle) and sample B (bottom).	219
Figure A 3: Zoomed region total ion chromatogram of sample 'A' WHOLE oil (top) and extracted ion chromatograms for (middle) nC17 (m/z 240) and pristine (m/z 183), and (bottom) nC18 (m/z 254) and phytane (m/z 197).	219
Figure A 4: Zoomed region total ion chromatogram of sample 'B' WHOLE oil (top) and extracted ion chromatograms for (middle) nC17 (m/z 240) and pristine (m/z 183), and (bottom) nC18 (m/z 254) and phytane (m/z 197).	219

List of Tables

Table 2-1: Global oil sample with different properties (Oil and Gas Journal Data Book, 1987/2004 Editions).....	20
Table 3-1: Properties of KSG crude oil (Sample A) supplied by Roemex (U.K.).....	54
Table 3-2: C10-60 standard Volume.....	65
Table 3-3: The chemistry of chemical wax inhibitors	66
Table 3-4: Blending of different Chemical Wax Inhibitors for improving efficiency.....	67
Table 3-5: Experimental test matrix for crude oil without chemical inhibitor in a straight pipe test-section	80
Table 3-6: Experimental test matrix for crude oil without inhibitor in flow rig equipped with two test-sections incorporates 45° and 90° bend	80
Table 3-7: Experimental test matrix for crude oil with blend ‘A’ wax inhibitor in straight pipeline test-section	81
Table 3-8: Experimental test matrix for crude oil with blend ‘A’ wax inhibitor in the pipeline with 45° bend test-section.....	81
Table 4-1: Physical and Chemical Properties of Three Crude Oil Samples	95
Table 7-1: Experimental and simulated deposit thickness (δ) in a straight pipeline section at temperatures from $T_{oil} = WAT + 15^{\circ}C$ to T_h at 15, 25 and 30°C.....	184
Table B1: Wax table before flash at fixed P and T	221
Table B 2: Screenshot of wax properties table compatible with OLGa software.....	222
Table B 3: Screenshot of PVT table compatible with OLGa software.....	222
Figure C 1: Bend loss coefficients for a pipe proposed by Babcock & Wilcox Co. (1978) (Sreenivas, 2011).	223
Table D1: Measured and computed wax deposition results at constant oil temperature (45°C), constant coolant temperature (15°C), Viscosity (0.0056 Pa) Density (915 kg/m ³).....	224
Table D 2: Measured and computed wax deposition results at constant oil temperature (45°C), constant coolant temperature (30°C), Viscosity (0.0056 Pa) Density (915 kg/m ³).....	225

List of Nomenclature

Symbol	Description
CCN	Critical Carbon Number (dimensionless)
ΔP_f	Frictional pressure drop (bar, psi and pascal)
ρ	Density (g/cm ³ , kg/m ³)
Q	Volumetric flow rate (l/min, m ³ /s)
D_w	Diffusion coefficient of dissolved wax molecules (m ² /s)
D_B	Brownian diffusion coefficient of solid wax crystals in the oil (m ² /s)
A_w	Area of wax deposition
dT/dr	Temperature gradient (°C/m)
$\frac{dM_w}{dt}$	Rate of deposition (kg/s)
M_w	Mass of solid wax (kg)
dt	Change in time (s)
$\frac{\partial u}{\partial y}$	Shear rate or velocity gradient perpendicular to the plane of shear (s ⁻¹)
$\frac{dc^*}{dr}$	Concentration gradient of dissolved wax with respect to distance
C^*	Change in concentration (m ³)
T	Absolute temperatures (°C)
μ	Dynamic viscosity (Pa·s)
V	Volume (m ³)
V	Velocity (m/s)
D_s	Shear dispersion coefficient (m ² /s)
γ	Shear rate at the pipe wall (1/s)
d_w	Wax particle diameter (m)
ϕ_w	Wax volume fraction precipitate out of the solution at the pipe wall
ρ	density (kg/m ³)
a	Particle diameter (m)
n	Power-law index
g	Acceleration due to gravity
K_p	Power-law consistency index
δ	Thickness of the wax layer (m)

f	Fanning friction factor (m)
r_o	Outside pipe radius (m)
r_i	Inside pipe radius (m)
h_c	Outside (coolant fluid) heat transfer coefficients W/(m ² K)
h_h	Inside (crude oil) heat transfer coefficients W/(m ² K)
SARA	Saturates/Aromatics/Resins/Asphaltene
S_{wet}	Wetted fraction of the circumference
NNu	Nusselt number
NRe	Reynolds (dimensionless quantity)
NPr	Prandtl numbers (dimensionless quantity)
Rc	Radius of curvature (dimensionless quantity)
API	American Petroleum Institute
SG	Specific gravity ($\rho_{\text{substance}} / \rho_{\text{H}_2\text{O}}$)
ASTM	American Society for Testing and Materials
PPT	Pour Point Temperature (°C)
WAT	Wax Appearance Temperature (°C)
CII	Colloidal instability index
HTGC	Higher temperature gas chromatography
HAN	High Aromatic Naphtha
R_b	Bend radius (m)
θ	Bend angle (°)
k_b	Bend loss coefficient
L_b	Length of the bend (m)
k_p	Thermal conductivity of pipe (W/(m·K))
k_w	Deposit thermal conductivity (W/(m·K))
U_{gly}	Overall heat-transfer coefficient (W/(m ² K))

Subscripts

w	Wax
o	Oil
d	Solid wax
gl	Glycol

Chapter 1

Introduction and Research Aim and Objectives

1.1 Introduction

Globally, energy demand is set to rise significantly in the coming decades due to population growth and economic development (IEA, 2019). The current IEA report shows that energy demand will grow by 1.3% annually to 2040; however, it has risen 2.3% in 2018, the fastest pace in the last decade. In many parts of the world, focusing on energy stability and security, along with the decline in onshore hydrocarbon production and shallow water reservoirs coupled with the developments in geological surveys, E&P has brought significant attention to hydrocarbon reserves from deeper offshore environments (Buller *et al.*, 2002; Bai and Bai, 2005; Lee, 2008; Guan, 2016; Rittirong *et al.*, 2017). Usually, this type of environment is found in most of the region in the world, including the North Sea, Gulf of Mexico, West Africa, and East coast Canada (Hammami & Ratulowski 2007; Huang *et al.*, 2015; Theyab and Diaz, 2016). The fields in such environments have more challenging reservoir fluids and activities that require more investment costs, 20 times higher than an onshore field (Lee, 2009); however, the returns on investments are considerably higher in the complex environments. So far, the Perdido platform is actually the most in-depth drilling and production platform on the earth, located about 321.869 km offshore in the Gulf of Mexico. Although, with 173 fully active drilling rigs, the North Sea is estimated to have the world's most massive offshore drilling environment (Swartz, 2015).

In general, hydrocarbons production in deeper offshore environments encounters harsh conditions that cause unfavourable flow assurance issues in; (i) System deliverability: pressure drop versus production, pipeline size, and boosting. (ii) Thermal behaviour: temperature distribution, temperature changes due to start-up and shutdown, insulation option and heating requirements. (iii) Production chemistry: hydrates, waxes, asphaltenes, scaling, sand, corrosivity and rheology. (iv) Operability characteristics: start-up, shutdown, transient behaviour (e.g. slugging) and (v) System performance: mechanical integrity, equipment reliability (Bai and Bai, 2005; Watson *et al.*, 2003).

Some of the factors that lead to most of these problems could be attributed to (a) the alteration in hydrocarbon composition, (b) the variation in flow rates (due to the drop in pressure), (c) the decrease in hydrocarbon temperature (due to the transfer of heat from the fluid to the surrounding pipeline environment), (d) the increase in water production with oil (as free-water) and (e) the solid production (Al-Safran and Brill, 2017). Usually, the average temperature at the seabed is typically about 4 – 16°C (Lee, 2008; Cawkwell and Charles 1989) and the increase in pressure drops from the reservoir to surface facility is extremely large (Hammami *et al.*, 2003; Theyab and Diaz, 2016; Teo, 2016;).

Therefore, in the flow assurance framework, engineers and the operators strive to develop effective strategies that are reliable and safe in production of hydrocarbon mixture with minimum operating costs from the main reservoir to processing facilities and point of sale (Shuqiang *et al.*, 2006; Hammami & Ratulowski 2007). This area is therefore crucial for safe operation and economic viability of any oil and gas field. Therefore, implementing appropriate flow assurance strategies is essential in any oil field either to avoid possible fluid problems entirely or to be able to intervene on a regular basis consistently. This research is therefore focused on the study of the behaviour of wax precipitation and deposition at subsea pipeline condition, along with the severity of wax deposition caused by the presence of bends in pipeline. The motivation of the study, aim and objectives alongside the thesis structure are presented in section 1.3, 1.4, and 1.5 respectively.

1.2 Waxes Deposition Challenges And Treatment

Wax deposition and the possible clogging of the production, transportation and storage facilities is one of the major problems in the oil and gas industry for decades, as this will lead to costly repair operations and plug remediation (Chala *et al.*, 2018; Fagin, 1945; Ford *et al.*, 1965; Goldman, Marcene S., 1957; Lira-Galeana *et al.*, 1996; Wang *et al.*, 2019). At the reservoir condition, waxes are soluble crystals in crude oil (70 – 150°C and pressures of around 50 – 100 MPa). The molecules of wax begin to precipitate as the bulk oil reaches a temperature below its wax appearance temperature (WAT), which increases oil viscosity and contributes to a pipeline pressure loss (Rittirong *et al.*, 2017; Zheng *et al.*, 2016). When wax molecules start to precipitate with temperature and pressure changes; the particles of the wax agglomerates and form a net-like or cage-like structure

called wax gelation. As the precipitation progresses, in the absence of any mitigation strategy, this gel begins to settle (deposit) on the wall of the production pipelines (Groffe *et al.*, 2001; Hao *et al.*, 2019; Zhu *et al.*, 2008; Zheng *et al.*, 2016; Singh *et al.*, 2000).

On the other hand, the deposition of wax has been reported to cause several problems in production, transportation and storage systems. Its occurrence leads to technical and economic problems such as increased surface roughness, increased pressure drop, decreased the inner diameter of the pipe, which eventually reduces the oil recovery. It can completely block the pipeline system and in the worst-case scenario and situations where the deposition is critical, contribute to the abandonment of the field (Bai and Bai, 2005; Zhu *et al.*, 2008). For instance, one of the typical oil fields abandoned due to severe and frequent wax deposition problems is the Staffa oil field in the UK operated by Lasmo Oil Company; after four years of production, the oil field reported over \$100,000,000 losses (Nguyen *et al.*, 2001; Singh *et al.*, 2000). In the cases where the abandonment is not necessary, the deposit induces high-yield stress for flow restarting (Chala *et al.*, 2018). This implies that in the event of restarting after shutting down, the system requires a higher pressure than the reasonable operating condition (Lee *et al.*, 2008; Bai and Bai, 2005). Figure 1-1 illustrated deposited wax received at the pig receiver in one of the North Sea platform. As revealed by Bai and Bai (2005), Rittirong *et al.* (2015), Rashidi *et al.* (2016), some of the fundamental factors affecting wax precipitation and deposition include the crude oil composition, the crude oil and the ambient temperature, flow rate, pipeline geometry and the system pressure.



Figure 1-1: Sample wax pig out of platform C in the North Sea (Labes-Carrier *et al.*, 2002)

In a nutshell, wax deposition issues affect the OPEC, CAPEX and the revenue generation along with the negative impact on the health, safety, and environment (Lee et al., 2008; Burger et al., 1981; Majeed *et al.*, 1990; Zheng et al., 2013). Wax deposition problems are usually studied by performing a laboratory experiment to find a suitable technique that can be used for its management. Some of the several researchers that have examined the problems in single-phase crude oil flow includes Bagdat and Masoud (2015), Burger *et al.* (1981), Chi *et al.* (2017), Creek *et al.* (1999), Dwivedi (2010), Gao (2003), Hoffmann and Amundsen (2010), Lee (2008), Rashidi *et al.* (2016), Singh *et al.* (2000), Theyab and Diaz (2016), Van Der Geest *et al.* (2019), Wang *et al.* (2019) and Zheng *et al.* (2013). Similarly, in two-phase oil and water flow, the deposition of wax has been studied by Couto (2004), Anosike (2007), Zhang and Liu (2010), Huang *et al.* (2011), Panacharoensawad and Sarica (2013), Kasumu (2014), Kasumu and Mehrotra (2013), Wang *et al.* (2019) and Zheng (2017) whereas, limited studies are reported in two-phase oil and gas flow (e.g. Apte *et al.*, 2001; Gong *et al.*, 2011; Kilincer, 2003; Matzain *et al.*, 2002; Rittirong, 2014; Rittirong *et al.*, 2016, 2017a, 2017b; Sulaiman *et al.*, 2017). Despite all these researches, so far there is no study on three-phase gas/oil/water wax deposition experiment (Duan *et al.*, 2016; Rittirong, 2014; Rittirong *et al.*, 2017; Sarica and Panacharoensawad, 2012).

It is worth noting that this research focuses only on using a single-phase oil flow, however, depending on the operating conditions, stages of experiment; the crude oil phase changes from liquid to gas and solid respectively. On the contrary, several studies were carried out by using mathematical modelling and computational simulation techniques in single-phase, two-phase and three-phase on wax deposition (Apte *et al.*, 2001; Giacchetta *et al.*, 2019; Huang *et al.*, 2011; Leporini *et al.*, 2019; Matzain, 1999; Matzain *et al.*, 2002a; Pinho *et al.*, 2011; Ramirez-Jaramillo *et al.*, 2004; Ramírez-Jaramillo *et al.*, 2001; Soedarmo *et al.*, 2017).

On the other hand, several methods for wax prevention and remediation have been developed in the laboratories and tested in the oil field. Despite the positive effects in some of the techniques, however, they have an economic drawback that has consequences on the CAPEX and OPEX in many ways. For instance; capital costs—preventive methods; such as the addition of subsea equipment and designing of strategies for solid deposits prevention, e.g. chemical wax inhibitors. Whereas, the operational

cost– corrective methods; such as injection of chemical, thermal method, pigging process and flow monitoring (Kennedy and Saint-Marcoux, 2015; Lee, 2008; Yang *et al.*, 2015). In many cases, none of the above techniques has been used as a stand-alone tool for the prevention and remediation of wax deposition purposes, particularly in a long-distance production system that required continues production with no interference and at minimum cost (Coto *et al.*, 2014; Fan and Llave, 1996; Li *et al.*, 2018; Yang *et al.*, 2015). The pigging is broadly well known to remove paraffin waxes. The thermal technique involves heating such as inductive heating for both removal and prevention method. Chemical treatment involved the use of wax inhibitors or pour point depressants for prevention of deposition (Birch, 2015; Wei, 2015). In most cases, two or more technique are combined, e.g. chemical with heating was used to achieve incredible treatment and to reduce cost (Kelland, 2009). Similarly, heating with the pigging method is tested to reduce energy consumption and environmental pollution (Mahto and Kumar, 2013; Yang *et al.*, 2015).

Chemical treatment has been practically the preferred prevention technique, especially for uninterrupted production, long-distance pipeline/flow lines and for reducing restart pressure and yield stress (Aiyejina *et al.*, 2011; Majeed *et al.*, 1990). Chemicals usually offer an improved rheology property by disrupting the orderly aggregation of the growing crystals, which decrease the viscosity, pour point and the WAT (Kelland, 2009). Unfortunately, the application of chemicals is usually limited to a specific oil well and deposit due to the different properties of the crude oils and origin. This implies that in all the types crude oil there is no single inhibitor developed to be suitable equally in each oil (Adeyanju and Oyekunle, 2014; Halim *et al.*, 2011; Kang *et al.*, 2014). Researchers have studied different chemical wax inhibitors, both analytically and using a flow loop system. The studies by analytical method have shown that the following chemicals effectively influence the crude oil properties such as polyethylene, copolymer esters, ethylene/vinyl acetate copolymers (Halim *et al.*, 2011; Jafari Behbahani *et al.*, 2015; Kang *et al.*, 2014), olefin/ester copolymers, ester/vinyl acetate copolymers, polymethacrylates (Al-Sabagh *et al.*, 2009; Song *et al.*, 2010; Wu *et al.*, 2012), alkylphenol resins, toluene and xylene (Jang *et al.*, 2007; Jennings and Newberry, 2008; Kang *et al.*, 2014). Nevertheless, a limited number of researchers used an experimental flow loop to test and determine dynamic efficiency of wax inhibitors on wax deposition (e.g. Adeyanju and Oyekunle, 2014; Hoffmann and Amundsen, 2013; Li *et al.*, 2018; Lim *et al.*, 2018; Theyab, 2017).

1.3 Motivation for Work

In recent years, wax deposition in production and transportation facilities has increasingly become a focus in the field of flow assurance. Although significant progress has been made in mitigating the problem, many questions around the full understanding of the depositional behaviour and the physical process mechanisms still remain unanswered. As discovered in the published literature, predominated researches works on wax deposition were carried out in straight pipes; horizontally, vertically, or slightly inclined. As the exploration and production of oil and gas advances in more challenging environments, it is unavoidable that the elbows, bends and inclination are used, particularly as essential components for subsea process equipment and some part of the production pipeline and riser. The effect of the pipe curvatures on the increased severity of wax deposition is not well studied.

As of today, very limited research work has been documented in the literature that investigates wax deposition in a flow rig equipped with curved or bended pipes (e.g. Bagdat and Masoud, 2015; Lee, 2008; Lee *et al.*, 2008; Rashidi *et al.*, 2016; Sarica and Volk, 2004). However, none of these studies suggested the degree of the severity of wax deposition in a restricted flow (i.e. in bends or elbows) and even the influence of the bends in pipes on the wax deposition at varied control parameters was not revealed. This also suggests a lack of experimental data on the extent to which curved pipes influence process mechanisms that govern the formation of waxes. Therefore, in this research, wax deposition in a flow loop with a straight pipe test section was investigated and compared with two different pipe sections with a 45° and 90° bend respectively. Overall, the effects and the severity of the wax depositional behaviour are studied in a single-phase flow in a laboratory-scale flow loop. The significance of the research is reflected that it provides the essential knowledge for the academics and industry engineers to develop robust and effective preventive strategies for wax mitigation and improve the existing model that has been used in the oil and gas industries.

Clearly, flow restriction (due to the presence of bend) significantly affects the global and local flow parameters; such as pressure drop, advection (i.e. altering the heat transfer characteristics) and particle interaction (causes secondary flows) (Wang *et al.*, 2004; Yadav *et al.*, 2014). Hence, it is expected that it shall affect wax deposition behaviour and

the mechanisms of the deposition (such as the molecular diffusion, Brownian diffusion, shear dispersion, gravity settling and shear stripping). The gap in knowledge necessitated further studies in this area to overcome wax deposition issues through a better understanding of wax deposition problems at the early stage of a project, which will lead to adequate mitigations plans through accurate prediction, and analysis of the deposition. In a nutshell, huge savings could eventually be achieved through improving the prediction of wax deposition and understanding the effect of deposition control parameters which, apart from the temperature that was regarded as the main factor and the pipe geometry.

Another aspect that is still under investigation and is of particular interest to the flow assurance experts is the understanding of the complex rheology of different crude oils and their mechanism of interaction with chemical inhibitors (Daraboina *et al.*, 2016; Hao *et al.*, 2019; Makwashi *et al.*, 2019b; Paso *et al.*, 2014). Unfortunately, several models are developed based on a specific crude oil property. In nowadays, a lot of simulation studies are carried out based on several assumptions of the oil property or by simulation with borrowed literature data. This affects performance, of course, and produced wrong predictions. On the other hand, it is well known that the use of chemical treatment in the industries has practically increased; however, chemicals are usually designed to fit specific properties of crude oil and environmental conditions (Jennings and Breitigam, 2010). Therefore, a typical chemical inhibitor is effective in a particular well but less effective or even fail in a different well of the same basin (Coto *et al.*, 2014; Towler and Rebbapragada, 2004).

Consequently, the interaction of chemical wax inhibitors with crude oil is not well known and still under scrutiny. Therefore various waxy oil samples with and without chemical inhibitors are characterised and analysed in this research. The study involved the use of rheometer— whereby different blended inhibitors were produced by mixing various fractions of commercial inhibitors. Similarly, pipeline flow loop system is used to test the inhibitor's improved performance and efficiency in reducing wax deposition. Hence, noting that the oil and gas industries are targeting a universal inhibitor that would be effective with different crude oils, which perhaps might be possible with advanced technologies. Through these analyses, fundamental understanding of wax deposition

phenomena and comprehensive waxy crude oil properties for simulation studies are achieved.

Overall, the relevant research questions arising from the motivations of this work to be investigated are as follows;

- i. Does the curvature of pipes matter in the production and transportation waxy crude oil?
- ii. And if so, what is the extent and what could be the percentage severity of wax deposition?
- iii. How will fluid dynamics affect the process mechanisms of wax deposition, mainly when the curvature of the pipe is changed?
- iv. What are the disparities in rheological behaviour between different crude oil samples with and without chemicals inhibitors?
- v. Does the blended wax inhibitor reduced or prevent wax deposition?, and if this is the case, to what extent (efficiency)?

1.4 Research aim and objectives

The aim and objectives of this research are shaped by the above questions and motivated by the fundamental knowledge gap in detailing wax deposition behaviour in different pipes curvatures under subsea conditions and the influence of various parameters and process mechanisms with or without chemical wax inhibitors. The aim of this research is, therefore, to provide comprehensive information through a novel experimental flow loop on the wax depositional behaviour of a single-phase waxy crude oil.

The main objectives of the research presented in this thesis are:

1. To systematically characterise three different samples of crude oil, one of which is synthetic oil, and study the onset of wax precipitation and deposition alongside with the influence of wax inhibitors on the rheological properties of oil samples.
2. To experimentally investigate wax deposition behaviour in a flow loop with a straight pipe section and compare with 45° and 90° curved pipes sections. Through which the influence of variables parameters on wax deposition are studied.

3. To analyse the efficacy of a blended wax inhibitor on wax deposition in the flow loop with straight and 45° curved pipes along under different flow conditions.
4. To visualise and quantify wax deposit thickness using different methods by which a new pressure drop model would be developed and tested.
5. To use the experimental results for comparison and validation of the existing OLGA models.

1.5 Achievement

The main achievements of this research are:

- (1) For the first time, the severity of wax deposition in different curvature pipes was successfully studied using a novel experimental flow loop designed and built in the Laboratory. This contribution presents an important scientific and practical advances into the prediction and the development of wax management strategies, which are still under the scrutiny of the flow assurance engineering community.
- (2) A new pressure drop correlation for measurement of wax thickness in curved pipes was established. The model combined the parameters that usually affect the deposition of wax due to the pressure drop by the frictional losses and the change of direction of fluid (momentum) due to the bends.
- (3) A synergy of different chemical inhibitors was tested and a new blended wax inhibitor was established. The inhibitor has proven to be effective and interfered with the wax crystals agglomeration, thereby reduces wax deposition and in some cases prevented the deposition completely.
- (4) Fully characterised two-naturally waxy crude oil and one synthetic crude oil through different standard techniques. The key finding includes the main parameters that defined the waxy oil behaviour and envelop in which the problem of wax deposition could be avoided. The results are essential for comparable prediction and simulation studies.
- (5) Attended several international conferences and drafted three Journal paper under review for publication.

- (6) Collaborated with other PhD students, strengthened capacity in the area of research and development. Through this process, two papers were published in the Journal of Analytical and Applied Pyrolysis and Society of Petroleum Engineers (SPE).
- (7) Successfully trained and managed two MSc students, with masters theses title as follows;
- i. Delcia Soraia David Barros (2019). Effect of a Blended Wax Inhibitor on Wax Deposition in Crude Oil Pipelines.
 - ii. Stephen Arome Akubo (2018). Experimental Study of Wax Depositional Behaviour in Single-Phase Oil Flow.

1.6 Publications (Conferences and Journals)

Makwashi, N., and Zhao, D. (No Date) The effect of pipe curvature on wax depositional behaviour: experimental results vs OLGA simulation data (**close to submission**)

Makwashi, N., and Zhao, D. (No Date) A Model for Determination of Thickness of Wax Deposition in Bend Pipelines using Pressure Drop Correlation (**close to submission**)

Makwashi, N., Sarkodie, K., Akubo, S., Zhao, D. and Diaz, P., 2019, June. Investigation of the Severity of Wax Deposition in Bend Pipes Under Subcooled Pipelines Conditions. In *SPE Europec featured at 81st EAGE Conference and Exhibition*. Society of Petroleum Engineers. <https://doi.org/10.2118/195559-MS>.

Makwashi, N., Barros, D.S.D., Sarkodie, K., Zhao, D. and Diaz, P.A., 2019, September. Depositional Behaviour of Highly Macro-Crystalline Waxy Crude Oil Blended with Polymer Inhibitors in a Pipe with a 45-Degree Bend. In *SPE Offshore Europe Conference and Exhibition*. Society of Petroleum Engineers. <https://doi.org/10.2118/195752-MS>.

Sarkodie, K., Fergusson-Rees, A., **Makwashi, N.** and Diaz, P., 2019, June. Slug Flow Monitoring in Pipes Using a Novel Non-Intrusive Optical Infrared Sensing Technology. In *SPE Europec featured at 81st EAGE Conference and Exhibition*. Society of Petroleum Engineers. <https://doi.org/10.2118/195449-MS>

Muhammad, I., **Makwashi, N.** and Manos, G., (2018) Catalytic degradation of linear low-density polyethylene over hy-zeolite via pre-degradation method. Journal of Analytical and Applied Pyrolysis. <https://doi.org/10.1016/j.jaap.2018.11.025>

Makwashi N., Akubo S.A., Sarkodie K., and Zhao D. (2018) Engaging Best Practices During Waxy Crude Oil Production to Prevent Deposition in the Subsea Pipeline. Available from: <http://www.lsbu.ac.uk/conferences/construction-professionalism-ethics>. p189 – 199.

Makwashi N., AhmedT., Zhao D., and Ismaila I. P. (2018) Pipeline Gas Hydrate Formation and Treatment: A Review (Published a full Paper in the Conference Proceedings). 3rd National Engineering Conference on Bridging the Gap between Academia and Industry (ACICon2018), Bayero University Kano, Nigeria. 14th – 16th November 2018.

1.7 Thesis Structure

This thesis is organised into eight different chapters, briefly discussed as follows:

Chapter 1 Introduces and outline the overall research project and the problem of the complex nature of wax precipitation and deposition with various mitigation methods, which raised research questions, aim and objectives of this work.

Chapter 2 reviews the literature relevant to this work and background information were presented related to the wax deposition problem. The proposed mechanisms of wax deposition and the factors that affect and control the wax deposition process. A review of wax mitigation methods, flow through a straight and bend pipes was presented. Relevant gaps in knowledge and rationale for this work was discussed.

Chapter 3 reveals the details design of the flow loop system and reviews different experimental methods and analytical techniques used for the crude oil characterisation (e.g. Rheometric analysis, SARA analysis, T-SEP® technique for HTGC analysis and Modified UOP 46-64 for wax content e.t.c) and wax thickness measurement (e.g. heat analogy, pressure dop and mass balance correlations).

Chapter 4 provides the full results of crude oil samples characterisation (such as n-paraffin distribution, WAT, pour point colloidal instability index). Screening results of four (4) commercial wax inhibitors mixed with different crude oil and the effects of blended inhibitors were presented.

Chapter 5 presents the results and the analysis of wax deposition in pipeline flow rig. The wax deposition behaviour in the straight pipeline was compared to those in curved pipes. Similarly, the chapter shows the results of the new wax thickness model and the disparity in the results were discussed.

Chapter 6 presents the performance and efficiency of blended wax inhibitor on wax deposition in a flow loop with straight and 45o curved pipes under different flow conditions.

Chapter 7 provides wax deposition simulation results in straight and 45o curved pipes. Experimental results were compared with the data obtained from OLGA simulation. A comparison between IRR, heat analogy and Matzain model are made alongside with the result from Multiflash for fluid modelling properties.

Chapter 8 presents the main conclusions and accomplishments of this research and provides suggestions for future works.

Chapter 2

Literature Review

2.1 Introduction

This chapter provides a review of the literature and background pertinent to this research, including an overview of the major flow assurance challenges (Section 2.4), with focused toward wax precipitation and deposition issue (Section 2.5). The deposition mechanisms and the factors that influence the deposition are presented in Section 2.5.4 and 2.5.5. The chapter also reviewed the prevention and mitigation techniques (Section 2.5.6) and the flow behaviour in the straight pipe and curved pipe (Section 2.5.9.1 and 2.5.9.2). Lastly, the gaps in this research identified based on the knowledge from the literature that unveils the novelty of this work are highlighted (Section 2.6).

2.2 Flow Assurance

The term “flow assurance” was first used in the oil and gas field in the early 1990s by Petrobras, which referred the term in Portuguese as Garantia do Escoamento, literally means “Guarantee of Flow”, or Flow Assurance (Irmann-Jacobsen, 2013; Ahmed, 2007). Flow assurance is often considered significant mostly in the area of field development for technical feasibility studies, detail design, economic efficiency. In some cases, it dealt with system selection such as processing facilities, pipeline and riser to deliver a successful operation (Bai and Bai, 2005). Flow assurance strategies are commonly applied in the oil and gas field to avoid all the problems that might affect the productivity and life span of the field, which could be in effect throughout the phases of production (Ahmed, 2007; Irmann-Jacobsen, 2013). One of the early problems of flow assurance (i.e. hydrate blockages) was recognised in the 1930s, which was solved by Hammerschmidt in 1939.

2.3 Flow Assurance Challenges

The critical task of flow assurance is mostly compounded at the subsea oil and gas environment, which is involved in system design and operation, primarily as a unit for

prevention and control of solid deposit. The three most common and well-known organic solid deposits that affect the assurance of fluid flow are; hydrate, paraffin wax and asphaltenes and in some cases, scale and sand are also a severe issue during production (Bai and Bai, 2005; Ahmed, 2007). Figure 2-1 illustrated the flow assurance challenges found in the deep-water environment, transportation through longer tiebacks, pipelines and flow lines.

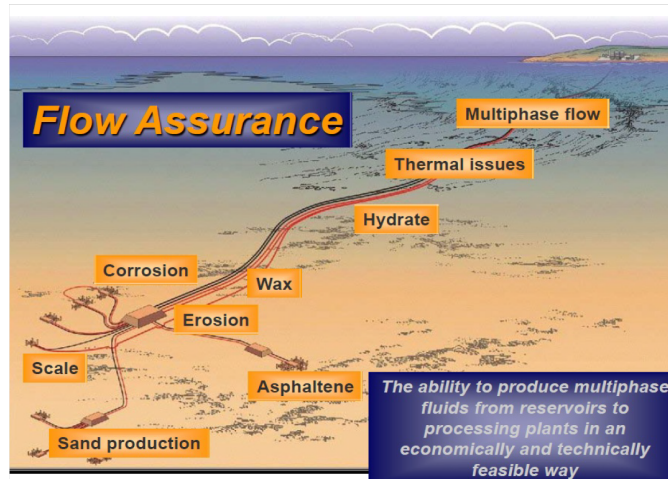


Figure 2-1: Typical flow assurance problems at a different stage of production (Serintel, 2017).

The challenges modelled above can be complicated due to the dynamic conditions and production profile over the life span of the field. Currently, the solutions employed as mitigation or prevention of these problems do not provide adequate desire target, mainly when dealing with long-distance production line (Akpabio, 2013; Chala *et al.*, 2018). The main organic deposits that affect the grantee of fluid flow are briefly discussed in the subsequent sections and more details on the general concept of wax deposition problems (as the central area of this research) are provided in Section 2.5.

2.3.1 Gas Hydrates

Apart from paraffin wax and asphaltene; gas hydrates formation is perhaps a major flow assurance problem in the oil and gas industry (Bai and Bai, 2005; Shuard *et al.*, 2017; Turner *et al.*, 2005). Study by Shuard *et al.* (2017) shows that, in the multiphase system, hydrate plugging constitutes the largest concern by order of magnitude compared to waxes, asphaltenes, and scales. Usually, the formation occurs in two ways; as a natural process and by the action of industrial activities 'technogenic' mostly within the oil and gas facilities (Brewer *et al.*, 1998; Kalorazi *et al.*, 1998). Gas hydrates' crystalline

compounds resembled snow or ice with densities smaller than ice. The structures are formed when small non-polar gas molecules are en-clathrate within the water at suitable conditions (Sloan and Koh, 2007). The following are the critical circumstances that promote the formation of gas hydrates in a system (Dutton, 2018; Jacobs and Writer, 2015; Dutton, 2018);

- Presence of free water: This is important for the formation of hydrates; normally, without free water, hydrate formation is not possible. Therefore, it is always important to remove water vapour from the hydrocarbon to avoid this problem.
- Low temperatures: Temperature of about 39 °F or lower is critical in any system that desires to avoid hydrates formation. Hydrates form, particularly when the temperature is below or at the hydrate formation temperature for a given pressure and gas composition.
- High operating pressures. Gas hydrates require pressure greater than 166 psi.
- Flow pattern: Hydrodynamic slug flow increases the rate of the formation of hydrates at the head of the slug. This is due to the greater interface between gas and water.
- Presence of H₂S and CO₂: These acid gases promote the formation of hydrate because they are far more water-soluble than the hydrocarbons.
- High velocities or agitation, or pressure pulsations.

Figure 2-2 shows the various stages encountered during the formation of hydrate crystals plug-in oil and gas pipeline.

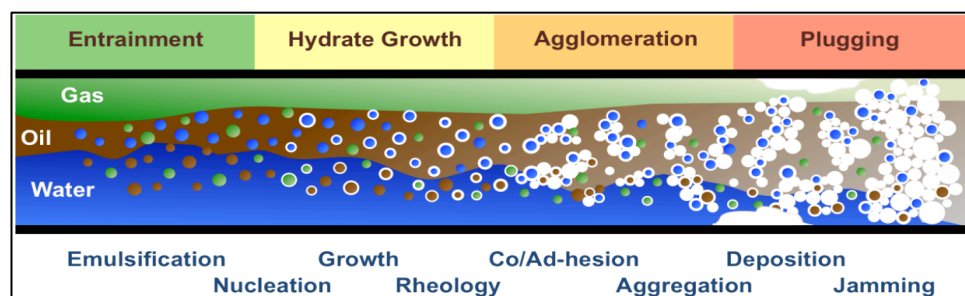


Figure 2-2: Typical conceptual hydrates formation, agglomeration and plugging in multiphase flow system (Sum, 2013).

At the beginning of production, the three-phases (gas-oil-water) are emulsified creating gas bubbles entrained in the oil and water, oil emulsified in water, and water emulsified in oil, which then produces the surface area for hydrate formation. Hydrates formation

begins as soon as the temperature and pressure in the system drop to a point within the hydrates stability region, which occurs at the interface between the water and hydrocarbon fluid (oil or gas) that forming a shell structure around the water/oil droplets (emulsified in oil/water). As typical mass transfer or heat transfer process, the growth of hydrates continues after this stage. As an exothermic process, once hydrated particles interact and agglomerate into larger aggregates, the particles continue to grow. They may form larger hydrated masses and deposition, resulting in an increase in slurry viscosity, causing an unacceptably large pressure drop, prohibiting flow and eventually creating a plug (Sum, 2013). The flow line becomes a plug similar to wax/asphaltene deposition as the particles slowly and continuously build-up over time (Shuard *et al.*, 2017; Singh *et al.*, 2000).

Unlike wax deposition remediation techniques, a pigging method is not recommended for removing of the hydrated blockage as this may cause more harm. The most effective solutions to this issue are therefore the use of chemical additives such as mono ethylene glycol (MEG) or methanol, pipeline insulation (mostly applied to flow lines and risers), depressurisation, direct electrical heating, or the cold flow method (Cha *et al.*, 2013; Cochran, 2003).

2.3.2 Asphaltenes

Asphaltenes appear as black, gummy, and slick component of crude oil (Brown, 2002). Asphaltenes are described as the collection of heavy polar components in crude oils that are soluble in aromatic solvents like toluene but insoluble in alkanes such as n-heptane and n-pentane. These components are perhaps the most complex fraction of crude oil that contributes to the formation of deposits in most of the crude oil processing facilities. Asphaltene solubility in crude oils depends on fluid composition, flow rate, pressure, and temperature (Brown, 2002; Trejo *et al.*, 2007). Any disturbance to these parameters during oil production or refinery operations can change the solubility value, resulting in precipitation of asphaltene fractions.

Prevention and removal of asphaltene can be achieved using similar techniques to paraffin wax. Methods such as chemical injection using solvents or mechanical method using scrapers are commonly apply (Chrisman *et al.*, 2012; Wasden, 2003). Combination of both mechanical and chemical methods is typically used, however, in any of the cases;

these operations are regarded as expensive and involve intensive processes which require a high degree of HSE management to execute and include potentially lengthy downtime (Chrisman *et al.*, 2012). Inhibitors added in one of the Haliburton production lines of asphaltenes have proven to be effective. It prevented the colloidal asphaltenes agglomeration without any formation of the deposit. Mechanical removal methods' using pigging is highly risky due to the prospect of the pig getting trapped in the production facility. It is stated by Wasden (2003) that the presence of asphaltene in waxy crude often rules out the standard pigging protocol for wax deposition management in waxy oil production. The asphaltene fraction in the waxy oil system promotes the interactions of waxes crystals and generally causes fouling (Alcazar-Vara *et al.*, 2012; Chanda *et al.*, 1998; Dickakian and Seay, 1988). In other words, during the wax deposition process, asphaltene serves as a nucleation site that promotes the deposition of crystals.

Hence, in this research, asphaltene fraction in three crude samples is analysed through precipitation techniques (Section 3.3.6). The colloidal instability index (Section 3.3.7) was analysed to understand the propensity of asphaltene aggregation of the crude oil samples. Figure 2-3: Appearance of asphaltene samples from crude oil. (a) A laboratory sample of n-heptane asphaltenes (Time, 2011) (b) Crude oil pipeline blocked by asphaltene and waxes shows the asphaltenes fraction obtained from an experiment and the co-precipitation and deposition of asphaltene and wax in the field pipeline.

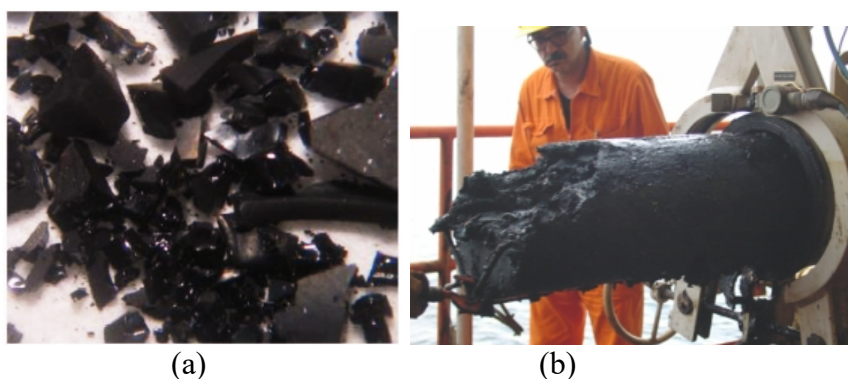


Figure 2-3: Appearance of asphaltene samples from crude oil. (a) A laboratory sample of n-heptane asphaltenes (Time, 2011) (b) Crude oil pipeline blocked by asphaltene and waxes (Headen *et al.*, 2007)

2.4 Paraffin Waxes

Waxes, also known as paraffin waxes (Escobar-Remolina *et al.*, 2009) is an old problem that has been in the oil industry since many decades (Fagin, 1945; Ford *et al.*, 1965; Goldman, Marcene S., 1957). Waxes in crude oil are one of the notorious pipe blockers, with asphaltenes as the second molecules (Siljuberg, 2012). The solubility of wax crystals is a function of temperature, whereas pressure hardly influences the solubility (Siljuberg, 2012). Typically, the precipitation of wax occurs at a lower temperature than asphaltenes and the problem are mainly found in the pipeline than within the flow lines. Also, compared to hydrate plug formation, wax deposition generally occurs slowly; however, the undesirable outcome is usually similarly if allowed to continue unchecked and unmitigated (Bai and Bai, 2005).

Paraffin waxes form a crystalline structure below their melting point range, either from their distinct compounds or from the combination of one another. The crystals' shapes are predominantly rhombic or monoclinic, usually with a low order of symmetry appearance (Mozes, 1982). Unlike other crystalline compounds, the paraffin wax crystal structure changes more below the melting point (i.e. at the equilibrium transition temperature) (Kasumu, 2014). Different authors (such as Hao *et al.*, 2019; Lee, 2008; Li *et al.*, 2018; Zheng *et al.*, 2016) have classified wax crystals into two types, (i) macro-crystalline and (ii) micro-crystalline paraffin wax molecules. Figure 2-4 shows a structural arrangement for these molecules.

The composition of paraffin wax has 80 to 90 per cent macrocrystalline. The remaining per cent are microcrystalline compounds (Rehan *et al.*, 2016). The macro-crystalline paraffin wax comprises of low molecular weight straight-chain n-alkanes (C₁₆ to C₃₆) that crystallises in needle or platelet shape crystals at low temperature (Lee, 2008; Li *et al.*, 2018). They are usually found in the production and transportation systems (Al-Safran and Brill, 2017; Hao *et al.*, 2019). Whereas, micro-crystalline wax are higher carbon number (C₃₀ to C₆₀) molecules; consisting of high fractions of branches and cyclo-alkanes. Hence, it tends to have a higher crystallization temperature and usually precipitates in the form of needles and mal-crystalline shapes (Japper-Jaafar *et al.*, 2016; Keeper, 2013; Kok and Saracoglu, 2000; Mansoori, 2009; Zheng *et al.*, 2016). Micro-crystalline is mostly found at the bottom of the sludge tanks (Al-Safran and Brill, 2017).

The mal-crystalline shape is small underdeveloped crystals that frequently agglomerate under fast cooling rate. Rapid cooling produces needles crystals forms, while slow crystallization favours the growth of the plate's shapes (Turner, 1971). In most cases, all these forms are usually produced in a single crystallization, although one of them often being the predominant one under a given set of conditions.

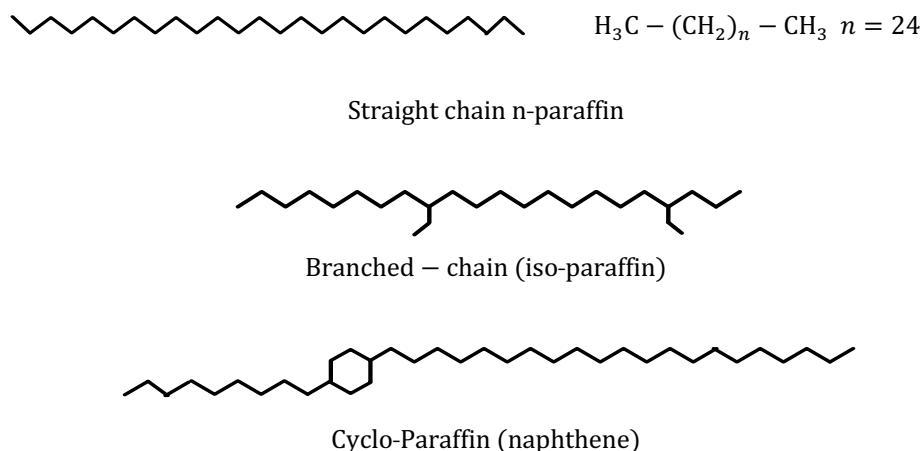


Figure 2-4: Paraffin waxes molecular structure (Hasbullah, 2011)

Hence, in this research, both the carbon chain (Section 3.3.8) and the morphology (Section 3.3.5) of different crude oil below the melting point are investigated. The study outlines the basic structure and identifies the region of macrocrystalline (C15-C36), and microcrystal (>C36) paraffin wax in the samples oil.

2.4.1 Waxy Crude Oil Properties

In many cases, it is vital to develop a good understanding of the physical and chemical properties of paraffin waxes in order to develop suitable management strategies. Paraffin is a member of homologous series; they are relatively inert with little affinity for chemical reagents, thus the name 'paraffin'. They are less dense than water and do not dissolve in water; their molecules are held together by covalent bonds (Kasumu, 2014; Sifferman, 1979). The non-polar molecules are held by weak and short-range van der Waals forces that act only between the surfaces of the molecules. Hence, Morrison and Boyd (1992) observed that the larger the n-alkanes molecules (indicates a large surface area), the stronger the intermolecular forces. Table 2-1 shows some of the critical properties of different waxy oil samples from different field around the world.

Table 2-1: Global oil sample with different properties (Oil and Gas Journal Data Book, 1987/2004 Editions)

SAMPLE NO.	CRUDE	API GRAVITY	WAX CONTENT wt %	WAT (°C)	Pour Point (°C)
1	Tapis, Malaysia	44.3	5.75	45	3.89
2	Bombay High, India	39.35	10.6	41	30
3	Brent, UK North Sea	38.16	3.1	44	-3
4	Brent Blend, North Sea	38	6.5	34	-15
5	Thistle, UK North Sea	37.03	7.7	26	12
6	Bonny Light, Nigeria	36.7	3.5	48	8
7	Forties, UK North Sea	36.6	7	23	-3
8	Dunlin, UK North Sea	34.9	5	27	6
9	Alaskan North Slope S5	34.02	18.1811	36.5	9
10	Soyo Blend, Angola	33.7	14.7	42	18
11	Cinta, Indonesia	33.4	30.3	52	4.56
12	Labuan Blend, Malaysia	33.2	2.34	28	11.11
13	Hout, Divided zone	32.8	14.5	30	-25
14	Khafji, Divided zone	28.5	13.9	50	-35
15	Belayim, Egypt	27.5	17.5	38	6

2.4.2 Precipitation of Wax Crystal

Wax precipitation or crystallization may be defined as the formation of a solid phase from a liquid phase, whereas deposition (discussed in Section 2.4.3) is termed as the formation and growth of a layer of the precipitated solid on a surface (Hammami and Ratulowski, 2007; Yang *et al.*, 2015). The precipitation process occurs when the temperature of the flowing fluid is less than or equal to the cloud point temperature (WAT). In general, the major mechanisms responsible for wax precipitation as publicised by Zhu *et al.*, (2008) and Yang *et al.* (2015) includes nucleation, growth and agglomeration stages. These processes do occur concurrently or individually, with one of the stages always predominating at a time. During the later process, formed wax crystals interlock, causing network formation in the system (Yang *et al.*, 2015).

2.4.2.1 Nucleation

The formation of the nucleus is reported as the first process of crystallization. In the nucleation stage, as the system experience decrease in temperature and pressure losses, the solubility limit of wax crystals is approached, and therefore, decrease the kinetic

energy. At this point, the motion of the wax molecules is negatively affected leading to the formation of a short-lived cluster of the wax molecules known as nuclei; this process is called nucleation process (Zhu *et al.*, 2008). Nucleation either can be spontaneous (homogenous nucleation) or induced artificially (heterogeneous nucleation). The usual thermal process that typically occurs from a pure sample with time-dependent nucleation sites is referred to as homogenous nucleation. In contrast, the heterogeneous nucleation may be either thermal or athermal, and therefore, all the nucleation sites are activated instantaneously (Turner, 1971). This form of nucleation occurs either on the pipe wall or because of the foreign particle within the system.

2.4.2.2 Crystal Growth

Following the formation of nuclei, as the temperature remained at or less than the WAT, more wax molecules continue to built-up, molecules attach themselves to the nucleation sites, becoming part of growing flats monolayers and subsequently built-up a crystalline lattice structure (Kasumu 2014; Zhu *et al.*, 2008). During the growth stages, the nearby molecules locate suitable parts of the nucleation sites where they can fit into in an orderly manner; and the growth stage continues mostly at the region of more high molecules concentration due to higher magnitude of the attractive force within the region (Turner, 1971). The nuclei with critical cluster size usually contain the high number of molecules, therefore, favours the conditions of wax growth. The initial formation of the monolayer is a relatively faster process than the subsequent addition of layer on the existing layer, due to further growth on the geometrically perfect crystal (Hammami *et al.*, 2003; Hammami and Raines, 1999).

2.4.3 Deposition of Solid Waxes

In the flow assurance, the terms precipitation is considered as precursors towards the deposition of solid, and it is also important to note that having precipitate solid crystals in the flowline doesn't necessarily guarantee deposition (Hammami *et al.*, 2003). Hence, according to Hammami *et al.* precipitation as a process is mainly a function of thermodynamic variables (such as temperature, pressure and composition). At the same time, dependent on the flow hydrodynamics, heat and mass transfer, and solid-solid and surface–solid interactions (Miao, 2012). As a function of temperature, if the temperature of oil in the pipeline equals or drops below WAT due to the ambient system temperature, the process of precipitation will gradually develop. During the process, the precipitated

wax particles from an interlocking network with a “house-of-card” configuration (Paso *et al.*, 2005; Zheng, 2017) as shown in Figure 2-5.

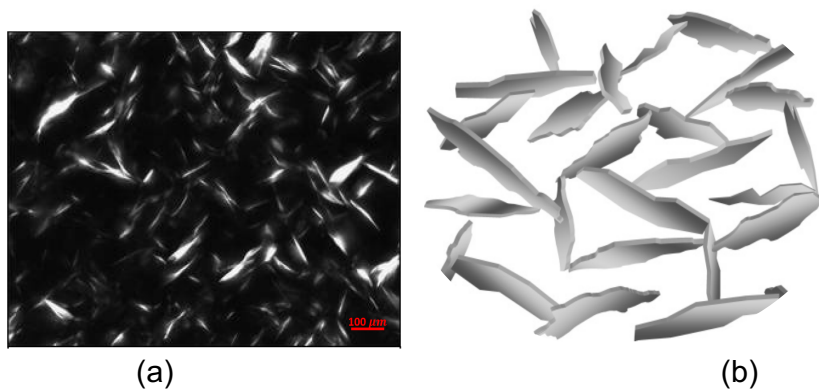


Figure 2-5: (a) Network of interlocking wax crystal by cross-polarised microscopic (b) a schematic of the “house-of-card” configuration of wax particles (Paso *et al.*, 2005; Zheng, 2017)

The solid interlocking network of wax particles can trap considerable quantity of crude oil (in liquid form) and form a stationary gel layer on the pipe surface. Researchers such as Holder and Winkler (1965) and Singh *et al.* (2000) revealed that a waxy gel could contain as low as 2-4 wt% of content solid wax and a high amount of entrapped oil of 98-96 wt%. Consequently, these low amounts of the solid wax crystal are enough to gel the fluid, provided the pipeline system are exposed to conditions that favour the process. Under favourable conditions, the wax gel continues to develop and deposit on the surface of the pipeline during production and transportation leading to reduction of the effective pipe diameter, posing severe threats to the oil recovery and processing facilities. The sooner the precipitation and deposition of waxes are diagnosed the better it will be from the financial, technical, and operational point of view (Tuner, 1971; Lee, 2008). One way to evaluate these data is through oil characterization and preliminary flow loop study in the laboratory. Hence, for these reasons, this research investigated and quantified the wax content and other vital properties of three crude oil samples using standard analytical methods before the flow rig experiments. Figure 2-6 shows the interpretation of waxes deposition process concerning temperature profile at a cross-section with a reduction of effective diameter.

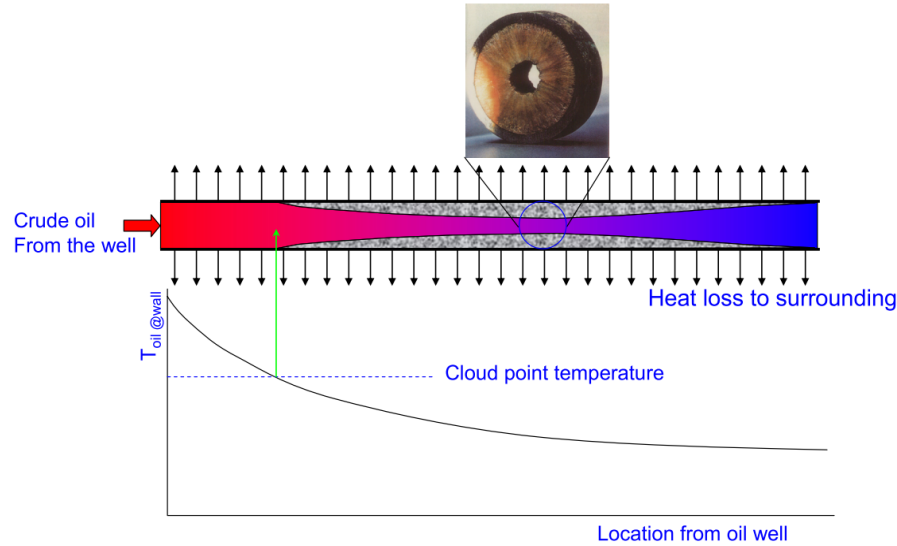


Figure 2-6: Wax deposition occurs when the inner wall temperature is below the wax appearance temperature (Lee, 2008)

Generally, four conditions must be met simultaneously for waxes to deposit within a pipeline system (Svendsen, 1993):

- i. The existence of wax components in the crude oil (with carbon number ≥ 20)
- ii. The temperature of the pipe wall at the deposition section must be less than WAT
- iii. The presence of the radial temperature gradient in the pipeline (i.e. the bulk temperature of the flowing fluid must be high than the pipe wall temperature)
- iv. There must be adequate attraction force within the wax crystals structure with the wall around the deposit location.

Similarly, the deposition of crystal waxes on the processing facilities follows five processes summarised below (Bai and Zhang, 2013; Singh *et al.*, 2000; Venkatesan, 2004):

- i. Formation of an incipient gel layer on the cold surface or in other terms gelation of the waxy oil
- ii. Diffusion (from concentration gradients) of waxes towards the gel layer from the bulk oil. In this stage, there is convection (from bulk fluid motion) of n-paraffin molecules with carbon numbers higher than the critical carbon number (CCN) into the gel layer from the bulk fluid.
- iii. Internal diffusion of these molecules through the trapped oil increases the gel layer thickness
- iv. Precipitation of the diffused n-paraffin molecules inside the deposit;
- v. Counter diffusion of de-waxed oil (light hydrocarbon components with a carbon

number lower than the critical carbon number) out of the gel deposit layer (Fig 2-7).

Step 3, 4, and 5 are responsible for the increase of the amount of solid wax content and the size at the active site and led to hardening of the gel deposit – usually the three steps are lopped together as ageing process of the wax deposit (Singh *et al.*, 2000; Zhu *et al.*, 2008). The ageing process of wax is investigated in this research.

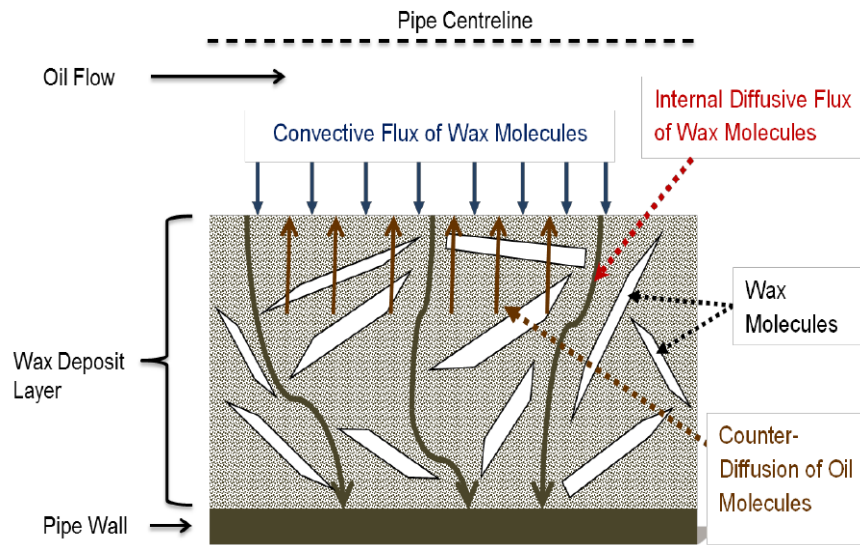


Figure 2-7: Process of deposition of crystal wax (Siljberg, 2012)

2.4.4 Mechanisms of Wax Deposition

Several studies have been done regarding the governing mechanisms of wax deposition. The following vital mechanisms are responsible for transportation of wax crystal from the bulk of fluid to the cold surface of the pipeline (i.e. wax deposition); molecular diffusion, Brownian diffusion, shear dispersion, gravity settling and shear stripping (Aiyejina *et al.*, 2011; Azevedo and Teixeira, 2003; Bern *et al.*, 1980; Brown *et al.*, 1993; Burger *et al.*, 1981; Giacchetta *et al.*, 2019; Majeed *et al.*, 1990; Singh *et al.*, 1999). These mechanisms are caused by different driving forces that transport the dissolved and/or precipitated paraffin to the pipeline surface. As of today, the actual relevance of some of these mechanisms and their impact on deposition is still questionable. It is crucial to develop a better understanding of these mechanisms and incorporate them into models for robust wax deposition predictions (Aiyejina *et al.*, 2011).

Generally, in this area, molecular diffusion is considered as the main mechanism responsible for the deposition of wax (Brown *et al.*, 1993; Burger *et al.*, 1981; Singh *et al.*, 2000). Whereas, shear stripping usually opposes the deposit growth in the pipe (Singh

et al., 2011; Aiyejina *et al.*, 2011). Already some of these mechanisms are being incorporated into the models, one of the good examples is the Matzain model that includes both shear move mechanism, known as shear stripping, alongside molecular diffusion and shear dispersion to simulate wax deposition (Giacchetta *et al.*, 2019; Leporini *et al.*, 2019). Some researchers such as Bern *et al.* (1980), Hao *et al.* (2019), Kelland, (2014), believed that wax deposition mainly occurs by molecular diffusion and shear dispersion, discarding the other mechanisms. The notable study by Burger *et al.*, 1981 that has been used as a reference by several researchers showed that gravity settling is insignificant in the wax deposition, whereas, Fusi (2003) revealed that the mechanism contributes to the deposition, however, to a lesser extent. This show needs to build a good understanding of deposition mechanisms. Therefore, a quick review of each of these mechanisms is made to highlight their role in the deposition process.

2.4.4.1 Molecular Diffusion

Molecular diffusion occurs immediately as the wax crystals precipitated due to drops in crude oil temperature below the WAT. At this point, it is believed that the oil is saturated with precipitated crystals wax in solution (Bern *et al.*, 1980). Imagine oil in a laminar flow, either through a pipe or in a thin laminar sub-layer adjacent to the pipeline surface; as soon as the oil is cooled in the pipeline, the fluid temperature gradient may occur in the liquid adjacent to the pipe surface. Therefore, at any point in that system, as the temperature drops below the WAT, the crystals wax separates from the solution and the liquid phase will be in equilibrium with solid phase, i.e. the liquid will be saturated with dissolved wax crystals (Azevedo and Teixeira, 2003; Zhu *et al.*, 2008). Therefore, the temperature profile close to the pipe surface or in another word the temperature gradient produces a concentration gradient of wax in the oil that is transported toward the pipe wall by molecular diffusion (Burger *et al.*, 1981; Zhu *et al.*, 2008).

Generally, molecular diffusion mechanism has been described in four steps (Huang *et al.*, 2015) as revealed in Figure 2.8):

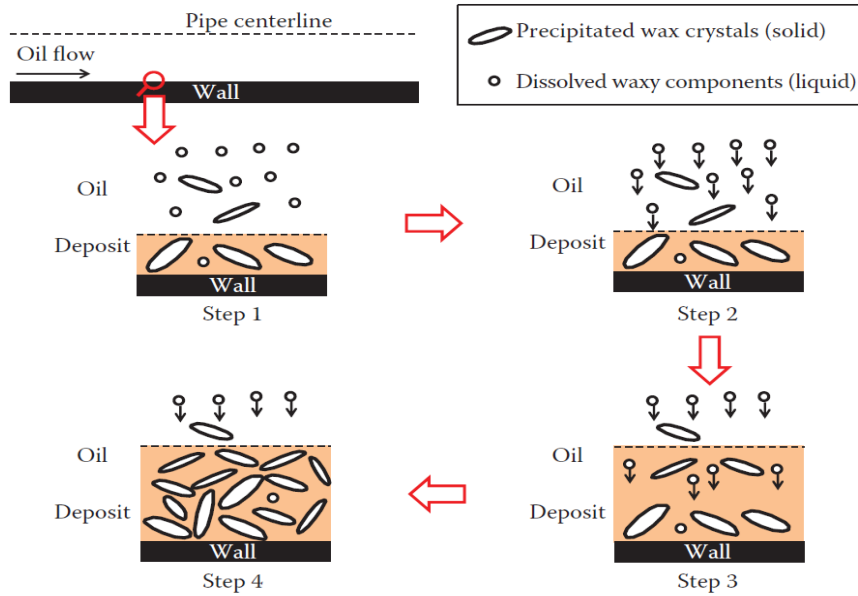


Figure 2-8: Schematic of molecular diffusion as the wax deposition mechanism (Huang *et al.*, 2015)

Step 1: *Precipitation of dissolved wax molecules*

The dissolved wax components in the oil begin to precipitate out and form crystals as the temperature of the flowing fluid drop below WAT. As the temperature decreases flowing fluid drop below WAT, the dissolved waxy components in the oil start to precipitate out and form crystals. As shown in step 1 (Figure 2-8), the crystal wax can be crystallised within the bulk oil and around the pipe wall as long as the temperature favours the precipitation. Some of the precipitated crystals in the bulk fluid continued to flow along with the oil, whereas, others agglomerates and formed an incipient layer of the wax deposit.

Step 2: *Generation of the radial concentration gradient of dissolved waxy components*

During the standard cooling below the WAT, the degree of precipitation of waxy components is usually higher at the pipe wall than within the bulk fluid. This resulted in a higher concentration of waxy components in the bulk oil than on the pipe wall, thereby creating a radial concentration gradient of the waxy components between the bulk oil and the wall. The concentration gradient results in the diffusion of the waxy components from the bulk oil towards the wall, which has a lower concentration of the dissolved waxy components.

Step 3: *Deposition of waxy components on the surface of an existing deposit*

As crystals close to the wall formed an incipient layer, the boundary of the oil region becomes the surface of the deposit. Therefore, as shown in the Figure, the precipitation of the dissolved waxy components on the deposit surface leads to further growth of the wax deposit. Hence, the diffusion of dissolved waxy components towards the deposit continues to take place as the waxy crude oil continues to flow through the pipe (Bai and Zhang, 2013).

Step 4: Internal diffusion and Precipitation of Waxy Components in the Deposit

Diffusion— as a driver, continue brings the molecules of waxy components to the oil–deposit interface, not all of these molecules that precipitated at the interface form a new deposit layer (Huang et al. 2015). Some of the dissolved wax crystals continue to diffuse into the wax deposit (interdiffusion), increasing the wax fractions in the wax deposit (known as deposit ageing). This could be because most of these dissolved waxy components in the deposit are above the solubility limit and could further precipitate to form crystals, resulting in an increase in the solid fraction in the deposit.

Therefore, the rate of transport of wax molecules to the wall is given by the Fick diffusion equation (Burger *et al.*, 1981 and Bern *et al.*, 1980) in terms of the concentration gradient of dissolved wax to distance, $\frac{dC}{dr}$, (per meter) as

$$\frac{dM_w}{dt} = \rho_w D_w A_w \frac{dC}{dr} \quad (2.1)$$

Eq. 2.1 was modified in terms of the concentration gradient of dissolved wax with respect to temperature, $\frac{dC}{dT}$, (per °C) as

$$\frac{dM_w}{dt} = \rho_w D_w A_w \left(\frac{dC}{dT} \right) \left(\frac{dT}{dr} \right) \quad (2.2)$$

Where $\frac{dM_w}{dt}$ is the rate of deposition (kg/s). Whereas ρ_w is the density of deposited wax, D_w and A_w are the diffusion coefficient of dissolved wax molecules (m²/s) and area of wax deposition. dT/dr is the temperature gradient, which can be derived from the solution of the energy equation of the pipe flow. Eq. 2.3 was proposed for the molecular diffusion coefficient (Wilke and Chang, 1955)

$$D_w = 7.4 \times 10^{-9} [T (\varepsilon M)^{1/2}] / \mu V^{0.6} \quad (2.3)$$

Where T and ε are the absolute temperatures and an association parameter. M and μ is

the molecular weight and dynamic viscosity of oil (as solvent), and V is the wax molecular volume (as a solute). Eq. 2.3 is reduced by Burger *et al.*, since ε and M are constant for a specific wax deposit and $V^{0.6}$ is proportional to absolute temperature

$$D_w = C_1/\mu \quad (2.4)$$

Where C_1 has been used as the adjusting constant parameter for fitting experimental deposition data.

Therefore, Eq. 2.4 was incorporated into a different model developed for wax deposition prediction (e.g. Creek *et al.*, 1999; Majeed *et al.*, 1990). Typically, the value of the diffusion coefficient of the waxy components in the oil ranges from 10^{-10} to 10^{-9} m²/s (Hayduk and Minhas, 1982), which is much smaller compared to that for gas systems.

2.4.4.2 Shear Dispersion

The term shear dispersion was introduced in the 1980s by Bern *et al.*, 1980, to describe particle deposition of wax. Wax deposition by shear dispersion occurs due to the dispersion of the precipitated particles toward the wall. For a shear dispersion to contribute to wax deposition, a sufficiently steep concentration gradient towards the wall must be present, see Figure 2-9 (Zhu *et al.*, 2008). Therefore, in shear dispersion mechanism, small particles are suspended in a fluid that is in the laminar motion process, the mechanism is said to contribute to the deposition at lower temperatures and low shear compared to the Brownian diffusion (Burger *et al.*, 1981). When particles are suspended in a fluid under laminar flow, the particles tend to move at the mean speed and in the direction of the surrounding fluid (Zhu *et al.*, 2008). The particle speed streamlines at its centre and rotates with an angular velocity, which is half the fluid shear rate. Each particle in a shear flow passes and interacts with nearby particles in slower or faster moving streamlines. According to Zhu *et al.* (2008), the multi-particle collisions result in net lateral transport and a dispersing of particles. There are two possible forces causes dispersion of particles located in a shear flow as detailed by Zhu *et al.*, (2008); Shear-induced lift forces and Shear-induced self-diffusion (see Figure 2-9 a).

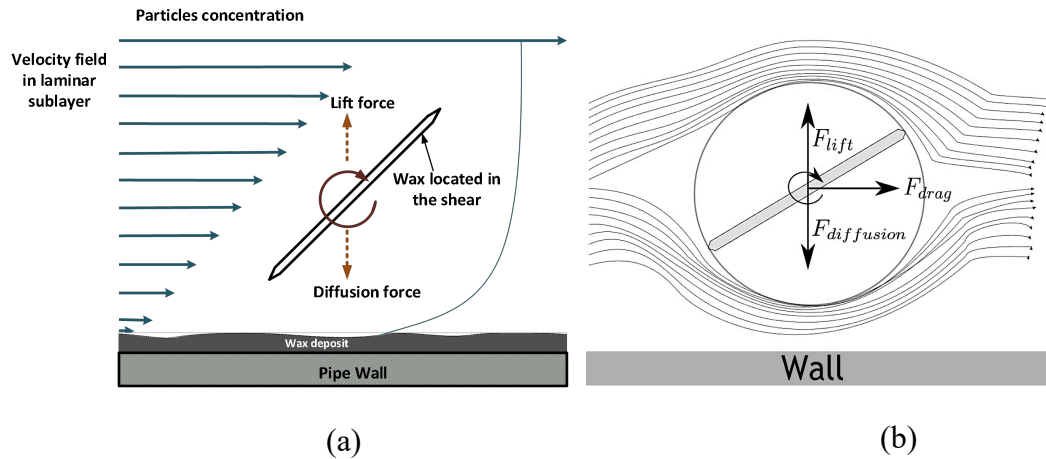


Figure 2-9: (a) Wax particle located in shear flow (Adapted from Siljberg, 2012). (b) Potential streamlines around a rotating particle in shear flow (Zhu *et al.*, 2008)

Shear-induced lift forces favour dispersion of particles away from the pipe wall. When fluid in motion past the surface of a body, an asymmetrical pressure distribution around the particle is formed. The flow field around the particle changes because of inertial effects (such as slip velocity and shear), which are summed up in two perpendicular forces, drag force and lift force (Figure 2-9 b). If the particle is exposed to strong shear, it experiences different fluid velocity on each of its sides. Since the pressure is higher in the lower streamlines, the lift force is in the direction of the increasing velocity (Zhu *et al.*, 2008).

On the other hand, **a shear diffusion force** favours dispersion in the direction of decreasing concentration, which requires rotating particles. Since the temperature profile decreases towards the wall, the concentration gradient increases towards the pipe centre. Therefore, the diffusion force drives wax particles back into the turbulent core. The concentration in the core can be so significant that diffusion contributes to deposition towards the wall. The shear rate near the wall is dependent on the particle concentration itself. However, an increase in particle concentration leads to a viscosity increase, hence a decrease in the shear (Zhu *et al.*, 2008).

Although, a review by Azevedo and Teixeira (2003) suggested that the contribution of shear dispersion as a mechanism for wax deposition is not significant. Similarly, Study by Bern *et al.* (1980) has shown that there is likely no propensity for the nucleation process to occur around the dispersed particles than those formed by the molecular diffusion process, particularly at turbulent flow. However, a study by Fusi (2003) considered both shear dispersion and molecular diffusion as important mechanisms for

wax deposition through the lateral motion of particles absorbed in a shear flow. In general, Burger *et al.* (1981) modelled the shear dispersion coefficient given by the equation below:

$$D_s = \gamma \frac{d_w^2 \phi_w}{10} \quad (2.5)$$

Where D_s , γ , and d_w are the shear dispersion coefficient (m^2/s), oil shear rate at the pipe wall ($1/\text{s}$), the wax particle diameter (m) and ϕ_w is the wax volume fraction precipitate out of the solution at the pipe wall.

2.4.4.3 Brownian Diffusion

Brownian diffusion mechanism is similar to the shear dispersion, which is responsible for the lateral movement of particles to be incorporated at the solid interface (Burger *et al.*, 1981). In shear dispersion, small particles are suspended in a fluid that is in the laminar motion process. This usually occurs at lower temperatures and low shear compared to the Brownian diffusion. Therefore, at a higher temperature and turbulent flow, shear dispersion mechanism is insignificant. However, due to the lateral movement of particles, the intensity and propensity for the nucleation process around the dispersed particles are higher. Accordingly, during the oil and gas production, as the wax crystals precipitated out of solution and suspended in the oil. The suspended particles collide with each other, which leads to an irregular wiggling motion of the crystals, in other words, small random Brownian movements of the crystals (Azevedo and Teixeira, 2003; Zhu *et al.*, 2008). If there is a concentration gradient of solid crystals, Brownian motion will lead to a net transport of these crystals in the direction of decreasing concentration.

In nature and mathematically, Brownian mechanism is analogous to diffusion (Zhu *et al.*, 2008; Azevedo and Teixeira, 2003) characterised by (crystals) Brownian diffusion coefficient and Fick's law of diffusion (equation 2.7) gives by

$$\frac{dm_B}{dt} = \rho_d D_B A \frac{dC^*}{dr} \quad (2.6)$$

$$D_B = \frac{RT_a}{6\pi\mu aN} \quad (2.7)$$

Where m_B is the mass of deposited wax (kg), ρ_d is the density of the solid wax deposit, D_B is the Brownian diffusion coefficient of solid wax crystals in the oil (m^2/s), A is the

area of deposition, $\frac{dC^*}{dr}$ the concentration gradient of dissolved wax with respect to distance (per meter).

Brownian diffusion has not been considered as a relevant deposition mechanism by several authors (such as; Hunt, 1962; Euchner, 1986; Brown et al., 1993; Ribeiro et al., 1997; Hsu et al., 1998; Singh et al., 1999; Weingarten and Weispfening, 2001). Nevertheless, the review Azevedo and Teixeira (2003) shows that there is no sufficient experimental evidence to support the above conclusion. Similarly, Burger *et al.* (1981), depicted the possibility of a Brownian deposition flux toward the wall, and flux away from the wall. Therefore, Brownian diffusion remains as a possible contributing mechanism for wax deposition.

2.4.4.4 Gravity Settling

The precipitated wax particles are usually denser than the surrounding fluid, thus, if there is no interaction, the particles settle in a gravity field and accumulate at the bottom of the pipes and tanks (Kok and Saracoglu, 2000). On the contrary, in an active oil and gas pipelines system, gravity settling does not seem to be a significant mechanism for wax deposition. It is believed that the shear dispersion mechanism or active fluid forces create a dispersion of precipitated wax particles, thereby eliminating gravity settling (Burger et al., 1981; Azevedo and Teixeira, 2003). However, in low flow rates, at typical shut-in conditions or in storage tanks, the gravity effect contributes significantly to wax deposition, particularly for low viscous fluids.

The settling velocity, U (m/s) reported by (Ajayi, 2013) is obtained by modified Stokes' law of settling crystals in a pseudoplastic fluid as follows:

$$U = \left[\frac{g\Delta\rho a^{(1+n)}}{18K_p} \right]^{1/n} \quad (2.8)$$

Where $\Delta\rho$ is the density difference (kg/m^3) between the settling wax and the oil, a is the particle diameter (m), n is the power-law index, g the acceleration due to gravity and K_p is the power-law consistency index.

2.4.4.5 Shear stripping

Shear stripping also is known as shear sloughing or shear removal mechanism. This removes wax from the walls due to shear stress exerted by a flowing stream of oil on the wax solid. The inflow velocity of fluid can sloughs pieces of wax from the deposition layer, thereby acting as a wax removal mechanism (Ajayi, 2013; Pan *et al.*, 2009). This mechanism is considered important in the wax deposition; for instance, Matzain model incorporates both shear stripping alongside molecular diffusion and shear dispersion as potential wax deposition models. The shear-stripping model serves as a wax reducing mechanism in the Matzain implemented model. Therefore, in turbulent flow, shear stress exerted by the flowing fluid on the deposit is sufficiently high to mechanically remove some of the deposits wax from the walls (Burger, 1981; Ajayi, 2013).

Therefore, the negative wax transfer due to shear forces is modelled as a function of the shear stress τ ($\frac{N}{m^2}$), the thickness of the wax layer $\delta(m)$, and the wax layer yield stress (Ajayi, 2013).

$$J^{sr} = c \frac{\delta\tau}{\omega^{2.3}} \quad (2.9)$$

The wax yield stress is reported as proportional to $\omega^{2.3}$ such that ω is the mass fraction of wax in the gel layer (Pan *et al.*, 2009). On the other hand, the wax-shearing rate is derived based on the shear rate equation as shown below (Edmonds *et al.*, 2008)

Where c represent the shear constant, ω is the mass fraction of wax in the gel layer, $\delta(m)$ is the thickness of the wax layer. The τ (N/m²) is obtained by the equation (2.11)

$$\tau = \frac{1}{2} f \rho_o u_o^2 \quad (2.10)$$

Where f is the fanning friction factor, ρ_o is the density of the flowing oil (kg/m³), and u_o is the oil velocity (m/s).

2.4.5 Factors Leading to Wax Precipitation and Deposition

Wax precipitation and subsequent deposition occurred when the soluble wax crystals in crude oil attained their solubility limit due to changes in equilibrium conditions in the crude oil. Some of the factors discussed in this section influence wax precipitation by shifting the solubility limit upwards and/or downwards, while, others provide favourable

conditions for wax deposition to occur (Zhu *et al.*, 2008). These factors include temperature, crude oil composition plus available solution gas, flow or shear rate, deposition time and pipe or deposition surface roughness and pressure of the oil, which affects the amount of gas in solution (Hammami and Raines, 1999; Zhu *et al.*, 2008). Hence, most of these factors formed the basis of this thesis and will be investigated experimentally, to further improved wax deposition prediction and mitigation strategy.

2.4.5.1 Effect of Temperature

One of the objectives of this research is to elucidate the onset of wax precipitation and depositional behaviour at varied cooling temperature. Temperature is the predominant and most critical factor that affect the solubility of wax crystals (Al-yaari, 2011; Zhu *et al.*, 2008). The paraffin solubility increases with an increasing temperature difference between the bulk fluid and the cold surface and decreases with decreasing temperature. Therefore, the precipitation and deposition of wax only occur when the operating temperature is lower or equal to the wax appearance temperature (WAT) of the crude oil. This, therefore, leads to a decrease in the amount of dissolved wax molecules near the pipe surface prompting a gradual radial change in concentration (Zhu *et al.* 2008; Singh *et al.*, 2000). Therefore, prevention of wax deposition could be achieved if the crude oil flows above WAT, or through a highly conductive pipeline maintained above a specific temperature given by Ed. 2.8 (Mehrotra and Bidmus, 2004).

$$T_h = \frac{h_c r_o}{h_h r_i} (WAT - T_c) \quad (2.11)$$

Where h_c and h_h are the outside coolant and inside crude oil heat transfer coefficients respectively, r_o and r_i are outside and inside pipe radii respectively, and T_h and T_c are the crude oil and coolant temperatures respectively.

In a nutshell, as wax started to deposit on the pipe wall, the rate of deposition is high (due to the availability of a large number of crystallisation sites). As the thickness of the wax deposit increases, it creates thermal insulation that limits the rate of heat transfer and reduces further improvements in the deposit mass (Al-yaari, 2011; Singh *et al.*, 2000; Zhu *et al.*, 2008).

2.4.5.2 Effect of Composition

Singhal *et al.* (1991) revealed that apart from temperature, crude oil composition is another key factor that significantly affects wax deposition. Therefore, another objective

of this dissertation is to investigate the onset of wax precipitation and depositional behaviour of different crude oil samples. The main composition of crude oil involves four chemical groups, specifically saturates, aromatics, resins, and asphaltenes. According to literature, crude oil with a mixture of different components such as heavy molecules such as long linear alkanes and Iso-paraffins tend to change phases at low temperature. Also, there is a transition towards more polar compounds due to the appearance of aromatic compounds and the presence of heteroatoms (e.g. oxygen, sulphur and nitrogen) in the fractions known as resins and asphaltenes (Akpabio, 2013). Valinejad and Nazar (2013) revealed that the amount of deposited wax is impacted by the concentration of paraffin, light ends, and nucleating or inhibiting materials in the crude oil.

Therefore, the step taken in this thesis to understanding oil composition based on the distribution by weight per cent of saturates, aromatics, resins, and asphaltene components is crucial. SARA provides a reasonable idea of the wax deposit potential of the crude and, hence, the oil stability (Zhu *et al.*, 2014; Towler *et al.*, 2011). Carbognani *et al.* (1999), reported the following trend highlighting the stable and unstable crude oils based on SARA analysis:

Unstable crude: Saturates > Aromatics > Resins > Asphaltenes

Stable crude: Aromatics > Saturates > Resins > Asphaltenes

This distribution is expected since the aromatics keep the heavy paraffin wax in solution, In contrast, a crude oil system that displays a large amount of saturates (paraffin) is likely to be unstable (Carbognani *et al.*, 1999) and thus precipitate and deposit wax. Zhu *et al.* (2008) revealed that the presence and deposition of asphaltenes could serve as nucleation sites for additional wax deposition. Besides, this research investigates the effect of compositional change based on the influence of chemical inhibitors. The presence of inhibitors changes the composition and the general behaviour of the sample.

2.4.5.3 Effect of Flow Rate and Shear Rate

The deposition of wax is directly proportional to the flow rate; a lower rate leads to high deposition in the system. This is because of the longer residence time of the oil in the tubing and/or pipeline, which permits more heat loss and give rise to lower oil temperature, thus, more particles available to deposit in the surface (Towler *et al.*, 2011). As the flow rate of the crude oil or waxy mixture is increased, wax deposition decreases

regardless of whether the fluid flow is in laminar or turbulent (Creek et al., 1999; Bidmus and Mehrotra, 2004) – as a result of an increased in shear dispersion within the turbulent flow region.

Similarly, the rate of shear at the wall causes a sloughing or shearing off the deposits that increases with increasing flow rate. This effect started to occur immediately when the rate of shear overcome the cohesive and adhesive forces of the paraffin wax molecules and the deposition surface (Bott and Gudmundsson, 1977). Hence, this studied the influence of a different range of flow rate covering both laminar and turbulent flow regime through the experimental flow rig and using OLGA software.

2.4.5.4 Effect of Pressure

Pressure drop is a vital parameter in the oil and gas field, which are experienced through the flow stream up to the surface facilities (Zhu *et al.*, 2008; Theyab, 2017). As the pressure dropped, lighter hydrocarbons outflow from the reservoir fluid, this leads to an increase in the solute-solvent (lighter component) ratio, which consequently decreases the solubility of the wax crystals. Compared to temperature, the pressure is not considered as an essential factor for wax deposition, especially for dead or stock tank oil (Valinejad and Solaimany 2013). Notwithstanding, Valinejad and Solaimany stressed that the pressure effect on wax deposition should not be neglected across the facilities. Accordingly, pressure serves significantly as an indicator for wax deposition, because as the wax formed on the pipe wall, the effective cross-section area of the pipe reduces, which causes a pressure drop in the system.

Therefore, in this research, two pressure sensors were used for monitoring the inlet and outlet pressure and the overall pressure drop. The existing pressure drop correlation is used to quantify the deposit thickness in a straight pipe, whereas a new model is developed for the curved pipe. The test section orientation of the flow loop is switched from horizontal to an inclined flow to study the effect of the gravitational field, which in turn influenced by the pressure drop.

2.4.5.5 Effect of Pipe Surface Properties

The pipeline material generally affected the process of wax deposition in a different way. According to a study by Kasumu (2014), the adhesion of the deposit onto a surface is a function of either wettability (free surface energy) and/or surface roughness. Therefore,

surface roughness acts as wax nucleating sites for the solid deposit. Quintella *et al.* (2006) discovered less deposition in pipelines coated with polypropylene than with those coated with high-density polyethylene and a vinyl acetate copolymer. These results show that the higher the contact angle, the lower the wettability between the flowing crude oil and the polypropylene lined pipes. More wax was deposited on the steel tubes than on the glass tubes, this attributed to the higher wettability of the steel tube surfaces. Hence, the rougher the surface, the higher the frictional force that will keep the deposit from sloughing away due to shear or flow rates (Kasumu 2014).

In this research, the influence of the surface property of pipe material is not one of the critical areas of investigation. However, it worth noting that the copper pipe was chosen in this research because of its thermal properties and surface roughness that facilitates wax deposition. The material is suitable for laboratory studies (Oyekunle, 2013; Theyab, 2017).

2.4.5.6 Effect of Deposition Time and Aging

In wax deposition problem, experimental time is considered an important parameter that affects the waxing process as publicised by different researches such as; Adeyanju and Oyekunle (2013), Huang *et al.* (2011), Hoffman and Amundsen (2010), Venkatesan, (2004). These studies have shown that the amount of wax deposited on the surface of pipeline increases with time until it reaches a steady-state condition.

In a laboratory-scale experimental study reported by different literature (such as Bidmus and Mehrotra, 2004; Parthasarathi and Mehrotra, 2005; Kasumu and Mehrotra, 2013; Kasumu, 2014) showed that a thermal pseudo steady state is achieved in less than 30 minutes during the wax-solvent mixtures deposition, under laminar and turbulent conditions. A small increase in the mass of the wax deposit after 4 hours of laboratory studies is being reported by Kasumu (2014). On the other hand, during the ageing process, the wax deposit becomes richer in heavier n-paraffin content. In contrast, the lighter n-paraffin content or the amount of entrapped oil reduces with time (Mehrotra and Bidmus, 2004). Therefore, different range experimental period was used to understand the influence of ageing in both straight and curved pipes.

2.4.6 Paraffin Wax Management

Paraffin wax management practices could either *preventive* or *corrective approaches* (Keeper, 2013). The prevention techniques are designed to avoid wax crystals deposits and growth throughout the system, while corrective (remediation) practice involves periodic removal of deposits waxes in the system. In a nutshell, the *prevention* or *correction* of wax deposit in the oil fields is usually done through (1) mechanical, (2) thermal, and (3) chemical methods (Nguyen, 2004; Lee, 2008; Rittirong, 2014; Theyab and Diaz, 2016). Usually, two or more techniques are combined in order to provide an efficient removal or prevention of the wax deposit (Towler *et al.*, 2011; Wei, 2015). Recently, other alternative methods with limited success were reported, such as bacterial and electromagnetic treatments (Towler and Rebbapragada, 2004), piezoelectric energy (Sulaiman *et al.*, 2011) and vacuum-insulated tubing (Singh *et al.*, 2007). In this research, a chemical method using wax inhibitors was used for prevention of wax deposition. A brief review of the mechanical and thermal method is given below.

2.4.6.1 Mechanical Method

Many industries have commonly employed the method for prevention of wax formation or removal of deposit solid. As removal techniques, oil industries used scrapers and cutters on the production tubing, whereas a “pig” is usually employed at the surface pipeline facilities as remediation method (Al-yaari, 2011; Nguyen, 2004). However, this method required a very good prediction on wax deposit (size, shape, and weight) to achieve better and efficient management. Pigging operation usually interrupted production, which significantly affects the production revenue. An effective pigging is made only for removing a thin layer of wax deposit; a highly thick wax deposit requires frequent pigging of the pipeline (Majeed and Bringedal, 1990).

Currently, frequent pigging operations are not recommended due to the high cost and the risk of the operation (Majeed *et al.*, 1990; Wei, 2015). If the operation is not properly managed, the pig can be stuck inside the pipeline, which caused a delay in production, in some cases the whole pipeline system around the affected area must be removed in order to remove the pig and replace the blocked section of the pipeline. Therefore, the understanding of deposition rate is fundamental as a mean to establish an appropriate pigging recurrence (Zheng, 2017).

2.4.6.2 Thermal Method

Precipitation of wax crystals from the solution mainly affected by the temperature, so thermal methods are assumed to be effective in preventing and removing wax deposition. This method is achieved through heat retention, active heating or heat tracing (such as resistive electrical element, tubing containing steam, hot water, or hot ethylene glycol) and use of suitable exothermic chemical reactions (Lashkarbolooki *et al.*, 2011; Kelland, 2009; Thota and Onyeonuna, 2016). For instance, hot water circulation – pipe-in-pipe system (HWC-PiP) is one of the active heating technologies reported to be successfully commissioned and operated in the offshore field (Ansart *et al.*, 2014) see

Figure 2-10. Unfortunately, this method is only applicable during steady-state production and required high power for preservation. Also, it involves the treatment of the injected water to avoid corrosion issues and only used at a short distance up to 500m water depth.

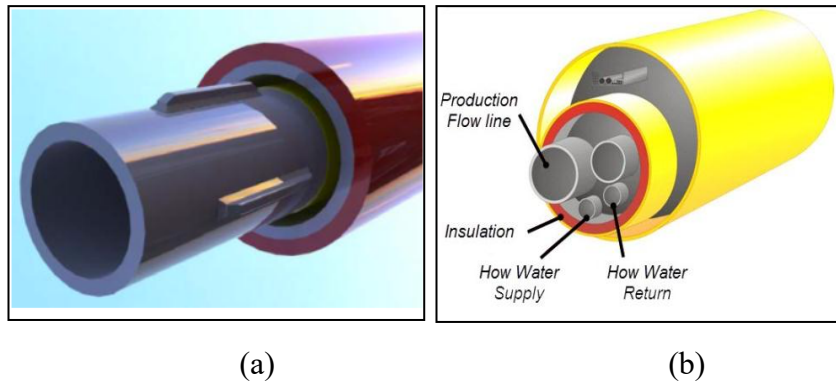


Figure 2-10: Hot Water Circulation (a) Wet insulated Hot Water Pipe (b) Hot Water Bundle (Leandro *et al.*, 2013; Ansart *et al.*, 2014)

On the other hand, heat trace cables are also used on onshore pipelines. The trace heating cables are directly laid on the flowline (shown in Figure 2-11), together with optical fibre cables to permanently monitor the internal fluid and cable temperature all along the flowline using distributed temperature sensing (Ansart *et al.*, 2014). The drawback of this method is that the tracing cables or splices cannot be repaired once installed subsea and the technique is only applicable for flow line with diameter limited to 12” and short distance. Consequently, the use of the mechanical and thermal remediation methods has become excessively uneconomical at extremely deep production, offshore drilling and some stages at ocean floor completions (Al-Yaari, 2011; Adeyanju and Oyekunle, 2014).

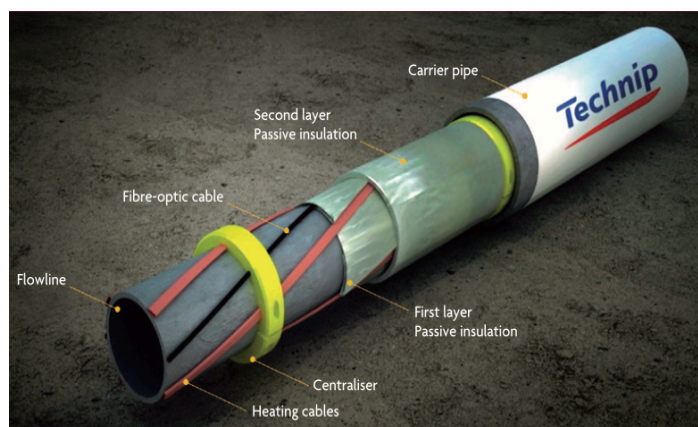


Figure 2-11: Electrically Trace Heated Pipe-in-Pipe ETH-PiP Structure (Ansart et al., 2014)

As a result, the use of chemical additives as wax deposition inhibitors is becoming more extensive (Jing *et al.*, 2017; Wei, 2015). Although in some cases, wax deposition may not be completely inhibited by inhibitors, it can effectively decrease the rate of wax deposits and delay wax deposit expansion (Pedersen and Rønningsen, 2003) and suitable for long distances flowlines without interrupting production. However, in most cases, industrial design is usually made to accommodate two or more method for high efficiency.

2.4.6.3 Chemical Method

Most of the chemical treatments reported in the literature are designed to prevent, delay, or minimise wax deposition. The technique is also applied for removal of the solid deposit in the system (Aiyejina et al., 2011; Kelland, 2009). Chemical inhibition is a practical approach to cope with wax deposition in crude oil pipelines; the use of chemical wax inhibitors has stood out. It has been the subject of several studies. Usually, the inhibitor disrupted the ordered aggregation of the growing wax crystals, thereby reduces the WAT and/or the pour point temperature of the crude oil (Kelland, 2009). The applications of chemical methods solely depend on thickness profile and fraction of the wax deposit as a function of axial location and time. Some of the advantages of chemical inhibitors includes improved rheology for example viscosity reduction (i.e. less energy requirement for transportation of crude oil), reduces the pipeline restart pressure due to yield stress reduction and suitable method without interruption of production for a long-distance pipeline/flow lines (Majeed and Bringedal, 1990; Aiyejina *et al.*, 2011). The method is powerful when combining with heating or pigging method (Kelland, 2009).

However, the efficiency of some the chemicals is limited due to cost, and another drawback is there is no universal type of chemical inhibitor developed for all kind of crude oil, due to the varying properties of the crude oils (Adeyanju and Oyekunle, 2014; Halim *et al.*, 2011; Kang *et al.*, 2014). As a result, the treatment is normally designed to fit a specific oil and environment conditions.

This research focused on using a polymer-based chemical wax inhibitor to prevent or reduce wax deposition in the pipeline. Wax inhibitors are polymeric chemicals in which the polymer molecular structure is similar to that of precipitating wax, thereby allowing wax molecules to co-precipitate by occupying the wax molecules site and forming larger crystals resulting in the disruption of wax crystals growth (Dobbs, 1999; Jennings and Newberry, 2008; Wei, 2015; Yang *et al.*, 2015). The four most frequently used chemicals are outlined below:

- **Wax Crystal Modifiers**

The crystal wax modifiers, otherwise known as pour point depressants are chemicals with similar molecular structure to the wax molecules (Pedersen and Rønningsen, 2003). Typically, these chemicals co-precipitate or co-crystallise with wax crystals by replacing wax molecules on the crystal lattices. Thus, preventing the wax molecules from networking to form a lattice structure that enriches the deposition of the precipitated wax crystals (Kang *et al.*, 2014; Pedersen and Rønningsen, 2003; Woo *et al.*, 1984) as clearly illustrated in Figure 2-12. Some of the wax crystal modifiers currently employed include polyethylene, copolymer esters, ethylene/vinyl acetate copolymers, olefin/ester copolymers, ester/vinyl acetate copolymers, polyacrylates, polymethacrylates and alkyl phenol resins (Dobbs, 1999; Kang *et al.*, 2014). However, the precise way in which these chemicals operate is still under study (Pedersen and Rønningsen, 2003).

Interestingly, as of today, the polymeric based polymer has been proven to be efficient (Hoffmann and Amundsen, 2013; Perez *et al.*, 2015). Hoffmann and Amundsen (2013) showed that polymer-based inhibitors could successfully reduce about 60%-90% of the wax deposit. Nonetheless, their performance differs based on molecular weight, which influenced the agglomeration.

- **Solvents**

Solvents are normally used for the treatment of solid wax deposit and remediation formation damage. The added solvent in crude oil increases the solubility of wax crystals in oil and dissolves already deposited wax. The most commonly used solvents include xylene, toluene, benzene, carbon tetrachloride, trichloroethylene, perchloroethylene, carbon disulfide, white or unleaded gasoline and pine-derived terpenes (Kang *et al.*, 2014).

- **Dispersants**

The dispersants such as polyesters and amine ethoxylates are usually employed as surface-active agents (Pedersen and Rønningsen, 2003). Usually, dispersants keep the pipe surface water wet, minimizing the tendency of the wax to adhere. These chemicals also help to disperse wax crystals into produce oil, thereby keeping the wax nuclei from agglomerating (Lee, 2008; Nguyen and Fogler, 2005). Nevertheless, the ability to maintain such a surface for an extended period is one of the operational problems with dispersants.

- **Surfactants**

Surfactants are used for the cleaning of pipelines and another part of the system where wax may have deposited. Usually, surfactants promote the formation of stable oil and water – emulsion, which is beneficial to pipeline transportation (Nguyen *et al.*, 2001; Singh and Fogler, 1998). Also, similar to dispersants; they could be adsorbed on the pipe surfaces and decrease the adhesion of waxes to the surfaces, and possibly change the wettability of the pipe surface. In other words, surfactants create an environment in which wax crystals are easily sheared off or adsorbed onto the wax crystals surface, which prevents sticking (Nguyen *et al.*, 2001; Singh and Fogler, 1998).

2.4.6.4 Interaction Mechanisms Between Chemical Inhibitors and Wax Crystals

One of the benefits of adding pour point depressant is to reduce the force of interaction among the wax molecules (Goia and Boccasari, 2016; Li *et al.*, 2018). As of today, the exact interaction mechanism of the wax molecules and the inhibitors such as polymeric pour point depressants are still under scrutiny (Chi *et al.*, 2016). Nevertheless, studies by Chi *et al.* (2016), Yang *et al.* (2015) and Li *et al.* (2018) have revealed some of the

mechanisms that include nucleation, adsorption, co-crystallization, and solubilization interactions.

During the nucleation process, as wax molecules precipitate below the WAT, a crystalline nucleus of a subcritical size is formed, leading to the formation of a larger compound wax crystal in Figure 2-12. Simultaneously, the high-molecular-weight polymeric inhibitor precipitates and acts as a crystalline nucleus for the wax crystals (Li *et al.*, 2018). Eventually, this leads to the formation of more subcritical nuclei of micelle-like aggregates. Subsequently, this inhibits the crystal growth and decreases the supersaturation. It is resulting in the creation of smaller wax crystals that are stable in the oil phase, implying improved flowability (Hao *et al.*, 2019; Yang *et al.*, 2015). Once the oil temperature drops below WAT, the precipitated wax molecules are adsorbed on the polymeric inhibitor nuclei with similar chemical structure, through co-crystallization. This modifies the morphology of the wax crystal (from long stick-like or large plate-like to small spherical-like), which delays the formation of new crystals (Hao *et al.*, 2019; Li *et al.*, 2018). According to Li *et al.* (2018), the changes of wax crystals reduce the specific surface area and decrease the surface energy, which makes it challenging to form three-dimensional network structure (Wang *et al.* 2014). Following the adsorption and co-crystallization processes, as the concentration of the inhibitor increases in crude oil, there will be the progressive formation of small spherulitic-like crystals in the crude oil system (Hao *et al.*, 2019; Li *et al.*, 2018). The crude oil (liquid) and precipitated wax crystals (the solid) act as disperse and continuous phase along with the system.

However, in the absence of pour point depressants in the system, the solid-liquid interface between the wax crystal and liquid phase as well as the energy of the system are large, resulting in an unstable system (Li *et al.*, 2018; Yang *et al.*, 2015). To minimise the energy of the system the solid-liquid interface has to be reduced, by doing that it would cause a union of the wax crystals, as a consequence, larger crystals will form and will create three-dimensional network structure. Thus, the addition of pour point depressants improves the dispersion of small wax crystals (Li *et al.*, 2018).

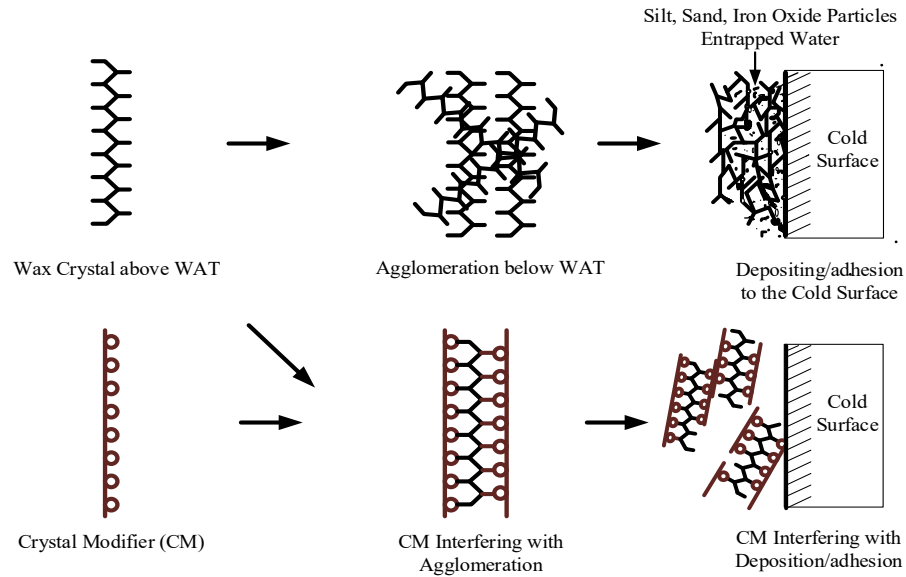


Figure 2-12: Interaction mechanism between wax crystals modifier with wax crystals (Adapted from Allen and Roberts, 1978, cited in Sousa *et al.*, 2019 and Al-yaari, 2011).

2.4.7 Wax Deposition Simulation

Several predictive wax deposition software has been developed, the best known and one of the few industry-standard tools for transient simulation of multiphase petroleum production is OLGA (Bendlken *et al.*, 1991; Giacchetta *et al.*, 2019). OLGA has an extensive package of standard and specialised modules built through extensive research and field measurements that can simulate complex multi-phase transport challenges (Bendlken *et al.*, 1991). Several numerical simulation studies have been carried out on wax deposition, which mostly predicts the depositional behaviour of wax and study the influence of different factors on the deposition. This data is useful, particularly for the deposited wax management process (Ajayi, 2013; Labes-Carrier *et al.*, 2002; Leporini *et al.*, 2019; Noville and Naveira, 2012; Pan *et al.*, 2009).

In this research, the experimental results and prediction from OLGA simulation are compared. However, before the simulation studies, Multiflash— as fluid modelling package was used to characterise the fluid, using Coutinho’s model that considered solid and liquid phases to be non-ideal solutions. Coutinho’s model gives good predictions of the fluid properties and behaviour (Coutinho *et al.*, 2001) compare to other models such as Won’s model, Erickson’s model, Pedersen’s model and its modified versions.

On the other hand, it is worth noting that OLGA incorporated modules that allow reproducing the wax deposition phenomenon, based on experiment or other field studies;

these include the Rygg, Rydahl and Rønningsen (RRR), Matzain and Heat Analogy (Matzain, 1999). Matzain model is used in this research as briefly described in the subsequent sections.

2.4.7.1 RRR model

The RRR (Rygg, Rydahl and Rønningsen) model is a multiphase flow wax deposition model that predicts deposition of wax in wells and pipelines. It is a semi-stationary model because wax deposition build-up is a slower process than pipeline flow disruptions and does not apply to laminar flow (Giacchetta *et al.*, 2019). RRR model considered molecular diffusion and shear dispersion as the only mechanisms responsible for wax deposition. “The RRR model does not take into account the removal of wax from the wall, in high velocity flows, due to the shear stress exerted by the oil” (Giacchetta *et al.*, 2019; Leporini *et al.*, 2019). The volume rate of wax deposition by molecular diffusion for a wax forming component (i) is calculated by (Giacchetta *et al.*, 2019):

$$Vol_{wax}^{diff} = \sum_{i=1}^{N_{wax}} \frac{D_{wo,i}(C_{wb,i} - C_{ws,i})S_{wet}M_{wax,i}}{\delta_{lam}\rho_{wax,i}} 2\pi rL \quad (2.12)$$

Where: N_{wax} is the number of wax components. $D_{wo,i}$ is the diffusion coefficient, S_{wet} is the wetted fraction of the circumference. $M_{wax,i}$ is the molar weight of wax component i (kg/mol).

2.4.7.2 Matzain Model

The Matzain is a semi-empirical model that integrates molecular diffusion and shear dispersion, and a wax reduction mechanism (i.e. shear stripping) to simulate wax deposit (Aiyejina *et al.*, 2011). “In this model, shear dispersion is considered of minor importance in respect to RRR model” (Giacchetta *et al.*, 2019; Leporini *et al.*, 2019). The rate of wax build-up is calculated by an empirical modification of Fick's law reported in Section 7.2.1.

2.4.7.3 Heat Analogy

According to Giacchetta *et al.* (2019), employ the heat and mass balances coupled with energy balances for its wax precipitation and deposition predictions. Heat Analogy model, like the RRR, includes the shear deposition effect, and, like the Matzain, it takes

into account the sheer stripping phenomenon (Ajayi, 2013; Giacchetta *et al.*, 2019). The heat transfer rate is given by:

$$\dot{Q} = h (T_{wb} - T_{ws}) \quad (2.13)$$

Where h is the heat transfer coefficient. Similarly, the mass transfer rate of the component i can be expressed as;

$$\dot{M}_i = m_i (C_{wb,i} - C_{ws,i}) \quad (2.14)$$

Where m_i is the mass transfer coefficient, the heat transfer coefficient is obtained from the Nusselt number (NNu), that is estimated from the Reynolds (NRe) and Prandtl numbers (NPr).

2.5 Fluid Flow Through Pipe Curvature

Practically, all piping systems contain bends (Dutta *et al.*, 2016; Fairbank and So, 1987). Pipe bends are an essential part of any network pipeline system as they provide routing flexibility (Dutta *et al.*, 2016). Therefore, investigations of the flow-through bends are of great importance, particularly for understanding and improving the prediction of wax deposition, the deposition mechanisms and minimising the losses caused by under or over-prediction of the problem. Brief reviews of the flow behaviour in both straight and curved pipes are presented as follows:

2.5.1 Fluid Flow Through a Straight Pipe – Single-Phase

Extensive studies have been carried on wax deposition in the straight pipeline (Huang *et al.*, 2015; Lim *et al.*, 2018; Mansourpoor *et al.*, 2019; Matzain, 1999; Panacharoensawad and Sarica, 2013; Venkatesan, 2004; Zheng, 2017). There are difficulties in a direct comparison between the results of one researcher to another, due to the differences in their experimental programmes such as the type of oil, pipe diameter, operating temperature, and flow rate. Figure 2-13 shows a simple schematic of a straight pipe showing fluid velocity profiles in laminar and turbulent flow regimes. In a straight pipe, the fluid flow experiences no secondary circulation or flow separation at any of the pipe boundary (Dutta *et al.*, 2016; Murty and Thandaveswara, 2014). Therefore, as the flow developed, the velocity gradient at the wall reduces and gradually more of the core fluid

becomes sheared. At the inlet of the pipe, the crude oil experiences higher pressure drop similar to the wall shear stress, which is higher and decreases steadily to the fully developed region. As waxy oil flow in a fully developed laminar flow, each particle moves in an orderly manner and at a constant axial velocity along the path line. On the other hand, for a fully developed turbulent flow, the fluid particles move in random and rapid fluctuations of swirling eddies throughout (Zhao, 2012).

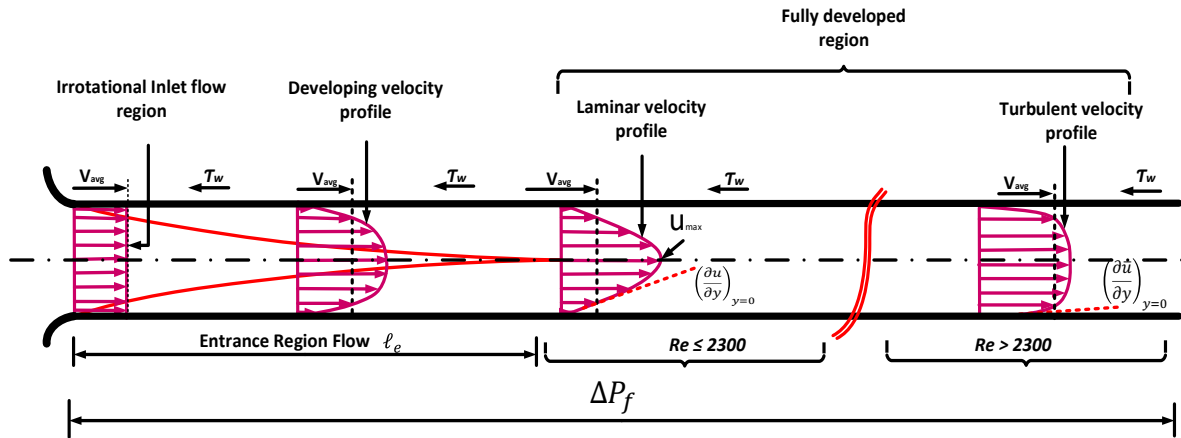


Figure 2-13: Schematic of a straight pipe with fully developed velocity profiles in laminar and turbulent flow regimes (adapted from UIO, 2004).

Numerous studies have been conducted in laminar and turbulent flow regime with different models developed covering these conditions. For instance, a study by Matzainn (1996) and Matzain *et al.* (2002) revealed that deposition of wax increase with time in laminar flow and produces a thicker and soft deposit than turbulent flow. This is because in turbulent flow the swirling eddies provide the wax crystals particle with an additional mechanism for mass, momentum and energy transfer that prevent the possible precipitation or deposition, unlike in the laminar flow condition, where the energy transfer is that rapid. In laminar flow, molecular diffusion is the main factor affecting the deposition (Bern *et al.*, 1980; Burger *et al.*, 1981) and there are higher mass, momentum and energy transfer across the region (UIO, 2004).

Hence, similar to mass and heat transfer; the pressure drop in a straight pipe are essential in the wax deposition. Pressure drop in a straight pipe is as a result of frictional loss (Chen *et al.*, 1997). Therefore, pressure drop from the Darcy-Weisbach equation (Eq. 2.15) was modified (see Section 3.8.1, Eq. 3.9) for quantification of deposit wax thickness. This is because, as the wax deposit builds-up on the pipe wall, the effective

diameter of the pipe reduces, leading to an increase in pressure drop. Similarly, heat analogy (Eq. 2.16) was used for the same purposed, see Section 3.8.3 for details.

$$\Delta P_f = 4f \frac{L}{d} \frac{\rho}{2} \left(\frac{4Q}{\pi d^2} \right)^2 \quad (2.15)$$

$$\frac{1}{U_{gly}} = \frac{1}{h_{oil}} \frac{r_o}{r_i - \delta_w} + \frac{r_o}{k_w} \ln \frac{r_i}{r_i - \delta_w} + \frac{r_o}{k_p} \ln \frac{r_o}{r_i} + \frac{1}{h_{gly}} \quad (2.16)$$

2.5.2 Fluid Flow Through a Curved Pipe – Single-Phase

The presence of bends in any piping system affects both the upstream and downstream flow since the pressure field in the bend gives rise to the secondary motion. Secondary flows can create points of maximum and minimum wall temperature and shear stress (Fairbank and So, 1987). Consequently, these are some of the significant parameters that influence wax precipitation and deposition behaviour. In a nutshell, fluid flow in bend pipes is characterised by the presence of a radial pressure gradient generated by the centrifugal forces acting on the fluid (Sreenivas, 2011). The flow is primarily associated with flow instability, separation, and strong secondary current, which mainly depend on Reynolds number, bend angle (θ) and the radius of curvature of the bend (R_b) (Dean, 1927; Sreenivas, 2011; Murty and Thandaveswara, 2014; Dutta *et al.*, 2016; Vester *et al.*, 2016).

Figure 5-9 (Section 5.4.1) and Figure 3-11 (Section 3.5), shows a typical fluid behaviour and velocity profile with a separated flow in a 45° and 90° bend pipes. These are the most common bends usually found in the oil and gas industries, particularly 90° bend (Dutta *et al.*, 2016; Zhao *et al.*, 2017). The fluid experiences a steady flow without velocity variation in the straight section of the pipe just before the bend. The central portion of the fluid accelerated to continue the constant flow through any cross-section of the pipe. Therefore, the overall pressure drop in bend pipes is defined as; the sum of the frictional pressure drop created within the straight pipe and the pressure drop due to momentum effect caused by the change in the flow direction. This depends on the curvature ratio and bend angle (Eq. 2.17) (Sreenivas, 2011; Prajapati *et al.*, 2015), see Section 5.4.1 for new the pressure drop correlation developed for quantifying thickness deposit.

$$\Delta P = \overbrace{4f \frac{L}{d} \frac{\rho}{2} (V)^2}^{\text{Pressure Drop due to Frictional loss}} + \overbrace{\frac{1}{2} k_b \rho V^2}^{\text{Pressure Drop due to Momentum change}} \quad (2.17)$$

It was evident that as crude oil flow through bend pipes, even for a smaller bend curvature ratio of $R_c/D \leq 1.5$ the adverse pressure gradient near the inner wall and immediately downstream of the bend could lead to flow separation and increases significant pressure losses (Idelchik, 1986; Dutta *et al.*, 2016). Which consequently affects the wax deposition behaviour and process mechanisms (molecular diffusion, Brownian diffusion, shear dispersion, gravity settling and shear stripping) that lead to the deposition of wax on the cold surface (Makwashi *et al.*, 2019a). In this research, the two curvature pipes– in horizontal and inclined flow are used to develop a better understanding and investigate the severity of wax deposition by comparing the behaviour with a straight pipe. Unfortunately, most of the researches discovered in the literature were carried out using a flow rig – with a straight pipeline test section. Few studies used a flow rig designed with a curved or bend pipes (Lee, 2008; Lee *et al.*, 2008; Bagdat and Masoud, 2015; Rashidi *et al.*, 2016) as highlighted in the next section.

2.6 Original Contribution to Knowledge

Achieving an excellent flow assurance during oil and gas production and transportation is a very challenging task, particularly with the potential for the complex physical phenomena of wax precipitation and deposition. By thoroughly examining the literature on experimental waxes depositions, it was found that several techniques and facilities have been used in the past to study and/or prevent these problems. Most of these studies were carried out using a straight pipeline flow loop, designed either in horizontal, vertical or inclined. The impact of pipes bend on the increased severity of wax deposition is not well studied, and indeed, the actual relevance of the deposition mechanisms and their effects on flow characteristic and the dynamics flow behaviour is still under scrutiny.

As of today, few researchers investigated wax deposition using flow loop designed with a bend or curved pipes (Bagdat and Masoud, 2015; Lee, 2008; Lee *et al.*, 2008; Rashidi *et al.*, 2016; Volk *et al.*, 2003) without any consideration of the influence of flow restriction (e.g. the pipe bends) and their effect on wax deposition. None of these studies attempted

to model experiments that adequately address the effect of curved pipes on the wax deposition. In reality, bends in pipes cause hideous problems in a typical fluid flow. Apart from flow restriction, pipe bends significantly affects the global and local flow parameters such as pressure drop, advection and particle interaction mechanisms (Wang *et al.* 2004; Yadav *et al.* 2014), and directly affects wax deposition mechanisms (Makwashi *et al.*, 2019a, 2019b). As already being highlighted in the literature, apart from molecular diffusion, other mechanisms also contributed to wax deposition process and are most likely to be manifested during production around the curved pipes.

However, there are several explicit studies in other area of flow assurance such as hydrate and multi-phase flow problems (e.g. slugging), which broadly investigates the effects of restrictions (e.g. bends and elbows) (Wang *et al.*, 2004; Xing *et al.*, 2013; Zhao *et al.*, 2017). For instance, a study by Xing *et al.* (2013) designed a flow loop that incorporated different pipes bend (i.e. 45 and 90-degree)– formed a wavy pipe test section. Xing *et al.* devised a method of mitigation severe slugging in three-phase (oil-water-air) flow. Accordingly, their results showed that pipe bends in a wavy form encourage flow oscillation and acceleration of oil and gas, which reduced the slug length in the pipeline riser system. Unfortunately, this study is limited by using a fluid with Newtonian characteristic only, without considering the effect of having fluid with non-Newtonian behaviour (such as waxy oil) in the system.

In view of the previous wax deposition studies revealed in the second paragraph; Lee (2008) and Lee *et al.* (2008) modelled a lab-scale pipeline system to develop an experimental technique and predict required gel breaking and restart pressure of the gelled in a U-shaped stainless steel pipe test section. The flow loop test section was slightly declined about 2° toward the outlet. Therefore, the experiment allows Lee to study different parameters and apply a hydrostatic head to reduce the gel breaking and the restart pressure. The study significantly decreases the required gel braking pressure by 50% in a U-shape flow loop pipe. However, the analysis did not show the curved parameters and no comparisons between a straight pipe and the U-shape test section — similarly, no information regarding the deposition mechanisms. Therefore, the effectiveness of the developed model is not justified.

In another study conducted by Bagdat and Masoud (2015) and Rashidi *et al.* (2016), the experiment flow loop is constructed with straight pipes joint by 90° elbows. The study

compared wax deposition behaviour with temperature, roughness and flow rate within different tested pipes (Polyvinyl Chloride (PVC), Ethylene - TetraFluoroEthylene (ETFE), and steel as reference material). The study provided solutions of wax deposition with ethylene tetrafluoroethylene (ETFE) plastic pipe coating. The drawback of these experiments is that the effect of deposition processes and the interaction of wax crystals around the curved pipe has not been elucidated.

University of Tulsa's wax deposition flow loop facilities (Volk *et al.*, 2003) modelled experiments in single-phase flow through U-shaped test section. Various studies with specific crude oil and varying parameters were performed to improve computer code for predicting deposition of paraffin in deepwater and surface pipelines. Similarly, the studies provided by Volk *et al.* (2003) did not describe the wax deposition effect of bend in the pipe and the actual relevance of the deposition mechanisms.

Therefore, in this research, wax deposition in a straight pipe and two curved pipes with 45 and 90° bend was investigated using a laboratory-scale flow loop. The results from the straight pipe (benchmark) were validated with published data, and this study improved the validation by using different wax measurement techniques. The research is significant and would enhance the understanding of wax deposition behaviour, wax crystals formation mechanisms and improve the current models for accurate prediction. Curvature pipes are believed to have had a similar effect on the waxing process in addition to other wax deposition control parameters mentioned in the previous sections. As such, it is the first time the waxing process and the severity of the deposition were studied and compared in different curved pipes test section– incorporated 0°, 45° and 90° bends. Most notably, this work considers the application of a new model for estimation of wax deposit thickness through pressure drop correlation.

Similarly, the research further improved the understanding of wax deposition prevention through the use of a blended wax inhibitor tested with different crude oil. Chemical treatment is currently regarded as the best solution to prevent wax accumulation in pipelines. However, oil industries usually developed wax inhibitors for a particular reservoir; as there is no universally acceptable inhibitor suitable for all crude oil types (Kang *et al.*, 2014; Adeyanju and Oyekunle, 2014; Halim *et al.*, 2011). The chemicals are highly selective to a specific waxy oil mixture. Characteristically, in most previous wax deposition models, the complex rheology of different waxy oil was ignored. This can

influence the accuracy of wax deposition prediction modelling behaviours. Therefore, this research analyses different waxy crude oil using standard analytical methods. The data developed are directly used for simulation studies of solid wax deposition.

In a nutshell, this research is focused on driving new sets of data valuable for improving wax deposition prediction and management strategies, particularly around subsea pipeline systems. The data would serve as validation tools for further improvement of the existing wax deposition model.

Chapter 3

Experimental Methods and Analytical Techniques

3.1 Introduction

This chapter focuses on the methods and procedure used to characterise the crude oils samples and relevant techniques used to quantify deposit wax thickness. Similarly, this chapter provides details design of the pipeline flow rig system and the wax chemical inhibitors. Together with the dynamic multiphase flow simulation study using OLGA and the embedded Multiflash 4.3.20 for validation of the wax models using the experimental data. Significant challenges in the experimental wax deposition study have been identified, including; control procedures, quantifications and characterization of both deposited wax and the crude oil. In general, the methods and systems are detailed in a sequential workflow (see Figure 3-1), from the pre-deposition to actual and the post-deposition stages, respectively.

The crude samples in this study described in terms of their API gravity, wax content, SARA fractions, n-paraffin distribution, wax crystals morphology, pour point, viscosity and the wax appearance temperature. On the other hand, the most reliable techniques, especially for single-phase system was used to measure the deposit thickness, e.g. the pressure drop method, weight–balance method, energy-balance method and the wet film-thickness gauge with the help of borescope camera. The details characteristics of the samples are crucial for understanding crude oil depositional behaviour. Similarly, it shows how the rheological properties of oil changed due to the interaction with paraffin wax (de Oliveira *et al.*, 2016; El-Dalatony *et al.*, 2019) Similarly, the data are used for gauging the flow rig capacity before the dynamic flow rig experiment and as input parameters in the simulation study.

Section 3.2 of this chapter outlines the crude oil sources and the synthesis procedure of the oil. Sections 3.3 and 3.4 describes the crude oil characterization, chemistry and

analysis and blending of chemical wax inhibitors. The details description of the pipeline flow rig design and operational procedure, including start-up and shut down, are provided in Sections 3.5 and 3.6, respectively. Section 3.7 and 3.8 are detailed the experimental matrices and the methods for quantification of deposit wax. Finally, Section 3.9 discusses the software package, procedure and sensitivity analysis used in this study.

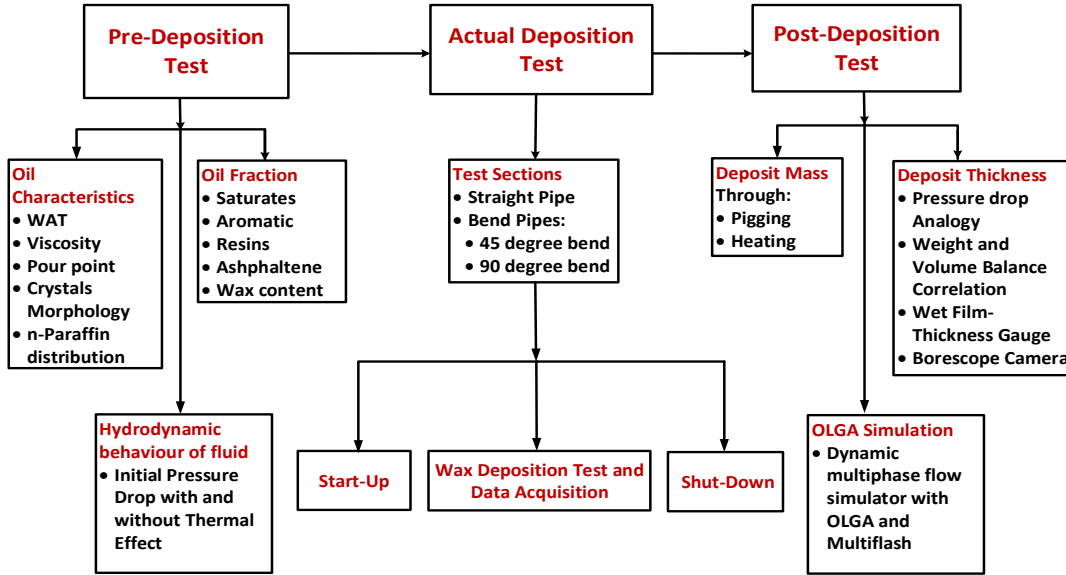


Figure 3-1: Sequential workflow for wax deposition experimental study. Highlights the overall stages and some of the most appropriate techniques and parameters obtained: before, during and at the end of the experiment flow study.

3.2 Crude Oil Sample Selection

Three crude oil samples are used in this study to develop a correlated understand of rheological behaviour and the physical properties. However, only one of them was employed in the flow rig and the simulation studies. Roemex Oilfield Service Company, UK– supplied two of the samples crude oil (Mwambe and KSG) with unknown origins and ranges of properties for only KSG crude oil (shown in Table 3-1). Hence, the Mwambe and KSG crude oil are referred to as sample A and B in this study. The third sample (dead oil) was provided by the Core Laboratories Limited (UK). The dead oil referred to as sample C in this study has shallow wax content (3 %wt), pour point (<1). Therefore, the three samples are characterised (see section 3.3) to obtain all the fundamental properties that defined their waxy nature through standard methods (see Table 4-1 for the results). However, prior to the

characterization, sample C was synthesized (see section 3.2.1) by blending dead oil with solid wax (source; Roemex) in order to increase the waxing properties of the sample.

Table 3-1: Properties of KSG crude oil (Sample A) supplied by Roemex (U.K.)

Properties	Unit	Value
Wax Appearance Temperature (WAT)	°C	28 - 30
Pour Point	°C	0 - 30
Wax Content	% wt	2 - 21
°API		25 - 37

3.2.1 Synthetic Crude Oil

The main rationale for synthesise sample C is to increase the wax content, which will directly affect other properties, e.g. the viscosity, pour point and WAT (Bai and Zhang, 2013; Rehan *et al.*, 2016). Therefore, increasing the wax content from 3 to 12 wt%, the sample can be treated as highly waxy crude. Noting that, with 3wt% original wax content, the non-Newtonian behaviour of the sample is not apparent. Generally, crude oils are treated as Newtonian fluid if the wax content is quite low; for instance, <5wt% (Abdel-Waly, 1997). As such, the wax content of the crude was increased as details below.

Five (5) litres of the dead crude oil was measured and heated using an electric hot plate to raise the temperature above crystallization temperature for 15 min. 544.34g of solid wax was mixed with the hot oil in two different containers, each contained 250 ml of hot oil (Figure 3-2). A LED digital overhead stirrer was used to stir the fluid at 550 rpm for 45 min. According Eq. 3.1 - 3.4, 544.3g of solid wax weight is required in 5 litres of sample C (3%wt wax content) to produce an overall wax content of 14 wt% as follows:

$$\text{wax content (\% wt)} = \frac{\text{weight of wax in crude (g)}}{\text{total weight of crude with wax (g)}} \times 100 \quad (3.1)$$

If γ = total weight of 5 litres dead crude with 3%wt wax content = 4254.8 g

The weight of solid wax in the 5 litres dead crude oil is given as;

$$3 \% = \frac{\text{weight of wax in dead crude (g)}}{4254.8} \quad (3.2)$$

$$\text{weight of wax in dead crude (g)} = 127.54\text{g}$$

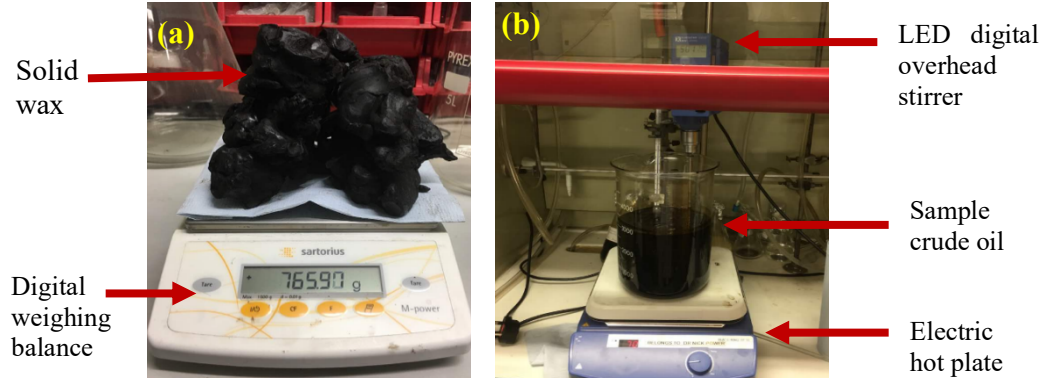


Figure 3-2: Wax sample: (a) Solid wax measured with weight balance (b) Set-up for mixing dead crude oil with solid wax at a constant temperature.

Note that, the target is to design a new oil with wax content of around 14wt%, therefore, from Eq. 3.1

$$14 \text{ wt\% (target wax content)} = \frac{\alpha + \beta}{\alpha + \gamma} \quad (3.3)$$

Where α = weight of wax to be added (g);

β = weight of wax in the original oil (g)= 127.54g and

γ = weight of original crude with 3 wt% wax (5 liters) = 4254.8 g

$$\therefore 14 \text{ wt\%} = \frac{\alpha + 127.54}{\alpha + 4254.8} \quad (3.4)$$

$$\alpha = 544.34 \text{ g}$$

Therefore, 544.34g of solid wax is required in 5-litres crude oil with 3wt% (wax content) to produce total 14wt% wax content. However, a modified UOP 46-64 method was used to compare the above result as shown in Table 4-1.

3.3 Crude Oil Characterization

In the oil and gas field characterization of crude oil is usually carried out before the front end engineering design (FEED) that comes after the completion of conceptual design and the feasibility study (Cochran, 2003; de Oliveira *et al.*, 2016). Similarly, crude oil characterization is mandatory before the use of a flow loop in the laboratory study. Therefore, in this work, understanding the natural properties of oil and rheological behaviour is significant. Problems related to fluid flow and solid

deposition concerning the change in pressure, temperature, and composition are resolved with adequate fluid characterization (Jamaluddin *et al.*, 2001; Jha *et al.*, 2014). The studies further emphasised that inaccurate crude oil characterization may lead to wrong designs of facilities and acts as bad input parameters for modelling and simulations. The results of specific crude oil characteristic cannot be straightforwardly generalised to other field scenarios.

Hence, in this study, a case-by-case investigation of crude oil assay and deposit wax characterisation was performed to address some of the unanswered questions highlighted in the literature through several standard methods that are usually employed by standard laboratories and the oil industries as follows;

3.3.1 Specific Gravity and API

API gravity is one of the fundamental properties of crude oil that provides insight into the quality of the oil. This property shows how heavy or light crude oil is compared to water, and is usually calculated using the equation shown below.

$$API = \frac{141.5}{SG} - 131.5 \quad (3.5)$$

Where SG is the specific gravity (dimensionless quantity), defined as;

$$SG = \frac{\rho_{oil}}{\rho_{water}} \quad (3.6)$$

In this work, a pycnometer was used to obtain the precise density of the crude oil in reference to a well-known density of water (1 g/cm³ or 1000 kg/m³).

3.3.2 Wax Content Analysis

In this study, the wax content of the oil samples was obtained using two different methods. (i) high-temperature gas chromatography (HTGC) (KAT 2009; Singh *et al.*, 2011) and (ii) a modified UOP46-64 method known as acetone precipitation technique (Hoffmann and Amundsen, 2010; Coto *et al.*, 2011; Fan and Buckley, 2002; Sarica and Panacharoensawad, 2012). The details procedure of HTGC method is incorporated in Section 3.3.8, whereas, the modified UOP46-64 technique was described as follows.

Initially, 5g of the oil sample was measured and mixed with 35 cm³ solvent (petroleum ether). The mixture is stirred in a beaker for about 15 min. To precipitate the wax content in the oil, acetone is added to the mixture in a ratio of 3:1 vol/vol (acetone: petroleum ether). The mixture is then chilled to -20 °C for 24 hours. The precipitate (i.e. waxes) are recovered by vacuum filtration using glass Buchner funnel with a vacuum pump connected to the sidearm of the filtration flask as shown in *Figure 3-3*. The filtered solid is washed with n-heptane to remove asphaltenes and the filtered liquid evaporated. Subsequently, the solid obtained after solvent evaporation is re-dissolved in n-hexane in order to remove asphaltenes content and filtered again. After solvent removal, the final product (wax) was weighted and the wax content (wt%) was calculated using Eq. 3.1.



Figure 3-3: Vacuum filtration set-up with Buchner funnel and flask for filtration of wax content from (A) crude oil sample B and (B) crude oil sample A and C after 24 hr cooling at -20°C

3.3.3 Pour Point of Crude Oil

The PP of crude oil samples was obtained using a slightly modified ASTM standard D97-08 method (Alcazar-Vara and Buenrostro-Gonzalez, 2011; Coto *et al.*, 2014; Roenningsen *et al.*, 1991). The result was compared with the PP obtained by the viscometric plot (Adeyanju and Oyekunle, 2013; Theyab and Diaz, 2016). Although, ASTM Standard D97-08 technique is the easiest and quickest method for pour point study of waxy crude oil. Section 3.3.4 describes the viscometric analysis, while the modified ASTM Standard D97-08 procedure started by using an appropriate amount of crude oil in a test jar and preheated to about 60 °C for 5 min. The complete set-up is made of a bath with crushed ice; the test jar sealed with a cork is placed in the bath. A thermometer is partially immersed in the sample crude through the sealed

cork to monitor the temperature changes. The pour point was observed and checked after every minute. The test Jar is removed and positioned horizontally, if the crude oil remained in that position for 5 seconds without sagging, the temperature reading is recorded as the PPT of the sample. Also, 3°C is added to the thermometer reading. According to ASTM D-97, the actual pour point is 3°C higher than the reading observed. The PPT from the viscometric plot is incorporated and details in Section 3.3.4 below.

3.3.4 Rheological Properties

In this study, the crude oil properties such as the oil viscosity, wax appearance temperature (WAT) and pour point temperature (PPT) are obtained using Bohlin Gemini II shear controlled Rheometer (**Figure 3-4**). The rheological study was performed according to Singh *et al.* (2011), Adeyanju and Oyekunle (2013), Wang *et al.* (2015) and Theyab and Diaz (2016). A rotating cone with a 4° angle, 40 mm diameter and a gap setting of 0.15 mm (0150) were used. The analysis was performed by controlling the temperature, shear and cooling rate. The oil sample was heated above the wax crystallization temperature– to eliminate the entire non-Newtonian characteristic. A pipette was used to introduce the sample oil on the stationary cylinder surface. The analysis begins by cooling down the crude oil from 50°C to 0°C at a constant cooling rate of 1.0 °C/min and a shear rate of 10 1/s. Once the oil sample reached 0°C, the sample is held at that temperature for 15 minutes with no shear. The data are captured and displayed immediately by a computer connected to the rig set-up shown below. The oil samples were analysed at a different shear rate of 10, 60, and 120 1/s, similar to the study reported by Singh *et al.* (2011), Adeyanju and Oyekunle (2013) and Theyab and Diaz (2016).

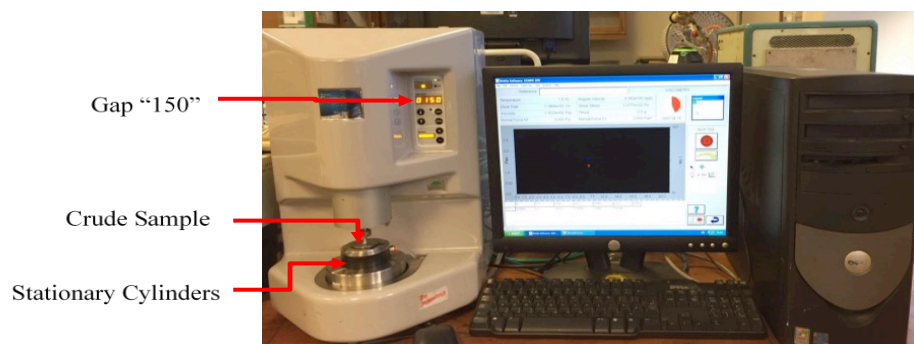


Figure 3-4: Bohlin Gemini II Rheometer for measurement of WAT, PPT and viscosity at specific shear and different temperature.

Figure 3-5 showed sample results from a complete experimental run, which defines the viscosity change (Red line) at different cooling temperature (Green line) and constant shear rate (Blue line). From the Figure, wax appearance temperature (Cloud point temperature) of the sample is usually characterised by any deviation point from the horizontal line of the viscosity line or an intersection of a baseline drawn from the Newtonian region and a tangent that fitted to the inflexion point (Alcazar-Vara and Buenrostro-Gonzalez, 2011; Huang *et al.*, 2015; Perez *et al.*, 2015; Ruwoldt *et al.*, 2018; Singh *et al.*, 2011a; Theyab and Diaz, 2016b; Anton, 2020), see chapter 4 for details results. Whereas, the point of intersect between two tangent lines drawn from the inflexion point after the WAT point is defined as the pour point. Hence, in the rheological data, the PP represents the property that corresponds to a phase's transition of flow behaviour from Newtonian to non-Newtonian characteristics. A clear representation can be found in Chapter 4 (Section 4.4).

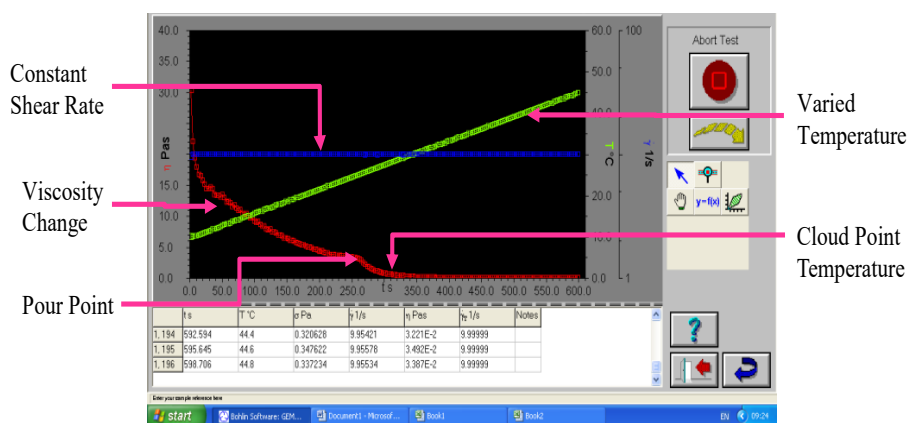


Figure 3-5: A snapshot of viscometric data from Bohlin II rheometer at varied cooling temperature (50 – 0°C), constant shear rate (120 /s)

3.3.5 Crystals Morphology of Waxy Crude Oil

A Carl Zeiss Axiovert S100 inverted optical microscope equipped with a Motic digital camera (Figure 3-6) was used to study the microscopic morphology of the crystalline wax molecules in the crude oil. Through this study, the strong interlocking and interactions of the wax crystals, which form the gelled network causing a complicated problem in the pipeline are evaluated. On the other hand, the study described the crystals as either needle-like or rod-like particles similar to the study by Coto *et al.* (2014) or Yang *et al.* (2014).

Similarly, the efficacy and the behaviour of chemical wax inhibitors was further comprehended using the inverted optical microscope. Therefore, the analysis was carried out using a doped and undoped crude oil with 1000-ppm chemical inhibitor (blend A, see Table 3-4), and the structures were captured. The presence of inhibitor which affects the structural formation of the wax crystals and agglomeration of particles are discussed.

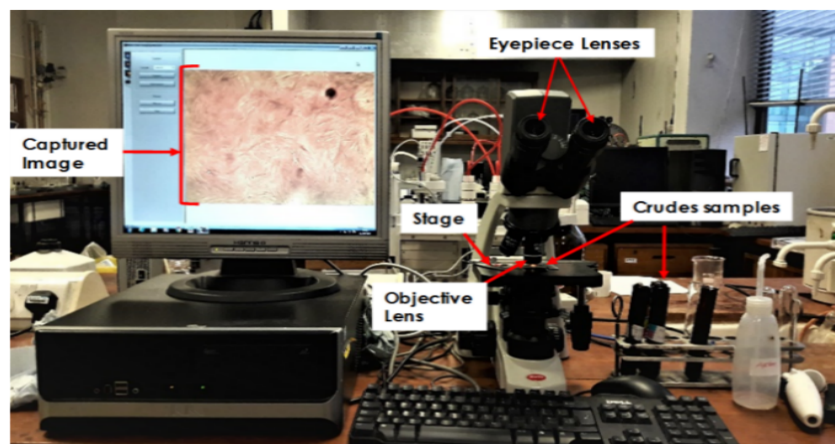


Figure 3-6: Carl Zeiss Axiovert S100 inverted optical microscope for the study of waxes crystals morphology in crude oil undoped and doped with a chemical inhibitor

3.3.6 SARA Analysis

In this study, the crude oil is separated into four significant petroleum fractions of Saturates/Aromatics/Resins/Asphaltene (Jewell *et al.*, 1972). The analysis is effective for assessing crude's fouling propensity, blending compatibility, and asphaltenic stability (Fan *et al.*, 2002; Yen *et al.*, 2001). Similarly, the study determine the oil quality, oil-to-oil correlations, and identify vertical and lateral oil quality gradients in reservoirs (Fan *et al.*, 2002; Roenningsen *et al.*, 1991; Wayne and Sue, 2015).

In this study, a modified ASTM D2549-02 method (elution chromatography) was used. The technique separates SARA fractions based on their polarities; hence, these fractions increases from low in saturates, to intermediate in aromatics, and high in resin. Asphaltenes fractions are the heaviest and most polar fraction formed by series of relatively large molecules containing aromatic rings, several heteroaromatic- such as nitrogen, sulfur, or oxygen atom, and naphthenic ring plus relatively short paraffinic branches (Deshannavar *et al.*, 2010). The procedure follows steps shown in *Figure 3-7*.

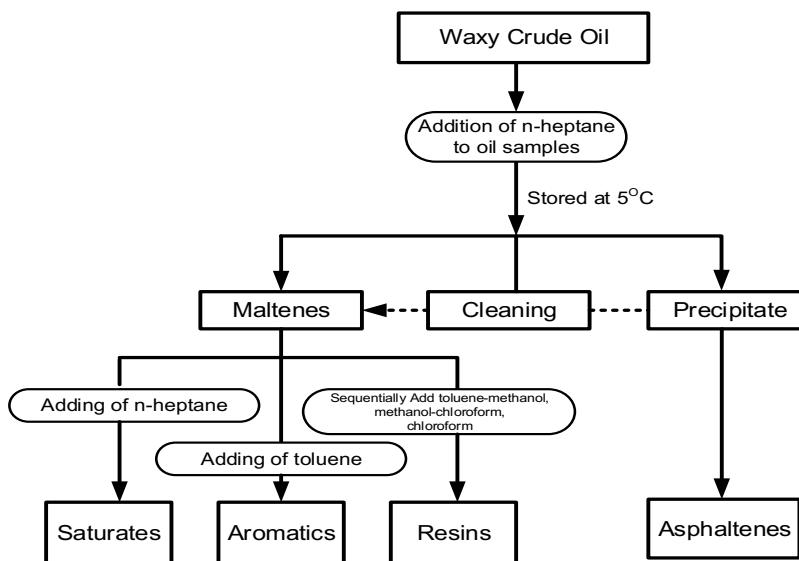


Figure 3-7: Flow chart adapted for crude oil sample fractionation (Zeng *et al.*, 2012).

The chemicals, suppliers and purities used include ethylene glycol–water mixture (IADA, 50/50%), dichloromethane (Scharlab, 99.9%), acetone (Scharlab, 99.8%), n-pentane (Scharlab, reagent grade), n-hexane (Scharlab, reagent grade) and alumina (Al_2O_3) as the solid adsorbent. Some of the apparatus includes; 2 x beakers, 2 x conical flasks, Pasteur pipette, and Buchner funnel etc.

Prior to the open column chromatography separation of maltene into saturates, aromatics and resins, the crude oil was de-asphaltene based on the Figure above and according to a modified ASTM D2007-80 method. The procedure is reported by Wang and Buckley (2002) with a little modification from Ronningsen *et al.* (1991) experimental work. According to the modified ASTM D2007-80 method, 7 g of crude oil was mixed with 160 ml of n-heptane on a ratio 1:40 vol:vol of solvent to crude oil. The mixture is wrapped with aluminium foil and stored at 5°C overnight. After ageing overnight, the precipitated asphaltenes is recovered using Whatman® glass microfiber filters, Grade 934-AH®. The funnel cup is rinsed with precipitants before removing the filtered asphaltenes. Finally, the percentage of weight fraction of asphaltene is calculated using Eq. 3.7 (Wang and Buckley, 2002)

$$\text{Asphaltene fraction (g/100ml)} = \frac{\text{weight of dried asphaltene (g)}}{\text{crude oil volume (ml)}} \times 100 \quad (3.7)$$

On the other hand, the maltene was first separated from solvent to possible amount using vacuum evaporation. Subsequently, 15 ml of maltene was charged to the

chromatographic column using a pipette (Figure 3-8). Subsequently, the sequential elution was done according to the studies by Jha *et al.* (2014). Initially, saturates fractions were eluted with 100 ml of n-pentane. While, for the aromatics fractions; 100 ml of toluene is added and the eluted aromatics are collected. The elution of polar resins was done in four runs, each elution was collected separately, and the final products were added. The sequence of elution began by mixing 100 ml of toluene-methanol solution in a ratio of 50:50. This is followed by running the second elution of 100 ml of methanol-chloroform solution in a similar ratio, third by using only 100 ml of chloroform and the finally eluting 100 ml of acetonitrile. All the eluted compounds were collected in a separate container and separated from the solvent using a rotary vacuum evaporator to recover the pure fraction of saturates aromatics and resins. The percentage of weight fraction was calculated using Eq. 3.7.

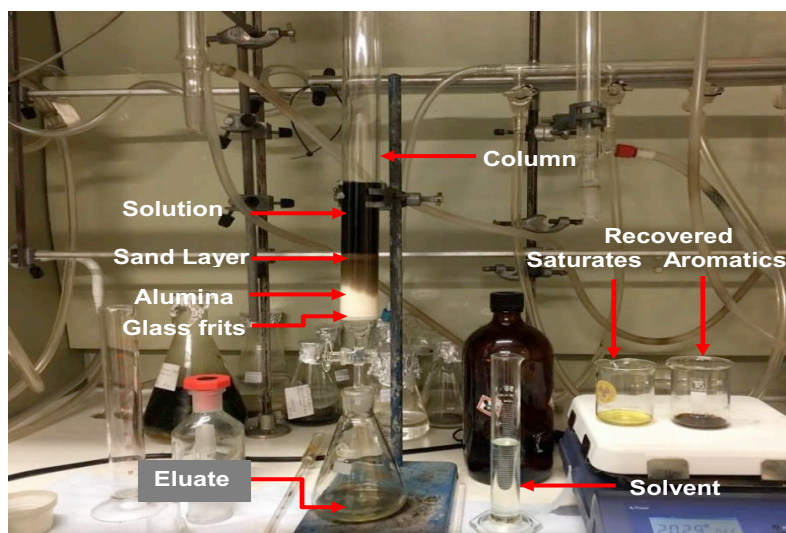


Figure 3-8: Open column chromatography set-up used for SARA analysis of a crude sample

3.3.7 Colloidal Instability Index (CII)

A colloidal instability index (CII) was reported by different researchers (such as Ashoori *et al.*, 2017; Yen *et al.*, 2001) and has been used as a screening criterion that showed the tendency of soluble asphaltene in crude and the extent of its problem. colloidal instability index considers crude oil as colloidal systems consisting of pseudo components of saturates/aromatics/resins/asphaltenes and is expressed as the ratio of the sum of asphaltenes and their flocculants (saturates) to the sum of their

peptisers (aromatics and resins) in crude oil (see Eq. 3.8) (Asomaning and Watkinson, 2000; Yen *et al.*, 2001).

$$\text{CII} = \frac{\text{Saturates} + \text{Asphaltenes}}{\text{Aromatics} + \text{Resins}} \quad (3.8)$$

Eq. 3.8 was used to scale the propensity of asphaltene aggregation of the crude oil samples used in this study. According to Asomaning and Watkinson (2000) and Yen *et al.* (2001b) if the oil CII value is above 0.9, the oil has a propensity to asphaltene aggregation and the oil is very unstable. Whereas, if the CII lower than 0.7, the oil has a solubilise asphaltene, hence, the oil is stable. However, if the CII falls between 0.7 and 0.9, the oil has moderate instability.

3.3.8 *n*-Paraffin Distribution of Crude Oil Samples

The distribution of *n*-paraffin and the wax content of the crude oil is usually obtained using higher temperature gas chromatography (HTGC) (Coto *et al.*, 2011; Singh *et al.*, 2011; Zheng *et al.*, 2016). In this study, a similar approach was used to determine the *n*-paraffin distribution and compare the wax content with the method used in section 3.3.2. An Agilent 6890 gas chromatograph equipped with flame ionization detector (FID) and a Varian Vf-5ht Ultimetall column (15m x 0.25mm x 0.1µm) is used (see Figure 3-9). The oven is programmed to run from 40 to 435 °C at 10 °C/min ramps before holding at 435°C for 10 min. Helium was used as carrier gas at a flow rate of 5 mL/min.

The study was carried out using a commercial technique in collaboration with the University of Plymouth. The method known as T-SEP[®] thermal separation technique was co-developed by the University of Plymouth and Kernow Instrument Technology, UK. Currently, the technique is used by most of the oil and gas industry, as this was regarded as one of the most reliable, reproducible and effective method compare to the simple conventional techniques employed by most laboratories available in the literature (KAT Lab, 2009). According to KAT, the method allows precise control of hydrocarbon by “*topping process*”, and in average the methods allows an additional of 20 carbon numbers of the *n*-paraffin to be observed and measured.



Figure 3-9: Agilent 6890 gas chromatograph (Picture was taken from Plymouth University)

3.3.8.1 Sample Preparation:

The crude oil sample is heated at 70°C for 1 hr. A small amount of heated oil is dispensed using foil-wrapped glass in two pre-weighed containers that were pre-heated at 110°C, which are then sealed and kept at room temperature. The two samples are prepared ready for analysis as follows:

Whole Sample: the whole sample is the unadulterated crude oil and made up to the required concentration of 5 mg ml⁻¹ with solvent (cyclohexane) and then analysed with HTGC at 0.5 µL. **Topped Sample:** the topped sample was prepared by topping procedure, which is not included in this work because of the preparation procedure is protected by various confidentiality agreements. Another part of this procedure is that the results of the whole and topped sample are normally merged to normalise between the two samples.

However, prior to the analysis of the *whole and topped samples*; the chromatograms of solvent blank (cyclohexane), the compound in C₁₀–C₆₀ standard (Table 3-2) and Polywax 655 external standard are workouts. The n-alkane peaks are quantified relative to the above standard. With response factors interpolated between C₁₀–C₆₀ (Table 3-2) and carbon numbers >nC₆₀ quantified using the response factor of nC₆₀. Whereas, the retention times are correlated with Polywax 655 external standard as shown in chapter 5.

Table 3-2: C10-60 standard Volume

Concentration (mg/ml)	Carbon Number	RT (mins)	Area (pA*s)	Sensitivity (pA*s/ng)
0.058	10	3.02	477.56	16.467
0.048	20	14.01	497.79	20.741
0.048	30	21.49	547.01	22.792
0.050	40	26.91	541.40	21.656
0.050	50	31.11	530.93	21.452
0.050	60	34.51	433.62	17.345

However, for clarity and understanding, it is essential to explain some part of the analysis and why do the topping of sample is necessary?. During the standard analysis of the whole oil sample, reported by KAT Lab (2009), the concentration of $nC_{10}-C_{20}$ is relatively higher. Those $>nC_{30}^+$ has low concentration, and they are very close or sometimes below the limit of detection of the HTGC instrument. Especially if the crude oil has a wider range of carbon ($>nC_{50}^+$), this implies that the reported heavier n-alkanes may not have a degree of accuracy. Therefore, by Topping procedure, these problems are eliminated, and in effect, the concentration $>nC_{15}^+$ are accurately measured and all the n-alkanes $<nC_{15}$ and unresolved complex mixture are reduced.

Analysis of Concentration

Unlike some laboratories that report the n-alkanes peak areas as a percentage of the total chromatogram signal area, in T-SEP® technique, the integrated peak area is converted to a mass (ng) by dividing the peak area (pA*s) by the sensitivity (pA*s/ng) of a relevant external standard (10-ppm of C15 will not give you the same peak area as 10-ppm of C60) (KAT Lab, 2009). The calculated mass shown in Appendix A (Table A1 and Table A2) is then represented as a weight per cent relative to the mass of the oil-injected (typically 10 µg). The main reason for this approach as stated by KAT Lab (2009) is because “the entire chromatographic area represents only the GC amenable part of the oil, so injecting the same mass of different oils will produce different total chromatogram areas, depending upon how much of each of the oils is GC amenable”.

3.4 Analysis of Wax Inhibitors Efficiency

The efficacy of chemical wax inhibitors on crude oil rheological properties was studied using Bohlin Gemini II Rheometer (Figure 3-4). Roemex supplied the four

chemical inhibitors used in the study, together with their chemistry as shown in Table 3-3 and Figure A1 (Appendix A). A constant volume (30 ml) of oil sample B was blended with an inhibitor in test tubes. Three concentrations (500, 1000 and 1500-ppm) of the inhibitor were used in the analyses. Before mixing the oil with different inhibitor, the sample oil was kept above WAT to ensure all the wax crystals are dissolved. The blended sample is stirred to make sure the chemical inhibitor is completely incorporated in the oil. The performance of these inhibitors in reducing viscosity, and influence on the cloud point, and Pour Point were analysed at different temperature, constant share and cooling rate.

Table 3-3: The chemistry of chemical wax inhibitors

Inhibitors	Inhibitors Chemistry		
	Compositions	Percentage %	CAS
W2001	Hydrocarbons, C ₁₀ , Aromatics, >1%	30% - 60%	n/a
	Naphthalene (HAN)		
	Olefinic polymer derivative	30% - 60%	1269781-05-6
W2003	Solvent naphtha (Petroleum), Heavy Aromatic	7% - 13%	64742-94-5
	Distillates (Petroleum), Hydrotreated light	7% - 13%	64742-47-8
	Naphthalene	1% - 3%	91-20-3
W2004	Alkenes, C ₂₀ -C ₂₄ Alpha-, Polymers with maleic anhydride, C ₁₈ -C ₂₂ alkyl esters	60% - 100%	n/a
	Solvent naphtha (Petroleum), Heavy Aromatic	7% - 13%	64742-94-5
	Distillates (Petroleum), Hydrotreated light	7% - 13%	64742-47-8
W2005	Naphthalene	1% - 3%	91-20-3
	Solvent naphtha (Petroleum), Heavy Aromatic	7% - 13%	64742-94-5
	Distillates (Petroleum), Hydrotreated light	7% - 13%	64742-47-8

However, out of the four samples, W2001 produces better performance, followed by W2003 (see Chapter 5 for details). Furthermore, the synergy of these four inhibitors was studied. 32 samples were tested, but only eight samples shows improvement. The eight samples were prepared by blending 70% of W2001 with the 30 of W2003, W2004 or W2005. And 50% of W2001 with the 50 of W2003, W2004 or W2005 (see Table 3-4). The mixing criteria were based on the inhibitor's performance and compositions. Hence, out of these blended samples, a new inhibitor with improved performance compared to the original four inhibitors is obtained.

Table 3-4: Blending of different Chemical Wax Inhibitors for improving efficiency

Inhibitors	Blended component
Blend A	50% W2001 + 50% W2003
Blend B	70% W2001 + 30% W2003
Blend C	50% W2001 + 50% W2005
Blend D	70% W2001 + 30% W2005
Blend E	50% W2001 + 50% W2004
Blend F	70% W2001 + 30% W2004
Blend G	50% W2003 + 50% W2004
Blend H	50% W2004 + 50% W2005

3.5 Pipeline Flow Rig Design

In this study, the fit-for-purpose experimental flow rig was designed using all the conditions that allow smooth flow of crude oil, and permits precipitation and deposition in a single-phase system. Some of the real subsea environmental conditions were considered in the design and are incorporated. These include the ambient subsea temperature, which changes with time, the bends angle and the monitoring devices e.t.c.

However, unlike in the laboratory study, in real subsea conditions the pipelines are strong enough to bear the high pressure and high temperature of the crude oil and are relatively non-corrosive (e.g. carbon steel and stainless steel). The length and pipe diameter are substantial in the field compared to the lab studies. Similarly, unlike in the various lab-scale researches, in a real oil field production, crude oil is being produced together with gas-phase. In cases, under higher temperature and pressure, some gaseous component or other light fractions are evolved (Hoffmann and Amundsen, 2010a; Lee *et al.*, 2008; Rittirong *et al.*, 2016). Notwithstanding, laboratory studies are so far being used as a benchmark, especially during most of the field development for making technical and economic strategic decisions.

In this study, three different test sections (a straight pipeline and two pipelines with bends) are designed for a comparative investigation. The base case– the straight pipe (pipe-in-pipe test section) was modified based on the previously published experimental study by Adeyanju and Oyekunle (2013) and Theyab and Diaz (2016). Unfortunately, there is no direct published study on wax deposition that can serve as

the basis for design test sections with a different bend (as detailed in chapter 2). However, studies by Rashidi et al. (2016), Xing et al. (2013) and Lee et al. (2008) were used as the preparatory for the flow rig design.

Rashidi *et al.* (2016) investigated wax depositional issues using a straight pipe test section joined by 90-degree elbows. Whereas, Lee et al. (2008) study waxy oil gel breaking mechanisms using a U- shaped stainless steel lab-scale flow rig. Xing et al. (2013) has the closest experimental set-up to the flow rig designed in this research. However, the study was based on hydrates formation and mitigation. Nonetheless, some of the information from Xing et al. has helped in designing the curved pipe test section.

Copper pipeline material of equal length was used for the three test-sections for a comparative study. The pipe diameter of 15 mm, O.D, and wall thickness of 0.7mm, t, were used, based on Theyab (2017) study. However, unlike the pipe length of 1500 mm used by Theyab (2017), this study uses a constant length of 1000 mm. This allows the establishment of a better developed and steady state flow – prior to the fluid advancement into the inlet port of the test section.

The straight pipe test-section was jacketed (pipe-in-pipe) in a 25 mm (O.D) pipe of the same material. The jacketed served as the shell (the annulus) where cold fluid (a mixture of water and glycol of 50% by weight) flowed. While the crude oil flows within the inner pipe – in counter-current direction. Unfortunately, the curved pipes test sections couldn't be jacketed in another pipeline. The curves are built using standard pipe bends commonly found in the oil industry. Copper compression fittings are used to join difference section. In a nutshell, the curve pipes test sections were installed in a flexible open tank as discussed in the subsequent section. Figure 3-10 shows the pipeline flow rig designed with a straight pipe and pipe with 45° bend and elevation.

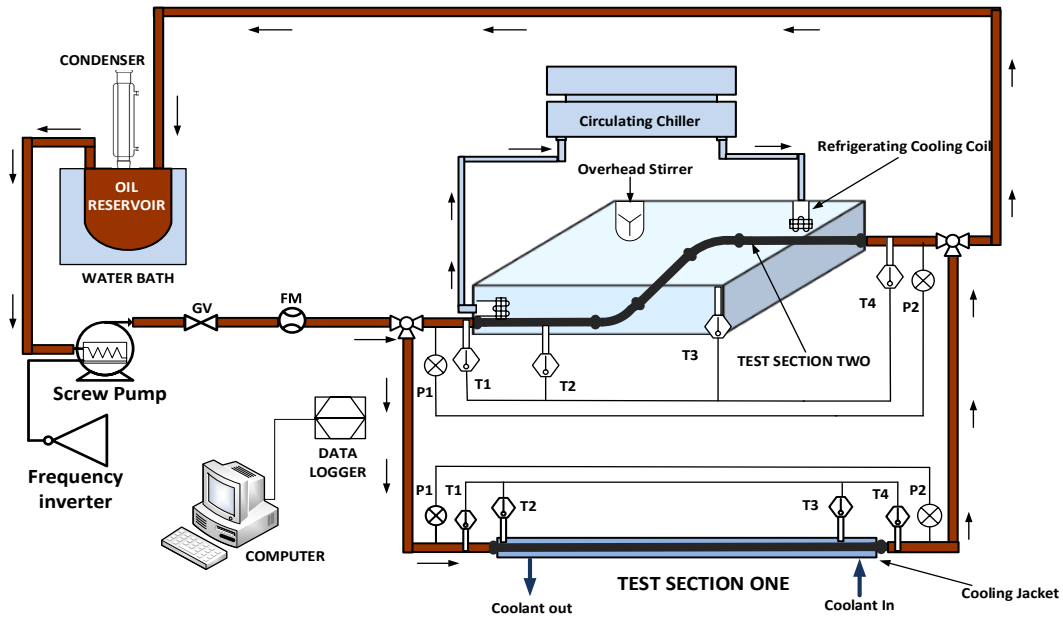


Figure 3-10: Wax deposition flow rig facility designed with Straight Pipe and 45° Bend Pipeline. Where; FM: flow meter, P1 and P2: inlet and outlet pressure of the test section, T1 and T4: inlet and outlet oil temperature, T3 and T2: the inlet and outlet coolant (water-glycol mixture) temperature.

Figure 3-11 shows the parameters of the curved pipeline test section assembled with the two bends. Including the bend radius ($R=45\text{ mm}$), angle of the bend ($\alpha=45^\circ$) and the elevation (350 mm) with velocity profile. The elevation is calculated using the trigonometric concept, from Figure 3-11: elevation (x)= $\sin(45) \cdot (30+220+220+30)$.

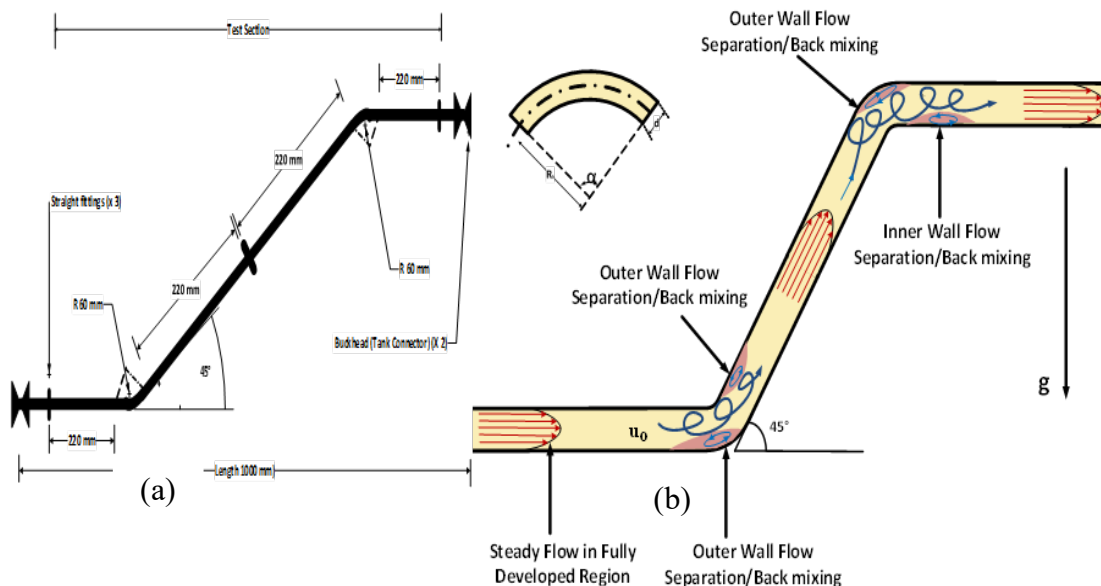


Figure 3-11: Schematic: (a) Design Parameters of Bend Pipeline Test Section with two 45-degree bends. (b) adapted from Idelchik (1986)

Figure 3-12 shows the second pipeline flow rig designed with a straight pipe and pipeline with 90° bend sections. The velocity profile and some parameters of the bend are shown in **Figure 2-13** (Section 2.5.1).

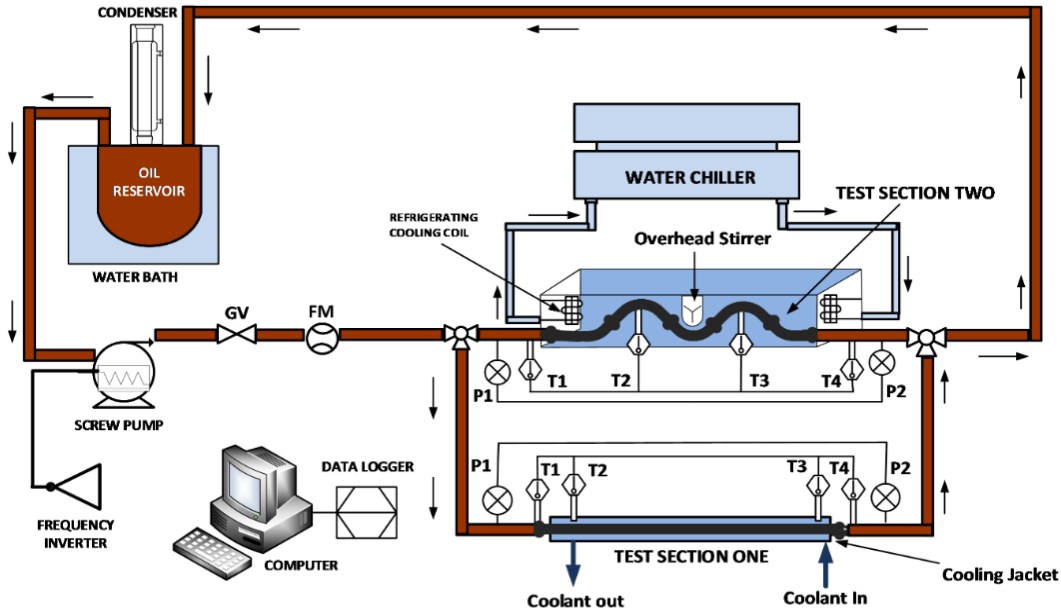


Figure 3-12: Wax deposition flow rig facility designed with Straight and 90° Bend Pipeline. Where; FM: flow meter, P1 and P2: inlet and outlet pressure of the test section, T1 and T4: inlet and outlet oil temperature, T3 and T2: the inlet and outlet coolant (water-glycol mixture) temperature

Other parameters of the pipeline including dimensions, two bulkheads used are shown in Figure 3-13.

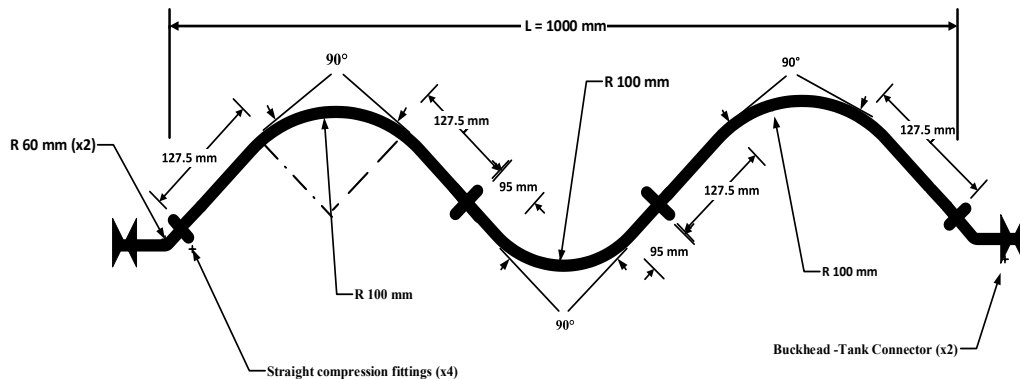


Figure 3-13: Parameters of the Pipeline test section with 90° bends ($L = 1000$ mm), with two bulkheads connected.

The test sections, for instance, Figure 3-11, somewhat mimics the pipeline geometry flow path at the subsea environment, which incorporates: the flowline, riser pipe and a pipe connected to the floaters on the surface. While Figure 3-13 was built similar to

Xing *et al.* (2013) design. The test sections were mounted in a feed and expansion cistern polypropylene tank (40 gallons capacity). Normally, the tank is filled with cold water fully covered the pipe sections (Figure 3-15), cooling the pipe surface. The water temperature is controlled according to the experimental matrix using a submerged refrigerating cooling coil connected to a high capacity circulating Chiller. The Chiller has a self-contained refrigeration bath for precise temperature control in a very wide temperature range (-30 to 100°C) with an accuracy of $\pm 0.02^\circ\text{C}$. In order to maintain uniform cooling water temperature in the tank, a powerful mechanical overhead stirrer- Heidolph RZR50 was used and operated at 500 r.p.m. Section 3.5.1.1 provides other details describing the test section, operation and control.

3.5.1 Flow rig components

The main components of the flow rig include the test section, crude oil pump, frequency inverter, crude oil reservoir, hot and cold water bath, chiller, pressure sensors, thermocouples, flow meter, data logger, and condenser. Others include Oscilloscope— PicoScope model 2204 and 8 channels thermocouple data logger connected to a computer for real-time recording of temperature and pressure readings.

3.5.1.1 Test Sections

These are the main unit of the flow rig where wax precipitation and deposition process occurs. As highlighted in section 3.5, the copper pipe used has a thermal conductivity of 401 W/m.k, density 8960 kg/m³, the heat capacity of 385 J/kg °C, and the roughness of 0.0015 mm. Whereas, the diameter and thickness are 15 mm (O.D) and 1.4 mm, respectively. Generally, due to the high thermal conductivity of copper pipe material, a rapid heat transfer between the hot crude oil and the cold environment is achieved, which could easily promote the precipitation of wax crystals and the deposition on the pipe surfaces, that significant to the lab-scale study.

The design, control and operation of each test sections were made flexible; detachable and rotatable in order to quantify the deposit wax thickness, measure the volume and weight of the deposit and for the study of the effect of inclination of the bend pipes. Each section could be run as a separate entity equipped, by disconnecting

the flow line directly from the inlet control valve. However, the systems can't be operated in parallel, as the test section share one crude oil reservoir.

3.5.1.2 Crude Oil Reservoir

A three-neck glass-boiling flask of 5000ml with 24/29 joint was used as the crude oil reservoir. The flask is made-up with a borosilicate glass 3.3, weight 0.8 kg and has a low linear coefficient of expansion and high annealing point. The glass can withstand a wide range of temperature (-80 – 200 °C) and pressure. The reservoir is placed in a controlled heating bath. The crude oil flows in and out of the reservoir through two different necks opening. While a condenser tube is mounted in the third neck for condensing the light end products.

3.5.1.3 Condenser

A Pyrex borosilicate glass condenser tube with 24/29 joints was used as reflux equipment for condensing gaseous components and agglomerating droplets that evolves in the course of the experiment. Two 1/4 inch hose nozzles for water in and out of the condenser are connected via a tube to a separate chiller filled with cold water and ice. The condenser has a body length of 200 mm, and weight 160 g.

3.5.1.4 Crude Oil Pump

The crude oil is transported in a closed loop and recycles system; from the reservoir into the test section and back to the reservoir using a horizontal close-coupled self-priming screw pump with an integral relief valve. Essentially, the Azcue BT-HM25D4 pump is on spec designed to transport waxy crude oil at varied viscosity; from light, medium and/or heavy oil. The pump provides a consistently smooth flow without pulsations or turbulence and is connected with a suitable motor for variable speed operation. The motor speed is controlled using an Optidrive variable-frequency drive and the pump operated at maximum capacity of 0.66 m³/h (11 l/min), at total head of 5-bars, and maximum temperature of 95 °C. The motor has a maximum frequency of 50 Hz at 0.55 kW.

3.5.1.5 Frequency Inverter

Invertek variable-frequency drive (VFD) for single Phase Motors (ODE-3-120070-1F12-01) was used to control the speed of the pump. Therefore, the VFD control AC motor speed and torque by varying motor input frequency and voltage. The

frequency of the pump is calibrated with the flow rate, which was recorded from the oval gear flow meter.

3.5.1.6 Flow Meter

Oval gear flow meter with a mounted display was used to monitor the flow rate at different pumping frequency. The flow metre is designed for online monitoring of flowrate using a computer and through a mounted display with a capacity between 1 - 30 l/min, fluid viscosity up to 1000 mPas and max pressure and temperature of 140 bars and 80°C. The crude oil flow rate is usually adjusted by regulating the frequency of the motor from the frequency inverter. A data logger from MadgeTech is connected for transmission and online monitoring of data.

3.5.1.7 Hot Water Bath

Generally, a water bath is preferred as the heat source for heating the crude oil instead of an open flame to prevent ignition of flammable components. Therefore, Grant GR150 stirred water bath equipped with stainless steel is used to provide outstanding temperature control up to a maximum temperature of 200°C. The bath is filled with water and heated to the desired temperature. Usually, the crude oil attained its desired temperature (45°C) when the water bath temperature is maintained at around 83 to 85°C. Therefore, the water bath incubates the crude oil temperature at 45°C throughout the study. A standard glass tube thermometer is used to ascertain the temperature reading displayed from the bath.

3.5.1.8 Circulating Chiller

Haake K20 C10 circulating Chiller type was used during this study. The Chiller has a self-contained refrigeration bath for precise temperature control in a very wide temperature range from -30 to 100 °C, with temperature accuracy of $\pm 0.02^\circ\text{C}$. The Chiller has a liquid capacity of 4.5 litres. A pump is mounted around the refrigeration bath, which recycled the coolant (glycol-water mixture). The coolant fluid at 7 l/min has pumped the shell of the straight pipe, as shown in Figure 3-14 (points 11 and 12).

On the other hand, at the same flow rate, the coolant fluid is pumped through a refrigerating cooling coil and recycled back to the chiller. The refrigerating cooling is fully immersed and placed at the middle of an open tank, which was initially filled with cold water and contained the bend pipe test sections. Heat transfer occurred

between the cold surface of the refrigerating cooling containing the coolant fluid and the cold water in the tank. The second heat transfer is between the cold water in the tank and the surface of the pipeline test sections (Figure 3-15, point 12).

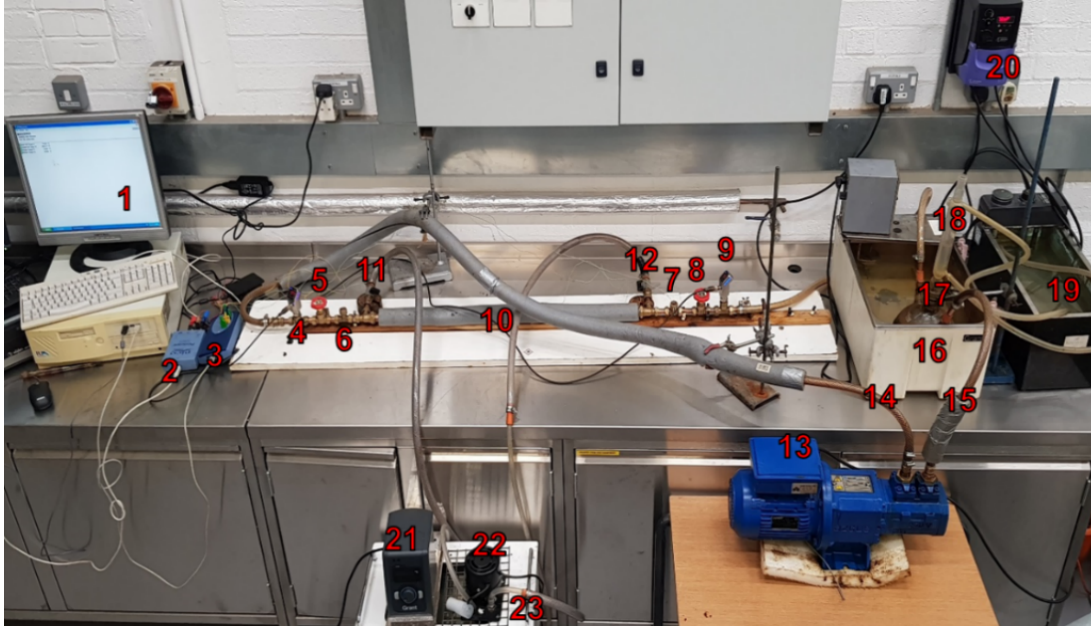


Figure 3-14: Flow rig set-up with straight pipe test section consists of; 1– Computer with the Software. 2– Pressure PicoScope. 3– Thermocouples Data Logger. 4&9– Inlet & Outlet Pressure Sensors. 5&8– Inlet & Outlet Control Valves. 6&7– Inlet & Outlet Oil Thermocouples. 10– Removable Jacked Straight Pipe Test Section. 12&11– Inlet and Outlet Coolant Fluid with Thermocouples attached. 13– Oil Pump. 14– Oil Flow out of the Pump. 15– Oil Flow into the Pump. 16– Hot Water Bath. 17– Oil Reservoir. 18– Condenser Tube. 19– Ice/Cold Water Bath for Condenser. 20– Oil Pump Frequency Inverter. 21– Chiller Programmable Temperature Controller. 22– Coolant Pump connected to the Test Section. 21– Circulating Chiller.

3.5.1.9 Pressure Sensor

The pressure drop across the test section was monitored using two GC35 pressure sensors manufactured by Ashcroft trust the shield. The sensors combined 3-in-1 analogue scaling/digital gauge, programmable switch outputs and transducer. It has a pressure compound ranges from 0 to 75 psi (0 -5 bar). The sensors are simple to configure that allow the user to adjust switch settings and analogue scaling. The sensor was installed as non-intrusive but invasive with the pipeline, connected to an Oscilloscope – PicoScope model 2204 and a computer for real-time monitoring and recording of pressure at the inlet and outlet of the test section of the flow rig. The GC35 sensors operate around a temperature between -20 to 70 °C and have an accuracy of $\pm 1.0\%$ F.S. The accuracy includes effects of linearity, hysteresis,

repeatability; zero offset and spans setting errors. Hence, sensors were first calibrated during the pre-deposition study based on the theoretical voltage value with corresponding pressure reading.

3.5.1.10 Thermocouples

In this study, two self-adhesive patch and two exposed tip thermocouples (type K) are used to monitor the temperature at a different location. The exposed tip thermocouples are made up of Nickel Chrome/Nickel Aluminium (NiCr/NiAl) (+/-) with tolerance class 1 (-40 to 1000 °C) and ± 1.5 accuracy. They have a probe diameter of 1.2 mm. On the other hand, the self-adhesive patch thermocouples (K calibration) are suitable for measurement of flat or curved surfaces temperature. They are rated for operation temperature between -50 and +250 °C and are made from PFA insulated thermocouple cable. The patch size is 25 x 20 mm, with 0.2 mm diameter solid PFA insulated twisted pair leads, and the lead length is 2 m.

In this study, the exposed tip thermocouples are used to monitor the temperatures of crude oil at the inlet and outlet of the pipe through suitable copper pipe T-coupling fittings used for temperature detection in a pipe. Whereas, the exposed tip thermocouples measured the coolant fluid temperature at the inlet and outlet points of jacked straight pipe. All the thermocouples are connected to a TC-08 channel thermocouple data logger. A thermometer is usually being used for verification of results.

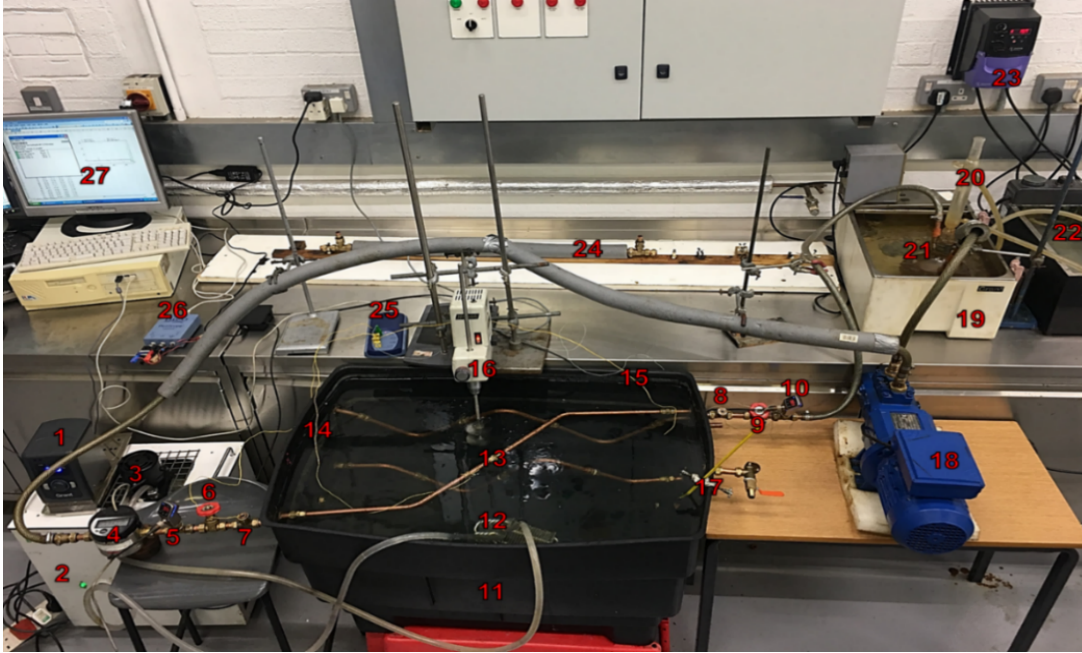


Figure 3-15: Flow rig set-up with bend pipe in an open cooling tank consists of; 1– Programmable Temperature Controller. 2– Circulating Chiller. 3– Water Pump connected to Fine Tube Heat Exchanger. 4– Flow Meter. 5&10– Inlet & Outlet Pressure Sensors. 6&9– Inlet & Outlet Control Valves. 7&8– Inlet & Outlet Oil Thermocouples. 11– Cooling Water Tank. 12– Fine Tube Heat Exchanger. 13– 45-degree bend pipe at zero elevation. 14&15– Water and Pipe Thermocouples. 16– Mechanical Overhead Stirrer. 17– Water Thermometer. 18– Oil Pump. 19– Hot Water Bath. 20– Condenser Tube. 21– Oil Reservoir. 22– Ice/Cold Water Bath for Condenser. 23– Oil Pump Frequency Inverter. 24– Detached Straight Pipe-in-Pipe Test Section. 25– Thermocouples Data

3.5.1.11 Borescope inspection

A USB borescope camera 5 m long was used for inspection of the deposit surface inside the spool piece and deposit thickness. A similar technique was used by Rittirong (2014) and Rittirong *et al.* (2015, 2016, 2017). According to these studies, borescope inspection permits better visual observation than the usual method. The camera can access any point around the pipeline, depending on the thickness of the deposit. Especially if the pipe diameter is small. However, significant observations on the deposit surface and thickness were made in this study. The camera is waterproofed with 5.5 mm (O.D) and screwed with a hook attached to the camera light to guide and create a mark on the wax deposit surface for analysis. Therefore, the mark of wax on the hook was used as a reference for thickness determination which gives a probability value of the thickness prior to the application of the standard method. The borescope camera is connected to a PC and usually, it supports OS, Windows and Android phones.

3.6 Deposition Testing Procedure

Initially, the pipeline flow rig was calibrated around the wax appearance temperature and pour point of the crude oil. The step-by-step procedure highlighted in three stages below was designed to achieve the objectives of this study.

Flow Rig Start-Up Stage:

This stage included the preliminary start-up when commissioned the flow rig and after each specific experimental run. At first, the flow rig was checked to ensure all the control valves are fully opened, and all the joints and fittings are airtight. Also, the thermocouples, PicoScope and data logger are connected. Similarly, the PC, Chiller and condensing system are put on. The experiment begins by heating the crude oil sample in the reservoir to a temperature above wax appearance temperature ($WAT + 15^{\circ}C$) for 30 min. Subsequently, the hot crude is circulated in the flow rig at a relatively high flow rate (9 l/min), by adjusting the motor speed of the pump from the variable-frequency inverter. The flow is maintained for 10 minute – without cooling. Through this sequence, the remaining deposits wax that stocked on the pipe wall from the previous test is melted and move along with the circulating hot oil to the reservoir. In this stage, the flow rig was operating without coolant fluid in the shell tube or the open tank as the case may be. This is done to avoid any possible thermal gradient in the test pipeline, which could lead to the formation of wax before the wax deposition stage. In some cases, coolant fluid is recycled within the shell tube from the chiller at high temperature (above WAT) to enhance rapid heating the test section. The system temperature is allowed to stabilise at T_{oil} , $45^{\circ}C$ (i.e. $WAT + 15^{\circ}C$) and at a specific flow rate based on the experimental matrix (see Section 3.7).

Wax Deposition Stage:

Wax deposition begins by controlling and monitoring the experimental parameters such as coolant temperature, flow rate, ageing period, and in the latter case, the concentration chemical wax inhibitor. The coolant fluid (based on the matrix) from the chiller is recycled through the jacked of the straight pipe test section, or through the refrigerating cooling coil for the open tank with curved pipeline section. This was done as soon as the system attained stable conditions in the start-up stage. A stopwatch is started immediately. On the other hand, a separated tank with water kept at a desired cooling temperature is always available to begin cooling along with

cold water from the chiller in the open tank contained the two pipe section. Similarly, the mounted overhead stirrer is put on to keep the water temperature homogenous all around the tank. Equally, a bucket full with crushed ice (from ice machine) is always available for any remediation of temperature either in the condensing or the chilling unit.

The wax build-up along the test sections are monitored according to the matrix using the pressure transducers and four different thermocouples connected to a computer at different locations. It is reported that a small piece of deposit along the pipe can cause pressure transducer reading and the outlet temperature of the oil to drops (Singh *et al.*, 2011). The results from the sensors at real-time are monitored and stored on the PC for further analysis.

Shut Down and Data Acquisition:

Once a specific experiment run is completed, the deposit mass, volume and thickness are measured. The flow rig was shut down in the following sequence; first, the coolant fluid from the chiller is turned off. The oil flow through the test section is stopped by shutdown the pump through the variable-frequency drive, and finally, the crude oil hot water bath is put off. At the same time, the test section was isolated by closing the control valve installed at the inlet of each test section.

The isolated section was tilted slightly for about 10 minutes to drain any fluids that remained on the deposited wax. This is followed by visual observation of the wax deposit through a borescope camera at a different location. Subsequently, the mass and volume of the wax deposit are measured using a weighing scale and measuring cylinder. This is achieved by pigging and scratching out (Sarica and Panacharoensawad, 2012; Theyab, 2017) the wax deposit in the pipe using a plastic conical attached to a flexible rod. On the other hand, the small amount of wax deposit that remained in the pipeline was melts and collected using hot water (60°C) recycled from the chiller through the jacked pipe. Whereas, for the curved pipe section; hot water from the water bath is used to heat up the outer surface of the disassembled pipe.

Immediately after the above steps, the removable test section is assembled back to the flow rig, with the two valves opened ready for the next run. The stored data

(temperature, pressure, volume and weight) were used to estimate the thickness of the deposited wax as describes in section 3.8.

3.7 Experimental Test Matrices

Crude oil “sample B” was used in all the flow rig experimental studies. The coolant (glycol and water) flow rate was kept at 7 l/min throughout the studies. Chosen the right conditions is essential and was considered to be necessary within which the flow rig configuration and crude oil samples and the inhibitor’s properties can be studied. A total of 111 test matrix was designed based on the analyses using the three test-sections and the chemical wax inhibitor (blend A) (see Table 3-5 to Table 3-8) as highlighted below:

- Investigation of the influence of thermal gradient at a varied coolant temperature, at 10, 15, 20, 25, 30, 35 and 40°C at a constant flow rate of 5 and 9 l/min (the two conditions under laminar and turbulent flow respectively) and constant experimental period of 2 hrs in a straight and bend pipeline test sections. The ranges of cooling temperature cover the conditions; below the crude oil pour point temperature (i.e 10, 15, and 20°C), around the pour point (i.e. 25°C), around the WAT (30°C), and above WAT (35 and 40°C) respectively.
- Evaluation of the dependency of wax deposition at a different volumetric flow rate of crude oil, at 2, 3, 5, 7, 9 and 11 l/min, at two different coolant temperature 15°C (below PP) and 30°C (at the WAT) and experimental period of 2 hrs. The flow rate covers both laminar to turbulent flow regime conditions; including 2, 3, 5, and 7 l/min that was found to be under laminar, whereas, 9 and 11l/min falls under turbulent flow regime. See Table D1Table D 2 (Appendix D) for the computed results.
- Examination of the consequence of the experimental period (2, 4, 6, and 8 hours) on wax deposit thickness at a constant coolant temperature of 25°C and flow rate of 7 l/min.
- Study the effect of blend ‘A’ inhibitor on wax deposit thickness at different concentrations (500, 1000, 1300, 1500 and 1800-ppm), constant ageing period of 2 hrs, varied flow rate (5, 7, 9 and 11 l/min) and coolant temperature (15, 25 and 30 °C) in straight pipeline. The concentration was varied to determine the optimal

value that gives higher inhibition efficiency. However, in the flow rig with the bent pipeline, the concentrations used were 500, 1000 and 1500-ppm.

- Examine the effect of switching the bent pipelines from horizontal flow to an inclined flow on wax deposition at the constant ageing period of 2 hrs and varied coolant temperature (15, 25 and 30 °C) and flowrate (5, 7, 9 and 11 l/min).

Table 3-5 and Table 3-6 showed the test matrix for the crude oil experiment without inhibitor for straight pipe and pipeline test-section with 45° bend (Figure 3-10) and 90° bend (Figure 3-12).

Table 3-5: Experimental test matrix for crude oil without chemical inhibitor in a straight pipe test-section

No of Tests	Objective	Variable Conditions			
2	Effect of DT	T _{cool} =15°C	Qo;5&9 l/m	t = 2 hr	T _{oil} = WAT + 15°C
2	Effect of DT	T _{cool} =20°C	Qo;5&9 l/m	t = 2 hr	T _{oil} = WAT + 15°C
2	Effect of DT	T _{cool} =25°C	Qo;5&9 l/m	t = 2 hr	T _{oil} = WAT + 15°C
2	Effect of DT	T _{cool} =30°C	Qo;5&9 l/m	t = 2 hr	T _{oil} = WAT + 15°C
2	Effect of DT	T _{cool} =35°C	Qo;5&9 l/m	t = 2 hr	T _{oil} = WAT + 15°C
2	Effect of DT	T _{cool} =40°C	Qo;5&9 l/m	t = 2 hr	T _{oil} = WAT + 15°C
2	Effect of Flow Rate	Qoil=2 L/m	T _c ;15&30°C	t = 2 hr	T _{oil} = WAT + 15°C
2	Effect of Flow Rate	Qoil=3 L/m	T _c ;15&30°C	t = 2 hr	T _{oil} = WAT + 15°C
2	Effect of Flow Rate	Qoil=4 L/m	T _c ;15&30°C	t = 2 hr	T _{oil} = WAT + 15°C
2	Effect of Flow Rate	Qoil=5 L/m	T _c ;15&30°C	t = 2 hr	T _{oil} = WAT + 15°C
2	Effect of Flow Rate	Qoil=7 L/m	T _c ;15&30°C	t = 2 hr	T _{oil} = WAT + 15°C
2	Effect of Flow Rate	Qoil=9 L/m	T _c ;15&30°C	t = 2 hr	T _{oil} = WAT + 15°C
2	Effect of Flow Rate	Qoil=11 L/m	T _c ;15&30°C	t = 2 hr	T _{oil} = WAT + 15°C
6	Effect of deposition Time	t = 2 hours	Qo;5&9l/min	T _c ;15,25&30 °C	T _{oil} = WAT + 15°C
6	Effect of deposition Time	t = 4 hours	Qo;5&9l/min	T _c ;15,25&30 °C	T _{oil} = WAT + 15°C
6	Effect of deposition Time	t = 6 hours	Qo;5&9l/min	T _c ;15,25&30 °C	T _{oil} = WAT + 15°C
6	Effect of deposition Time	t = 8 hours	Qo;5&9l/min	T _c ;15,25&30 °C	T _{oil} = WAT + 15°C

Table 3-6: Experimental test matrix for crude oil without inhibitor in flow rig equipped with two test-sections incorporates 45° and 90° bend

Test	Objective	Variable Conditions				Flow-Through Test Section with Bend	
24	Effect of ΔT, Flow Rate	T _{cool} =15,25&30°C	Qoil = 5,7,9&11l/min	t=2hr	T _{oil} =45°C	45° Horizontal	90° Horizontal
16	Effect of ΔT, Flow Rate	T _{cool} =15&30°C	Qoil = 5,7,9&11l/min	t=2hr	T _{oil} =45°C	45° Inclined	90° Inclined

However, the tables below showed a test matrix of experiment with a blend ‘A’ wax inhibitor in a straight pipe and pipeline with 45° bend test-sections.

Table 3-7: Experimental test matrix for crude oil with blend ‘A’ wax inhibitor in straight pipeline test-section

Test	Objective	Concentration	Variable		Conditions	
1	Effect of wax Inhibitor	500 ppm	Qoil = 5 L/m	Tcool = 15	t = 2 hr	T _{oil} = 45°C
1	Effect of wax Inhibitor	1000 ppm	Qoil = 5 L/m	Tcool = 15	t = 2 hr	T _{oil} = 45°C
1	Effect of wax Inhibitor	1300 ppm	Qoil = 5 L/m	Tcool = 15	t = 2 hr	T _{oil} = 45°C
1	Effect of wax Inhibitor	1500 ppm	Qoil = 5 L/m	Tcool = 15	t = 2 hr	T _{oil} = 45°C
1	Effect of wax Inhibitor	1800 ppm	Qoil = 5 L/m	Tcool = 15	t = 2 hr	T _{oil} = 45°C
1	Effect of wax Inhibitor	500 ppm	Qoil = 7 L/m	Tcool = 15	t = 2 hr	T _{oil} = 45°C
1	Effect of wax Inhibitor	1000 ppm	Qoil = 7 L/m	Tcool = 15	t = 2 hr	T _{oil} = 45°C
1	Effect of wax Inhibitor	1300 ppm	Qoil = 7 L/m	Tcool = 15	t = 2 hr	T _{oil} = 45°C
1	Effect of wax Inhibitor	1500 ppm	Qoil = 7 L/m	Tcool = 15	t = 2 hr	T _{oil} = 45°C
1	Effect of wax Inhibitor	1800 ppm	Qoil = 7 L/m	Tcool = 15	t = 2 hr	T _{oil} = 45°C
1	Effect of wax Inhibitor	500 ppm	Qoil = 11 L/m	Tcool = 15	t = 2 hr	T _{oil} = 45°C
1	Effect of wax Inhibitor	1000 ppm	Qoil = 11 L/m	Tcool = 15	t = 2 hr	T _{oil} = 45°C
1	Effect of wax Inhibitor	1300 ppm	Qoil = 11 L/m	Tcool = 15	t = 2 hr	T _{oil} = 45°C
1	Effect of wax Inhibitor	1500 ppm	Qoil = 11 L/m	Tcool = 15	t = 2 hr	T _{oil} = 45°C
1	Effect of wax Inhibitor	1800 ppm	Qoil = 11 L/m	Tcool = 15	t = 2 hr	T _{oil} = 45°C

Table 3-8: Experimental test matrix for crude oil with blend ‘A’ wax inhibitor in the pipeline with 45° bend test-section

Test	Objective	Concentration	Variable		Conditions	
1	Effect of wax Inhibitor	500 ppm	Qoil = 5 L/m	Tcool = 15	t = 2 hr	T _{oil} = 45°C
1	Effect of wax Inhibitor	1000 ppm	Qoil = 5 L/m	Tcool = 15	t = 2 hr	T _{oil} = 45°C
1	Effect of wax Inhibitor	1500 ppm	Qoil = 5 L/m	Tcool = 15	t = 2 hr	T _{oil} = 45°C
1	Effect of wax Inhibitor	500 ppm	Qoil = 7 L/m	Tcool = 15	t = 2 hr	T _{oil} = 45°C
1	Effect of wax Inhibitor	1000 ppm	Qoil = 7 L/m	Tcool = 15	t = 2 hr	T _{oil} = 45°C
1	Effect of wax Inhibitor	1300 ppm	Qoil = 7 L/m	Tcool = 15	t = 2 hr	T _{oil} = 45°C
1	Effect of wax Inhibitor	500 ppm	Qoil = 11 L/m	Tcool = 15	t = 2 hr	T _{oil} = 45°C
1	Effect of wax Inhibitor	1000 ppm	Qoil = 11 L/m	Tcool = 15	t = 2 hr	T _{oil} = 45°C
1	Effect of wax Inhibitor	1300 ppm	Qoil = 11 L/m	Tcool = 15	t = 2 hr	T _{oil} = 45°C

3.8 Quantification of Deposit Wax Thickness

Generally, wax deposition is quantified in thickness, mass and volume. There are different methods used to determine deposit thickness in the pipeline. In this study, four techniques were selected based on previous studies. These include the pressure drop method, weight–balance and volume correlation methods, heat transfer method

(Chen *et al.*, 1997; Hoffmann and Amundsen, 2010; Chi *et al.*, 2017; and Rittirong *et al.*, 2017; Theyab, 2017b) and wet film-thickness gauge method (Panacharoensawad and Sarica, 2013; Rittirong *et al.*, 2016). These techniques were reported to be suitable in single-phase conditions, which are considered fundamental in this study. However, these techniques are inadequate in multiphase flow conditions, due to the increase in uncertainty especially in predicting pressure and temperature gradients (Sarica and Volk, 2004; Chen *et al.*, 1997). Some of the parameters required for calculating the thickness are shown in Figure 3-16.

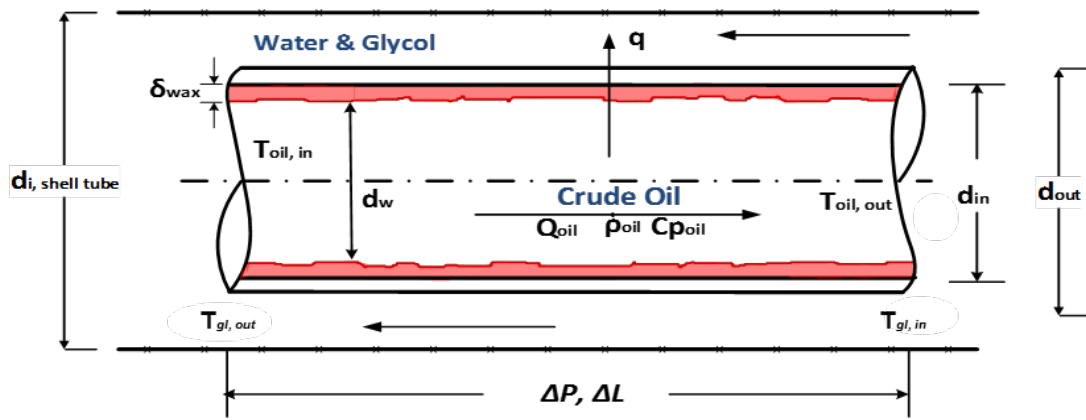


Figure 3-16: A Segment of Pipe-in-Pipe Cross Section with different Parameters (adapted from Sarica and Volk, 2004): The crude oil flow in the inner section of the pipe whereas, the mixture of water and glycol (coolant) flow in the shell section of the jacked pipe.

Where δ_w is deposit wax thickness, d_w is effective internal diameter after deposition, d_{in} is the inner pipe diameter, d_{out} is the outer pipe diameter, C_p is the specific heat capacity of oil and T_{gl} the temperature of glycol mixture.

3.8.1 Pressure Drop Method

This is considered as an online method for quantifying wax thickness in the pipeline, which does not require interrupting the flowline, depressurisation or restart of the system (Chen *et al.*, 1997; Botne, 2012). The method is one of the most reliable techniques, especially in a single-phase flow (suitable for this study) and was extensively used by several researchers (such as Hoffmann and Amundsen, 2010; Singh *et al.*, 2011; Panacharoensawad and Sarica, 2013; Rittirong *et al.*, 2017; and Adeyanju and Oyekunle, 2013). However, pressure drop method is not suitable when the frictional pressure drop is very low and for multiphase flow due to the

complex character of pressure loss (Chen *et al.*, 1997; Huang *et al.*, 2011; Rittirong, 2014).

The deposit thickness is back-calculated using the Eq. 3.15 (Chen *et al.*, 1997) once the pressure drop across the test section, the flow rate, density and viscosity of the crude oil are known. In the equation, the pressure drop is related to the diameter of the pipe and the wax thickness. This is significant because as the wax deposit builds-up on the pipe wall, the effective diameter reduces that led to anomalies in the system (Chen *et al.*, 1997; Bai and Bai, 2005). Therefore, the thickness equation was derived from a well-known frictional pressure drop equation (Chen *et al.*, 1997).

$$\Delta P_f = 4f \frac{L}{d} \frac{\rho}{2} \left(\frac{4Q}{\pi d^2} \right)^2 \quad (3.9)$$

f , is the frictional factor, Q is the volumetric flow rate and ρ is the fluid density.

The friction factor is defined as $f = \frac{c}{(Re)^n}$ (3.10)

Whereas, Reynolds number is defined as

$$Re = \frac{v\rho d}{\mu} = \frac{4\rho Q}{\pi\mu d} \quad (3.11)$$

$$Q = \frac{v\pi d^2}{4}$$

Substituting the above relationship into Eq. 3.9

$$\Delta P_f = \frac{4c\rho L(\pi\mu d)^n}{2(4\rho Q)^n d} \left(\frac{4Q}{\pi d^2} \right)^2 \quad (3.12)$$

Re-arranging and collect the like term gives

$$\Delta P_f = \frac{2c\rho L}{d^{5-n}} \left(\frac{\mu}{\rho} \right)^n \left(\frac{4Q}{\pi} \right)^{2-n} \quad (3.13)$$

This implies that any reduction of the effective inside diameter (d) of the pipeline causes an increase in the frictional pressure drop across the pipe section, which increases the fluid velocity and d in the above equation is new or the reduced diameter of the pipe due to deposit wax. Therefore, from Figure 3-16, $d = d_w = d_i - 2\delta_w$,

$$\text{Hence,} \quad (d_i - 2\delta_w)^{5-n} = \frac{2c\rho L}{\Delta P_f} \left(\frac{\mu}{\rho}\right)^n \left(\frac{4Q}{\pi}\right)^{2-n} \quad (3.14)$$

Where δ_w is the average thickness of the deposited wax, d_i and μ are the bore inside diameter of the pipe and the apparent viscosity of the crude oil, c and n are constant parameters; for laminar flow ($NRe < 2100$), $c = 16$ and $n = 1$ while for turbulent flow $c = 0.046$ and $n = 0.2$ ($NRe > 2100$) (Chen et al., 1997).

$$\therefore \delta_w = \frac{d_i - \left(\frac{2c\rho L}{\Delta P_f} \left(\frac{\mu}{\rho}\right)^n \left(\frac{4Q}{\pi}\right)^{2-n}\right)^{\frac{1}{(5-n)}}}{2} \quad (3.15)$$

However, Eq. 3.15 is particularly essential for calculating wax deposit thickness in a straight pipeline since only the frictional pressure loss across the pipeline was considered in the deposition process (Chen *et al.*, 1997; Burger *et al.*, 1981). Hence, in this study, this equation was used in the cases where the wax deposition was studied with straight pipe test section.

On the other hand, apart from the frictional pressure loss as a result of resistance to flow; the flow of fluid through a pipeline with bend experiences other abnormalities caused by the change in the direction of the flow. Similarly, pressure loss could be increased by the increase in elevation— i.e. hydrostatic pressure, due to the gravitational effect. Consequently, in the elevated pipe, there is more pressure at a lower fluid elevation due to the increased depth and weight of the fluid above the reference point, and vice versa. As described in chapter 2, the fluid around the pipe bend is primarily characterised by flow instability, separation, and strong secondary current (Dean, 1927; Sreenivas, 2011; Murty and Thandaveswara, 2014; Dutta *et al.*, 2016; Vester *et al.*, 2016). Hence, a new model (Eq. 3.16) was derived following the studies by Sreenivas (2011) and Prajapati *et al.* (2015). The equation incorporated all the curvature parameters that cause instabilities. Details of the mathematical correlations and more descriptions of the extent to which these parameters influence the flow and cause instability are given in section 5.4.1.

$$\delta_w = \frac{d_i - \left[\left(\frac{1}{\Delta P}\right) \left[(128Q\mu) \left(\frac{\theta R_b}{180}\right) + \frac{8Q^2 k_b \rho}{\pi^2}\right]\right]^{\frac{1}{4}}}{2} \quad (3.16)$$

Where μ is the viscosity of the fluid, R_b , the bend radius; θ , the bend angle; and k_b , the bend loss coefficient obtained from Babcock & Wilcox chart. On the other hand, Eq. 3.16 can be further modified by including the parameters of hydrostatic pressure drop due to the gravitational effects.

3.8.2 Weight–Balance and Volume Correlation Method

Weight balance is another typical method applied in a single-phase flow and under low-pressure wax deposition study (Chen *et al.*, 1997; Matzain *et al.*, 2002). Hence, the method is suitable for this work, which requires a complete shutdown of the system to “take-out” the removable test section from the flow rig. The published experimental results by Hoffmann and Amundsen (2010) and Panacharoensawad and Sarica (2013) has shown that the weight balance and the back-calculation from the pressure drop methods produced roughly the same wax thickness.

Unlike, pressure drop method, weight balance involves careful and precise measurement of the deposit weight by pigging the solid wax and melting the remaining wax that might be stuck on the wall after pigging operation. Before the pigging procedure and melting, the test section is tilted and positioned for about 5 – 10 minute to drain any residual oil that remains on the deposit surface. In some cases, the removable section is weighed two to three-times after the experiment and work out the difference with the original weight of the empty pipe section, as previously revealed by Hunt Jr (1962). A sample of pigging operation showing the solid wax pushed out of the pipe section and the layers of wax thickness are presented in chapter 5. Equation (3.24) shows the deposit thickness equation used by different researchers (Hoffmann and Amundsen, 2010; Panacharoensawad and Sarica, 2013; Chen *et al.*, 1997; Matzain *et al.*, 2002). Starting from the correlations below (Figure 3-16);

$$m_{total} = m_{wax} + m_{oil} \quad (3.17)$$

Similarly
$$m_{wax} = V_{wax} \rho_{dep} \quad (3.18)$$

$$V_{wax} = V_{inner\ of\ pipe} - V_{reduce,\ due\ to\ wax} \quad (3.19)$$

$$V_{wax} = (\pi R_{in}^2 - \pi R_{red}^2)L \quad (3.20)$$

Note
$$\delta_w = R_{in} - R_{red} \quad (3.21)$$

$$V_{wax} = \pi[R_{in}^2 - (R_{in} - \delta_w)^2]L \quad (3.22)$$

$$\frac{m_{wax}}{\rho_{dep}L\pi} = R_{in}^2 - (R_{in} - \delta_w)^2 \quad (3.23)$$

$$\delta_w = R - \sqrt{R^2 - \frac{M_{dep}}{L\pi\rho_{dep}}} \quad (3.24)$$

δ_0 is added as the excess oil layer thickness due to residual oil

$$\therefore \delta_w = R - \sqrt{R^2 - \frac{M_{dep}}{L\pi\rho_{dep}}} - \delta_0 \quad (3.25)$$

However, δ_0 is usually assumed to be negligible (Hoffmann and Amundsen, 2010; Panacharoensawad and Sarica, 2013). Where δ_w is the actual deposit thickness, R is the inner pipe radius, M_{dep} is the deposit weight, L is the length of the test section, and ρ_{dep} is the deposit of deposit. The M_{dep} of 915 kg/m³ is used for the thickness calculation, which was predicted obtained from Multiflash (see Section 3.9.1 and Appendix B, Table B1) using the actual crude oil properties.

On the other hand, the volume method was reported by Theyab (2017). The volume of deposit was obtained by measuring the volume of the pipe before and after the deposition. Therefore, the volume of wax that will drop out of the system is related to the deposit thickness as follows:

$$V_{wax} = V_{inner} - V_{reduce, \text{ due to wax}} \quad (3.26)$$

Where $V_{inner} = \frac{\pi d_{in}^2}{4}L$, and $V_{reduce} = \frac{\pi d_{reduce}^2}{4}L$

$$\therefore V_{wax} = \frac{\pi L}{4} (d_{in}^2 - d_{reduce}^2) \quad (3.27)$$

Re-call: $d_{red} = d_{in} - 2\delta_w$,

Or from Eq. 3.22 $V_{wax} = \pi[R_{in}^2 - (R_{in} - \delta_w)^2]L$

From Eq. 3.27 $(d_{in}^2 - d_{red}^2) = \frac{4V_{wax}}{\pi L}$ (3.28)

$$(d_{in} - d_{red}) = \sqrt{\frac{4V_{wax}}{\pi L}} \quad (3.29)$$

$$d_{red} = d_{in} - 2 \sqrt{\frac{V_{wax}}{\pi L}} \quad (3.30)$$

$$d_{in} - 2\delta_w = d_{in} - 2 \sqrt{\frac{V_{wax}}{\pi L}}$$

Hence,

$$\delta_w = \sqrt{\frac{V_{wax}}{\pi L}} \quad (3.31)$$

Where V_{wax} , is the volume of wax that drops out of the system.

3.8.3 Energy–Balance Method

The process of wax deposition has been described as a non-isothermal driven by the heat flux between the flowing fluids and the surroundings (Lashkarbolooki *et al.*, 2011). An acceptable and accurate wax thickness can be achieved using energy balance method as long as the temperature measurement, deposit thermal conductivity, film heat transfer coefficients on the inside and outside pipe walls are adequately known (Chen *et al.*, 1997; Hernandez, 2002; Sarica and Panacharoensawad, 2012). However, the major difficulty in applying the heat-transfer method is uncertainties from temperature measurement and the value of thermal conductivity of the deposit, which depended on wax content analysis (Huang *et al.*, 2011; Wang and Huang, 2014). Prior to the formation of wax deposit layer on the pipe surface, there is a total resistance to heat transfer from the bulk fluid to the surrounding area, which comprises; (i) the resistance due to heat transfer by convection between the flowing fluid and the pipe wall, (ii) the heat transfer by conduction between the pipe wall and the insulation materials and the appropriate heat transfer between the pipe and the environment (Chen *et al.*, 1997).

However, as the deposition begins, it creates a thermal resistance due to the heat conduction through the deposit. And the convective heat transfer takes place at the interface between the flowing fluids and the layer of deposited wax. Therefore, a thermal resistance term due to conduction within the layered wax is added to the total resistance to the overall resistance to heat transfer (Chen *et al.*, 1997). This added thermal resistance is approximately proportional to the wax thickness layer. Hence, Eq. 3.32 (Chen *et al.* 1997; Sarica and Volk, 2004; Lashkarbolooki *et al.*, 2011) was

used to calculate the layer's thickness by measuring the crude oil and coolant temperatures and performed heat balance.

$$\frac{1}{U_{gly}} = \frac{1}{h_{oil}} \frac{r_o}{r_i - \delta_w} + \frac{r_o}{k_w} \ln \frac{r_i}{r_i - \delta_w} + \frac{r_o}{k_p} \ln \frac{r_o}{r_i} + \frac{1}{h_{gly}} \quad (3.32)$$

Where δ_w is the thickness of the wax layer. r_o and r_i are the outside and inside of the pipe radius. h_{oil} and h_{gly} are the convective heat-transfer coefficient of the oil and the convective heat-transfer coefficient of the cold fluid (a mixture of glycol and water). k_p and k_w are the thermal conductivity of pipe and the deposit thermal conductivity respectively. k_w , is assumed to be equal for the waxy crude oil. Whereas, U_{gly} is the overall heat-transfer coefficient calculated from the total heat-transfer rates in the test section defined by

$$Q = U_{gly} A_{gly} \Delta T_{lm} = m_{oil} C_{p_{oil}} (T_{oil(in)} - T_{oil(out)}) \quad (3.33)$$

Where $A_{gly} = \pi d_o L$, $C_{p_{oil}}$ is the specific heat capacity of oil and ΔT_{lm} is the log mean temperature difference in the heat exchange region. For a countercurrent heat exchanger, ΔT_{lm} is written as

$$\Delta T_{lm} = \frac{(T_{oil(in)} - T_{gly(out)}) - (T_{oil(out)} - T_{gly(in)})}{\ln \left(\frac{T_{oil(in)} - T_{gly(out)}}{T_{oil(out)} - T_{gly(in)}} \right)} \quad (3.34)$$

According to Lashkarbolooki et al. (2011) and Sarica and Volk (2004), the inside (oil) convective heat-transfer coefficient (h_{oil}) in Equation 3.35 is defined according to the two correlations describes below,

$$h_{oil} = \frac{N_{Nu,o} k_w}{d_w} \quad (3.35)$$

Where d_w is the diameter of the pipe open to flow. Equation 3.36 defined $N_{Nu,o}$ for laminar flow conditions (Hausen correlation 1973), while Equation 3.37 Sieder and Tate correlation (1936) for turbulent flow.

$$N_{Nu,o} = 3.66 + \frac{0.19(N_{pe} \frac{d_w}{L})^{0.8}}{1 + 0.117(N_{pe} \frac{d_w}{L})^{0.467}} \quad (3.36)$$

$$N_{Nu,o} = 0.023 + N_{Re}^{0.8} N_{pr}^{1/3} \left(\frac{\mu_{o,b}}{\mu_{o,w}} \right)^{0.14} \quad (3.37)$$

Where $N_{pe} = N_{Re}N_{pr}$ and $N_{pr} = \frac{\mu_o C_{p_{oil}}}{k_{oil}}$.

On the other hand, the outside (glycol) heat transfer coefficient, h_{gly} , is calculated using the Petukhov correlation (1970).

$$h_{gly} = \frac{N_{Nu,gly} k_{gly}}{d_{i,gly} - d_o} \quad (3.38)$$

Where $d_{i,gly}$ is the internal diameter of the shell pipe and d_o is the outer diameter of the pipeline. Whereas, $N_{Nu,o}$ is calculated using the Equation below

$$N_{Nu,gly} = \frac{\left(\frac{f}{8}\right) N_{Re} N_{pr}}{1.07 + 12.7 \sqrt{\frac{f}{8}} (N_{pr}^{2/3} - 1)} \left(\frac{\mu_{gly,b}}{\mu_{gly,w}}\right)^\eta \quad (3.39)$$

Where f is the friction factor defined as $f = (1.82 \log_{10} N_{Re} - 1.64)^{-2}$. The ratio of viscosities (Eq.) is assumed to be equal to 1.25 and $\eta = 0.25$ (Lashkarbolooki *et al.*, 2011).

3.8.4 Wet Film-Thickness Gauge

Panacharoensawad and Sarica (2013), Rittirong *et al.* (2016) and Rittirong *et al.*, (2017) have used this method to measure the wax thickness using a dip-type wet film thickness gauge. However, according to the ASTM D 4414 standard, the original purpose of this type of gauge is to measure the wet paint film thickness. Nevertheless, previous studies have managed to carefully measure the local thickness of deposit wax by inserting the dip-type film gauge into the test section. In this study, similar equipment was used and measured the thickness at three different locations— inlet, outlet and midpoint— 500mm apart. The dip-type wet film thickness gauge is attached with a long handle to measure the deposit thickness inside the test section. Pictures of the dip-type wet film thickness gauge are shown in Figure 3-19.

The gauge was inserted into the test section and dip on the deposit surface slowly to perform the measurement. As the tick mark of the scale was perpendicular to the surface a small mark is created on the deposit surface. When the gauge was dipped into the deposit, some teeth of the gauge were coated with oil from the deposit. At that point, the gauge is dragged horizontally to allow the teeth that touch the deposit pick up more mass onto the teeth. Once the measurement with the dip-type gauge is done, the deposit thickness was determined to be in between the most prominent vale

coated or wet tooth and the next shortest tooth that was not covered with oil (Panacharoensawad and Sarica, 2013).

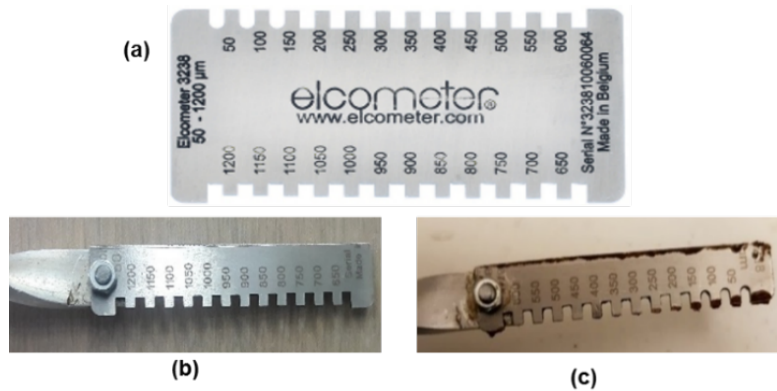


Figure 3-17: (a) Dip-type wet film thickness gauge scaled from 50 – 1200 μm (<https://www.elcometer.com>). (b) Constructed dip-type wet film thickness gauge scaled from 650 – 1200 μm attached with a long handle. (c) Constructed gauge scaled from 50 – 600 μm with measured deposit thickness from the test section.

3.9 OLGA: Multiphase flow simulator

In general, OLGA is used for modelling and simulation of wax deposition problem. The use of OLGA in the oil and gas field has become a norm in designing strategies that could manage or prevent flow assurance problem. The practice is real, especially when the experimental laboratory cases indicates the presence of wax, and when the wax appearance temperature (WAT) is within the wax envelope (SPT Group, 2015). Hence, as shown in the properties Table 4.1, the wax content of the three crude oil samples A, B and C are higher (11.5, 19.7 and 15.3 wt%), which consequently could lead to a serious depositional problem during production. However, in the simulation study, sample B crude oil and *OLGA: multiphase flow simulator* was used for validation of the experimental results.

The three existing wax deposition models in OLGA (RRR, Matzain, Heatanalogy) are used to comparative analysis. Therefore, it is essential to model the temperatures (heat transfer) accurately to achieve accurate simulation. One of the goals of this study is to be able to replicate the actual heat transfer condition used in the experimental conditions for validation purposes. As such, the surroundings conditions of the pipeline such as the inlet and out cooling temperature, the heat transfer coefficient h_{gly} (coolant fluid) and other critical experimental parameters (WAT, PP and SARA) are vital. Therefore, one of the three existing options in the

OLGA software was selected, i.e. to specify properties of the ambient fluid (HOUTEROPTION=OTHER / WATER / AIR, requires TEMPERATURE=WALL in OPTIONS). This option allows the user to control the ambient conditions and the heat transfer to fit a specific study. Accordingly, water is used as coolant similar to the experiment.

OLGA calculates the outer heat transfer coefficient by specifying the following as input data: (i) the minimum heat transfer coefficient (HMININNERWALL) of water (0 W/m²-C, default value). (ii) The speed of the ambient fluid at the inlet and outlet of the pipe section (INVELOCITY and OUTVELOCITY), which is constant at 0.13 m/s (i.e. 11 l/m) and (iii) the ambient temperature as the inlet and outlet boundary temperature (INTAMBIENT and OUTTAMBIENT). After that, OLGA performed interpolation based on the input conditions to predict a linear temperature profile for the distance along the pipeline. However, the outer heat transfer coefficient is not affected by the interpolation (SPT Group, 2015), which is calculated using Eq. (3.38).

3.9.1 Crude Oil Properties for Wax Table and PVT Table files

Wax table file (.wax) and PVT table files (.tab) are the two most essential table files required to run a simulation study using OLGA. These files contained all the properties of wax forming components and PVT parameters. In this study, a fluid package called Multiflash 4.3 version was used to generate the table files. Multiflash is a tool embedded within the OLGA software, which is designed specifically for fluid characterization using a thermodynamic wax model known as *Coutinho solid solution model*. This model is applicable to both live and dead oils and presented wax as a single solution (OLGA, 2014). Similarly, *Multiflash* was used to understand the waxing behaviour of crude oil and predicts both wax appearance temperature, the amount of wax precipitated at different temperatures and other properties such as deposit density.

The input parameters required to flash a sample crude include the oil compositions and its properties, e.g. the n-paraffins pseudo-components i.e. those with 15 carbon number or higher (defined as the main forming wax fractions in the fluid model). Other parameters are the density of oil, SARA fractions, wax content, API and WAT

(Table 4.1). Also, the files the system temperature and pressure ranges. Therefore, the temperature ranges between -5 to 150°C and pressure between 5 psi (< 0.5 bar) to 1000 psi (69 bar) respectively. Note that, in the experimental study, the lowest temperature and pressure are 15°C and <1bar. However, in the real field, a negative temperature is reported and can be up to 69 bar.

Based on the above data, Multiflash generates other unknown properties of wax and oil, presented in Appendix B “table files” (Table B1Table B 2Table B 3). These include enthalpy, density and entropy of the liquid and the wax phase. Similarly, the continuous distribution of n-paraffin single carbon number (SCN) species, the wax precipitation envelops as a function of pressure and temperature, and the PVT phase envelop are generated. Some of these parameters are compared with the experimental results (see Chapter 6). However, unlike other studies (e.g. Theyab, 2017), a good prediction (e.g. WAT, SCN with n-Paraffin) was achieved without further tuning from experimental data.

3.9.2 Wax Deposition Simulation and Sensitivity Analysis

The simulation study is carried out using the actual experimental matrix, and the flow rig boundary conditions. However, some data (e.g. wax porosity) are from SPT Group (2015). Two of the experimental flow rig sections– a straight pipeline and pipe with 45-degree bend and elevation are considered in this study. Initially, a base case simulation was created using the straight pipeline of 1000 mm long. However, the pipeline was extended to about 7000 mm (i.e. 600 mm extra length) for a more developed flow in the simulator. Figure B1Figure B2 (Appendix B) shows the two pipeline geometry before adding the extra length. However, the 45-degree curved pipe with elevation is replicated in the simulator by considering an elevation only. This is the only practical approach to mimic the flow rig section in the OLGA simulator. Therefore, an elevation of 350 mm was used as described in section 3.5. A copper pipe material was used for all the flow path. The crude oil is allowed to enters the flow line at a constant temperature of 45°C (above WAT) and constant mass flow rate according to the matrix. Other input parameters include the wax porosity, copper pipe heat capacity, thermal conductivity, density, roughness, diameter and thickness (reported in section 3.5.1.1).

After flow path and material definition, wax deposition option was turned ON in the model browser of the OLGA, and the RRR model was selected. Whereas, a steady-state in the OPTION is turned OFF. The wax diffusion coefficient multiplier is set to 1 (the default value); however, the contribution of the deposited wax to the wall roughness is not considered, i.e. WAXROUGHNESS=0 by default. The porosity of wax 0.6 (default value) and the simulation end time (hours) was varied. See Appendix B for further details on the steps.

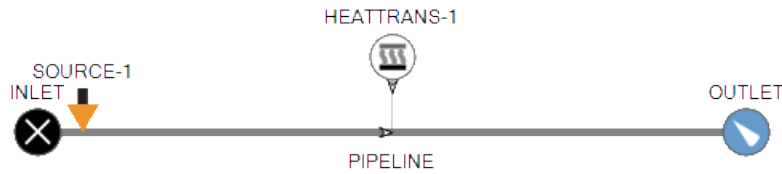


Figure 3-18: Single flow path diagram in the OLGA software with closed inlet node where the source is located and the heat transfer source around the flow line and a pressure outlet node.

Before the simulation study, sensitivity analysis is carried out to determine the appropriate wax porosity (%)– between 0.6, 0.8 and 0.9 based on the previous studies and models (between RRR, Matzain and Heat analogy) that would best predict the appropriate wax deposition behaviour with reference to the experimental results. Thereafter, the study investigates the influence of different parameters including the oil flow rate between 5 and 11 l/min (i.e. mass flow rate 0.07, and 0.15 kg/s), which are within the laminar and turbulent flow regimes. Three wax porosity of 0.6, 0.8 and 0.9 based on the previous studies and finally, the impact of varying coolant temperature (15 and 25⁰C). The results predicted from the simulation are then compared with the experiment.

Chapter 4

Results and Discussion

Analysis of Crude Oil Characteristics and Effect of Inhibitor on Rheological Properties

4.1 Introduction

Undoubtedly, a full evaluation of waxy crude oil's properties is challenging. However, it is crucial to examine the main fundamental crude oil compositional properties of fluid before the flow rig study, in order understand the depositional behaviour as well as to select the best mitigation and/or prevention strategy. Therefore, the analysis of results presented in this chapter include the API gravity, density, SARA fractions, pour point, wax appearance temperature, viscosity, n-Paraffin distribution and colloidal instability index (CII). Similarly, a study of the crude oil structural network below and above wax appearance temperature, doped and un-doped with chemical inhibitor are also carried out. Also, the chapter presented the results of the study of a new blended wax inhibitor, which proven to be effective and better than the commercial inhibitors (Makwashi *et al.*, 2019b).

The analysis of the API gravity, density and the specific gravity of the samples (Section 4.2) reveal that sample A is heavier than samples B and C. However, higher wax content is found in sample B crude oil (19.7 wt%) compared to A and C (12.05 and 15.3 wt%) as discussed in Section 4.3. SARA fractions of the samples (Section 4.4) indicate the presence of high saturates in all the three samples; sample B having the highest value. The results in Section 4.5 show the rheological properties including the viscosity, WAT (28.5, 30 and 25.5°C) and the pour point (23, 25.5 and 14°C) for sample A, B and C. The results in Section 4.7 show the n-paraffin distribution; sample A contains high fractions of macro-crystalline (C18 to C36) components than the other sample. The morphological analysis of samples in Section 4.6 shows the presence of the needle-like or rod-like particles. However, the

presence of blend A wax inhibitor affects the structure of the wax crystals, which is transformed from needle-like or rod-like to agglomerate to small particles dispersed in the oil matrix. Given the complexity and heterogeneity of waxy crude oil, the typical behaviour of the crude oil under different shear is studied and the influence of varying wax inhibitors are discussed (Section 4.5.3). The results in this chapter (summarised in Table 4-1) provide a direct observation of the development of micro and macro-structure of wax crystals with and without inhibitor. The physical and chemical measurements from this work serve as valuable input parameters to modelling wax deposition processes.

Table 4-1: Physical and Chemical Properties of Three Crude Oil Samples

Properties	Unit	Crude Oil Sample			Method
		A	B	C	
Appearance		Black	Brown	Black	Visual
Density	kg/m ³ (15°C)	865	835	858	Measurement
Sp. Gravity	60°F/60°F	0.865	0.835	0.858	Calculated
API Gravity	—	32.1°	35°	33.4°	API Method
Wax Content	wt%	11.5	19.7	15.3	Modified UOP 46-64
Wax Content	wt%	12.05	20.05	14 ^a	HTGC (n-C15+)
Pour Point	°C	22	25.5	19.5	Rheometry
Pour Point	°C	23	26	20	Modified ASTM D-97
WAT at 120 1/s	°C	28.5	30	28	Rheometry
WAT at 10 1/s	°C	34	35	30	Rheometry
Viscosity	Pa.s (at 45°C >WAT)	0.0102	0.0056	0.0091	Rheometry
Viscosity	Pa.s (at 15°C <WAT)	2.31	3.89	1.20	Rheometry
Saturates Fraction	wt%	55.04	73.25	63.11	elution chromatography
Aromatics Fraction	wt%	34.67	21.2	31.01	elution chromatography
Resins Fraction	wt%	6.15	5.14	4.15	elution chromatography
Asphaltene Fraction	wt%	4.14	0.41	1.73	Modify ASTM D2007-80
CII	—	1.45	2.798	1.84	Calculated

where the superscript “a” represented the wax content from correlation (see Equation 3.4), Sample A, B and C are the Mwambe, KSG and synthetic crude oil.

4.2 Analysis of API Gravity, Density and Specific Gravity

In general, the API gravity is widely used to describe the crudes oil based on their gravities, which is influenced by the oil composition. According to the American Petroleum Institute (2011) crude oil is divided into heavy and light crudes. Hence, the lighter the crude oils are usually less dense and possess high API gravities (gravity $> 33^{\circ}\text{API}$), high paraffinic content and high amount of dissolved gases. Whereas, the denser crudes are those with low API gravity ($< 28^{\circ}\text{API}$), more asphaltenes, high aromatic/naphthenic content and a small amount of dissolved gas fractions (American Petroleum Institute, 2011; Sifferman, 1979).

In this work, the API gravity of crude oil samples (A, B and C) is 32.1, 35 and 33.4 $^{\circ}\text{API}$. As seen in Figure 4-1, sample A is relatively denser with a density value of 865 kg/m³ than samples B and C (835 and 858 kg/m³). The high-density value in sample A resulted in the lowest API value among the samples. This could be due to the higher fraction of asphaltene with low presence of the light component.

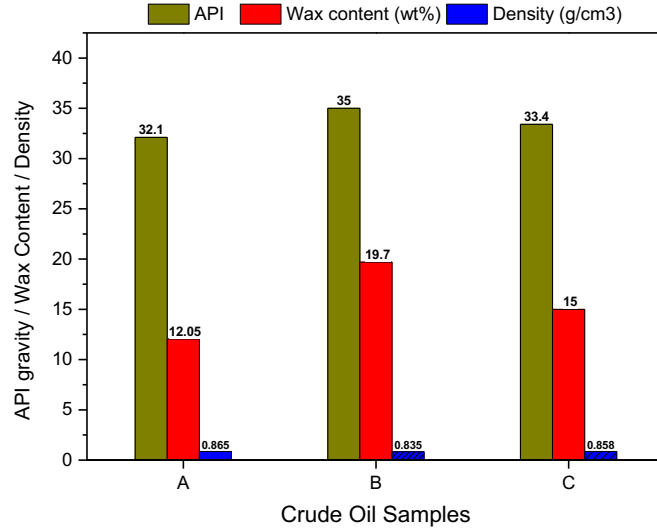


Figure 4-1: Correlation between the API, density, and wax content of three crude oil samples

4.3 Study of Wax Content

In this work, understanding of wax content of the crudes oil is extremely significant. The wax content in need to understand and predicts the severity of deposition phenomenon and model validation purposes. As highlighted in this thesis, a crude oil containing as little as 2% by mass of wax can potentially cause deposition problem

in the flow lines, pipeline, and separators at suitable conditions that favour the process (Holder and Winkler, 1965; Kasumu, 2014). The wax content of crude oil has a linear relationship with the aromatic and saturate fractions of the sample (see Section 4.4), WAT and pour point (see Section 4.5). It is revealed that the higher the wax content of crude oil, the more the presence of a saturating component with a lower amount of aromatic fraction and vice-versa (Ekaputra *et al.*, 2014).

Therefore, In this work, wax content obtained from the modified UOP 46-64 and HTGC method characterised crude oil samples as waxy crudes. As observed from Figure 4-1, sample B crude has higher wax content of 19.7 wt% (UOP 46-64) and 20.05 wt% (HTGC, nC₁₅⁺) compared to sample A that has 11.5 wt% (UOP 46-64) and 12.05 wt% (HTGC, nC₁₅⁺) and sample C with 15.3 wt% (UOP 46-64) and 14 wt% (equation 3.4, Section 3.2.1) respectively. The methods used in this work produced approximately the same result and these methods have been the most reliable in this area (Sarica and Panacharoensawad, 2012). The results in **Figure 4-1** show proved that the higher the high paraffin content, the less dense the oil with high API gravities (gravity > 33°API).

Based on these results, mitigations strategies are necessary during production, transportation or storage of any of these crudes. As the crudes sample in this work is sufficient to cause wax deposition problem.

4.4 Analysis of SARA Fraction

The purpose of this study is to fractionate the crudes samples into – saturate, aromatic, resin and asphaltene. According to Zhu *et al.* (2008), SARA analysis is useful tools in assessing crude oil stability for wax related issues. Studies of individual fraction in crude oil showed that these fractions significantly influence the viscosity, crystallization and deposition of waxes in a production system, transportation and storage (Jewell *et al.*, 1972; Fan *et al.*, 2002; Pierre, 2004; Johnson, 2009).

According to a study by Zhu *et al.* (2008) crude oil with more than 50% fraction of saturates (flocclulants) are most likely to precipitate and deposited wax in the facilities. As shown in Figure 4-2, the crudes samples contained sufficient fractions of saturates, which indicates high paraffin content. As established in the literature,

crude oil with a high content of saturating fraction is regarded as highly unstable (see Section 4.4.1) with respect to wax deposition (Moura *et al.*, 2010).

Therefore, it is observed that the more saturates fractions of the crude oil, the higher the CII and generally, the crude oil become unstable. It is seen that sample B crude oil has high saturates fractions of 73 wt% compared to sample A and C 55.04 and 63.22 wt%. Hence, saturates fractions in crude oil has a linear relationship with the amount of wax content. Therefore, as seen in **Figure 4-2** the crude with high wax content, possessed more saturate fraction (Ekaputra *et al.*, 2014).

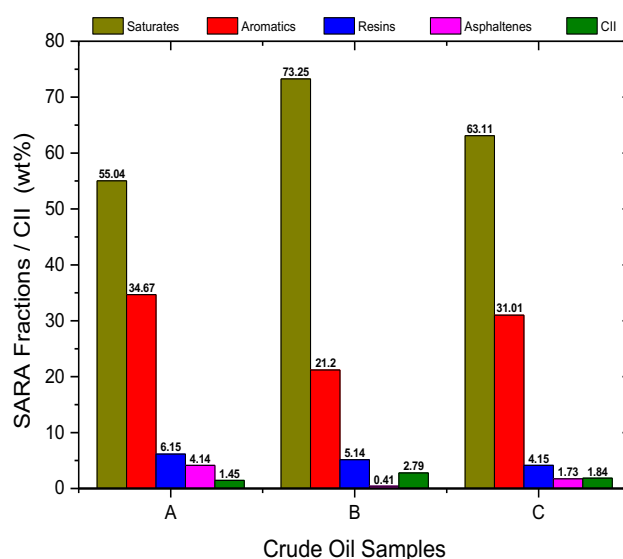


Figure 4-2: SARA fraction of crude oil sample and colloidal instability index (CII).

On the other hand, the aromatic components are more polarizable differently (Ashoori *et al.*, 2017). Therefore, aromatics are a good solvent for asphaltene molecules in crude oil, which acts as a bridge between the mixed micelle and saturates, make the mixed micelles effectively dispersed in saturates (Ashoori *et al.*, 2017; Fan *et al.*, 2002). This mean, sample A with high asphaltene fraction (4.14 wt%) also has higher aromatic component, which serves to retard the gel structuring process via steric interference (Paso, 2014), resulting in a significantly weaker gel structure. Therefore, this fraction weakens the chains of asphaltene, which usually promote the interactions of waxes crystals and generally causes fouling (Chanda *et al.*, 1998; Dickakian and Seay, 1988). It is expected that the oil sample with a higher aromatic component to be more stable with respect to wax deposition (Figure 4-3).

Similarly, resin molecules in crudes oil prevent any significant aggregation of the asphaltenes, as a result. the risk of asphaltene precipitation decreases as the resin content increases (Aske *et al.*, 2002; Pereira *et al.*, 2017). Equally, Paso (2014) reported a study which describes resins natural affinity to paraffin wax crystals in crude oil, which act as natural gelling point depressants. The study postulated that the resins assemble on the wax crystals and inhibit the interlocking process. Therefore, the stability of asphaltene in waxy oil would be improved by the presence of resin and aromatic molecules. As shown in Figure 4-2, the amount of resin in the crude sample A is 4.14 wt% compared to samples B and C that has 0.4 and 1.73 wt% respectively. However, the higher saturate component and low resins and aromatics influence the stability of the crude as discuss in section 4.4.1.

Furthermore, a visual inspection of the SARA fractions was carried out (Figure 4-3). It worth noting that oil samples A and C appeared as black, whereas sample B is brown. The result from the SARA fractions showed that saturated fraction of sample A and C are pale yellow, while sample B is more pure yellow. On the other hand, the aromatic fraction is found to be dark brown liquid, while the resin fraction is Gardner or clear light brown liquid. On the other hand, the asphaltene fraction is found to be coloured black suspended solid. In general, the colours depicted in this Figure agreed with those reported by Benedek (2000) and Odebunmi *et al.* (2002).

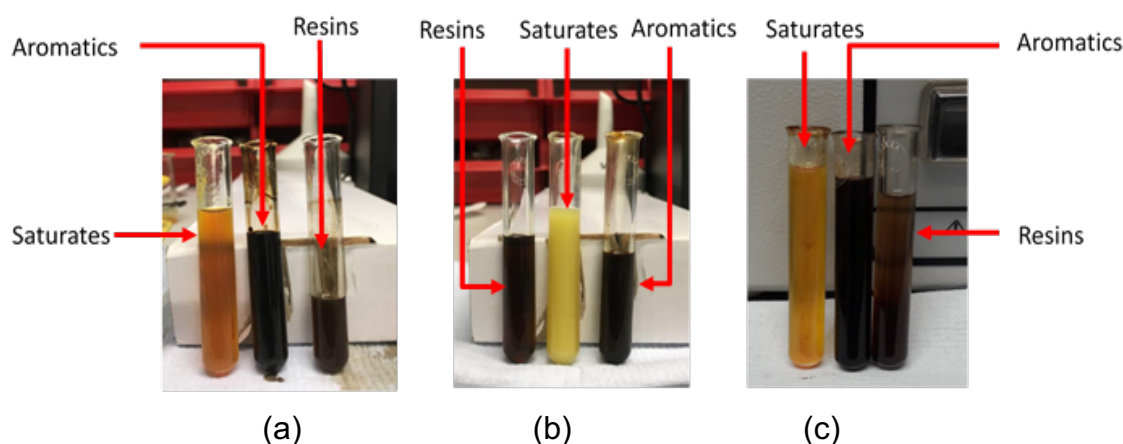


Figure 4-3: Samples of Saturate, Aromatics and Resins fraction obtained from crude oil sample A, B and C.

4.4.1 Analysis of Colloidal Instability Index (CII)

This section describes more propensity of asphaltene aggregation and identifies the ratio of crudes fraction that may cause deposition problem – unstable crude oil. This

study is carried based on the reported by Ashoori *et al.*, (2017) and Choiri and Hamouda (2011). As seen in Figure 4-3 and Figure 4-4, the three crude oil samples are found to be unstable. Similarly, the CII value of the crudes samples is > 0.9 , which implies highly unstable samples, as describes in section 3.3.7 (Equation 3.8). As seen in Figure 4-4, the stability of the oil sample increases with a higher fraction of aromatics and saturates as suggested by Ashoori *et al.* Whereas, higher saturate, and asphaltene fraction is associated with instability in the crude oil sample. The same behaviours were observed from the results in this work.

As shown in Figure 4-2, sample A has higher asphaltene fraction (4.14 wt%) and higher resin value (6.15 wt%) making this sample with relatively lower CII value of 1.45, compared to 2.79 and 1.84 for sample B and C respectively.

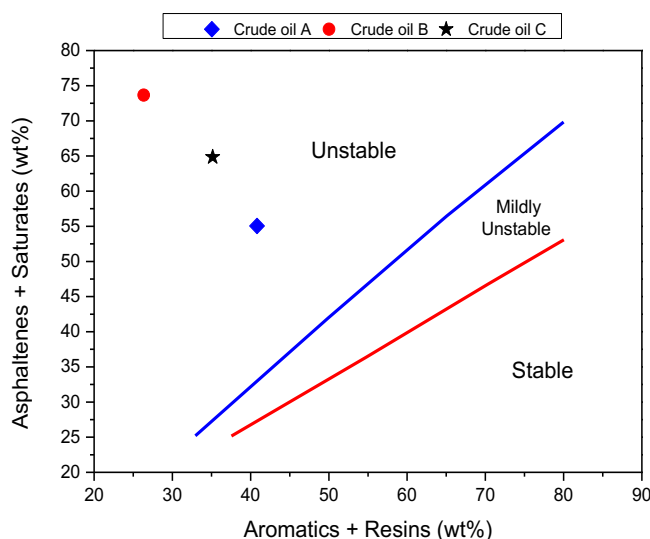


Figure 4-4: Evaluation of crude oil samples stability of using Yen's model

4.5 Rheological Behaviour of Crude Oil Samples and Wax Inhibitors

In this work, the properties of crude oil such as the viscosity, wax appearance temperature (WAT), wax disappearance temperature, and pour point was studied with the rheometry technique. Four of the commercial inhibitors were screen using the same method. Overall, the study was carried out at different shear rate, temperature, rate of cooling, time of shearing, and composition of the crude oil. The fluid behaviour was characterised as Newtonian and/or non-Newtonian fluid.

Similarly, the results in this chapter show the synergy of the four commercial chemical inhibitors, with the goals of achieving further inhibition performance from the eight new samples generated. The properties and fluid behaviours above are essential in wax deposition and prevention study. They usually influence the modelling of wax deposition as well as wax deposit growth rate in the lab study.

4.5.1 Effect of Temperature and Shear Rate on Viscosity, WAT and Pour Point

Initially, the properties (WAT, viscosity and PP) are defined directly from the Bohlin Gemini II Rheometer results (see Figure 3-4, section 3.3.4). It is essential to mention that in this section, the parameters such as WAT and pour point are approximated similar to the study by Singh *et al.* (2011) Adeyanju and Oyekunle (2013), Paso (2014), Ronningsen *et al.* (1991), Theyab and Diaz (2016) Anton (2020). Figure 4-5 shows the results of crudes oil behaviour analysed at varied temperature (0 – 50°C) and shear rate (10, 60 and 120 1/s). It is seen that as the crude oil temperature drops, the pseudoplastic behaviour begins to appear, which affects the viscosity, WAT and pour point. Similar behaviour was reported by Alcazar-Vara and Buenrostro-Gonzalez (2011), Perez *et al.* (2015), Wardhaugh *et al.* (1988). Similarly, it was observed that the crudes samples behave more as non-Newtonian fluid at the lower temperatures, i.e. below the pour point. Therefore, the crude viscosity varies as a function of the shear rate, as shown in Figure 4-5. Otherwise, the crudes typically behave as Newtonian fluid above the pour point temperature.

The Figure below clearly demonstrates the behaviour of crude oil viscosity at different temperature and shear rate. It is observed that the viscosity of crude oil samples (A, B and C) varies inversely with shear rate and temperature. Therefore, it is understood that the increase in oil viscosity with a decrease in temperature causes the formation of a gel network in the crude oil structure, which creates the risk of wax precipitation and deposition in the oil facilities. Similarly, the profile in Figure 4-5 shows that the oil viscosity decreases with an increase in temperature and shear rate. The decrease in viscosity with shear rate causes the wax appearance temperature to drop as a result of the declining in the intermolecular attraction, between the wax crystals in the system towards the deposit surface. This means the

cohesive and the adhesive force between the wax molecules and the deposition surfaces are overcome.

For example, at a low shear rate of 10 1/s, high viscosity and a relative high WAT values are seen in the three crude oil samples. In sample ‘A’ crude, a viscosity of 30 Pa.s was seen at 10 1/s and 10 °C. Which reduces to 15 and 5 Pa.s at 60 and 120 1/s at 10 °C. Similarly, in sample A crude, the WAT increases from 28.5°C to 35°C as the shear increase from 10 to 120 1/s. The same behaviour was seen in sample B and C; WAT increases from 30 to 36°C and from 28 to 33°C at 10 and 120 1/s respectively. Perez *et al.* (2015) and Theyab and Diaz (2017) reported similar typical crude oil behaviour.

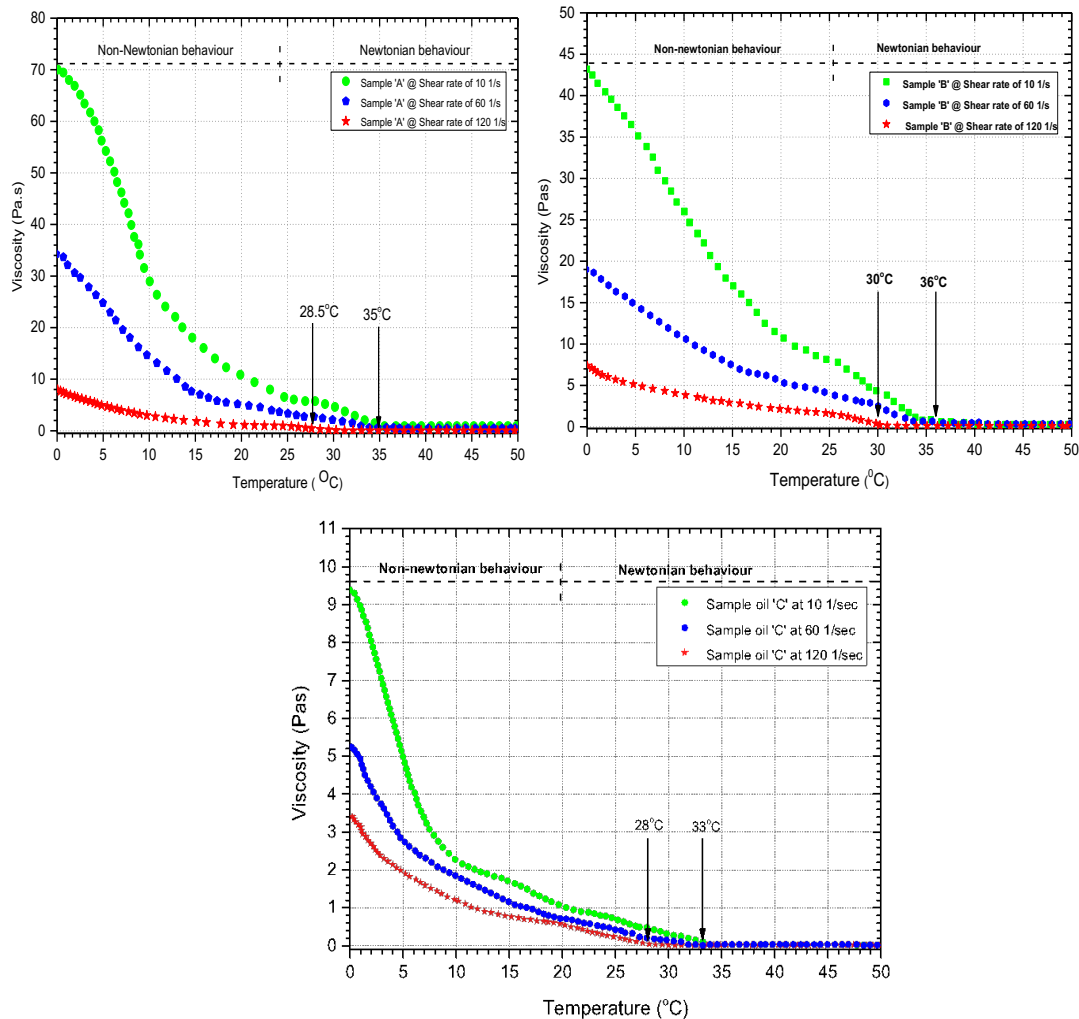


Figure 4-5: Effect of shear rate on viscosity and wax appearance temperature at different temperatures. Top left: Sample A crude oil. Top right: Sample B. Bottom: Sample C.

The effects of shear rate and temperature on viscosity are further described in Figure 4-6. As stated in the previous paragraph, the viscosity decreases with an increase in the shear rate. For instance, it is observed that at 5°C, the oil viscosity decrease from 55.5 Pa.s to 24.5 and 5 Pa.s as the shear rate increases from 10 to 60 and 120 1/s for sample A crude oil. Similarly, at the same varied shear rate but a relatively higher temperature (25°C), the oil viscosity decreases further. In real pipeline flow rig, this phenomenon is studied by increasing the oil flow rate at constant cooling temperature, which in sequence decreased the wax deposition.

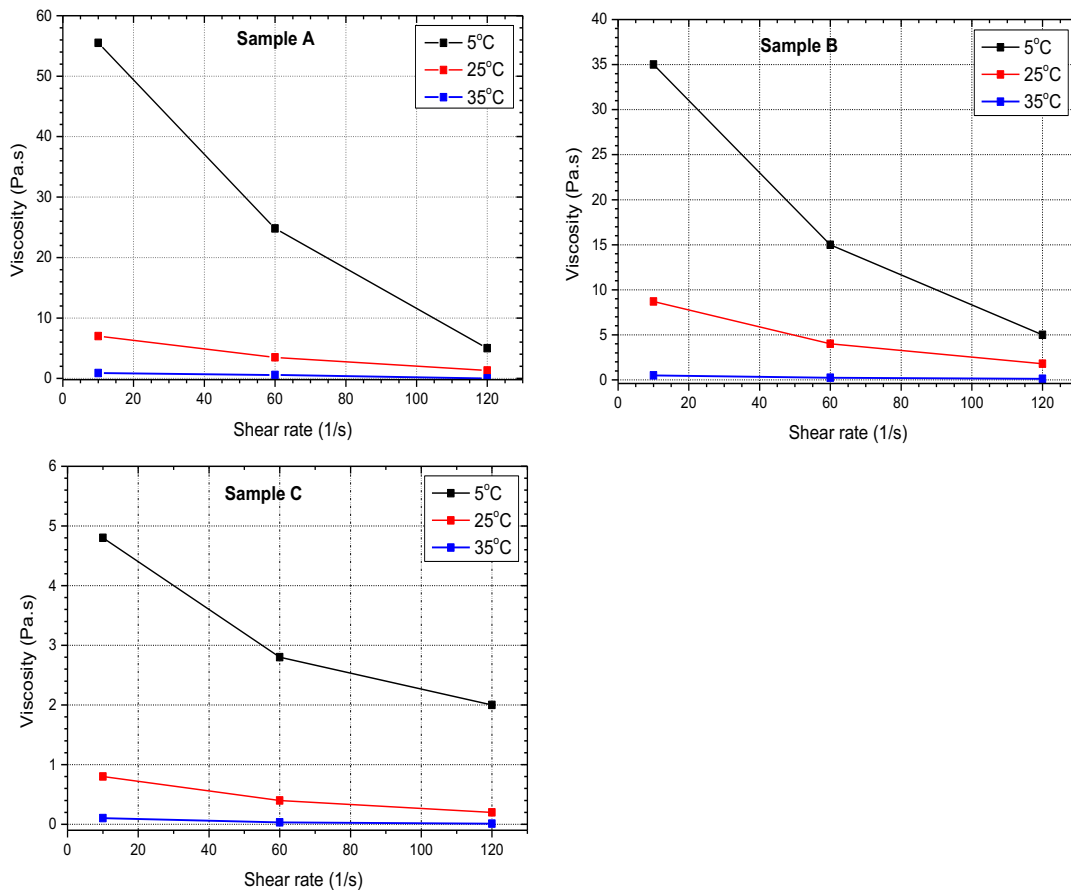


Figure 4-6: Influence of shear rate on crude oil viscosity at three different temperature (5, 25, 35°C) using samples A (top left), B (top right) and C (at the bottom)

Hence, in this thesis, a shear rate of 120 1/s was used to report the properties of crude oil samples, and the same shear rate was used in the analysis of chemical wax inhibitors (Section 4.5.2). It appears that the results obtained at this shear rate are within the range of the properties of sample A provided by Roemex Oilfield Service Company (see Table 3-1). Similarly, the modified ASTM D-97 method used for pour point analysis gives approximately the same pour point obtained from the

viscometric at 120 1/s. Also, considering the oil field operation, the use of higher shear rate in this work is considerate, as the shear experienced in the oil field by the fluid is far higher than those experimented in the Lab.

As a result, the crudes oil behaviour was studied at a constant shear rate (120 1/s) and at varied temperature, which is fixed between 0 – 50°C; below the pour point and above the WAT of the crudes samples (Figure 4-7). The WAT was measured instantaneously as the wax crystal precipitated – this defined the beginning of paraffin wax crystallization. The technique used for characterizing the WAT and pour point was described in Section 3.3.4 according to previous studies (Alcazar-Vara, 2011; Perez *et al.*, 2015; Huang *et al.*, 2015; Theyab and Diaz, 2017; Ruwoldt, 2018). As seen in Figure 4-7, sample B crude has the highest pour point (25.5°C) and WAT (30°C). This result provides an insight into the waxy content of these samples. This implies, the higher the wax content of the sample, the easier the wax appearance, and the higher the pour point of crude oil. A similar result was reported by Oseghale and Akpabio (2012), Bai and Zhang (2013).

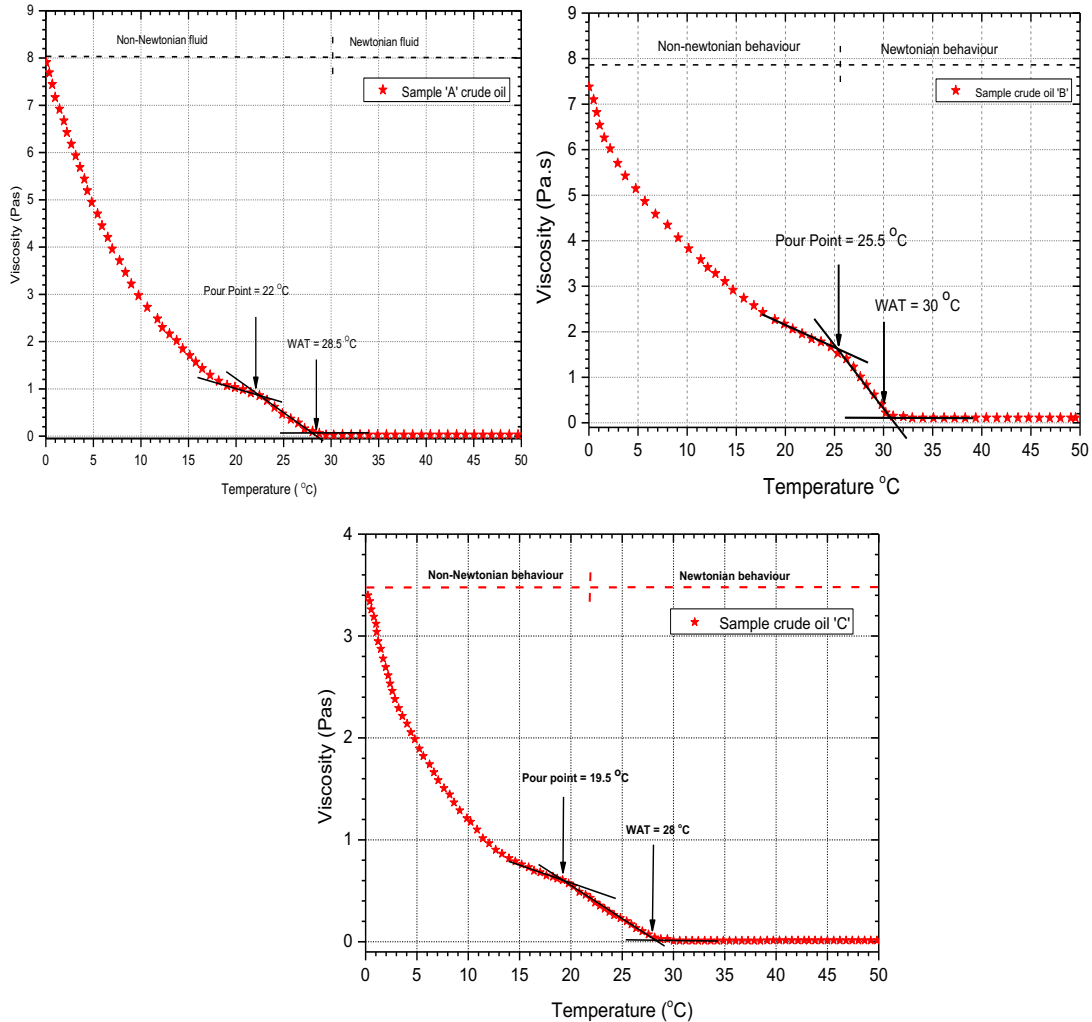


Figure 4-7: Rheological behaviour of crude oil sample A, B and C at a shear rate of 120 (1/s) and different temperature

Therefore, it can be concluded that as the temperature drops, the propensity of sample B crude to crystallise and form solid wax is higher compared to other samples. Also, a possible re-start problem is observed in the whole samples due to the high pour point value, which is generally related with high paraffin content (Ekaputra *et al.*, 2014; Zheng, 2017; Bai and Zhang, 2013).

The followability of crude oil is usually determined from yield stress (Section 4.5.1) and its viscosity; it plays a significant role in the wax deposition rate. As expected, the more viscous the oil sample is, the higher the wax content as observed in figure below. However, sample A has a highly viscous of 2.1 Pa. s (as 15°C) and 0.03 Pa. s (at 50°C) compared to sample B and C, perhaps this due to the high asphaltene content in the sample.

4.5.2 Measurement of Yield Stress

During the waxy oil production, the characteristic feature of non-Newtonian behaviour dominates the system as the temperature of flowing fluid drops below the wax appearance temperature. This behaviour is due to wax precipitate of the soluble wax molecules, which usually possesses plasticity and shear-thinning properties, unlike the Newtonian fluid (Zheng *et al.*, 2016). The dynamic yield stress indicated in Figure 4-8 was defined as the minimum stress required to maintain flow (Kumar *et al.*, 2016; Zheng *et al.*, 2016). Therefore, any shear stress below this point would not be enough to cause the flow of crude oil. As shown in Figure 4-8 the dynamic yield stress measurement is carried out at a different temperature and shear rate (10, 60, 120, and 180 1/s) based on Zheng *et al.* (2016) study. **Figure 4-8** shows the existence of dynamic yield stress as the shear approach zero. This behaviour gives evidence of the plasticity of the waxy crude oil. Whereas shear-thinning of the oil sample observed in Figure 4-5 (viscosity - shear rate plot) occurred as the apparent viscosity decrease with an increase in shear rate (represented by the decreasing slope of the curve).

In general, high shear stress breaks down the micro-structures that bind the crystal wax together. Therefore, there is a lower rate of gelling, as shear stress increases in the system. For instance, at 180 1/s and 15°C, shear stress of 98.7 Pa is observed, as compared to a lower shear stress of 10.12 Pa at the same shear rate but relatively higher temperature (35°C). This behaviour shows that within the Newtonian fluid region (above WAT), the shear stress is very low. Therefore, it is essential to highlight that in wax deposition phenomena, the wall shear stress increases with velocity. Hence, during the deposition process in a pipeline flow rig, the shear stress at the wall increase due to the increase in wax deposit build-up cause b continuous precipitation of wax crystals (Botne and Gudmundsson, 2012; White and Mungal, 2008).

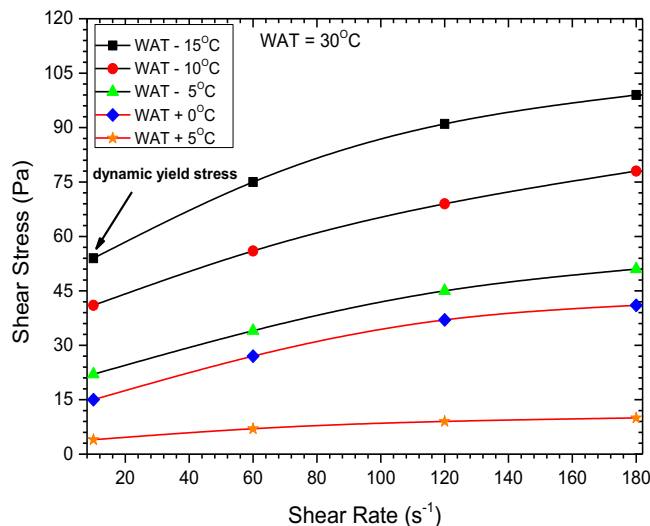


Figure 4-8: The relationship between shear stress and the shear rate at different temperature

4.5.3 Effect of Wax Inhibitors on Crude Oil Rheological Properties

In this section, a preliminary study prior to the flow loop experiment is carried out. As such, the commercial chemical wax inhibitors (commercial codes; W2001, W2003, W2004 and W2005) were screened in this section and their synergies were investigated – for improve inhibition performance towards decreasing the oil viscosity, WAT and pour point. It should called that in Section 1.4, the aim was to study the efficacy of the commercial inhibitor, however, improving the inhibition performance, if possible, is paramount to flow assurance Engineers. The study is carried out at using sample B crude oil, and at constant shear rate of 120 1/s and different cooling temperature (0 – 50°C).

Figure 4-9 shows the results of the commercial inhibitors at different concentrations from 0-ppm (un-doped), 500-ppm, 1000-ppm and 1500-ppm concentration. It is observed that each of the commercial inhibitors has successfully decreased the oil viscosity, thereby reducing the wax appearance temperature and pour point of the crude sample. Therefore, the chemicals could be used to interfere with the nucleation, growth, and agglomeration processes of the wax crystals in the flow rig study. Unfortunately, the interfering mechanism of the inhibitors has yet been fully understood (Jennings and Newberry, 2008). However, the main theory on this process indicated that polymer inhibitors having a similar structure to the wax crystals, easily incorporated themselves into the active sites of the wax crystal,

thereby preventing the crystals growth and promotes the formation of smaller aggregates particles (Jennings and Newberry, 2008; Adeyanju and Oyekunle, 2014).

In this work, it is seen that the performance of these inhibitors reduces at low concentration and wax inhibitor W2001 provided the best inhibition performance. Overall, the inhibitors performance decreases in the order of W2001 > W2003 > W2005 > W2004. This implies that, apart from the concentration, the performance is influenced by the composition of the inhibitors. Similar behaviour was reported by Kuzmić et al. (2008), Hoffmann and Amundsen (2013), Pedersen and Rønningsen (2003).

However, the complete composition of the commercial inhibitors was not provided due to the proprietary issue; nevertheless, based on the details in Section 3.4 and Table 3-3, it is possible to conclude that the higher performance of inhibitor W2001 could be correlated to its composition. It is seen that the inhibitor (W2001) is made up of a mixture of Olefinic polymer derivative, which perhaps enhances the activity of the sample compared to the others. Other compositions included hydrocarbons C10, Aromatics, >1% Naphthalene in different percentages.

W2003 is found to be the second-best inhibitor consists of solvent naphtha, heavy Aromatic, distillates (petroleum), hydrotreated light Naphthalene, Alkenes: C20 - 24, Alpha-Polymers with maleic anhydride, C18-22 alkyl esters. However, a very small inhibition performance differences are observed at 1000 and 1500 ppm between W2003 and W2005 inhibitors. This is because the two inhibitors have relatively the same composition except for Naphthalene (in W2003). Inhibitor W2004 displayed the least performance amongst the tested samples.

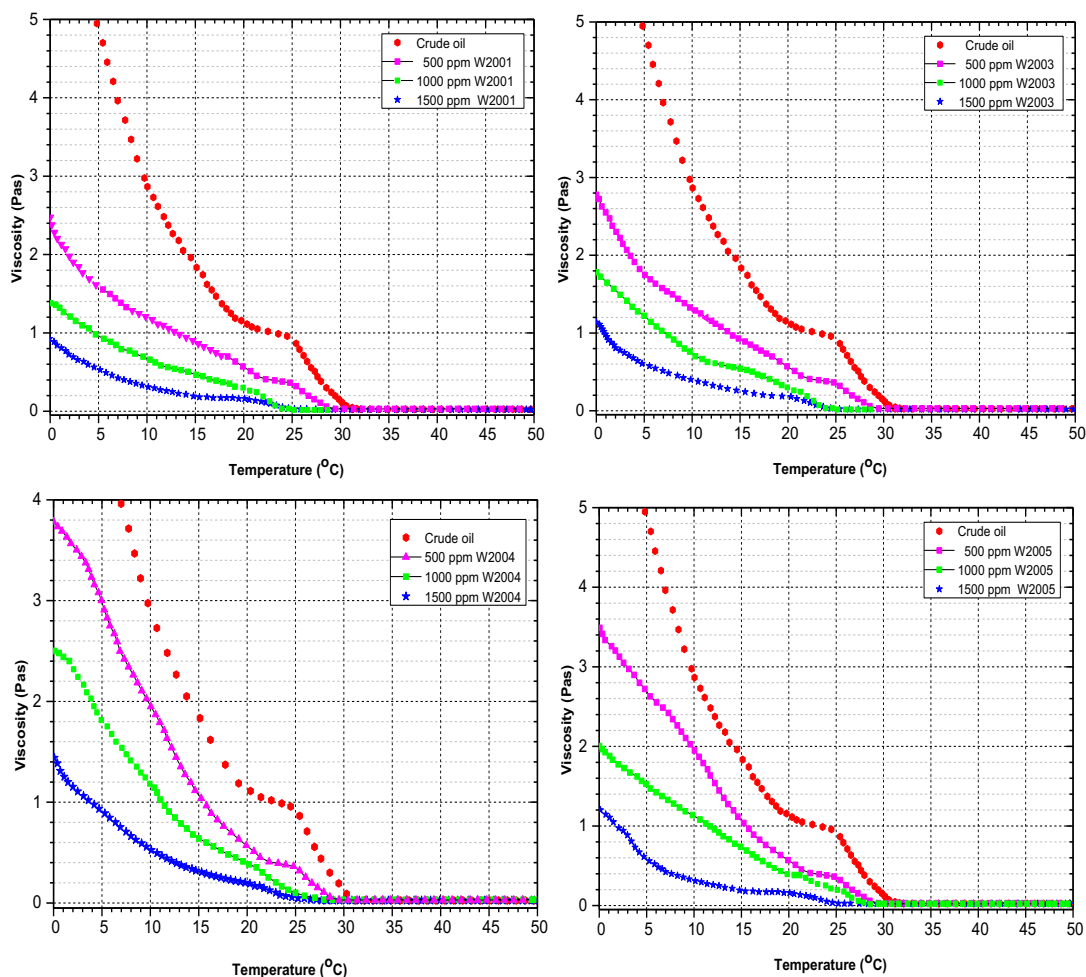


Figure 4-9: Rheological behaviour of sample B crude mixed with different inhibitor at a constant shear rate of 120 1/s and varied concentration (500, 1000 and 1500ppm). Top left: W2001. Top right: W2003. Bottom left: W2004. Bottom right: W2005 inhibitor.

4.5.3.1 Viscosity, Wax Appearance Temperature and Pour Point Behaviours

It is observed that the viscosity crude oil was strongly affected by adding the W2001, W2003, W2004 and W2005 inhibitors individually at 1500 ppm, compared to the lower concentrations (such as 1000 and 500-ppm). For example, during the control cooling experiment at 5°C, the viscosity at 500 ppm of the undoped sample B crude oil reduces from 5 Pa.s (Figure 4-7) to 2.9 Pa.s and 2.60 Pa.s for W2004 and W2005 inhibitors (**Figure 4-9** bottom left and right) and further reduced to 1.75 and 1.6 Pa.s for W2001 and W2003 inhibitors at the same condition. The pour point and WAT of crude oil give further evidence if the effectiveness of W2001 wax inhibitor compared to others. It is observed that by adding W2001 wax inhibitor at 500, 1000 and 1500 ppm, and the pour point of crude oil sample B decreases from 25.5°C to 22°C, 20.5

and 17°C (Figure 4-10). Whereas a small decrease in the pour point was observed at 500 ppm in the other samples.

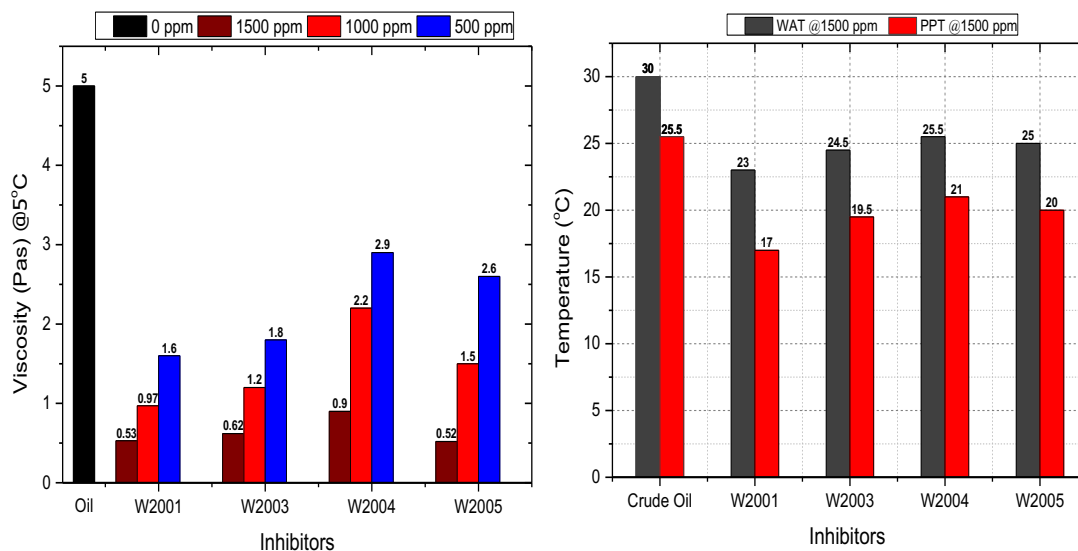


Figure 4-10: Effect of chemical inhibitors on (a) viscosity at 5°C and shear rate of 120 1/s and (b) pour point at a shear rate of 120 1/s at varied cooling temperature (0 – 50°C)

Therefore, in this work, it is noteworthy that at 500 ppm, the inhibitors have poor inhibition performance. Because, at this concentration, there is not enough inhibitor to prevent the wax formation process effectively. Typically, increasing the concentration of chemical inhibitor provides additional structural interference which leads to the decrease in crude oil sample pour point and wax appearance temperature. On the other hand, the wax appearance temperature of the crude oil doped with W2001 decreases from 30°C to 29, 25.4 and 23°C at 500 ppm 1000 and 1500 ppm, respectively. In a similar manner to the viscosity and pour point, the WAT reduction is observed to be higher with W2001 inhibitor compared to W2003, W2004, and W2005.

Overall, it is well comprehended that the concentration and composition of chemical wax inhibitors influence the rheological properties of crude oil. However, other factors such as; shear rate, shear stress, and temperature considerably affect the inhibition performance. Therefore, as highlighted in the previous sections, an increase in temperature leads to a decrease in crude oil viscosity by melting the wax crystals in the crude oil. Also, the wax appearance temperature decrease due to the increase in the shear rate leads to an increase in shear forces.

4.5.3.2 Study of Blended Wax Chemicals Inhibitor on Oil Rheology

It should be recalled that the objective of achieving further inhibition performance is desired in this work. Therefore, this section presented the results of the synergies between the four chemical inhibitors, generating eight new samples. The results of the eight samples, which are blended based on the percentages (see Table 3-4, section 3.4) were analysed at constant shear of 120 1/s and a concentration of 1500 ppm only. The performance of each sample was compared with the four original inhibitors (Figure 4-11). An improved inhibition performance was observed from the blended samples compared to others. It is observed that at 1500-ppm concentration, blend 'A' inhibitor provides much better inhibition by decreasing the crude oil viscosity and reduces both wax appearance temperature and pour point.

Similarly, at a fixed temperature of 5°C, the viscosity of undoped crude oil reduces from 5 Pa.s (Figure 4-7) to 0.35 Pa.s – the viscosity of crude oil with blend 'A' wax inhibitor (Figure 4-11). Unlike the high viscosity (0.53 Pa.s) obtained by doping crude oil with W2001 (best commercial inhibitor). On the other hand, the pour point and WAT of the crude oil were compared from the same Figure. The pour point and WAT of crude oil doped with blend A inhibitor reduces from 25.5 and 30°C (undoped with inhibitor) to 13°C and 17.5°C respectively. Hence, blend A produced better inhibition performance compared to other tested inhibitors. This could describe as due to the compositional properties of sample A inhibitor, which has more inhibition characteristic than the rest of the inhibitors. As shown in Chapter Three, the improvement is as a result of blending 50% of W2001 inhibitor with another 50% W2003. Therefore, blended A inhibitor provided more structural interference with the nucleation, growth, and agglomeration of the wax crystals.

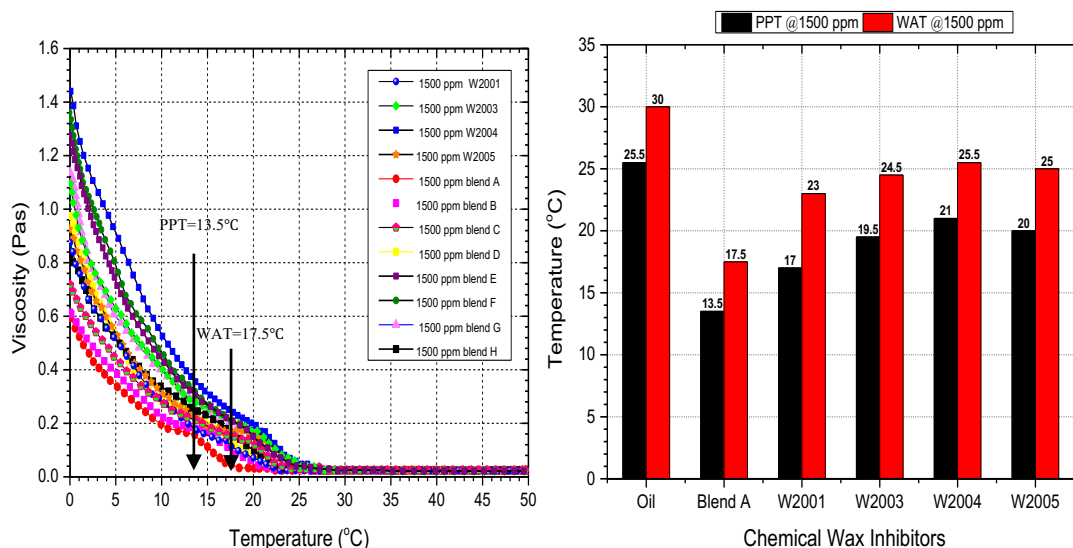


Figure 4-11: Performance of different inhibitors. Left results: Rheological behaviour of four commercial inhibitors compared to other blends inhibitors. Right: Effect of four commercial inhibitors and blend ‘A’ inhibitor on WAT and pour point.

4.6 Microscopic analysis of crude oil

The purpose of this section is to perform a microscope examination of the crude oil samples (A, B and C) with 0 ppm and 1000-ppm of blend ‘A’ inhibitor. The comparative crude oil morphology of the prepared samples is shown in Figure 4-12. The strong interlocking and interactions between the wax crystals are observed. The interaction of the crystals formed structural network defined as needle-like or rod-like particles, see Figure 4-12 (A, B and C). This assembly of wax crystals is usually the source of gel formation, which is an obstacle for the production systems. Similar behaviour was reported by other researchers (such as Coto *et al.*, 2014) using different waxy crude oil.

A strong network of the wax crystal is observed in sample B oil compare the other samples. This further proves the presence of higher wax crystal density with higher wax content in the sample B. The hierarchy of this behaviour is evidenced by the amount of wax content in each sample (Table 4-1). On the other hand, sample A*, B* and B* displayed the micrographs of the crude oil doped with blend ‘A’ inhibitor at 1000 ppm. It is observed that the presence of blend A wax inhibitor in the oil samples affects the structural morphology of the wax crystals. As seen in **Figure 4-12** (A*, B* and C*), the inhibitor transformed the needle-like or rod-like crystals (A, B and C) into an agglomerate and small particles dispersed in the oil matrix.

Therefore, in this case, the inhibitors disrupt the strong interactions of the wax crystals around the microsphere through steric hindrance effect. This behaviour demonstrated that the presence of inhibitor effectively inhibits the development of wax crystal network structure.

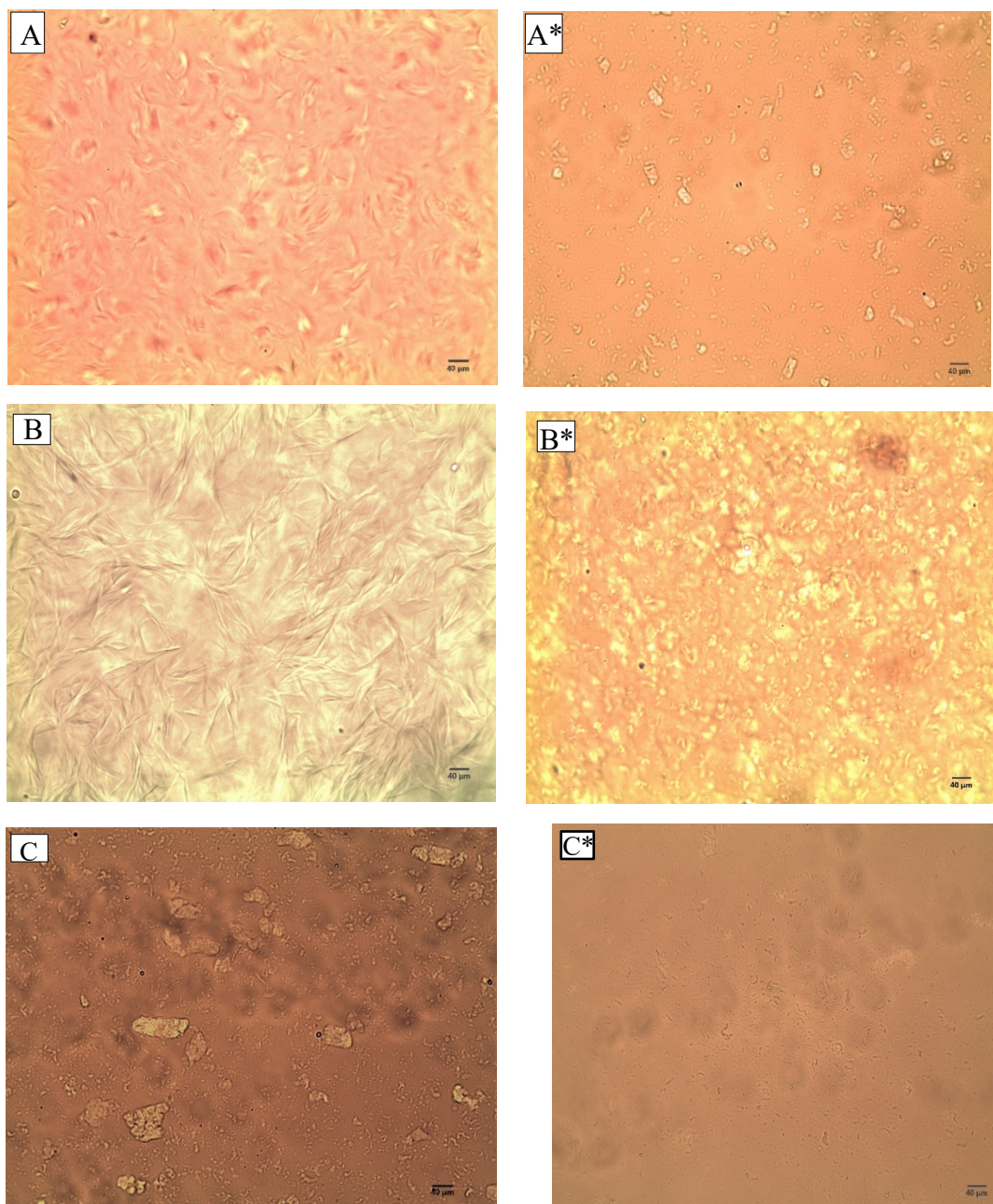


Figure 4-12: Evaluation of macroscopic morphology of crude oil samples (A, B and C) mixed with blended A wax inhibitor (A*, B* and C*) Wax Crystals Morphology with.

4.7 n-Paraffin Distribution of Crude Oil Sample

The study of *n*-Paraffin distribution is carried using HTGC in collaboration with the University of Plymouth using the proprietary commercial method (known as T-SEP® “thermal separation technique”) (see Section 3.3.8). The technique has proved to be more reliable, reproducible and effective than the simple conventional methods employed by most laboratories, which gives the *n*-paraffin distribution and wax content a particular crude sample. As the aim in this section was to demonstrate the use of HTGC– T-SEP for understanding higher molecular weight compounds of two waxy crude oil (A and B) in the form of macro-crystalline ($\leq C_{36}$) and micro-crystalline (C_{30} to C_{60}^+) molecules and for validation of the wax content. As reported by França et al. (2018) “Macro- and micro-crystalline waxes have different functional properties (including viscosity and melting point) due to the differences in their hydrocarbon content (linear or branched)”.

Therefore, in this work, the *n*-paraffin distributions are used as the input parameters to the thermodynamic models of wax precipitation process (see chapter 6). The wax content obtained in this section was compared to the content obtained using modified UOP 46-64 method (discussed in section 4.3). As mentioned in Section 4.3, the two methods produced approximately the same results wax content, which proves the claims made by Sarica and Panacharoensawad (2012). The outcomes from the analysis of the *n*-paraffin distribution (elaborated in Section 4.8.3) revealed that the two crudes oil are naturally high paraffinic comprising carbon chains length between C_{15} - C_{74} and C_{15} - C_{67} for the sample A and B respectively.

Before the analysis of key results, it is noteworthy to discuss some of the studies of the solvent blank (cyclohexane), the compound in C10-60 standard (see Table 3-2) and Polywax 655 external standard used. Their chromatographs are worked out, as shown in Figure 4-13. In the blank solvent (cyclohexane) chromatography (Figure 4-13 Top Left), two peaks around 2.2 and 3.5 minutes are detected as impurities. It is observed that the impurities appeared in each subsequent chromatographs. The chromatograph on the right of Figure 4-13 showed an integrals peaks of C_{10} , C_{20} , C_{30} , C_{40} , C_{50} and C_{60} standard, whereas, Figure 4-13 shows the Polywax standard contained an even-numbered *n*-alkanes for retention matching of peaks that make up the missing component in the C10-60 standard.

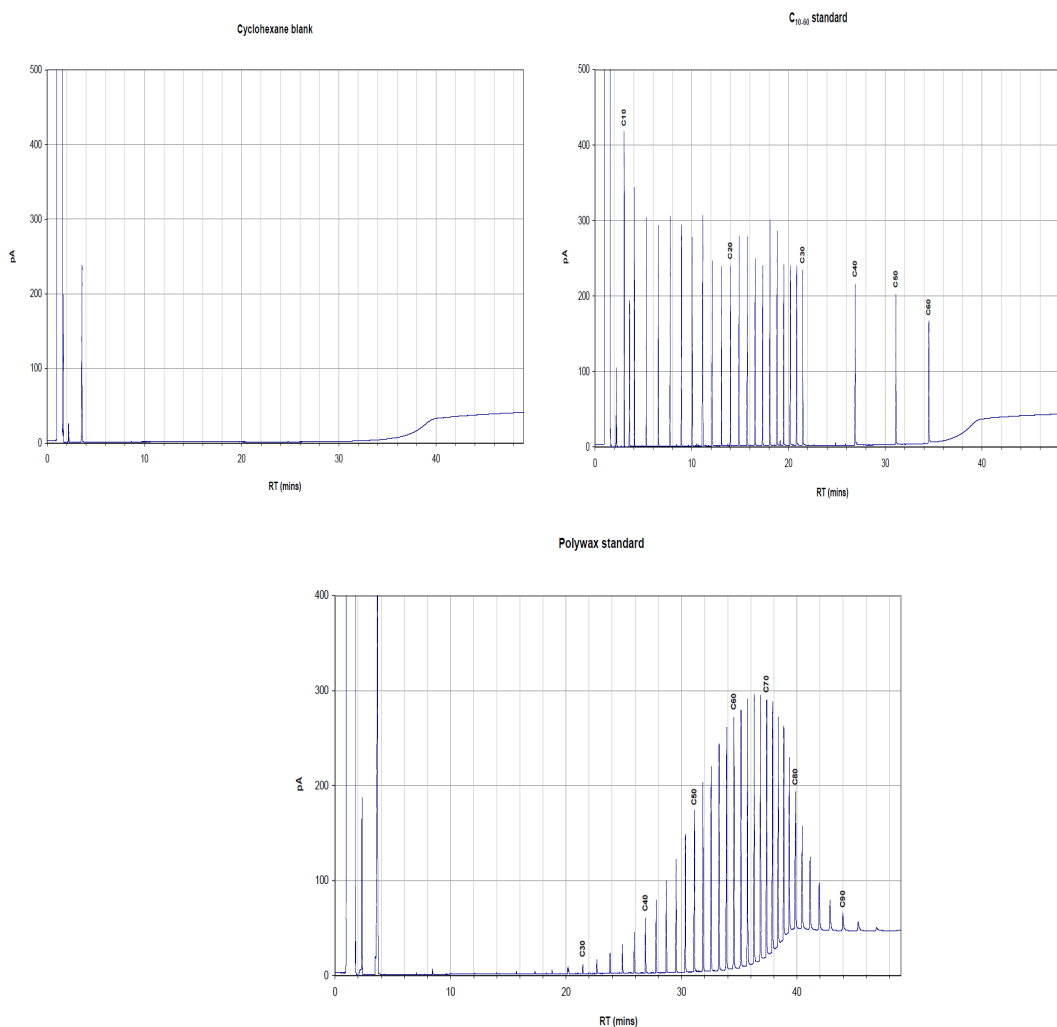


Figure 4-13: Chromatograms of different solvents. Top Left: The solvent blank (cyclohexane). Top Right: A standard consist of some even carbon number from C10 to C60. Bottom Left: A typical chromatograph of Polywax 655 external standard.

Subsequently, the whole oil and top oil samples (see Section 3.3.8 for preparation procedure) were characterised based on T-SEP® technique, in which the n-Paraffin distribution and wax content are obtained as follows.

4.7.1 Whole Oil and Topped Oil Chromatograph

The analysis of the whole oil resulted in a series of chromatograms characterised as resolved peaks and unresolved complex mixtures (UCMs) as shown in Figure 4-14 and 4-15. The unresolved complex mixtures (UCMs) are often found during the HTGC analysis (Hasinger *et al.*, 2012; KAT Lab, 2009) and generally affect the accuracy of the results. It is observed that crude oil sample B (Figure 4-14) depicted higher peaks in the region of relatively heavier n-paraffins component compared to sample A (Figure 4-15). The peak intensity was observed to decreased sequentially

from n-Decane C10 – C30 (n-Triacontane) and almost diminishes around C40 – C60 in both Figures.

In reality, the whole oil chromatographs did not reflect the actual n-paraffin distribution within the oil samples, and therefore, the n-paraffins content is underestimated. Which implies that in the “whole” oil sample, the n-paraffins fractions above C30⁺ are considered to be below the detection limit of HTGC (KAT, 2009), and the presence of the UCMs affect the elution of other higher fractions compound. For these reasons, the topping of whole oil is carried out using an *undisclosed solvent* (T-Sep procedure) due to the proprietary issue with the method. As shown in Figure 4-14 Figure 4-14, the Topped oil procedure increase the intensity of the signal, which allows the heavier compounds to be detected with higher precision (KAT, 2009). Also, the unresolved component mixture (UCM) in the “whole” oil chromatographs is minimised to a great extent.

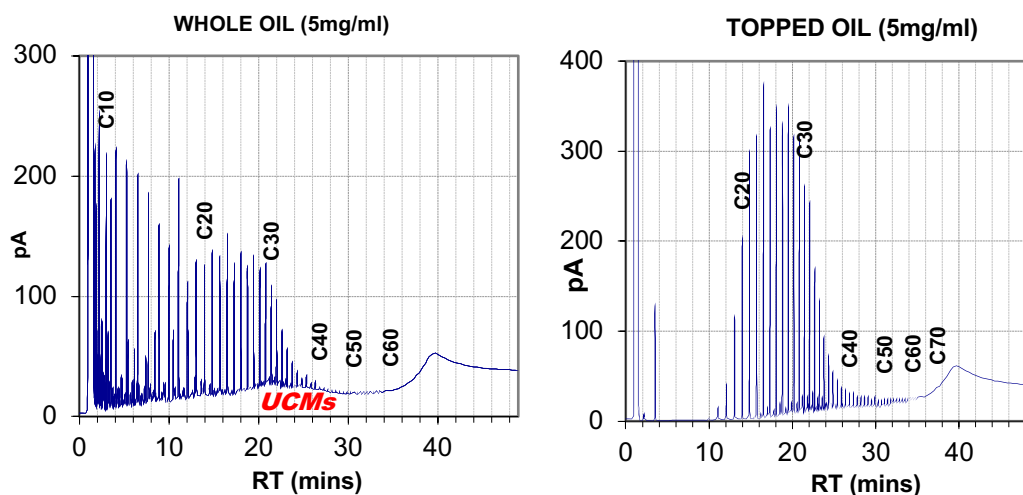


Figure 4-14: Chromatogram of crude oil sample A. Left: Whole oil chromatogram.
Right: Topped oil chromatogram

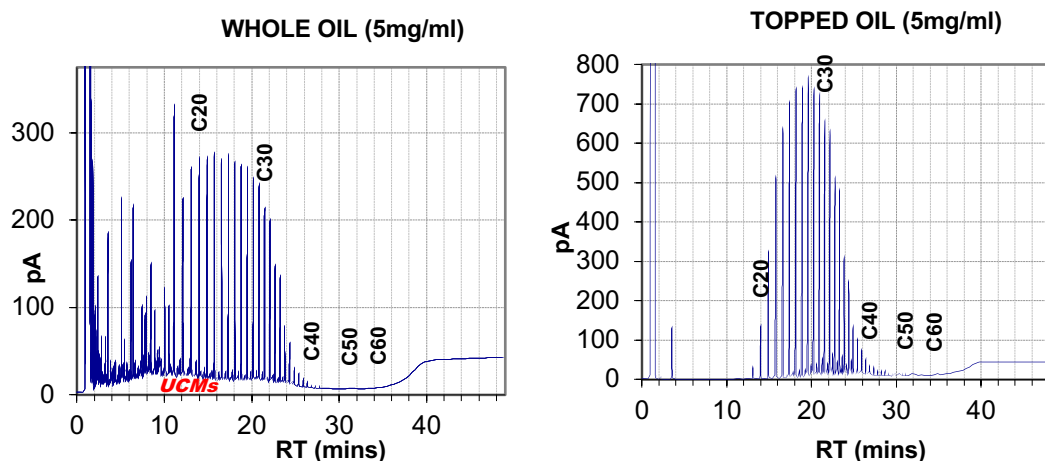


Figure 4-15: Chromatogram of crude oil sample B. Left chromatogram: Whole oil chromatogram. Right chromatogram: Topped oil chromatogram

Therefore, as shown above, the peaks of n-alkanes fractions above C_{30+} are more pronounced and the peaks around $C_{15}-C_{35}$ (macro-crystalline compound) are intensified in the topped sample. From these results, it is seen that the n-paraffin distribution chains between C_{15} to C_{74} and C_{15} to C_{67} for sample A and B crudes. However, the intensity and the amount of the n-paraffin fractions are higher in sample B (Table A2, Appendix A), which are related to the amount of wax content in the sample. Whereas, the larger chains of n-paraffin in sample A could be traced back to the higher asphaltene content in the sample.

Based on the T-SEP® procedure (KAT Lab, 2009), the data of ‘whole’ and ‘topped’ oil were merged to produce a new “adjustable value” which represents the actual n-paraffin distribution in the oil sample as discussed in the next section.

4.7.2 Merging the ‘Whole’ and ‘Topped’ Data

Merging of data is carried out using a mathematical correlation developed as part of T-SEP® technique (see Appendix A, Table A1 and Table A2). Figure 4-16 and Figure 4-17 show the results of the adjustable components, which represented the actual and accurate carbon number distribution in each sample. This implies that the distribution of n-paraffin carbon number (shown in Figure 4-18) was generated based on the integration of chromatograms of the “Whole and Topped” oil samples. The boundary between the macro and micro-crystalline waxes is clearly shown in the Figure. Accordingly, as stated in the literature, microcrystalline wax is smaller and thinner than that of macro-crystalline waxes. It is clearly observed that the

microcrystalline wax crystallises at a higher temperature compared to macro-components, where stronger gels are formed (Figure 4-18).

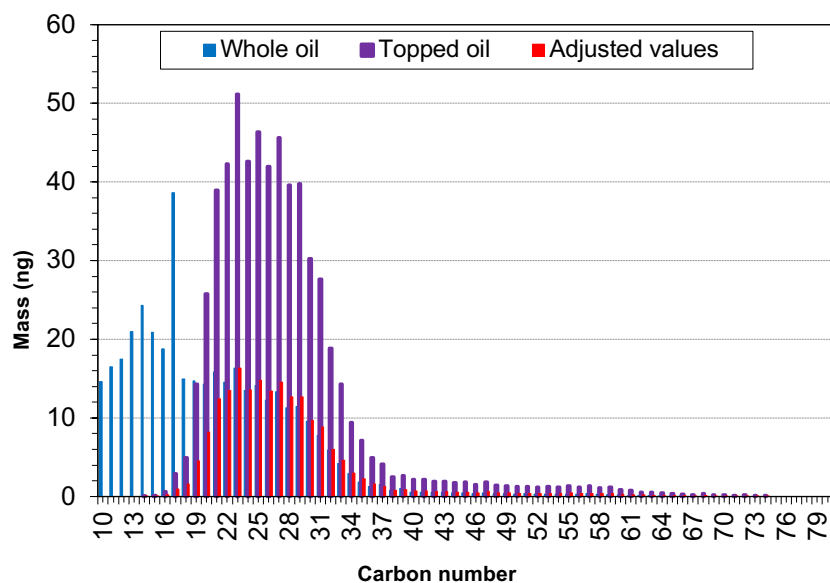


Figure 4-16: Correlation chart for waxy crude oil sample A

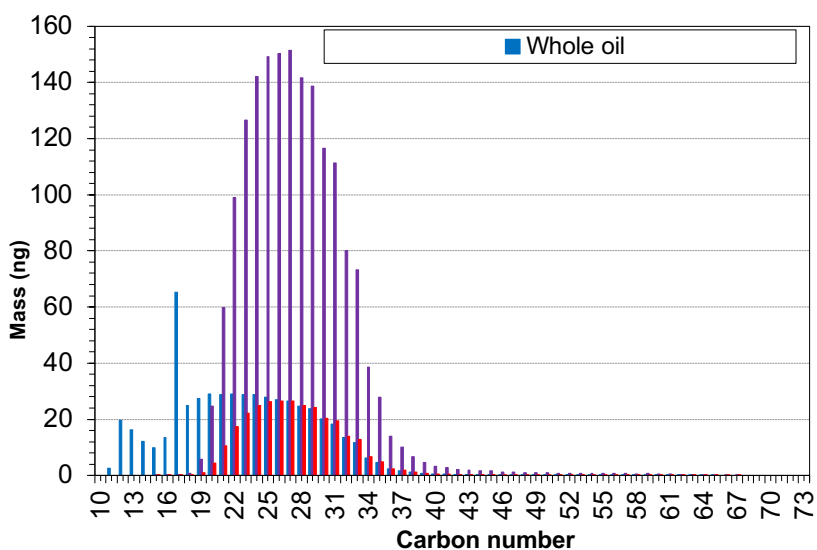


Figure 4-17: Correlation chart for waxy crude oil sample B

Initially, the distribution n-paraffin carbon around the macro-crystalline wax fraction increase from C_{15} to around C_{27} (Figure 4-18), which shows the richness of paraffin content in the two samples. The fractions gradually decrease towards the higher molecular weight component (micro-crystalline wax). This behaviour followed the same trend with other research findings (García *et al.*, 2000; El-Dalatony *et al.*, 2019; Japper-Jaafar *et al.*, 2016).

Higher fractions of n-paraffin were seen in sample B, with the macro-crystalline wax (C_{15} - C_{36}) varies between 0.196–1.161 wt%, compared to the fraction micro-crystalline wax that varies from 0.0003-0.097. On average, each fraction of macro-crystalline wax (C_{15} - C_{36}) for sample A is around 0.92wt%. Compared to micro-crystalline wax that exists in small quantity (0.014 wt%). Whereas, in sample A, the macro-crystalline wax (C_{15} - C_{36}) varies between 0.092–0.835wt%, and 0.001–0.063w% for the micro-crystalline wax molecules. This indicates the presence of more microcrystalline wax crystals in sample A. It is seen that there is more microcrystalline wax in sample A than in B, compared to the higher presence of macrocrystals in sample B, which qualify it as highly paraffinic. The macrocrystals crystallise in needle shape mostly in the production and transportation systems (Al-Safran and Brill, 2017).

A unique peak was seen at C17 with percentage fractions of 2.31 and 1.546 wt% for sample A and B (Figure 4-18). It is noted that some fraction of Pristane ($C_{19}H_{40}$) colludes nC_{17} , particularly as their boiling point, is approximately the same, which give rise to such behaviour. The inability to resolve these two compounds using HTGC (T-Sep technique) is a limitation of this method (KAT, 2009). However, this will not affect the accuracy of the results; in fact, the component of nC_{17} exhibits considerably less effect on wax deposition problem compared to other heavy components. This behaviour was indicated in a standard GC-MS analysis shown in Appendix A (Figure A3 and A4).

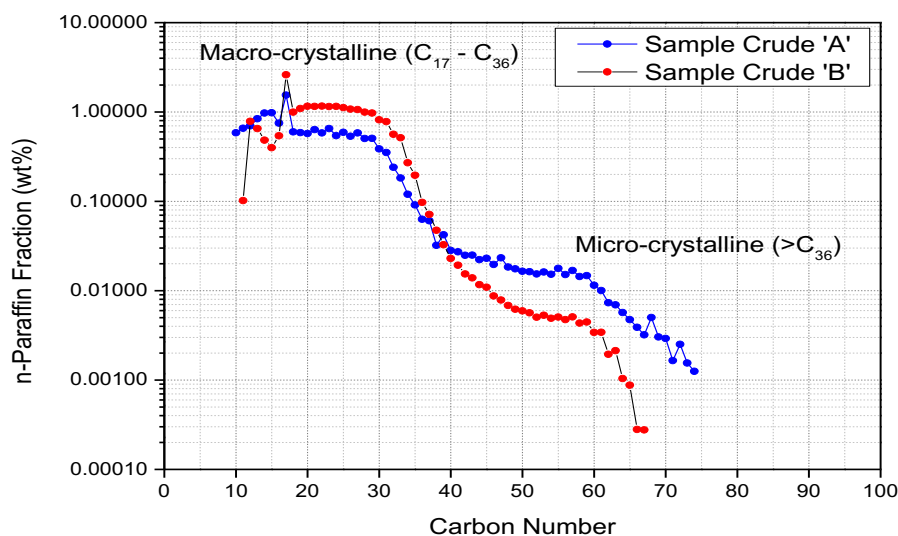


Figure 4-18: n-Paraffin distribution of waxy crude oil samples A and B

Therefore, based on the n-paraffin distribution and wax contents; sample B crude oil poses a highly flow assurance issue during production, and transportation compared to sample A and generally sample C based on the other properties. However, with a high fraction of asphaltene content, sample A might cause other serious problem during storage or as the operation shutdown.

Chapter 5

Results and Discussion

Analysis of Wax Deposition in Pipeline Flow Rig

5.1 Introduction

The primary aim of this chapter is to present and discuss the severity of wax deposition results in straight and curved pipes obtained through different methods; including weight and volume measurement, pressure drop and heat transfer correlations and wet film thickness gauge method. It is worth noting that the results from weight balance technique and pressure drop produced nearly the same results and hence, were suitable for the overall analysis of the deposit thickness in both curvature pipes. A new model for deposit thickness measurement in bend pipes was developed and compared with the existing methods. The results of the study create a better understanding of wax deposition process correlated with different mechanisms involved during the deposition (such as molecular diffusion, shear dispersion, Brownian diffusion, gravity settling and shear stripping) and the effect of variables-control parameters (e.g. cooling temperature, crude oil flowrate and deposition period).

Section 5.3 presents the results and analysis of the deposit thickness measured in a straight pipeline through different techniques. Section 5.4 provides the analysis of wax deposition results measured in curved pipes with the new model established for the overall wax thickness measurement in a curved pipe described in section 5.4.1. It was found that the severity of wax depositional rate (in relative percentage) could be increased if the curvature of the pipe changes from straight pipe to 45° and 90° bend pipes at different conditions.

5.2 Pressure and Temperature Response from the Flow Rig

In this study, it is essential to understand and accurately measure the pressure drop between the inlet and outlet of the test section and temperature response between the fluid and the ambient condition before and during the deposition experiment. Therefore, this section analysed the pressure and temperature data captured at the preliminary phase of the experiment. However, it should be noted that there is no calibration data available for the pressure sensors. Therefore, the pressure sensors were first calibrated based on the flow rig capacity, and linear interpolation was used that enabled the voltage reading to be converted to pressure readings in bars (Eq 5.1). The two similar pressure transducers PT1, and PT2 (range 0 – 5 bars) corresponded to an output of voltage of 3.84 – 20V.

$$\frac{P_i - P_{min}}{P_{max} - P_{min}} = \frac{V_i - V_{min}}{V_{max} - V_{min}} \quad (5.1)$$

$$P_{cal} = 0.37V_i - 1.43$$

Where P_i is the pressure value at a sample interval (calculated) and V_i is the instantaneous reading of the voltage obtained from the pressure sensors.

In general, it is known that in any system producing waxy crude oil, the pressure drops as soon as the wax particles begin to precipitate out of the oil and deposited on the pipe wall. Therefore, the transient pressure drop data and temperature responses at different locations have been analysed to estimate the average wax deposit growth rate (in thickness). Figure 5-1 (a) shows a voltage to time (trend) plot for the pressure responses – at channels A and B, which represent the inlet and outlet of the test section. Figure 5-1 (b) presented the temperature responses for the coolant fluid and the crude oil. The data is obtained at two different conditions; at $\Delta P_{t=0}$, i.e. the pressure drop is zero, and at $\Delta P_{t=26}$ pressure measurement after 26 minutes.

For the voltages (pressure) responses, at $\Delta P_{t=0}$, which represent no-flow conditions, channels A and B is represented by blue and pink line. Whereas, the observed initial increase in pressure drop after 26 min is constant, which indicates the pressure drop prior to the deposition of wax. Though, it is expected that as soon as the wax build-up in the pipe, the pressure drop will increase. This behaviour was monitored

throughout the experimentation, and the instantaneous reading of the voltage is converted to pressure (in bars) to determine the deposit thickness (see section 3.81; Eq 3.15 and 3.17). It is observed that at 26 minutes of the testing period, under constant oil flow rate (7l/m), the temperature responses for the coolant fluid (inlet and outlet) and the crude oil (the inlet and outlet) are 15 and 45°C respectively. This demonstrates that prior to the deposition of wax; the frictional pressure drops and the change in temperature for both cold and hot fluid remain constant. However, as the wax precipitation begin– due to the temperature gradient between the pipe wall and the flowing fluid, the pressure drop increases. Similarly, the crystals wax that travelled along with the bulk fluid reached the outlet thermocouple, which causes the temperature to drops very slowly. When the wax molecules simultaneously build-up and deposited on the pipe wall, the decrease in the outlet temperature is usually rapid.

Usually, the outlet temperature drops with an increase in pressure drop remained constant until the wax formation is interrupted– through any of the strategy reported in the literature. Otherwise, as the deposition continues, the deposit itself could form a thick layer that usually acts as an insulator and prevent further deposition of wax.

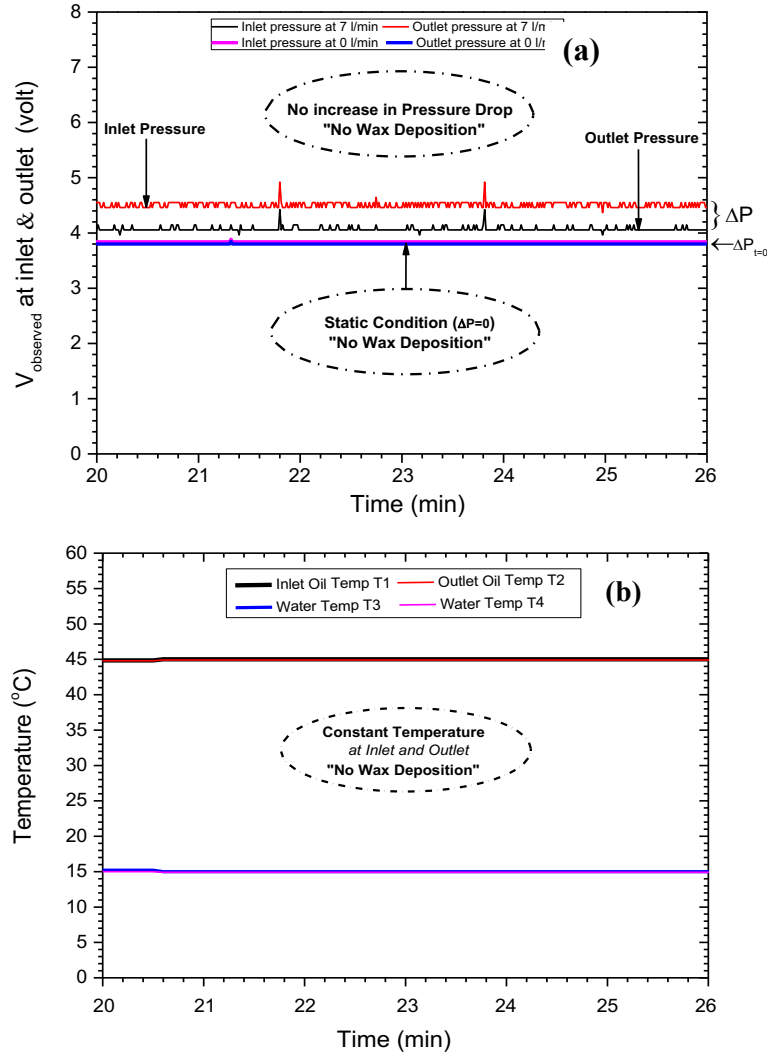


Figure 5-1: Pressure and temperature sensors responses. Q_{oil} , 7 l/min prior to the wax deposition. (a)– Voltage (Pressure) reading at $\Delta P_{t=0}$ i.e. the pressure drop is zero, and at $\Delta P_{t=26}$ pressure measurement after 26 minutes of the test. (b)– Temperature correlation after 26 minutes of the test

5.3 Wax Deposition Analysis in Straight Pipe

The results presented in this section were performed in a flow rig equipped with a straight pipe only (see Figure 3-14). In this work, since there are no direct published results discovered in the literature that could be used to compare the study of wax deposition in bend pipes; the results in the straight pipe were used as the benchmark (or base-case scenario) for the comprehensive study and comparison. On the other hand, different techniques– established in the literature were used to precisely and qualitatively measure the deposit thickness from the straight pipe. In order to ascertain the quality of data obtained, the results– in straight pipe are compared with other studies that have used similar flow rig configuration, crude oil composition,

method of quantifying deposit thickness and experimental matrix, which includes; Adeyanju and Oyekunle (2013), Panacharoensawad and Sarica (2013), Theyab and Diaz (2016) and Rittirong *et al.* (2017) – these study are based on the laboratory scale level. Also, the standard offshore case study by Singh *et al.* (2011) was looked at for understanding and establishing realistic data. Therefore, the next section investigates and discussed the influence of fundamental parameters that control wax deposition behaviour.

5.3.1 Effect of Temperature Gradient on Wax Deposition

Several experiments conducted were based on the experimental matrix (see section 3.7). Literature and the results in Chapter 4 have shown that temperature is the primary factor for wax precipitation and deposition and was studied alongside the shear rate effect and other parameters. It is comprehended that a successful production and transportation of waxy crude oils or gas condensate could be achieved at temperature conditions higher than the wax appearance temperature of a particular oil– i.e. as a means to prevent wax deposition (Hoffmann and Amundsen, 2013). Therefore, the influence of the thermal gradient was investigated by varying the pipe wall temperature by controlling the cooling temperature at 15, 20, 25, 30, 35 and 40°C, respectively.

Figure 5-2 shows the effect of the cooling temperature, which was carried out at two different constant flow rates (5 and 9 l/m) – that are within the laminar and turbulent flow region (Makwashi *et al.*, 2019a). The experiments were performed at a constant crude oil temperature of 45°C (WAT+15°C) and experimental period of 2 hrs. These set of temperatures was chosen mainly to examine different conditions frequently encountered in the subsea environment and to study the crude oil temperature envelope– which is below and above the pour point, below and above the WAT.

It is observed that at the lower cooling temperature, particularly below the pour point (15°C), the thickness of the wax deposit is higher. This is because, below the pour point, the waxy crude oil behaves as viscoelastic material (Visintin *et al.*, 2005; Zhang and Chen, 2007). Similarly, at this point, the structure of the wax crystals are strong enough to form a network structure that makes the crude oil behaves gel-like and lose fluidless, especially in the case of the pipeline shut down (Makwashi *et al.*, 2019a, 2019b; Zhang and Chen, 2007). Therefore, below the pour point (15°C) and

after the system is shut down, the waxy crude oil can flow again only if the structure is destroyed or its yield stress overcome (see Figure 4-8, section 4.5.2).

Therefore, in this study, thickness of 1.93mm was measured at 15°C cooling temperature and 5 l/min (Figure 5-2, a) and $\delta_{wax} \approx 1.46\text{mm}$ at 9 l/min (Figure 5-2, b). The disparity in these deposit thickness at the same cooling temperature is due to the shear removal effect (known as shear stripping mechanism). This implies that at a higher flow rate (9 l/min), which is under turbulent conditions, less wax deposit thickness was observed compared to the low flow rate. Some researchers, such as Kang *et al.* (2019) and Matzain (1999), has experimentally and empirically represented this effect– which shows the reduction rate of deposit formation caused by shear forces.

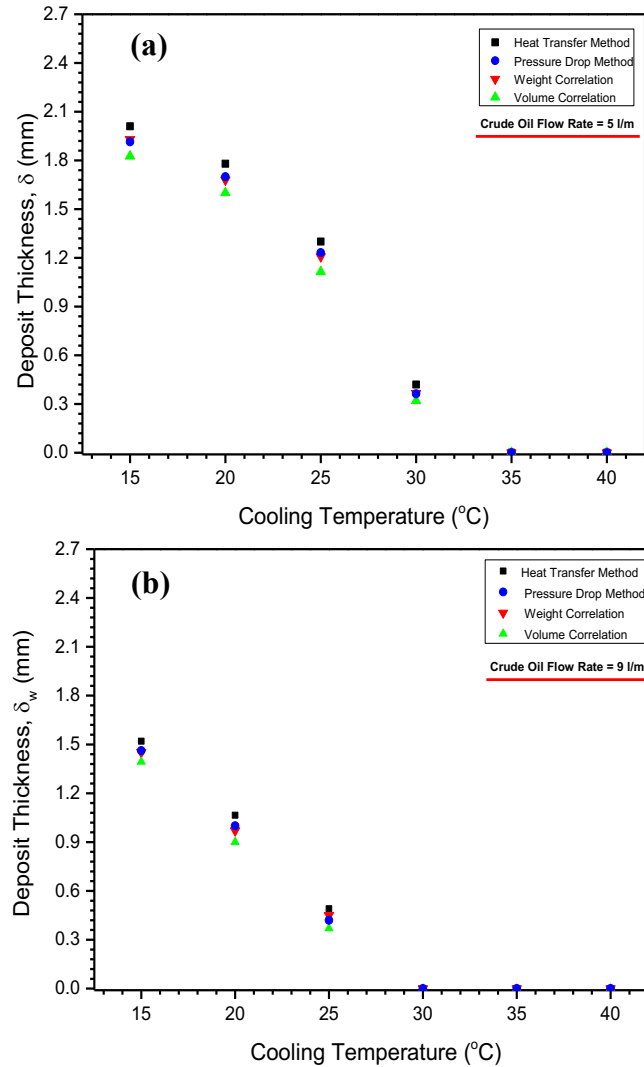


Figure 5-2: Effect of varied cooling temperature (15, 20, 25, 30, 35 and 40 $^{\circ}\text{C}$) on wax deposition at constant crude oil temperature (45 $^{\circ}\text{C}$) and experimental time of 2 hrs. (a) – Experiment at a constant oil flow rate of 5 l/min (laminar flow). (b) – Experiment at a constant oil flow rate of 9 l/min (turbulent flow).

Similarly, as seen in the Figure above, the deposit thickness reduces as coolant temperature is increased from 15 to 20 $^{\circ}\text{C}$ and 25 $^{\circ}\text{C}$. For instance, at 25 $^{\circ}\text{C}$, which roughly equates to the pour point temperature of the crude sample (25.5 $^{\circ}\text{C}$), the thickness at 5 l/min and 9 l/min reduces from 1.93mm at 15 $^{\circ}\text{C}$ to 1.21 mm at 25 $^{\circ}\text{C}$ (Figure 5-2, a) and from $\delta_{wax} \approx 1.46\text{mm}$ at 15 $^{\circ}\text{C}$ to 0.45mm at 25 $^{\circ}\text{C}$ (Figure 5-2, b) respectively. This behaviour is similar to the study reported by Panacharoensawad and Sarica (2013) Singh *et al.* (2000) and Theyab and Diaz (2016).

The results demonstrated that decreasing the coolant temperature (pipe wall temperature) causes the crude oil temperature to drops, which is due to the decrease

in the radial temperature gradient. Several studies collectively reported that molecular diffusion mechanism (Eq. 5.2) is highly and likely the dominant mechanism for the deposition of wax under laminar flow condition as modelled by Burger *et al.* (1981) using Fick's law of diffusion. Whereas, a combination of both molecular diffusion and shear stripping effect (Eq. 5.3) at turbulent flow (Bern *et al.*, 1980; Burger *et al.*, 1981; Zhang *et al.*, 2014).

$$\frac{dM_w}{dt} = \rho_w D_w A_w \frac{dC}{dr} = \rho_w D_w A_w \frac{dC}{dT} \frac{dT}{dr} \quad (5.2)$$

Where $\frac{dM_w}{dt}$ is the rate of wax deposited (kg/s), ρ_w is the density of the solid wax (kg/m³), D_w and A_w are the diffusion coefficient of the wax in the oil phase (m²/s) and the area of wax deposition (m²), $\frac{dC}{dr}$ is the wax concentration gradient (1/m) of wax concentration over pipe radial coordinate r (m), $\frac{dC}{dT}$ and $\frac{dT}{dr}$ are the solubility coefficient of the wax crystal in the oil phase (1/°C) and the radial temperature gradient of the wall (°C/m). d_w is the wax particle diameter (m) and ϕ_w is the wax volume fraction out of the solution at the wall.

Similarly, it is observed that as the coolant temperature develops near to the wax appearance temperature, the wax deposit thickness decreases significantly, especially at the higher oil flow rate, which makes the thermal driving force less significance. Based on the preceding statement, a very small deposit thickness was observed at 30°C under laminar flow (5 l/m, $\delta_{wax} \approx 0.35mm$) and hence, no-wax deposition ($\delta_{wax} \approx 0mm$) under turbulent flow (9 l/m) at the same temperature. In both cases (5 and 9 l/m.), it was observed that the effect of temperature as a driving force is highly insignificant particularly above the WAT, therefore, no wax deposition (i.e. at 35 and 40°C, $\delta_{wax} \approx 0mm$). This is because there is no precipitation of wax molecules as the pipe wall temperature is maintained above WAT, which means that the solubility level of the wax molecules at this point is very high.

On the other hand, following Bern *et al.* (1980) study, it is believed that at higher temperatures and high heat flux conditions, molecular diffusion is dominant deposition process, whereas, at lower temperatures and low heat fluxes shear dispersion is the dominant mechanism. In the latter case, the lateral movement of

wax molecules close to the pipe wall due to the shear dispersion mechanism leads to the transport of more precipitated wax from the turbulent core to the surface of the pipe. This behaviour could result in the formation of a deposit on the pipe wall or connect with wax already deposited by molecular diffusion (Bern *et al.*, 1980). Therefore, increase in shear rate usually encourage more wax crystals to diffuse towards the pipe wall, whereas, the corresponding increase in wall shear stress causes more loosely held deposits to be stripped from the pipe wall (Venkatesan, 2004; Bott and Gudmundsson, 1977). Eq. 5.3 defines shear stripping (i.e. the negative wax transfer due to shear forces) as a function of the shear stress τ , and thickness of the wax layer δ (m) based on the Pan *et al.* (2009) and Ajayi (2013) study.

$$J^{sr} = C \frac{\delta \tau}{\omega^{2.3}} \quad (5.3)$$

Where C is the shear constant, ω is the mass fraction of wax in the gel layer

According to the literature, both shear dispersion and Brownian diffusion mechanisms are responsible for the lateral movement of particles (Burger *et al.*, 1981). In shear dispersion mechanism, small particles are suspended in a fluid that is in the laminar motion process. This usually occurs at lower temperatures and low shear compared to the Brownian diffusion. The coefficient of Brownian diffusion (D_B) and shear dispersion (D_s) are defined by Burger *et al.* (1981) as

$$D_B = \frac{RT_a}{6\pi\mu aN} \quad (5.4)$$

$$D_s = \gamma_o \frac{d_w^2 \varphi_w}{10} \quad (5.5)$$

Where R is the gas constant, T_a is the absolute temperature, μ is the oil viscosity, a is the Brownian particle diameter (m), and N is the Avogadro's number, whereas γ_o is the oil shear rate at the pipe wall (s^{-1}), d_w is the wax particle diameter (m), and φ_w is the wax volume fraction out of the solution at the wall.

It should be noted that in a straight pipe, shear dispersion and Brownian diffusion are considered less probable mechanisms or insignificant when compared to the bend pipes (see section 5.4). Studies have shown that there is likely no propensity for the

nucleation process to occur around the dispersed particles than those formed by the molecular diffusion process (Bern *et al.*, 1980). However, due to the lateral movement of particles and fluid separation around the bend pipes, the intensity and propensity for the nucleation process around the dispersed particles are higher. These disparities are well discussed in the subsequent sections.

Currently, a model by Matzain has already incorporated three of these mechanisms (i.e. molecular diffusion, shear dispersion and shear stripping), which is one of the reliable wax deposition predicting model included in OLGA simulator alongside IRRR and heat analogy.

5.3.2 Influence of Crude Oil Flow Rate

In a similar way to the temperature effect, the crude oil flow rate has shown to be significant in the wax deposition process (Kang *et al.*, 2019). In this work, the impact of different oil flow rates (i.e. 2, 3, 4, 5, 7, 9, 11 l/min) was investigated over two varied pipe wall temperature (15 and 30°C; which are below and above the pour point), at constant oil temperature and experimental time of 45°C and 2 hrs respectively. These flow rates cover the two dynamics flow regimes, i.e. laminar (2, 3, 4, 5 and 7 l/min) and turbulent flow (9 and 11 l/min). This allows us to thoroughly evaluate the effect of this parameter within the lower and higher rate conditions. For instance, the laminar (5 l/min) and turbulent flow (9 l/min) conditions used in section 5.3.1 are considered to be higher flow rate around the laminar flow regime and lower or medium flow rate around the turbulent flow regime.

As shown in Figure 5-3: Effect of varied crude oil flow rate; 2, 3, 4 and 5 l/min (laminar regime) and 7, 9 and 11 l/min (turbulent flow) on wax deposit thickness: (a) – cooling at 15°C (below pour point). (b)– cooling at 30°C (at wax appearance temperature), wax deposition rate decreased with an increase in the crude oil flow rate and vice versa. It is seen that the severity of the deposition (in thickness) is higher– even at a turbulent flow around high flow rate of 11 l/min, as long as the coolant temperature falls below the pour point (15°C). Illustrated in the Figure 5-3 (a), at cooling temperature of 15°C, the deposit thickness decreased very slowly from 2.38 mm at 2 l/min to 1.89, 1.45 and 1.26 mm at 5, 9 and 11 l/min. However, over the same range of flow rate, as the pipe wall temperature equals to the wax

appearance temperature (WAT) (30°C), i.e. above the pour point; the deposit thickness decreases significantly, especially at higher flowrate. For instance, it was observed that at turbulent flow condition under high flow rate Q_{oil} , of 9 and 11 l/min, there is no wax deposition observed, i.e. $\delta_{wax} \approx 0mm$. Similarly, a very small wax deposit was seen at a lower flow rate (e.g. at 2 l/min, $\delta_{wax} \approx 0.84$ mm) (Figure 5-3, b).

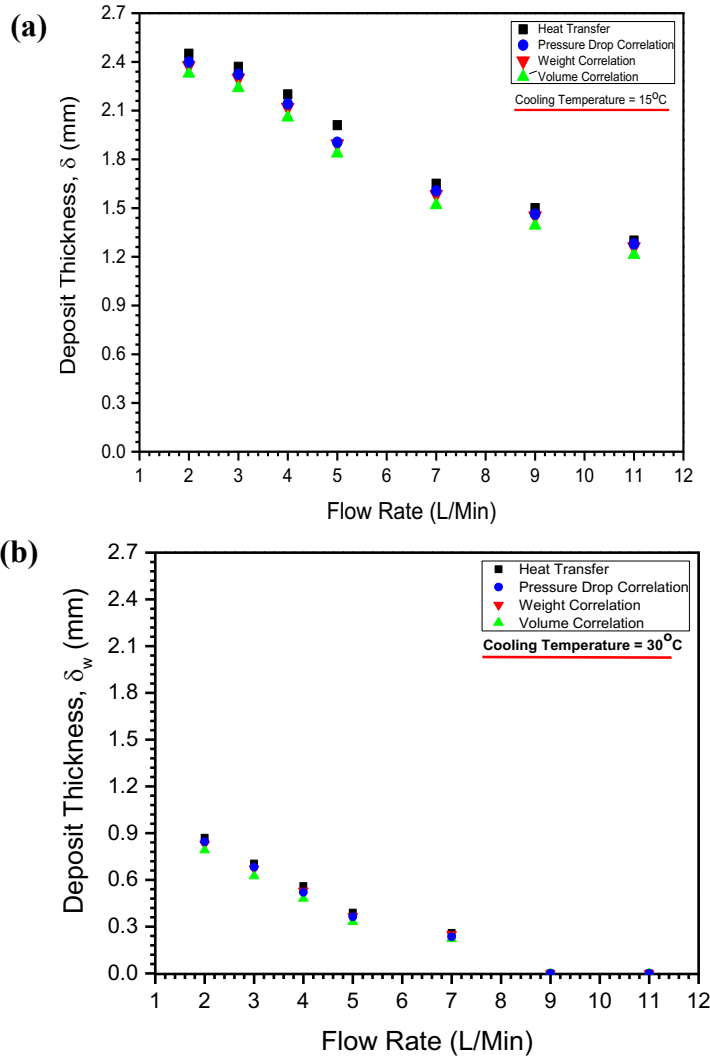


Figure 5-3: Effect of varied crude oil flow rate; 2, 3, 4 and 5 l/min (laminar regime) and 7, 9 and 11 l/min (turbulent flow) on wax deposit thickness: (a) – cooling at 15°C (below pour point). (b)– cooling at 30°C (at wax appearance temperature)

Accordingly, at the lower flow rate, the high deposit thickness could be related to the high residence time experiences by the circulating oil that led to additional heat losses between the fluid and cold surface. Consequently, this resulted in lowering the crude oil temperature and rapid precipitation of the wax particles. Therefore, in this case, the

internal heat transfer coefficient increases with an increase in the radial temperature gradient, which led to a much higher concentration of wax molecules diffused towards the pipe wall and deposited (Adeyanju and Oyekunle, 2013; Creek et al., 1999). In this scenario, it is believed that both molecular diffusion and shear dispersion contributed to the deposition process at low conditions. This is following the previous studies such as Burger *et al.* (1981), which considerably believed that shear dispersion and molecular diffusion (Brown *et al.*, 1993; Hsu and Brubaker, 1995) are the dominant mechanisms in a wax deposition when the oil temperature is much lower than the WAT.

On the other hand, a high flow rate underpins a lower residence time and lowers internal heat transfer coefficient that reduces the radial temperature gradient. Similarly, in this case, there is an increase in shear stress between the liquid-deposit interface. This condition (higher flow rate) increased the intensity of the shear stripping alongside with molecular diffusion of molecules. As a result, in this case, no deposition at $Q_{oil} = 9$ and 11 l/min or lesser wax deposit ($\delta_{wax} \approx 0.25$ mm) is seen at $Q_{oil} = 7$ l/min. As such, similar to experimental studies by Creek *et al.* (1999), Hernandez (2000) and Matzain (1999) shear removal effect on wax deposits, particularly under turbulent conditions has been observed.

On the other hand, Figure 5-4 shows the rate of deposition in terms of volume and weight of the deposit measured under varied conditions. The results further proved the behaviour reported in deposit thickness. It was noticed that increasing the flow rate decreased the amount of wax deposited (volume and weight). For instance, at a cooling temperature of 15 °C, the mass and volume of the deposit decrease from 77 g and 121 ml at 2 l/min to 43 g and 45 ml at 11 l/min (*Figure 5-4, a*). Similarly, the deposition rate increased with a decrease in coolant temperature (pipe wall temperature). It reached the maximum as the temperature near the usual seabed condition (i.e. below the PP of the sample) at a low flow rate (2 l/min). Besides the explanation given in the previous section, it is interesting to be aware that increasing the fluid velocity leads to an increase in the viscous drag force that tends to remove the accumulation as it exceeds the shear stress within the deposited wax (Zhu *et al.*, 2008).

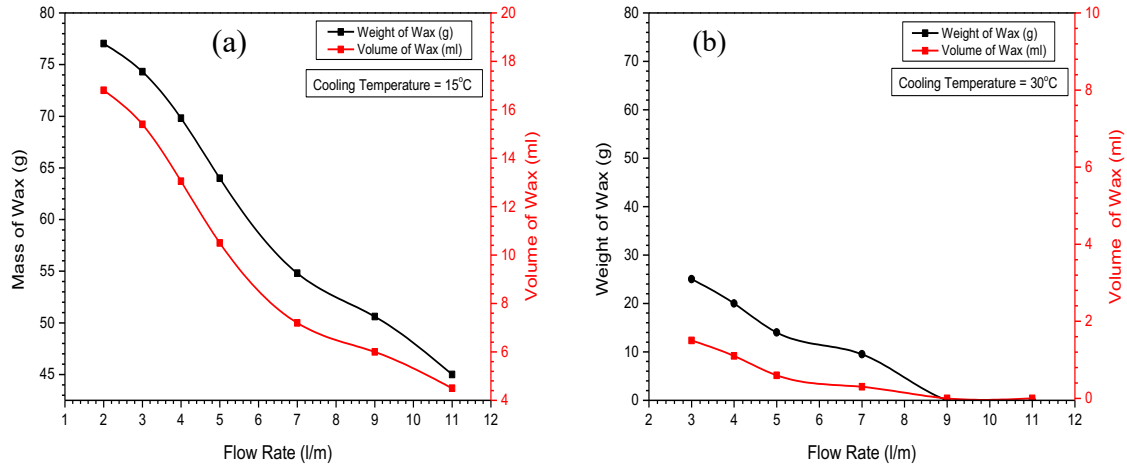


Figure 5-4: Effect of varied flow rate on weight and volume of the deposited wax. (a)- at a constant cooling temperature of 15°C. (b)- at a constant cooling temperature of 30°C.

5.3.3 Error Analysis in Deposit Thickness Measurement

In this work, a parity plot is used to evaluate the accuracy of the techniques used to determine wax deposit thickness (δ_w) (i.e. weight–balance, pressure drop, volume correlation and the heat transfer method) based on the experimental conditions and results in Figure 5-2 and Figure 5-3: Effect of varied crude oil flow rate; 2, 3, 4 and 5 l/min (laminar regime) and 7, 9 and 11 l/min (turbulent flow) on wax deposit thickness: (a) – cooling at 15°C (below pour point). (b)– cooling at 30°C (at wax appearance temperature).

Parity plot– as a scatter plot was reported as one of the methods used to compare reference data chosen with experimental results (Baby and Balaji, 2019). In the analysis, a parity line, also known as a mean line or a reference is usually drawn, which is defined by equation $y = x$ to compare the set of experimental data. In the case where the experimental data fall on the mean line or parity line, then it is interpreted as a perfect fit, indicating there is no error between the data sets. However, if the data falls below or above the parity line, it is either underestimation (-ve), or overestimation (+ve) the measured data. Outliers data may not be included in the error margin given the extreme deviation from the cluster of data in the experiential results.

The error margin or deviation from parity margin is hence determined based on the maximum deviation of points from the mean line. Hence, the error margin is the standard deviation scaled according to the maximum value of the data sets. It is also referred to as the root-mean-square error (RMSE) or root-mean-square deviation (RMSD) between the reference and experimental data sets. Equation 5.8 gives the formulas. Lashkarbolooki *et al.* (2011) used another expression through the average percentage relative error (E_r) between the reference data and the rest of the experimental data sets defined as

$$E_i = \left[\frac{T_{exp} - T_{ref}}{T_{ref}} \right]_i * 1000 \quad i = 1, 2, \dots \dots n \quad (5.6)$$

$$E_r = \frac{\sum_{i=1}^n E_i}{n} \quad (5.7)$$

Which give a similar result to RMSE method

$$RMSE = \sqrt{\frac{\sum_{i=1}^n (x_i - y_i)^2}{n}} \quad (5.8)$$

The resulting RMSE error is then obtained +/- absolute value that defines the error margin lines in shot dashed black line. Furthermore, a percentage of the RMSE can be computed based on the maximum scale from the data set. Therefore, **Figure 5-5** and Figure 5-6 show parity plots of wax deposit thickness (δ_w) at varied temperature and flow rate. Figure 5-5 represent a parity plot based on the data set from Figure 5-3, whereas, Figure 5-6 is based on data set from Figure 5-2. As shown in the Figures, the data from the weight balance method is used as the mean line, i.e. as the reference data. The reference method is deemed to be accurate based on the established results in this work and the data reported in the published literature by Chen *et al.* (1999) and Matzain *et al.* (2002). Hence, this work has proved Chen *et al.* and Matzain *et al.* claim and further discovered that both weight balance and the back-calculation from the pressure drop method produced roughly the same wax thickness, similar behaviour was observed in a study by Hoffmann and Amundsen (2010) and Panacharoensawad and Sarica (2013).

It is seen that the data from the pressure drop method (red points) fall within the mean line (reference), thereby revealing a perfect match without errors. A very slight

disparity is observed from the pressure drop data (Figure 5-6) which could be due to the uncertainty of pressure drop measurement at a low flow rate (i.e. 2, 3, 4 l/min). Zhang (1999) error analysis shows that pressure drop approach is suitable for higher flow rates studies, but not for low flow. However, based on the overall results from the parity plot it can indeed conclude that pressure drop and weight–balance methods are the most reliable techniques for calculation of wax thickness in this work as agreed with other literature. Hence, weight correlation was used in all the subsequent deposit wax measurement.

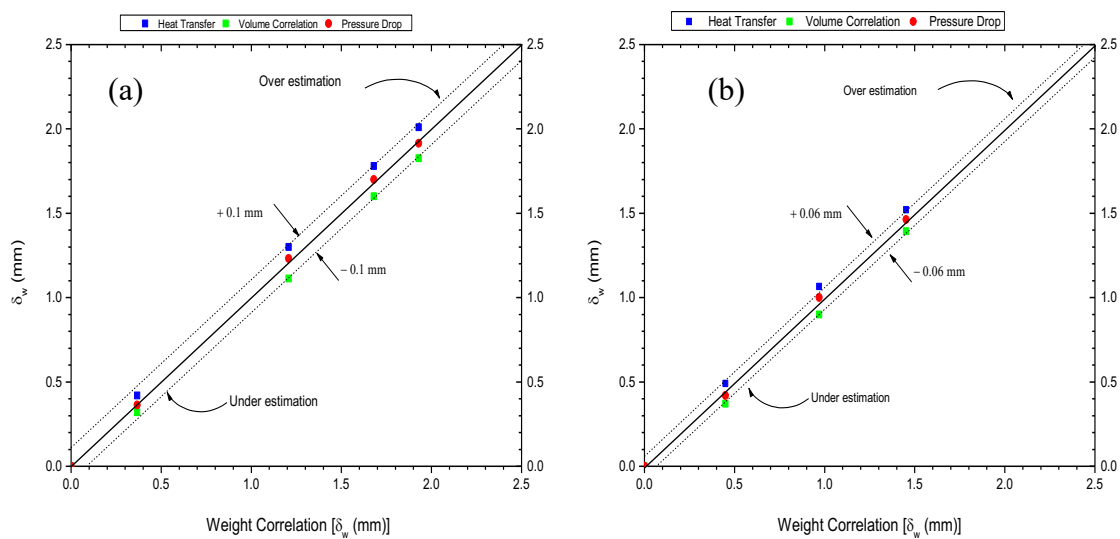


Figure 5-5: Parity plot validation of deposit thickness (δ_w) obtained from weight–balance (reference data) and pressure drop method with volume correlation method and heat transfer methods. (a)– Thickness at $Q_{oil} = 5$ l/min and $T_{coolant} = 15, 25, 30,$ and 35°C . (b)– Thickness at $Q_{oil} = 9$ l/min and $T_{coolant} = 15, 25, 30,$ and 35°C .

On the other hand, it is observed that the heat transfer methods overestimate the deposit thickness relative to the thickness obtained using the weight method, whereas, the volume correlation underestimate the thickness. In Figure 5-5 (a), the overall error margin of ± 0.1 mm is computed and compared to an error margin of ± 1.06 mm (Figure 5-6, b). Whereas, Figure 5-5 (b) and Figure 5-6 (b), produced ± 0.06 mm as compared to ± 0.05 mm for heat transfer and volume correlation methods relative to weight method. This uncertainty band infers a good agreement with other published data. For instance, Volk *et al.* (2003) revealed that the heat transfer method might not be reliable to give an accurate measurement of the wax thickness given the uncertainty associated with the thermal measurement of the conductivity of the wax deposit. Hence an error margin of ± 0.11 mm was

estimated in their study. The uncertainties of volume measurement come from the pigging of the deposit wax and measurement the volume of the fluid (human error).

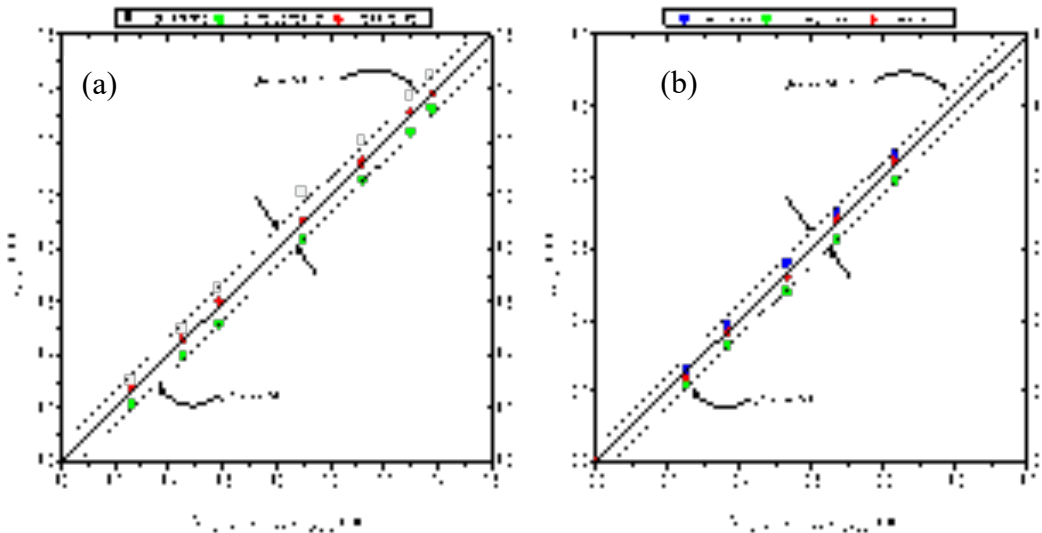


Figure 5-6: Parity plot, validation of experimental deposit thickness (δ_w) obtained from weight–balance (reference data) and pressure drop method with volume correlation method and heat transfer methods. (a)– Thickness at $constant T_{coolant} = 15^\circ\text{C}$ and $Q_{oil} = 2, 3, 5, 7, 9$ and 11 l/min. (b)– Thickness at $constant T_{coolant} = 30^\circ\text{C}$ and $Q_{oil} = 2, 3, 5, 7, 9$ and 11 l/min.

A sample of pigging operation showing the solid wax pushed out of the pipe section is shown in Figure 5-7. Whereas, a sample of the deposit thickness layer on the pipe wall can be found in Figure 5-16.

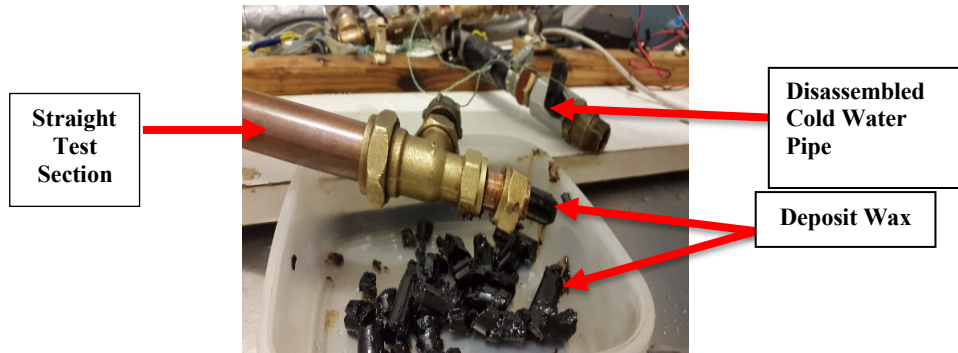


Figure 5-7: Sample of wax pigging operation inside the jacked test section obtained in the laboratory.

5.3.4 Deposit Thickness Variation with Time

The influence of wax deposition ageing on the severity of the deposition is studied in this section. Understanding this behaviour is essential for the successful remediation and control of wax built-up in the facilities. A study by Al-yaari (2011) has shown that the incipient wax gel grows as time progresses, while there are radial thermal

and mass transfer gradients as a result of heat losses to the surroundings. In a nutshell, wax molecules diffusion into the wax deposit due to the concentration gradient across the deposit, and therefore, wax ageing affected the overall deposition process (Zhang *et al.*, 2014). According to the results shown in Figure 5-8, the parameter investigated has relatively influenced wax deposition. Figure 5-8 shows the wax deposit thickness profile along with the experimental time increases (2, 4, 6, and 8 hrs). The study is carried out at a different cooling temperature of 15, 25 and 30°C, over two different flow rates of 5 l/min (Figure 5-8, a) and 9 l/min (Figure 5-8, b).

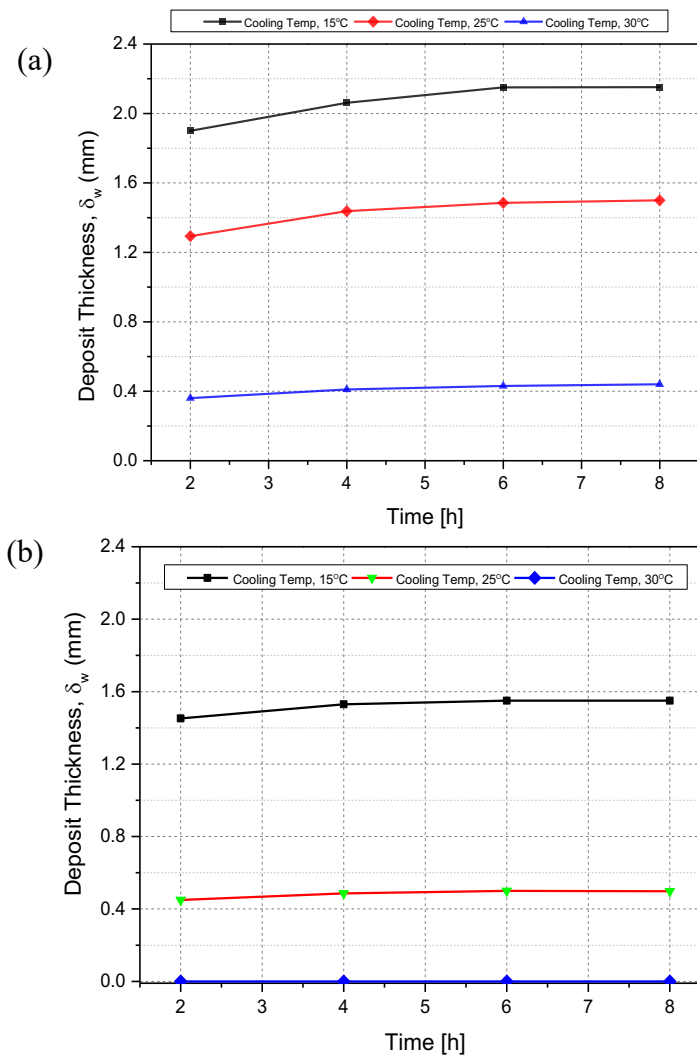


Figure 5-8: The effect of different experimental time on the wax deposition measured in thickness as a function of different cooling temperature. (a)– at laminar flow regime (5 l/min). (a)– at turbulent flow regime (9 l/min).

It is clearly seen in Figure above that, initially, the wax deposition rate starts at a relatively higher value during the initial experimental time from 2 hr and then increases slowly about 4 hrs and then 6hrs. Therefore, the growth of the deposit reached a steady-state after 8 hrs experiment. It is believed after these 8 hrs experimental times the deposited wax layer acted as thermal insulation between the hot crude oil and the surrounding pipe surface (cold). This means the growth of the deposit wax layer continues until a thermal steady-state is achieved. Such that the rate of thermal energy gained by the coolant is equal to the rate of heat transfer through four thermal resistances in series, namely the mixture (convection), deposit layer (conduction), tube wall (conduction), and coolant (convection) (Ehsani *et al.*, 2019). On the other hand, the shear removal effect could prevent continuous wax built-up with time (Zhang *et al.*, 2014). This means at a specific flow condition, the wax deposition rate is balanced with the shearing rate after a particular time, and the overall growth of wax deposits stops.

Following other studies, it is understood that the oil molecules can continually diffuse out of the wax deposit matrix, creating a hard deposit, despite the overall growth of the wax deposit stops after 8 hours. Similarly, wax molecules diffuse into the wax deposit due to the concentration gradient across the deposit leading to an increase of the wax fraction in the deposit and gel strength (Zhang *et al.*, 2014; Singh *et al.*, 2000). In a nutshell, different literature and studies by Al-yaari (2011), Pinho *et al.* (2011) and Theyab (2017) also support the behaviour observed in this work.

5.4 Wax Deposition Analysis in Curved Pipes

Having developed a good understanding of wax deposition behaviour using a straight pipe section and validated the results of this study following theories and similar technique used by previous studies. Therefore, the study and results obtained in the straight pipe section serves as the based for the comparative analysis on the severity of wax deposition with curved pipe. Recalled that the deposition in straight pipe is highly controlled by mechanisms such as molecular diffusion, shear dispersion and shear stripping. However, the latter is believed to oppose the deposition process. On the other hand, mechanisms such as Brownian diffusion and gravity settling have an insignificant impact on the deposition in a straight pipe. Although with curvature in

pipe, the depositional behaviour changes perhaps due to the factors discussed in Section 5.4.1 and 5.4.2.

In gravity settling mechanism, the precipitated molecules denser than the surrounding fluid settled on the pipe wall. An experimental study by Burger et al. (1981) investigates the gravity settling mechanism by switching a straight pipe test section from horizontal to vertical flow, with no effect to the gravity settling been observed. Perhaps due to the shear dispersion effect, which redispersion of the solids particles on the pipe wall – which could occur either in vertical or horizontal flow (Burger et al., 1981; Kok and Saracoglu, 2000). On the other hand, the Brownian diffusion mechanism is said to be insignificant in straight pipeline flow, as a result of lateral transport of particles by diffusion. Studies have shown that lateral transport of particles may also occur in molecular diffusion and shear dispersion (Burger *et al.*, 1981; Kok and Saracoglu, 2000) – therefore, the influence of Brownian diffusion is less compared to the other two mechanisms in a straight pipe.

In another study by Zhu et al. (2008), suggested that in laminar flow regime, mechanism by shear removal, Brownian dispersion, and gravity settling mechanisms could be ignored while molecular diffusion becomes the dominant mechanism for wax deposition. Hence, the study of wax in curved pipe and the results discussed in subsequent sections are vital, which look at the problem of wax deposition in different angle – compare to the previous studies. Therefore, the impact of pipe curvature on the increased severity of wax deposition that had been left unanswered problems in the literature is studied. Prior to the main results and discussion (section 5.4.2), the new model for deposit thickness quantification in bend pipe, and its significance is discussed below.

5.4.1 New Model for Deposit Thickness Quantification in a Bend Pipe

It is worth recalling that the current model used for deposit thickness calculation (see Eq. 3.15) was based on the pressure drop equation (Chen *et al.*, 1997), which is as a result of frictional loss in pipe. Having understood that wax deposition could be affected by a curve or bend pipe, in which the flow is characterised by the presence of a radial pressure gradient generated by the centrifugal forces acting on the fluid (Sreenivas, 2011). Thus, the presence of a bend in pipes might affect the global and

local flow parameters such as the additional pressure drop, advection and particle interaction (Wang et al., 2004; Yadav et al., 2014), which might consequently influence the mechanisms of wax deposition. Hence, a new model is developed, which incorporated some of these parameters that are primarily associated with flow instability and separation at some boundary area. These mainly depend on Reynolds number, bend angle (θ) and the radius of curvature of the bend (R_b) (Dean, 1927; Dutta *et al.*, 2016; Murty and Thandaveswara, 2014; Sreenivas, 2011; Vester *et al.*, 2016)

Therefore, in the new model, the total pressure drop is defined as a sum of the frictional pressure drop within the straight pipe and the pressure drop due to the change in the direction of flow– momentum change. The latter effect depended on the parameters such as the bend radius (R_b), the bend angle (θ), and the bend loss coefficient (k_b) (Dean, 1927; Sreenivas, 2011; Prajapati et al., 2015). This indeed, is the case because the flow of fluid in a straight pipe experiences a steady flow without velocity variation, particularly in a laminar flow. However, if the fluid passes through a bend, the pressure losses in the bend pipe increased due to the centrifugal forces, which in turn (can) cause the flow to separate at the inner wall of the bend pipe (Dean, 1927; Prajapati *et al.*, 2015; Sreenivas, 2011; Vester *et al.*, 2016) and could affect the deposition process. Therefore, in a bend, some portion of the fluid accelerated in a constant flow through the cross-section of the pipe. Whereas, the separated fluid from the bulk fluid experienced low velocity and back-mixing due to the localised disruption of the flow around the bend pipe (see Figure 5-9). Eventually, this could cause loss of energy, and consequently, experiences a high thermal gradient than the bulk fluid.

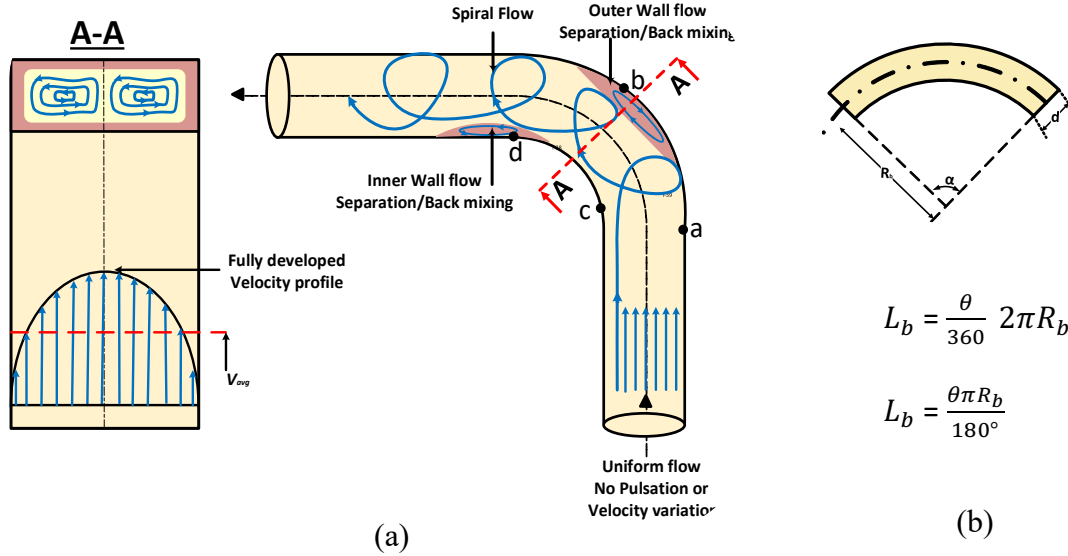


Figure 5-9: Typical velocity profiles with a separated flow in pipe bend: (a) Longitudinal and rectangular cross-section around the 90° bends (Adapted from Idelchik, 1986), (b) Bend parameters

Therefore, the deposit thickness measured along a section with bend was modelled starting from the pressure drop correlation in Eq. 5.9 (Sreenivas, 2011; Prajapati et al., 2015).

$$\Delta P = \underbrace{4f \frac{L}{d} \frac{\rho}{2} (V)^2}_{\text{Pressure Drop due to Frictional loss}} + \underbrace{\frac{1}{2} k_b \rho V^2}_{\text{Pressure Drop due to Momentum change}} \quad (5.9)$$

Substituting the bend parameters in the pressure drop due to the frictional loss defined in Figure 5-9 into Eq. 5.9 gives

$$\Delta P = 4f \frac{\rho(V)^2}{2d} \left(\frac{\theta \pi R_b}{180} \right) + \frac{1}{2} k_b \rho V^2 \quad (5.10)$$

The friction factor in Eq. 5.10 is defined as $f = \frac{c}{(R_e)^n}$

Therefore, for laminar flow condition

$$f = \frac{16}{(Re)^1} = \frac{16 \pi \mu d}{4 \rho Q}$$

Equation 5.10 becomes

$$\Delta P = \frac{4}{2d} \left(\frac{16 \pi \mu d}{4 \rho Q} \right) \rho (V)^2 \left(\frac{\theta \pi R_b}{180} \right) + \frac{1}{2} k_b \rho V^2 \quad (5.11)$$

By eliminating all the common terms and factorised velocity of the fluid, Eq. 5.11 is expressed as

$$\Delta P = \left(\frac{8 \pi^2 \mu}{Q} \right) (V)^2 \left(\frac{\theta R_b}{180} \right) + \frac{1}{2} k_b \rho V^2 \quad (5.12)$$

$$\Delta P = (V)^2 \left[\left(\frac{8 \pi^2 \mu}{Q} \right) \left(\frac{\theta R_b}{180} \right) + \frac{1}{2} k_b \rho \right] \quad (5.13)$$

Therefore, expressing the velocity in terms of flow rate from $Q=VA$; $V = \frac{4Q}{\pi d^2}$

$$\Delta P = \left(\frac{4Q}{\pi d^2} \right)^2 \left[\left(\frac{8 \pi^2 \mu}{Q} \right) \left(\frac{\theta R_b}{180} \right) + \frac{1}{2} k_b \rho \right] \quad (5.14)$$

$$\Delta P = \left(\frac{16Q^2}{\pi^2 d^4} \right) \left[\left(\frac{8 \pi^2 \mu}{Q} \right) \left(\frac{\theta R_b}{180} \right) + \frac{1}{2} k_b \rho \right] \quad (5.15)$$

However, as the wax begins to form, the diameter of the pipeline reduces; therefore, the new internal diameter of pipe open to flow is reduced by $2\delta_w \Rightarrow d_w$ (see Figure 3-16, section 3.8).

Hence, $d = d_w = d_i - 2\delta_w$. Therefore, Eq 5.15 is expressed as

$$\Delta P = \left(\frac{1}{d^4} \right) \left[(128Q\mu) \left(\frac{\theta R_b}{180} \right) + \frac{8Q^2 k_b \rho}{\pi^2} \right] \quad (5.16)$$

$$(d_i - 2\delta_w)^4 = \left(\frac{1}{\Delta P} \right) \left[(128Q\mu) \left(\frac{\theta R_b}{180} \right) + \frac{8Q^2 k_b \rho}{\pi^2} \right] \quad (5.17)$$

$$\text{Let } A = \left[(128Q\mu) \left(\frac{\theta R_b}{180} \right) + \frac{8Q^2 k_b \rho}{\pi^2} \right]$$

Equation 5.17 can now be written as

$$\begin{aligned} \therefore di - 2\delta_w &= \left[\left(\frac{1}{\Delta P} \right) [A] \right]^{\frac{1}{4}} \\ \delta_w &= \frac{di - \left[\left(\frac{1}{\Delta P} \right) [A] \right]^{\frac{1}{4}}}{2} \end{aligned} \quad (5.18)$$

Substituting for A, the overall formulated model can be express as

$$\delta_w = \frac{di - \left[\left(\frac{1}{\Delta P} \right) \left[(128Q\mu) \left(\frac{\theta R_b}{180} \right) + \frac{8Q^2 k_b \rho}{\pi^2} \right] \right]^{\frac{1}{4}}}{2} \quad (5.19)$$

Equation 5.19 represents the new model. Where μ is the viscosity, R_b is the bend radius, θ , the bend angle, k_b , the bend loss coefficient and ρ the density of wax.

Before using the model (Eq. 5.19) to calculate wax thickness, the effect of curvature parameters was studied using Babcock & Wilcox chart. The curvature ratio and the bend loss coefficient were verified (Appendix, Figure C 1). Therefore, based on the flow rig design, the curvature ratio (R_c/D , 45/13.6) is significant and can cause flow separation and increases large pressure losses around the pipe bend. According to the literature a minimum R_c/D of 1.5 is enough to cause issues related to the fluid flow (such as Sreenivas, 2011; Murty and Thandaveswara, 2014; Dutta *et al.*, 2016; Vester *et al.*, 2016). Similarly, the bend loss coefficient obtained from the Babcock & Wilcox chart has further proved the impact of this model. For the pipeline with 90° bend $k_b \approx 0.24$, whereas 0.15 for 45° bend.

Furthermore, a parity plot (Figure 5-10) was used to measure the disparities of the deposit thickness (δ_w) calculated using the new model compared to the existing correlation (reference technique). It is observed that the new model did not match the predictions of the reference method (i.e. weight correlation) with data error margin within the -1.5 mm and -0.35 mm (Figure 5-10) – therefore, the method underestimated the deposit thickness. This could be because the pressure drop measured from the test section of the flow rig did not include the actual pressure drop around the bend. Therefore, as seen from the flow rig, only the inlet and the outlet pressure were measured; consequently, the effect of the additional increase in

pressure loss around the bend is not properly measured. However, it is worth noting that even if the actual pressure drop around the bend is accurately measured, it will make a little difference, particularly in this work. This could be due to the size (small) and the length of the pipe sections used, leading to the small disparity seen between the deposit thickness from the new model and the weight correlation (reference method) (Figure 5-10). However, the disparity could be significant, particularly in the field study or using a larger size and long-distance pipe.

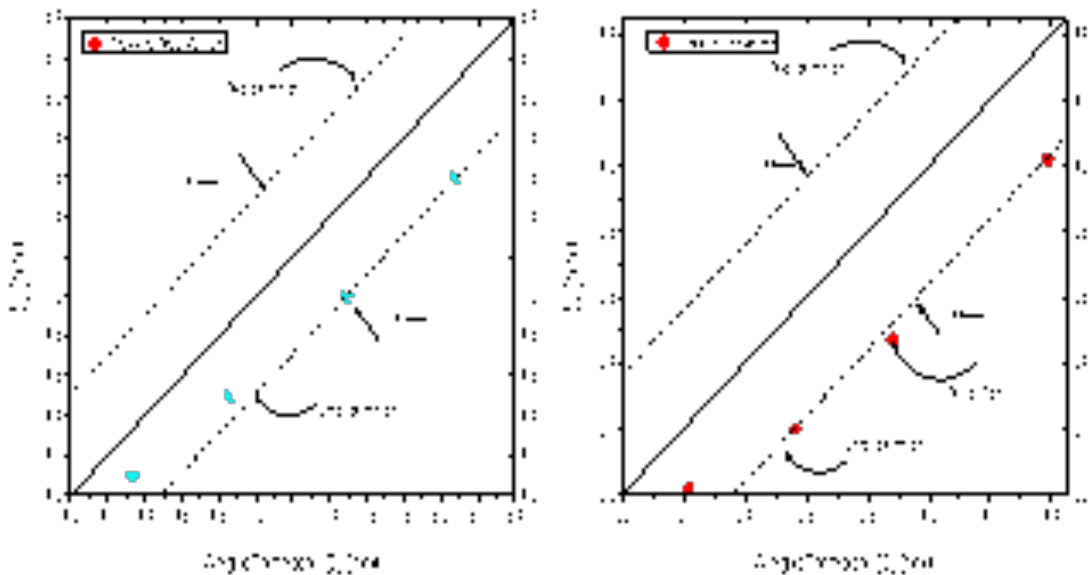


Figure 5-10: Parity plot– comparison of the new model with the existing correlation weight–balance (reference data). Left– Thickness at constant $T_{\text{coolant}} = 15^{\circ}\text{C}$ and $Q_{\text{oil}} = 5, 7, 9$ and 11 l/min. Right– Thickness at constant $T_{\text{coolant}} = 30^{\circ}\text{C}$ and $Q_{\text{oil}} = 5, 7, 9$ and 11 l/min.

A significant pressure drop would be measured in a long-distance pipe and is expected to vary at a different location, particularly, before the pipe bend, immediately after the bend and at a distance far away from the bend. Meaning that by ignoring the pressure losses at the bend the wax that formed around the inner part of the pipe, which might have further increase the pressure drop couldn't be predicted accurately using the new correlation. Therefore, to fully appreciate the new model, it is recommended to modify the test section, to accommodate many sensors for wax film measurement, visual inspection and pressure drop monitoring around the bend. Currently, the flow rig used in this study has no sensors to measure the local wax thickness in and around the bend. However, it does incorporate two vital sensors that measured the overall pressure drop of the test sections. Therefore, the

study, assumed that wax film is symmetrically distributed in the pipe. Although, the assumption may not be valid particularly, for a larger diameter pipe.

5.4.2 Study of the Effect of the Main Control Parameters on Wax Deposition in Curved Pipes

The study is carried out according to the flow loop designed in chapter 3 (section 3.5) with experimental matrix presented in Table 3-6. Therefore, the effect of thermal gradient over different range of cooling temperature at 15, 25 and 30 °C, the crude oil flow rate, including $Q_{oil} = 5$ and 7 l/min (laminar flow) and $Q_{oil} = 9$ and 11 l/min (turbulent flow) and the experimental time of 2, 4, 6 and 8 hrs were investigated. The studies were carried out using the two pipe test section– that is 45° and 90° bend pipes in horizontal and incline flow.

Figure 5-11 shows a comparison of wax deposition rate (in deposit thickness) using a horizontal and inclined 45° bend pipes section. In both orientations, a higher deposition rate was seen, particularly around the laminar flow regime. For instance, at Q_{oil} of 5 l/min and at 15°C cooling temperature a deposit thickness δ_{wax} , of 3.1 mm and 4.2 mm is observed in the horizontal and inclined 45° curved pipe. As expected, the severity of the deposition decrease as the coolant temperature increase from 15 to 25 and 30°C. Therefore, at the same flow rate (5 l/min) the thickness decrease from 3.1 mm to 2.2 and 1.1 mm for the horizontal pipe and 4.2 mm to 3.6 and 2.05 mm for the inclined 45° bend pipe. This demonstrates that as the coolant temperature develops towards the wax appearance temperature, the wax deposit thickness decreases significantly, especially at higher oil flow rate due to the influence of the driving force, which is becoming less significant. The thickness reduces further with the increase in flow rate, especially around the turbulent flow regime (e.g. 9 and 11 l/min). Similar to the straight pipe experiment, in two of the cases studied in this section, it is observed that at a cooling temperature above the WAT (i.e. at 35 and 40°C) no wax deposition and $\delta_{wax} \approx 0mm$. This is because above the WAT, the solubility of the wax crystals is high, which keep the wax crystal in the oil– that liquid phase.

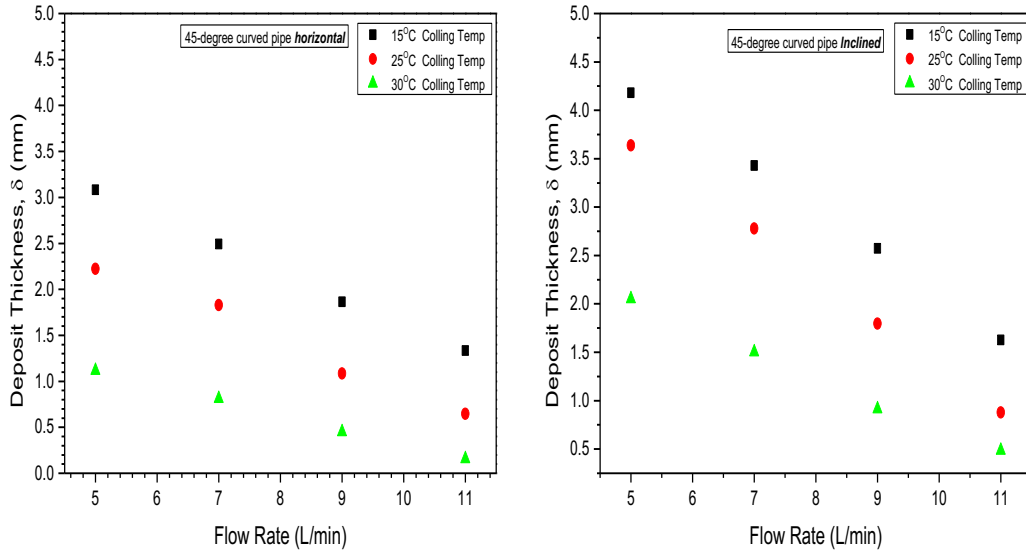


Figure 5-11: Effect of varied cooling temperature under different flow rates on wax thickness in 45° bend pipe test-section: Left – Horizontal flow experiment. Right – Inclined flow experiment.

In contrast to the deposition in a straight pipe, a higher deposit thickness was seen particularly at a condition that was not expected, i.e. at a relatively higher cooling temperature of 30°C (WAT) and high flow rate ($Q_{oil} = 11$ l/min). At these conditions, a thickness of around 0.2 mm is measured in horizontal flow, while 0.45mm in an inclined flow (elevation) (Figure 5-11). It is important to recall that in the straight pipe experiment no deposition was seen under the same conditions, i.e. the deposit thickness $\delta_{wax} \approx 0$ mm at 30°C (WAT) and 11 l/min (Figure 5-13).

Similarly, Figure 5-12 presented results of deposit thickness from the second curved pipe– with 90° bend pipes section (horizontal and inclined). It is seen that at a constant flow rate and cooling temperature of 5 l/min and 15°C the deposit thickness δ_{wax} , increases from in 3.5mm in horizontal flow to 3.85mm in an inclined pipe. Similar to the severity observed in 45° bend pipe section (Figure 5-11); the deposition in 90° bend pipe section (horizontal and inclined) decrease as the coolant temperature increase from 15 to 25 and 30°C. Also, increasing the flow rate Q_{oil} , from 5 l/min to 7, 9 and 11 l/min interfered the overall deposition rate. Therefore, increasing the Q_{oil} causes more oil at high temperature to be pumped through the test section, thus, leads to shorter residence time and consequently reduced the deposit thickness. However, as discussed in the previous paragraph, this behaviour is less significant in bend compared to a straight pipe test section. For instance, in the

straight pipe, the deposition is reduced significantly at higher cooling temperature and equal zero at a higher flow rate (11 l/min). Unlike, in the bend pipes where the deposition is noticed even at higher flowrate and cooling at WAT. See Figure 5-13 for a comparison of results between straight pipe and 45^o and 90^o bend pipes section (horizontal and inclined).

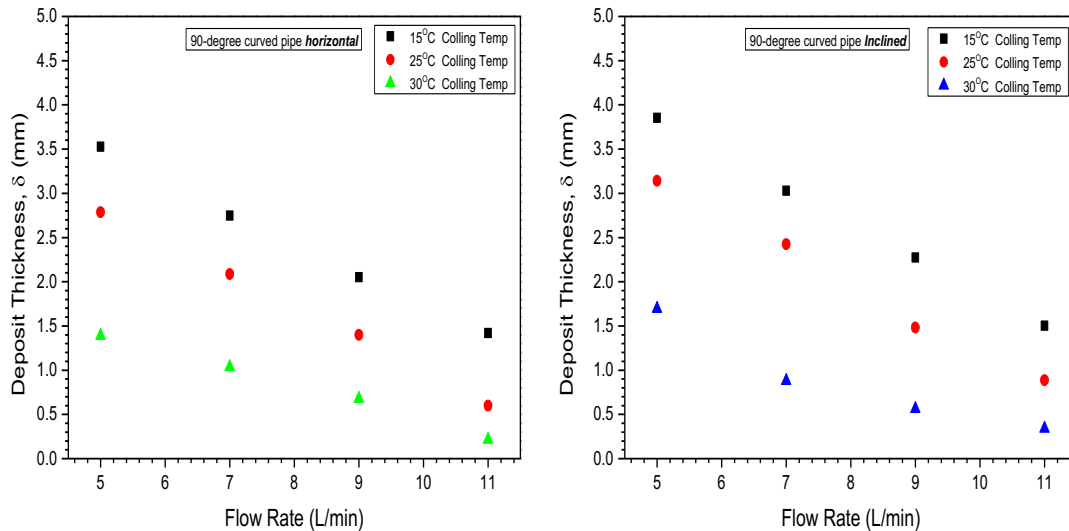


Figure 5-12: Effect of varied cooling temperature under different flow on wax thickness in 90^o bend pipe test-section: Left – Horizontal experiment. Right – Inclined experiment.

The higher depositional behaviour observed in the bend pipes could be because as the waxy crude oil flow horizontally through the inner core of the pipe bends some fraction of the oil experiences segregation and isolation from the bulk fluid and back mixed within the same region. This behaviour leads to higher residence time, in which the segregated fluid undergoes before exiting the area, which experiences high internal heat transfer, leading to an increase in the radial temperature gradient that could cause high transport of wax molecules toward the pipe wall by the influence of different mechanisms. The effect of wall shear rate, particularly at a higher flow rate is substantial in a straight pipe. However, this factor is considered less in a bend, particularly around the inner core area at the exit of the curve, causing relatively high deposition. Already, it is established that molecular diffusion gathers widespread acceptance as the most relevant wax deposition mechanism (Sousa *et al.*, 2019b). However, the behaviour experienced in horizontal bend pipe is attributed to the additional mechanisms such as the Brownian diffusion, and or shear dispersion (see

Eq 5.4 and 5,5). These mechanisms might have interfered the stripping effect at a higher flow rate and contributes to additional deposit in the system (around the inner section of the bend) compared to the impact around the outer core of the bend, where a low deposition is observed. See Figure 5-16 for the layers of the sample deposited on the walls of a straight and bend pipe. Therefore, at low flow conditions, some portion of oil around the bend could be forced to experience a large thermal difference, which could result in a swift deposition process or transport of the wax particles towards the cold surface, despite the oil flowing at a relatively higher temperature. Similarly, the high wax thickness (in observed at a higher flow rate and higher temperature (e.g. 9 l/min and 30°C), could be as a result of the combined effect of Brownian diffusion or dispersion in the pipeline. This implies that the precipitated particles could be suspended in the oil and moved laterally (Azevedo and Teixeira, 2003) towards the cold surface by molecular diffusion. Hence, the suspended particles are transported in the direction of decreasing concentration due to the Brownian diffusion. Indeed, Brownian diffusion was regarded as insignificant to the growth of wax deposits, particularly in a straight pipe (Erickson *et al.*, 1993). Due to the dominant combined effect of molecular diffusion with shear dispersion, particularly at a lower cooling temperature and shear stripping at a relatively higher shear rate (i.e. higher flow rate).

It is worth noting that in horizontal flow under 90° bends pipe section, the higher wax thickness was observed compared to the horizontal flow under 45° bend pipes. This could be related to the effect of bend parameters, particularly the bend radius. According to the literature, the higher the bend radius, the more flow is separated, and the more isolated fluid would be found around the bend. On the other hand, the deposition is higher under 45° bend pipes in an inclined orientation than under 90° bends pipe section. As per the flow rig design, the fluid flowing in the inclined 90° bend pipes section experienced both upward (friction dominant) and downward flow (gravity dominant). This could lead to higher shear stripping or sloughing effect (less wax deposit) compared to an inclined 45° bend pipes section with an elevation of 350 mm.

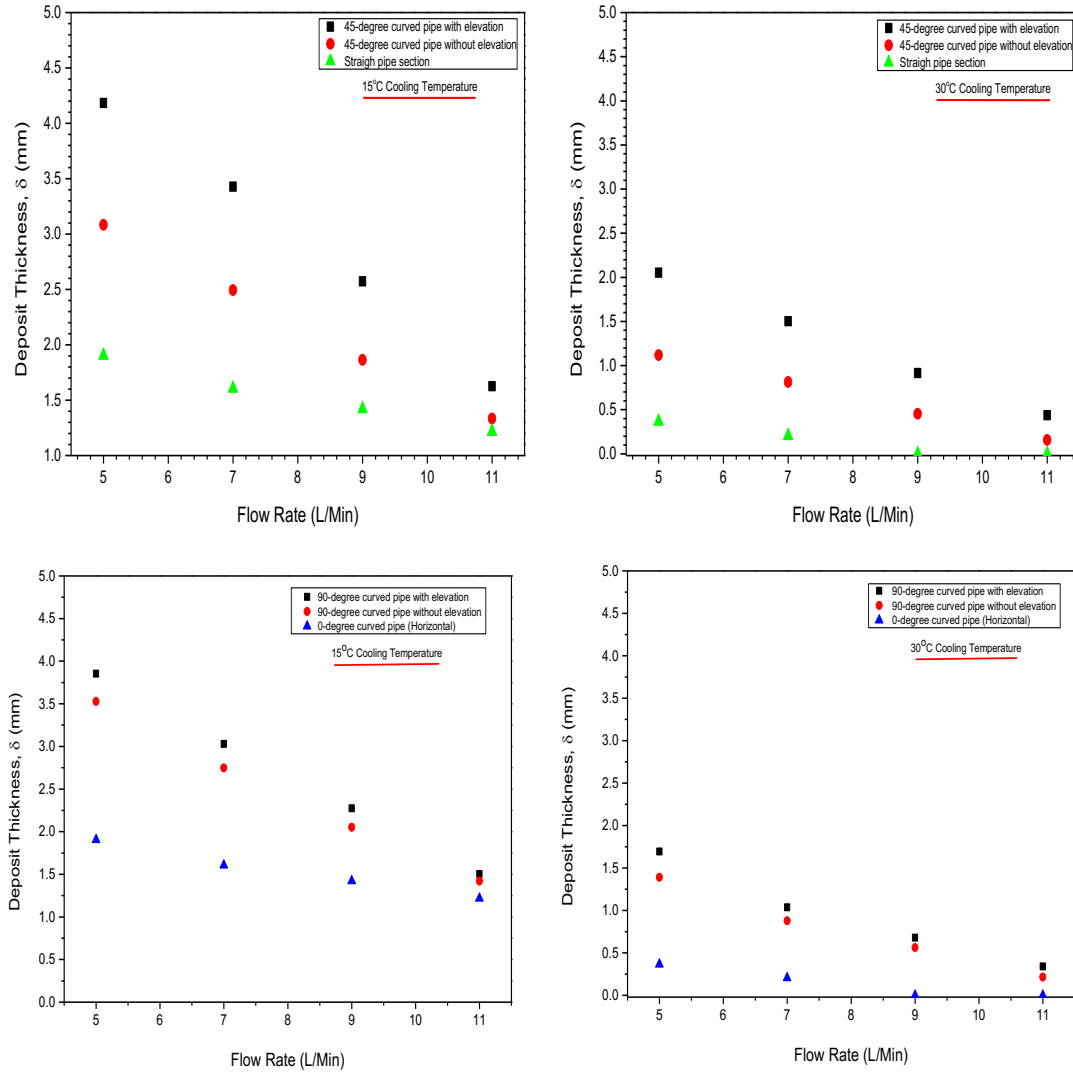


Figure 5-13: A comparison between deposit thickness in the straight pipe (horizontal flow) with 45° bend pipe section (the top Figures) and 90° bend pipe section (the bottom Figures) in horizontal and inclined flow. Left– cooling at 15°C (below pour point). Right– cooling at 30°C (above pour point).

In this work, the region where segregation of fluid occurs could experience an increase in the concentration of the precipitated wax because of the decrease in the solubility of the wax under lower temperature. In general, the lateral transport rate of solid wax particles to the pipe wall is described in a model by Burger *et al.* (1981). The model combined the effect of mechanisms causing lateral movement, i.e. by Brownian diffusion and shear dispersion coefficients.

$$flux = \rho_d(D_B + D_s) \left. \frac{dm_B}{dt} \right|_{wall} \quad (5.20)$$

where $\left. \frac{dm_B}{dt} \right|_{wall}$ is the radial concentration gradient of waxy material out of solution at the pipe wall. However, it is proposed that the rate of incorporation of solid particles into the immobile deposit must be equal to the rate of transport of these particles to the wall (Eq. 5.20). The study by Burger et al. have shown that “If the volumetric concentration of solid is low, the particles are noninteracting” (Burger *et al.*, 1981). As a result, it is comprehended that in relatively all of the cases presented in section 5.4, there is enough concentration of solid wax that transports the particles and deposited on the pipe wall. Therefore, the rate of deposition is directly proportional to the wall shear rate, thus, Eq. 5.21 is proposed as the rate of deposition of solid wax. The Equation shows that the rate of deposition W_{BS} due to Brownian diffusion and shear dispersion is proportional to the surface area available and wall shear rate (γ).

$$\frac{dm_i}{dt} = W_{BS} = k^* C_w^* \gamma A \quad (5.21)$$

Where k^* is the deposition rate constant analogous to the rate of reaction constant for a chemical reaction. C_w^* is the concentration of solid particles at the solid-liquid interface.

On the other hand, the rate of deposition in which molecular diffusion of dissolved wax combined with lateral transport is modelled in an equation, which gave the total rate of wax deposition at the pipe wall (W_T)

$$\frac{dm_T}{dt} = W_T = \rho_d D_m A \frac{dC}{dT} \frac{dT}{dr} + k^* C_w^* \gamma A \quad (5.22)$$

Therefore, Brownian diffusion and dispersion causing lateral transport are considered significant to the deposition, which should be incorporated with another mechanism for the overall deposition growth towards the cold surface. The phenomena of Brownian mechanism and shear dispersion effectiveness to the wax transport and deposition of wax on the cold surface (in horizontal flow) was supported by Azevedo and Teixeira (2003) and Singh *et al.* (2000). However, not many existing deposition models take it into account.

On the other hand, the gravity settling effect of particles claimed to be irrelevant by many studies (Burger *et al.*, 1981) was observed relatively observed in this work. The deposit thickness increased as the pipe orientation is switched from horizontal to an inclined flow.

Figure 5-14 shows a more close comparison between the two curved pipes sections in horizontal and inclined flow. A study reported by Burger *et al.* (1981) has demonstrated that wax deposition curved in horizontal and vertical flow in a straight pipe is indistinguishable within the levels of experimental uncertainty. Burger *et al.* suggested that shear dispersion might re-disperse the settling of the solids particles, which may eliminate any effect of gravity settling. However, similar to the findings of this work, Hamouda and Ravnøy (1992) discovered the influence of gravity settling mechanism in a flow rig experiment, although, according to their study, the deposit growth is less compared to the molecular diffusion, Brownian diffusion and shear dispersion.

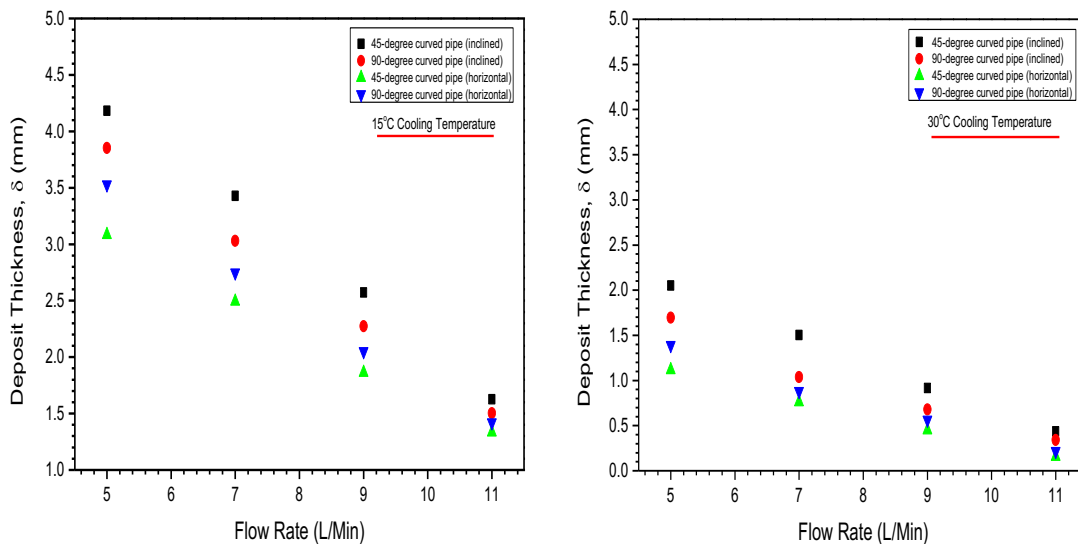


Figure 5-14: Comparison of the severity of wax deposition in 45° and 90° curved pipe in horizontal and inclined flow at a different oil flow rate. Left— cooling at 15°C. Right— cooling at 30°C.

Ajayi (2013) suggested that the influence of gravity settling mechanism would be felt, particularly in a lower flow rates system, especially during typical shut-in conditions or in the storage tanks. Golchha *et al.* (2015) have proved Ajayi (2013) prediction, which studied wax deposition in near-gelling systems under quiescent conditions, the study found that gravity settling mechanism affected the deposition of

wax particles. The predictions and the discoveries by these studies are somewhat in agreement with the results obtained in this work, especially at lower experimental conditions of cooling temperature and flow rate. It is believed that some of the experimental condition in this work has an attributed this behaviour. For instance, the restriction and flow separation around the bend alongside with the pipe materials– as the copper pipe has a higher thermal conductivity that allows rapid heat transfer, unlike the study by Burger *et al.* that uses stainless steel and a straight pipe of 6.35-mm-OD.

Therefore, the settling velocity of particles is modelled based on the balance of the buoyancy and the viscous forces presented in the Eq. 5.23 (Buongiorno, 2006).

$$V_g = \frac{d^2(\rho_p - \rho_f)g}{18\mu} \quad (5.23)$$

Where ρ_p and ρ_f are the particle and fluid density, d is the particle diameter, n the power-law index, g the acceleration due to gravity and μ is the fluid viscosity.

In a nutshell, the relative percentage of the severity of wax deposition is compared for the three-curvature pipes– i.e. 0, 45 and 90-degree bend pipes under horizontal flow (shown in Figure 5-15). For instance, Figure 5-15; Top left, show the results at a constant cooling temperature of 15°C (below pour point) and under laminar flow regime of relatively high flow rate (5 l/min). According to this Figure, the severity of the deposition measured in percentage between the three curvatures in horizontal flow shows that only 22% of the wax would be deposited in the system with straight pipe section compared to 36% and 43.5% in a pipe with 45° bend pipes and 90° bend pipe section. Similarly, at these conditions, the relative percentage showed that up to 14% and 19% of wax deposition problems would inherit if the curvature of the pipe is changed from straight pipe (which considered to have 0%) to a pipe with 45° and 90° bend.

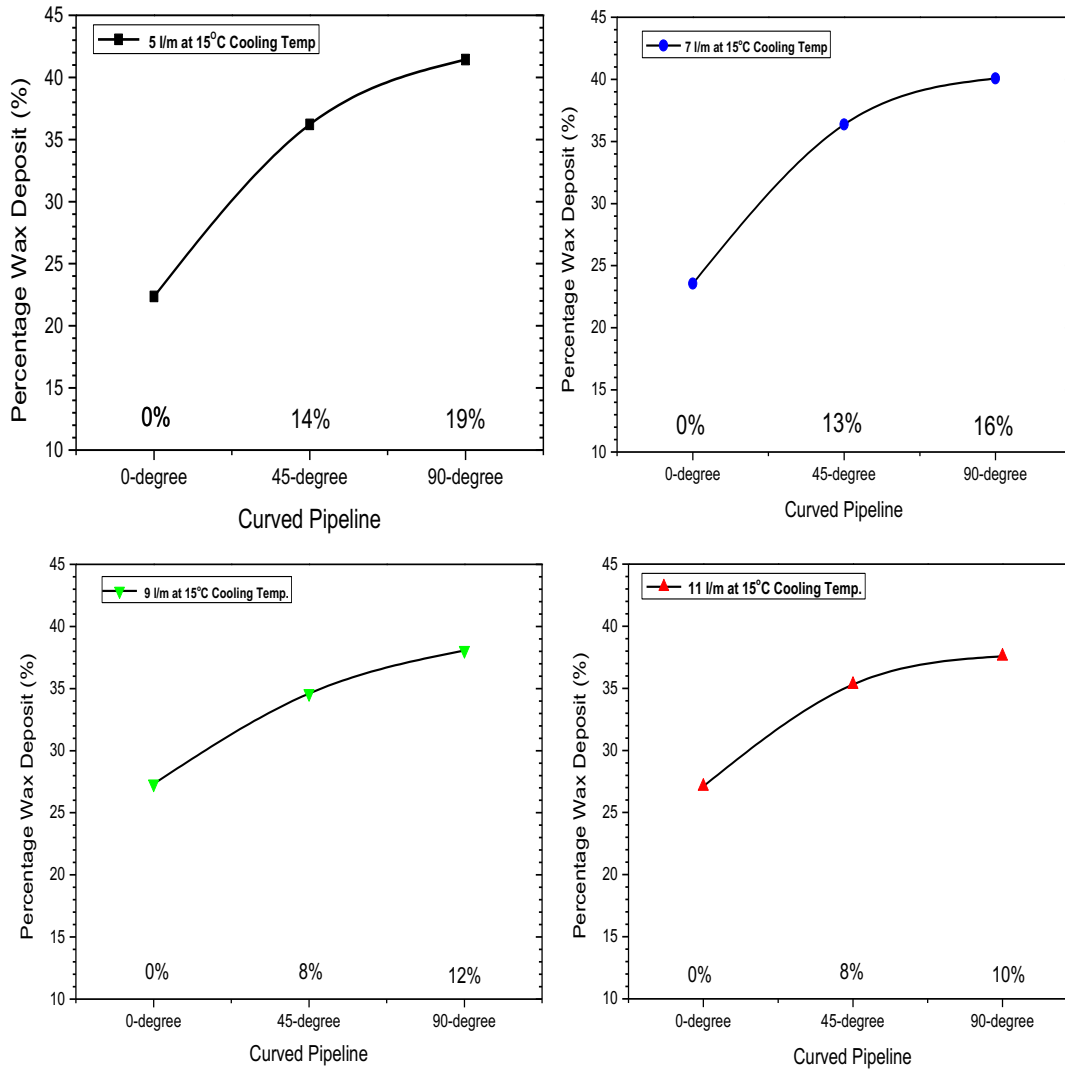


Figure 5-15: Relative percentage severity of wax deposition for three-curvature pipes (i.e. 0, 45 and 90-degree bend pipes) under horizontal flow. Top Left and Right: at 5 and 7 l/min and at constant cooling at 15°C. Bottom Left and Right: at 9 and 11 l/min and a constant cooling at 15°C.

Similarly, at the same cooling temperature of 15°C, but under turbulent flow regime of higher flow rate (11 l/min), the severity of wax deposition rate decreased. It is seen that only 8% and 10% more wax deposition issues would be encountered if 45° and 90° bend pipes are used instead of a straight pipeline (Figure 5-15; Bottom right). Overall, contrarily to some previous studies on the paraffin deposition, this work has demonstrated that wax deposition behaviour is influence by curved pipes and the severity increased by changing the orientation of the pipe from horizontal to an inclined flow within the precision operating conditions and the curvature used.

A cross-sectional view of Deposit thickness layered samples in a straight and curved pipe is shown in Figure 5-16. The wax deposits layer was seen to be is higher, thicker and more compact around the inner core area where the separation of fluid occurred. On the other hand, the deposit thickness in the straight pipe section is found to be uniform circumferentially for most of the cases. The non-uniform circumferential thickness was observed at a high flow rate. Similar results were reported by (Rittirong *et al.*, 2016, 2017). Therefore, indeed, these results provide some experimental evidence that validates the results and discussion made.

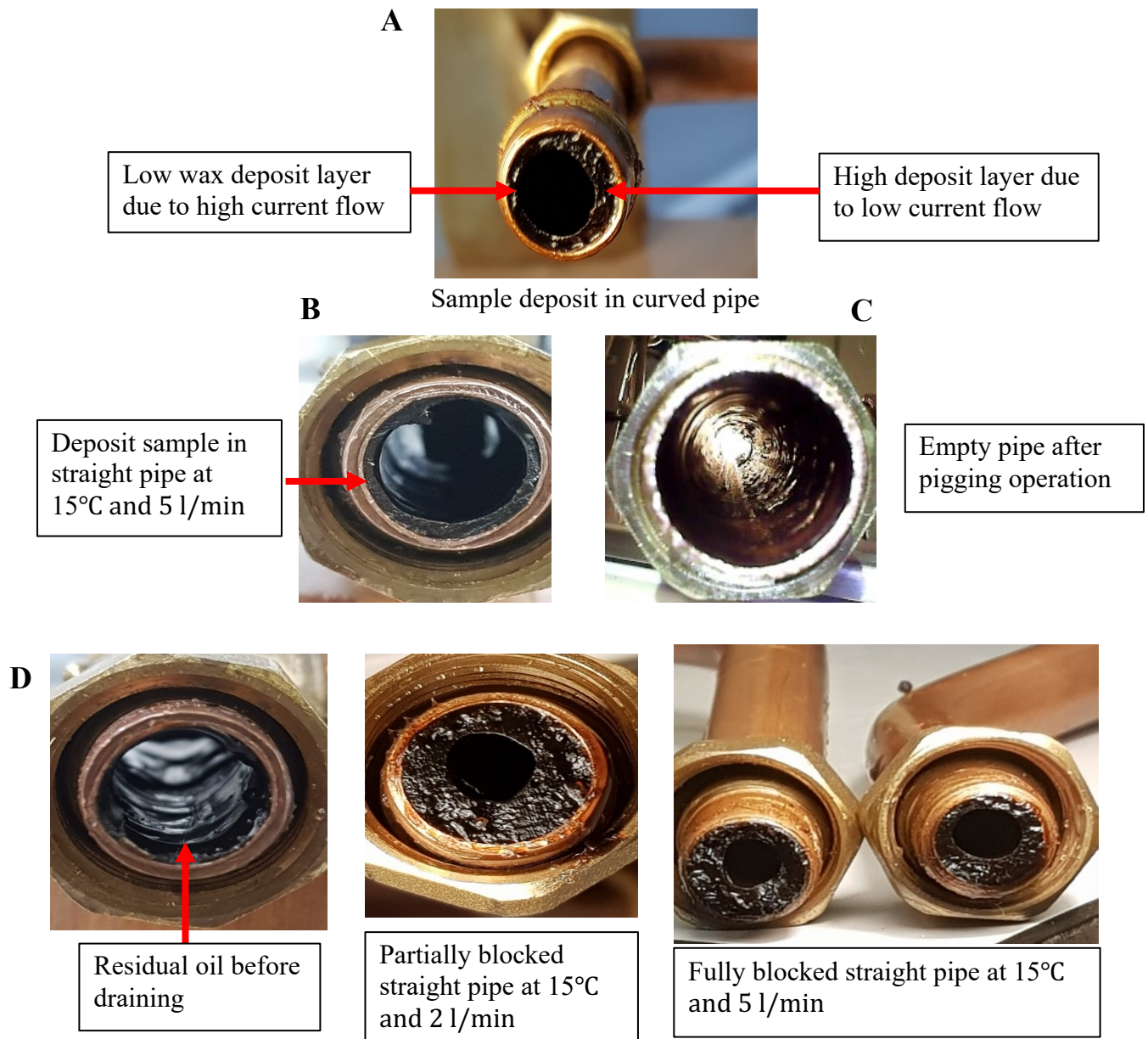


Figure 5-16: Cross-sectional view of the deposit thickness on the pipe wall: A – wax deposit after 45° bends in inclined flow, B – wax deposit at 2l/min and 10°C, C – Empty pipe and D – Various waxing problem in straight and curved pipe.

Chapter 6

Results and Discussion

Effect of Blended Wax Inhibitor on Wax Deposition

6.1 Introduction

Chapter 4 and 5 have shown that wax crystals found in the crude oil could remain dissolved until its solubilisation limit is reached, which leads to its precipitation and deposition in the pipeline. The study in chapter 5 has shown that the severity of wax deposition could be increased by introducing bends in a straight pipeline. It also showed that the deposition causes a problem such as pressure anomalies as a result of the restriction in pipes, which consequently affects the oil recovery rate. Hence, out of the several techniques developed for mitigation and prevention of wax deposition, the use of chemical inhibitors for the prevention of wax deposition has been widely considered as the best way to deal with wax deposition problems. Therefore, this chapter presents an experimental investigation of the performance of a new blended “A” polymer base wax inhibitor using a flow rig designed with a straight and 45° bend pipe sections. Blend “A” wax inhibitor was found to be the best in terms of its inhibition characteristic– interfered with the nucleation, growth, and agglomeration of the wax crystals than the rest of the tested inhibitors. See chapter 4, section 4.5.3 for the wax inhibitor screening results.

Therefore, in this chapter, a series of experiments were performed to examine the impact of this inhibitor at different concentrations (500, 1000, 1300, 1500, and 1800-ppm). The studies were carried out over two major wax deposition control parameters, i.e. the cooling temperatures (15, 25, 30 and 35°C) and the crude oil flow rates; under laminar (5, and 7 l/min) and turbulent (9, and 11 l/min) conditions. The crude oil (sample B) temperature and experimental period were kept constant throughout at 45 and 2 hrs. The study has shown that the interaction between the blended inhibitor and the wax crystals provides an improved inhibition performance

in the system even in extreme cases of this study ($Q_{oil} = 5$ l/min, $T_{cool} = 25^{\circ}\text{C}$ and 500-ppm). More than 50% of wax deposition issue is reduced at these conditions. Significantly, it is observed that 100% inhibition efficiency is achieved in different experimental settings, particularly at the pour point temperature.

6.2 Effect of the inhibitor at varied temperature – Straight pipe section

The transportation, production and storage of waxy crude oils could be achieved successfully as long as it is made at higher temperature conditions, particularly above wax appearance temperature of that particular oil (Hoffmann and Amundsen, 2013; Makwashi *et al.*, 2019a, 2019b). Indeed, the behaviour of wax deposition could be related to the basis of the classical Fick's mass diffusion law (Lim *et al.*, 2018), as the wax deposit formation relies on the influence of thermal gradient. At a low cooling temperature, both the radial temperature gradient and the concentration gradient increased, which eventually produced a mass transfer of dissolved wax towards the cold surface and consequently results in deposition of wax (Lim *et al.*, 2018; Zhang *et al.*, 2010).

Therefore, as aimed in this section, the depositional behaviour of a waxy crude oil doped with chemical inhibitor at different concentration has been studied over a range of different cooling temperatures of 15, 25, 30 and 35°C. The temperatures ranges were mainly chosen to investigate the deposition behaviour below the pour point and above the WAT of the waxy crude oil. On the other hand, five ranges of the polymeric inhibitor concentration (500, 1000, 1300, 1500, and 1800-ppm) were selected based on the rheological study (chapter 4, section 4.5.3) to determine the optimum concentration based on the dosage and the performance of the inhibitor interference with the deposition under flow rig experiment. The crude oil temperature and experimental period were kept constant at 45°C and 2 hrs throughout the study. Two different oil flow rates (5, and 11 l/min) were used, as shown in Figure 5-16.

Therefore, the results in Figure 5-16 shows the depositional behaviour of the crude oil sample undoped and doped with the inhibitor at different concentration. It is worth recalling that addition of inhibitors in the system change the rheology of the

fluid (Kelland, 2009), and improves the dispersion of small wax crystals as it contains a similar structure to the wax crystals structure (Li et al., 2018). Due to the same structure, the inhibitors usually cover the wax area, therefore preventing further wax crystal growth and in combination with other structural characteristics the crystallization of wax is disrupted (Jennings and Newberry, 2008). Thus, at the lowest cooling temperature (15°C)– below pour point, under a lower flow rate (5 l/min) conditions, a higher wax thickness was observed in the undoped oil (without inhibitor) and doped oil (with inhibitor) (Figure 6-1). It is believed that a lower cooling rate, facilitates the nucleation processes (Lira-Galeana and Hammami, 2000). It is seen that under the same condition (15°C and 5 l/min), the deposit thickness without the inhibitor (undoped oil) (i.e. 1.93mm) reduces to 1.19, 0.91, 0.8, 0.73 and 0.7mm when blended with the inhibitor at 500, 1000, 1300, 1500, and 1800-ppm (Figure 6-1 (a)). At the same flow rate, these thicknesses reduced significantly as the coolant temperature increased to 20, 25 and 30°C. It is observed that at 25°C cooling temperature, the deposit thickness decreased to 0.58, 0.42, 0.35, 0.3 and 0.28mm at 500, 1000, 1300, 1500 and 1800-ppm. The thickness is nearly zero at 30°C (i.e. equal to WAT) under laminar flow ($Q_{oil} = 5$ l/min), particularly at 1300, 1500 and 1800-ppm (0.09, 0.07, and 0.07mm).

These phenomena could be explained as follows; lower cooling temperature (15°C) is believed to increase the precipitating ability and the decrease in the dissolving capacity of wax particles in the oil. Therefore, the potential of the wax molecules to precipitate on the cold surface increased and the driving force of the wax molecules' diffusion from the bulk oil to the cold surface is strengthened, particularly under the low flow rate ($Q_{oil} = 5$ l/min). This is because at laminar flow the tendency of the wax to adhere to the cold surface is higher, besides, the time in which oil flows in the pipe is extended, thus, leading to agglomeration of wax particles and consequent deposition in the pipe surface (Lee, 2008; Nguyen and Fogler, 2005; Zhu *et al.*, 2008).

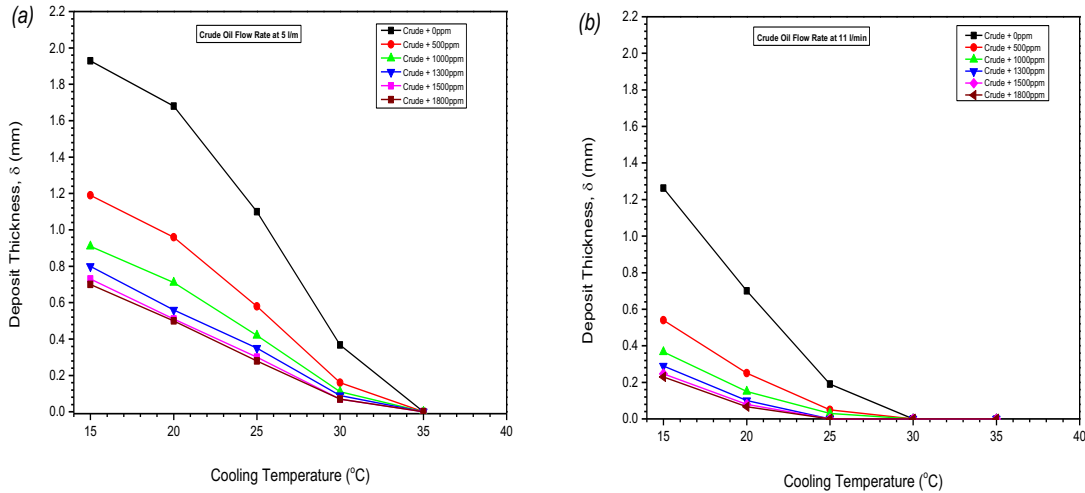


Figure 6-1: Effect of varied cooling temperature on wax deposit thickness in straight pipeline test section at (a) laminar flow (5 l/min) and (b) turbulent flow (11 l/min)

However, as the fluid flowed under the turbulent flow condition, the thicknesses reduced more rapidly, i.e. more wax is reduced from the system. Figure 6-1 (b) shows that as the flow rate increases to 11 l/min, the deposit thickness measured without inhibitor δ_{wax} , is 1.26 mm. The deposition becomes zero ($\delta_{wax} = 0\text{mm}$) at pour point temperature (25°C) under 1000, 1500 and 1800-ppm. At this point, it is believed that the polymeric inhibitor precipitates and acts as a crystalline nucleus for the wax crystals (Li et al., 2018), which eventually leads to the formation of more subcritical nuclei of micelle-like aggregates. The aggregate particles are transported along with the bulk of crude oil due to high shear rate, and sometimes the particles itself inhibit the deposited wax by stripping effect in the system.

It worth noting that blended inhibitor is effective even at the lowest inhibitor dosage (500 ppm), however, this dependence upon the experimental conditions. It is seen that the efficacy of this inhibitor increases with increase in the concentration, particularly around 1500-ppm that produced almost equal effectiveness with 1800-ppm. Previous studies have suggested that the differences in dosage efficacy of inhibitor are perhaps due to the action of the mechanism of the active polymers as wax solubilises, wax crystal modifiers, and interfacial active agents (Paso *et al.*, 2014; Yang *et al.*, 2015). It is also believed that the adsorption and co-crystallization processes of the inhibitor progressively drive the formation of small (spherulitic-like) crystals in the system, which as a result of increasing the concentration of inhibitor in crude oil (Li et al., 201; Hao et al., 2019). Similarly, at a higher concentration, the

inhibition performance becomes increasingly better, particularly around the turbulent flow regime due to the shearing effect (Bern et al., 1980; Makwashi et al., 2019). More details on the influence of this factor are given in the next section.

Interestingly, the combined effect of flow rate, temperature and inhibitor concentration on the wax deposition (in mass) is presented in a surface 3D plot shown in Figure 6-2 and Figure 6-7 for curved pipes. At oil flow rate of 5 l/min and cooling temperature of 15°C, the measured wax deposition without inhibitor is 63.16 g (Figure 6-2 (a)), which decreases to 42.5 g with inhibition at 500-ppm. Similarly, the amount of wax deposited reduces further from 39.5 and 13.89 g to 21.7 and 6.0 g as the cooling temperature is raised to 25 and 30°C at the same concentration (500ppm) and flow rate (5 l/min). However, at the same flow rate and a relatively higher concentration of inhibitor, for instance, 1500-ppm, the mass of deposit wax reduced to 27, 11.6 and 2.6g at 15°C to 25 and 30°C respectively. The deposition becomes zero at a relatively higher flow rate (7, 9 and 11 l/min) and inhibitor concentration of 1000 and 1500-ppm (Figure 6-2, b and c). A similar trend is also observed in curved pipes (Figure 6-7).

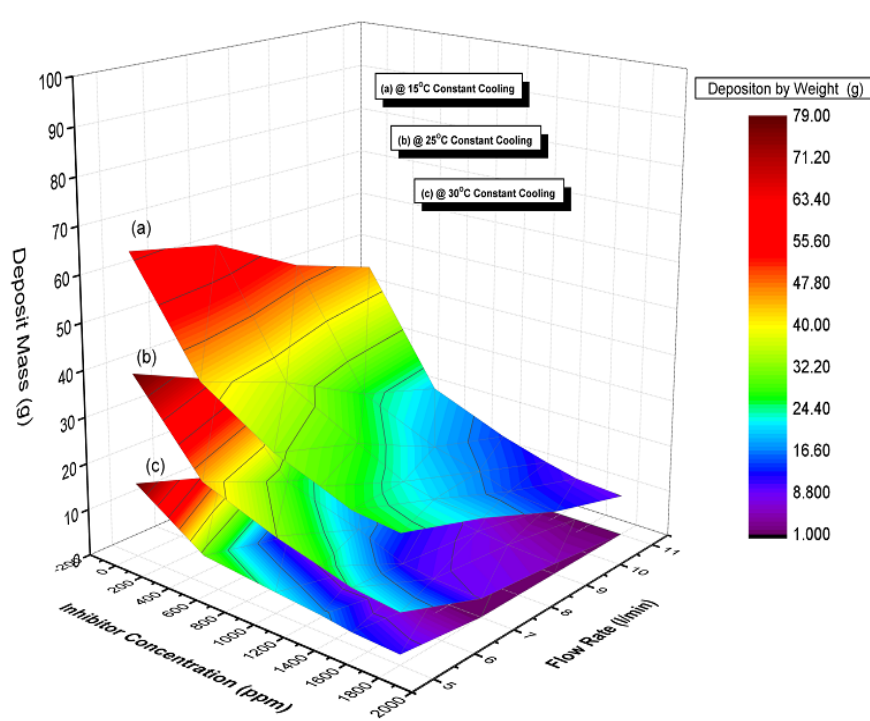


Figure 6-2: Combined effect of varied flow rate, cooling temperature and inhibitor concentration on wax deposition (in mass) – through Straight Pipeline Test Section.: (a) at $T_{cool} = 15^\circ\text{C}$, (b) at $T_{cool} = 25^\circ\text{C}$, and (c) at $T_{cool} = 30^\circ\text{C}$

In this work, the optimum concentration of inhibitor was identified, which is an essential factor when using inhibitor for prevention or migration of wax deposition in the oil and gas field due to the cost of the inhibitor and environmental issues. As observed in the results in Figure 6-1 and 6-2 and those in Figure 6-3, out of the tested dosage of inhibitor, 1500-ppm was chosen as the optimal concentration. This is because, maximum inhibition performance was recorded at this concentration, as the inhibitor concentration is increased above 1500-ppm the corresponding decrease in wax thickness remain the same. For instance, at 1800 ppm the inhibition performance was found to be relatively the same. Similar behaviour was reported by Lashkarbolooki *et al.* (2011) (optimum inhibitor 800-ppm) and Daraboina *et al.* (2016) (optimum inhibitor 500-ppm); although both studies uses different inhibitor. This also suggested that optimum concentration varies for a specific crude type, composition of the inhibitor and experimental settings/operational conditions.

Therefore, it is suggested that further increase in inhibitor concentration is not always an indication of further inhibition. Thus, under this experimental setting, 1500-ppm that yields a better inhibition performance is considered as the optimal (concentration). Although one might argue that 1300-ppm should be optimum concentration, as this dosage is lower and produced inhibition performance very close to 1500-ppm. However, the efficiency and performance at 1300-ppm reduces, particularly at a low cooling temperature (Figure 6-3 (a)). As a result, 1500-ppm inhibitor concentration is regarded as the optimum.

Figure 6-3 presents the analysis of the wax inhibition efficiency (WIE) at different concentration, and varied cooling temperature and flow rate. WIE is calculated using Eq. 6.1 following the study of Bello *et al.* (2006), Chi *et al.* (2017) and Wang *et al.* (2003). A clear and distinctive trend is seen for all the inhibitor concentrations; the higher the inhibitor concentration, the higher the efficiency in decreasing the amount of deposits on the cold surface. At the highest concentrations (1500 and 1800-ppm) more than an 80 % reduction in the deposition was seen at a high flow rate (9 and 11 l/min). The most significant differences between the efficiency of the inhibitor appear at the lower concentrations and low temperature and flow rate, for instance at 500ppm inhibitor concentration, the effectiveness of the inhibitor at reducing the

deposition ranges from 33 % at 15°C and 5 l/min (Figure 6-3 (a)) to around 62 % at 30°C and 5 l/min (Figure 6-3, c).

$$WIE (\%) = \frac{W_f - W_t}{W_f} \times 100 \quad (6.1)$$

Where W_f , is the amount of wax deposit without inhibitor (in grams) and W_t is the amount of wax deposit with inhibitor treatment at different concentrations.

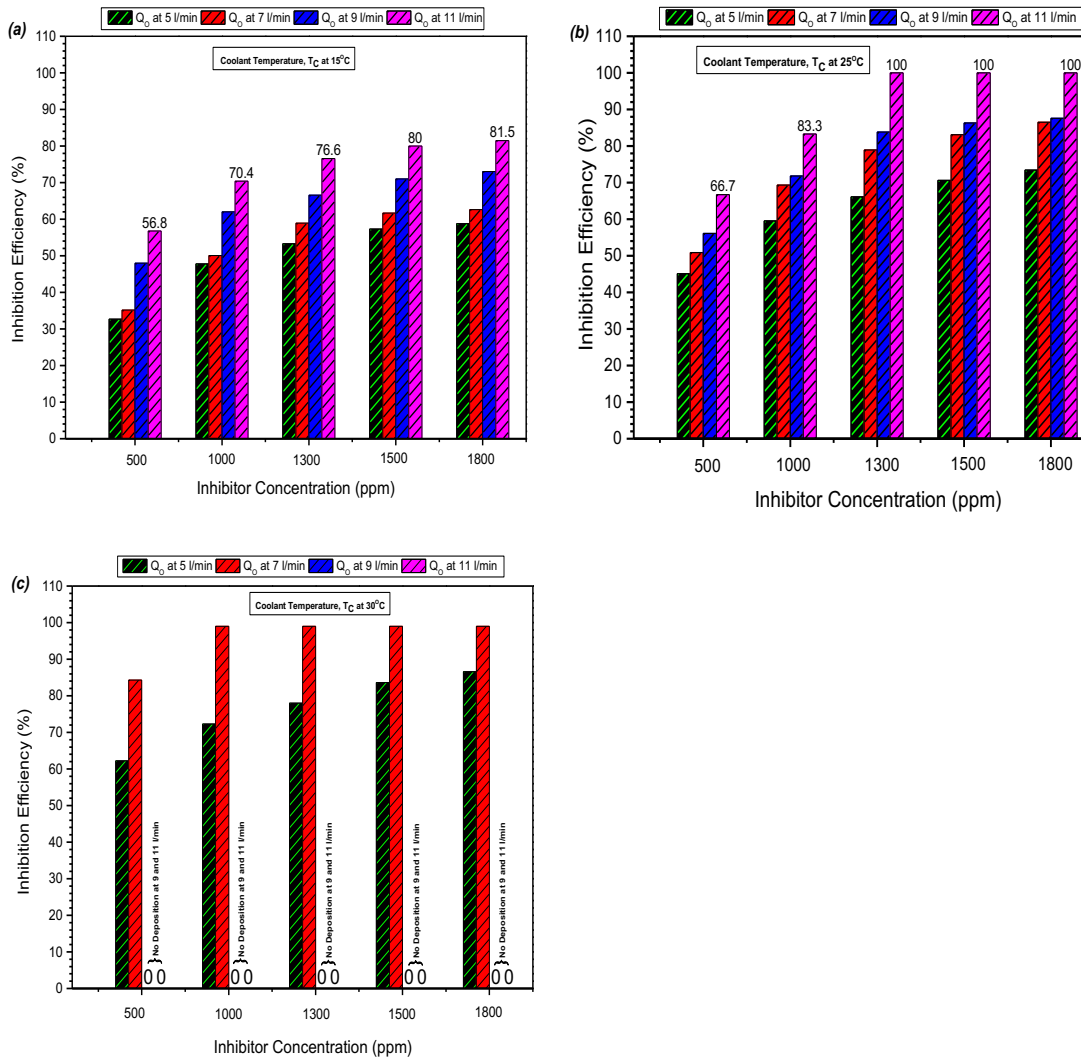


Figure 6-3: The percentage efficiency of blended wax inhibitor at a different flow rate in a straight pipe section (a) at 15°C cooling temperature (below pour point). (b) at 25°C cooling temperature (at pour point). (c) at 30°C cooling temperature (at WAT).

6.3 Effect of the Inhibitor at Varied Flow Rate– Straight Pipe Section

Similar to ambient temperature condition; another critical parameter that controls wax deposition is the oil flow rate (Makwashi *et al.*, 2019a; Miao, 2012; Seyfaee *et al.*, 2012; Wang *et al.*, 2019, 2008; Zheng *et al.*, 2013). Chapter Five and Seven of this work has demonstrated the significance of this parameter and showed that a system must be operated above the wax precipitation envelope to avoid deposition problems. In this section, besides the flow rates already used in section 6.1, two more flow rate were added alongside with different concentration of inhibitor to develop a better understanding of the parameters. Therefore, the four flow rates studied in this section include; 5 and 7 l/min (within laminar flow regime) and 9 and 11 l/min (turbulent flow regime) over three selected cooling temperatures (i) 15°C, considered as one of the extreme cases (below the pour point and WAT), (ii) 25°C, around the pour point and (iii) 30°C, at wax appearance temperature. Clear and distinctive wax deposition behaviour at these flow rates and a specific cooling temperature is shown in Figure 6-4, which is a similar trend to those in section 6.1.

Therefore, in both cases, the inhibition performance increased with an increase in flow rate, inhibitor concentration and cooling temperature. A high wax deposition rate was seen within the laminar flow condition of low flow rate (5 l/min) compared to the high flow rate (7 l/min), particularly at the extreme temperature condition (Figure 6-4 (a)). The higher deposition rate at a low flow rate is related to high residence time experiences by the circulating oil within the test section leading to rapid heat losses between the flowing fluid and cold surface. This behaviour promotes further agglomeration of the wax crystals, thus, deposited on the pipe surface (Zhu *et al.*, 2008). At the same cooling temperature, a small decrease in the deposit thickness was seen even at higher flow rates (9 and 11 l/min). This could be because at low temperature (15°C) more precipitated particles are available to adhere on the pipe surface and the increase in the radial temperature gradient, thus causing further growth of wax deposit thickness even within the turbulent flow regime. Similarly, in both cases, better inhibition performance was seen at higher inhibitor concentration.

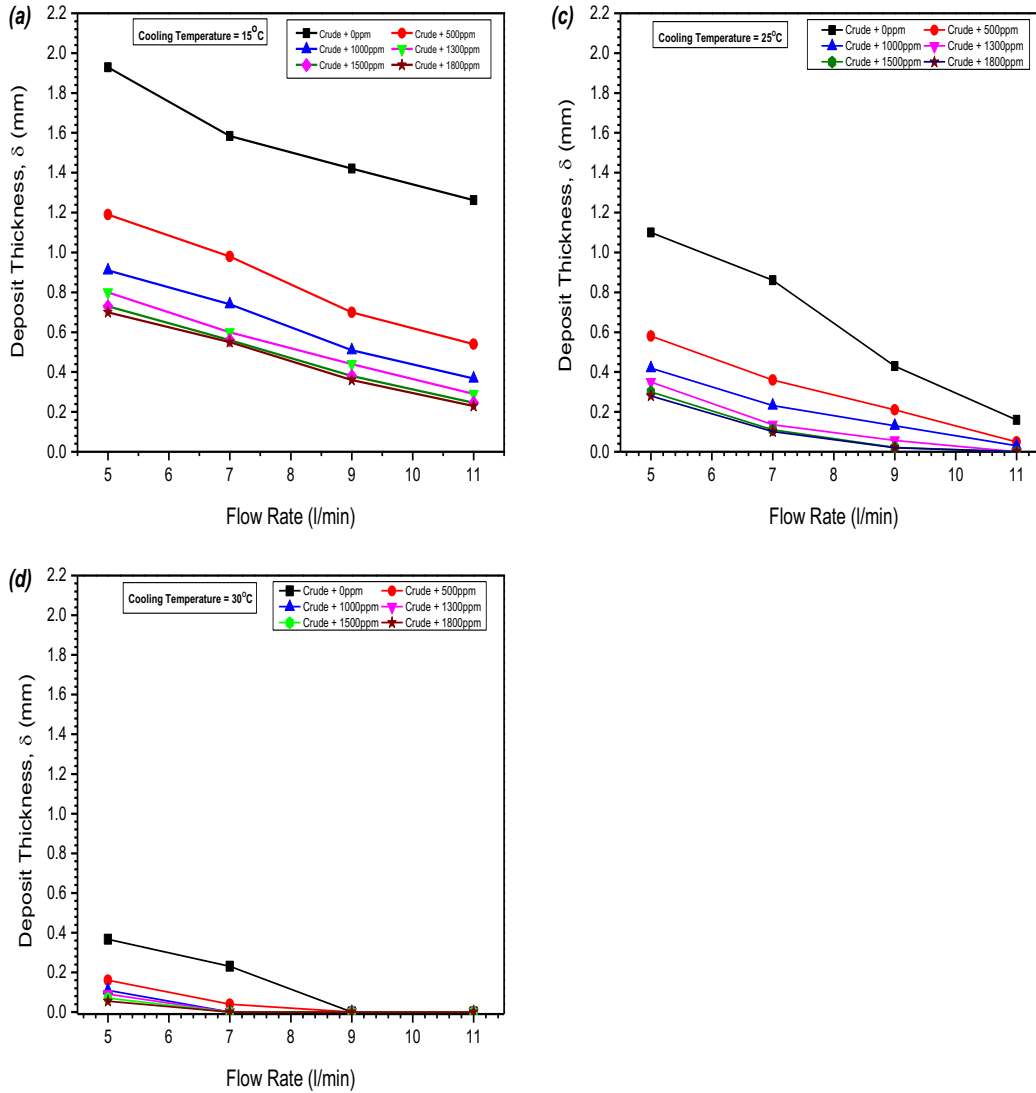


Figure 6-4: Effect of variation of flow rate, and inhibitor concentration on Wax Deposit Thickness at (a) $T_{cool} = 15^\circ\text{C}$, (b) $T_{cool} = 25^\circ\text{C}$, and (c) $T_{cool} = 30^\circ\text{C}$ through Horizontal Straight Pipeline Test Section

However, as the flow rate increased at a relatively higher temperature (25°C) (Figure 6-3 (b)), a remarkable performance of the inhibitor was observed within the turbulent flow of lower (9 l/min), no wax deposition was seen at 1500-ppm. Similarly, at 25°C , the same performance is observed within the laminar flow regime (i.e. at 7 l/min) where 100% wax inhibition was recorded at 1000, 1500 and 1800-ppm. Whereas, at turbulent flow (9 and 11 l/min), the used of lower concentration (500-ppm) provided 100% wax inhibition. In a nutshell, this behaviour could be related to the shear stripping effect and small residence time. However, even if the flow rate is higher, the temperature needs to be relatively at or above the pour point of the crude oil before any significant effect of flow rate can be noticed. This is demonstrated in

Figure 6-4 (a) and (b). For instance, the thickness measured at a low flow rate (5 l/min) and at relatively higher cooling temperature (25°C) is relatively equal to the deposit thickness measured at a higher flow rate (11 l/min) and lower cooling temperature (15°C).

Therefore, at some particular experimental conditions seen in sections 6.2 and 6.3, 100% wax inhibition can be achieved in a flow line using the new blended chemical. Therefore, even at pour point temperature and the low concentration (500ppm), 100% wax inhibition could be achieved, but then, the fluid must be maintained at 9 or 11 l/min. Similarly, as the temperature increase around the WAT, the lower dosage of the inhibitor (500-ppm) could satisfactorily inhibit the deposition under laminar flow condition. Unfortunately, the blended chemical studied in this work could not provide 100% wax inhibition at the severe case of 15°C (cooling temperature), under any of the tested flow rate conditions for 2 hours experimental period (Figure 6-4 (a)). Therefore, to completely prevent deposition at this lower temperature, the chemical method (wax inhibition) must be combined with other prevention is recommended (e.g. thermal or mechanical method). This statement follows with other studies such as Adeyanju and Oyekunle (2014), Coto *et al.* (2014), Singh *et al.* (2007) and Theyab (2018). This implies, in real field system, depending on the specific scenario, none of these measures is 100% effective in preventing wax deposition.

6.4 Study of the inhibitor in flow rig with bend pipes sections

The inhibition performance of the blended wax inhibition was studied in horizontal and inclined flow with 45° bend pipe test section (Figure 6-5). As already established in chapter 5 and 7, these test sections produced severe deposition scenarios compared to the straight pipe section. Therefore, the analysis in this section is intended to lead to a further understanding of the degree to which the blended inhibitor could further reduce wax deposition in a critical condition. It is already established in chapter 5, the severity of wax deposition in horizontal 45° bend pipe is 14% higher compared to the straight pipe test section at 15°C cooling temperature in laminar flow regime at lower flow rate (5 l/min). The severity is yet substantial in a

turbulent flow region (11 l/min) at the same temperature. About 8% more wax would be inherited as the curvature changed from straight pipe to a pipe with 45° bend. The deposition rate increases as the curved pipe are inclined to flow, which may be due to the gravitational settling effect of particles drives by the influence of bend parameters, especially at lower temperature and laminar flow conditions (Makwashi *et al.*, 2019a).

Therefore, in this section, the behaviour and influence of wax crystals interaction with the blend ‘A’ wax inhibitor are studied in flow rig with 45° bend section in horizontal and inclined flow at different concentration (500, 1000 and 1500-ppm), cooling temperature (15, 25 and 30°C) and flow rate (5, 7, 9 and 11 l/min). Figure 6-5 (a, b and c) shows the result of inhibition performance in a horizontal pipe with a 45° bend at a different flow rate and concentration. Figure 6-5 (a) shows that in the extreme case (i.e. at $T_{cool} = 15^{\circ}\text{C}$ and 5 l/min) without inhibitor, the measured deposit thickness of 3.08 mm was reduced to 1.8, 1.4 and 0.9 mm by doping the crude oil with inhibitor at 500, 1000, and 1500-ppm (Figure 6-5, a). This implies at these concentrations, the deposition was reduced from 43% (without inhibitor) to 25.3%, 19.1% and 12.6% at 500, 1000 and 1500-ppm.

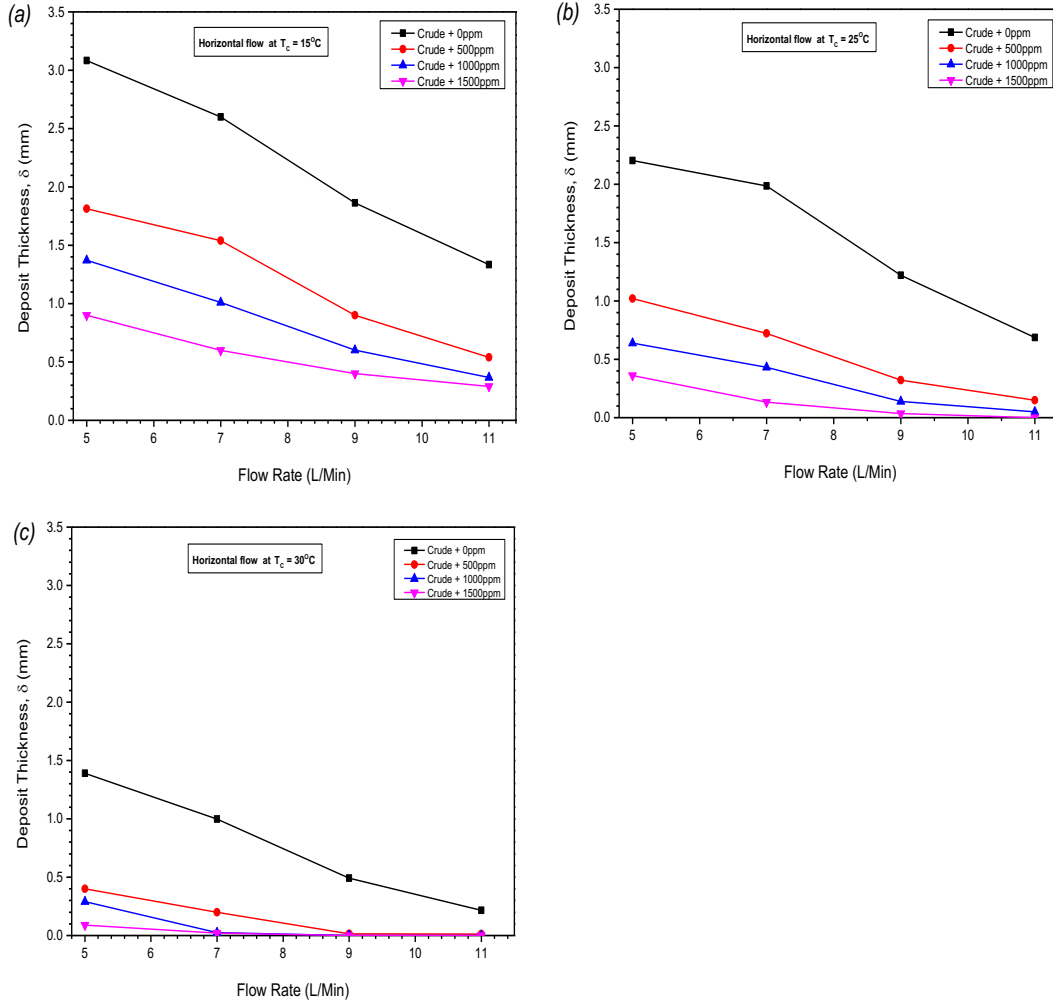


Figure 6-5: Effect of varied flow rate and inhibitor concentration on wax deposit thickness—through horizontal 45° bend pipe section at (a) $T_{cool} = 15^\circ\text{C}$ (b) $T_{cool} = 25^\circ\text{C}$ and (c) $T_{cool} = 30^\circ\text{C}$.

However, as the coolant temperature increases to 25 and 30°C (Figure 6-5, b and c) the inhibition performance increases considerably. Similar to the straight pipe results (Figure 6-4, b), no deposition is observed at higher turbulent flow (11 l/min); however, a small deposit was seen at low turbulent flow 9 l/min under 25°C cooling temperature. Unlike, in the laminar flow regime, where the thickness at 1500-ppm is relatively higher, i.e. $\delta_{wax} \approx 0.36\text{mm}$ at 5 l/min and $\delta_{wax} \approx 0.132\text{mm}$ at 7 l/min respectively. The thicknesses are still higher in the bend pipe than the straight pipe. This could be because in the bend pipe under laminar flow, the concentration of precipitated wax is higher due to the combined effect of molecular diffusion, shear dispersion and Brownian diffusion mechanisms.

On the other hand, Figure 6-6 (a, b and c) shows the results obtained with the

inclined 45° bend test section at a different flow rate and concentration. As described in a study by Makwashi *et al.* (2019a) and reported in chapter 5, wax thickness increases as the horizontal pipe test section with 45° bend are switched to an inclined flow. As shown in the Figure below, the wax thickness measured with undoped crude oil (0-ppm) at $T_{cool} = 15^\circ\text{C}$ and $Q_{oil} = 5 \text{ l/min}$ is $\delta_{wax} \approx 4.12 \text{ mm}$. Unlike in horizontal study, at the same condition the δ_{wax} measured is 3.1 mm , which could be due to the influence of the ‘gravity settling’ mechanism. Therefore, in both cases, as shown in the Figure below, the severity of wax deposition decreases with increasing the flow rate, cooling temperature and inhibitor concentration.

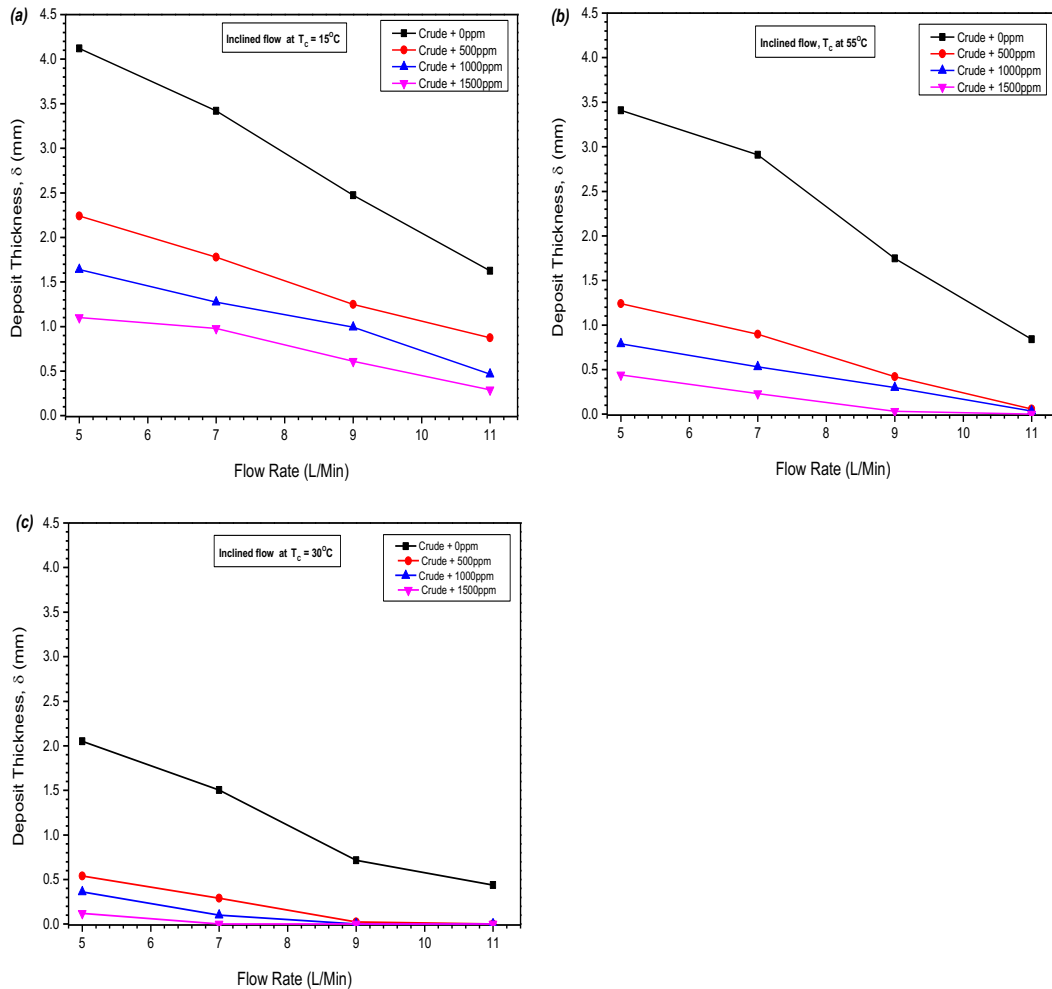


Figure 6-6: Effect of varied flow rate and inhibitor concentration on wax deposit thickness—through inclined 45° bend pipe section at (a) $T_{cool} = 15^\circ\text{C}$ (b) $T_{cool} = 25^\circ\text{C}$ and (c) $T_{cool} = 30^\circ\text{C}$.

Although the measured thickness is higher in 45° bend pipe section, the inhibitor performance is still promising at a relatively higher temperature (25 and 30°C). It is

evident that at 9 l/min and cooling at 25 and 30°C, no wax deposit was measured at 1500-ppm. As this flow rates increase to 11 l/min at 30°C, 100% inhibition efficiency was achieved at all the turbulent condition. It is suggested that higher shear rates and higher cooling rates are thought to influence the nucleation process, which is likely to control the marginal impact that paraffin inhibitors may have on the nucleation process of wax particles. This behaviour is similar to the results reported in a straight and horizontal 45° bend pipe. At high laminar flow (7 l/min) and 1500-ppm, almost 100% inhibition efficiency was achieved at the same cooling temperature. Therefore, this further proves that increasing the oil flow rate tends to increase turbulence in the pipe, thus, reduce the residence time for the deposition. Even though wax formation could occur, the deposition process is, however, not encouraged to a great extent, due to these shearing effects in any of the curvature pipe. This behaviour continues to demonstrate the influence and the effectiveness of the blend 'A' wax inhibitor used in this work, particularly at temperature \geq pour point and a relatively high flow rate. Similar to the results in section 6.2, the mass of the wax deposit (in grams) are presented in a surface 3D plot (Figure 6-7), as a function of different flow rate, cooling temperature and inhibitor concentration.

The results indicate a reduction in the amount of wax deposition by increasing inhibitor concentration and flow rates at varying cooling temperatures of 15°C, 25°C and 30°C. As shown in the Figure, at a constant flow rate of 5/min and 15°C cooling temperature, the mass of the wax deposit without inhibitor reduced from 94g, 73g and 40g to 61.5, 48.2 and 32.8g when an inhibitor is added at 500, 1000 and 1500ppm at the same condition. The deposit mass decreases continue with an increase in temperature and flow rate, as the cooling temperature reached 30°C, the system experiences zero deposition even at low concentration (500ppm). Hence, the decrease in the deposit mass with increasing concentration at varied control parameters further revealed the significance of these parameters in the wax deposition as a prevention strategy. In a nutshell, it is imperative for operators in the oil field to carefully consider these combined effects (i.e. the temperature, flow rate and inhibitor concentration) to minimise wax deposition in the pipe. In a practical approach, the influence of temperature and concentration of the wax inhibitor in the pipeline could be modelled and implemented to reduce wax deposition, since the flow rate is a set deliverable.

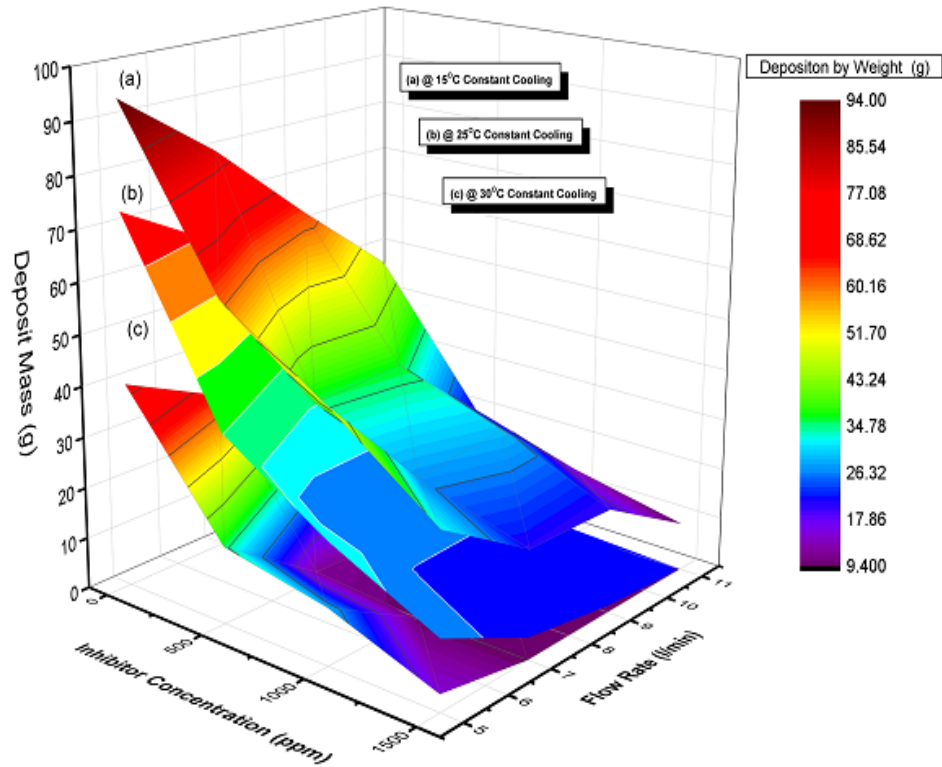


Figure 6-7: Combined effect of varied flow rate, cooling temperature and inhibitor concentration on the mass of the wax deposit (in grams) through horizontal 45° bend pipe test section: (a) at $T_{cool} = 15^{\circ}\text{C}$, (b) at $T_{cool} = 25^{\circ}\text{C}$, and (c) at $T_{cool} = 30^{\circ}\text{C}$.

Chapter 7

Simulation of Wax Deposition

7.1 Introduction

This chapter focuses on the simulation of wax deposition using OLGA dynamic multiphase flow simulator. The severity of wax deposition in the straight and curved pipes are predicted and compared. It is worth noting that in this study, similar boundary conditions used in the experimental work were employed in the simulation study. However, only two of the pipe curvatures (straight pipeline and pipe with 45-degree bend and elevation) used in the experiment was considered in this simulation. The pipe with 45° bend and elevation is simulated in OLGA by considering the straight section and the elevation– which is the only practical approach to mimic the flow rig section in the software. Before simulating wax deposition along the pipeline, the fluid is characterised with the total wax content of 19.7wt% using Multiflash – a fluid modelling package, which gives the fluid properties, phase behaviour and single carbon number (SCN) distribution. Two feed files containing these properties data are generated with the Multiflash, which are essentially required for simulation of wax deposition with OLGA. The comparison of the experimental results and predicted values from the simulation are discussed.

7.2 Analysis of Fluid Characteristics and WAT

One of the possible explanations for this interesting study presented in this section is the use of a well-known and the most accurate predictive tool to evaluate and compare the fluid properties such as PT flash properties, which includes individual wax and liquid phase fractions and their density, average molecular weight and thermal conductivity. These properties have a significant effect on the overall wax deposition and are necessary for the simulation study. Therefore, appropriate data files are generated with correct fluid characteristics prior to the simulation study; otherwise, it results in the inaccurate prediction of wax deposition rate. Similarly, it should be noted that the study provides the percentage amount of wax that

precipitated per degree temperature (unknown in the previous studies) and predicted WAT value is compared with the WAT reported in Chapter 4. The study is carried out at different temperature (below and above the WAT) and at a varied pressure to help better understanding of the wax deposition behaviour. Therefore, results discussed here included WAT, wax precipitation at varying temperature and pressure, phase envelope and single carbon number (SCN) distribution of n-Paraffin.

7.2.1 Analysis of WAT and Wax Precipitation

The results and discussions presented here and in section 7.2.2 are based on the thermodynamics model known as Coutinho solid solution model, implemented in Multiflash fluid package (Coutinho *et al.*, 2001, 2006; Edmonds *et al.*, 2008; SPT Group, 2015; Zhang *et al.*, 2014; Zhu *et al.*, 2008). These studies described the Coutinho model as a predictive local compositional model that accurately predicts wax solubility and the waxing behaviour of waxy crude oil. The studies also revealed that the model could be used to evaluate the physical and transport properties of the crude oil sample in comparison with other thermodynamics wax models such as the studies by Won (1989), Erickson *et al.* (1993), Pedersen (1995), Lira-Galeana *et al.* (1996) and Pan *et al.* (1997). The Coutinho model is based on sound thermodynamic wax phase behaviour from high-quality laboratory data (Zhu *et al.*, 2008; Coutinho *et al.*, 2001). Unlike other models that have no direct experimental evidence to show that the assumptions made in their models are correct to predict key thermodynamic parameters, but only rely on the experimental measurements of WAT to validate their models. However, Coutinho *et al.* (2001) reported that WAT measurement might be associated with uncertainties of $\pm 5^{\circ}\text{F}$.

Coutinho *et al.* (2001) highlighted three main factors controlling the thermodynamics of wax formation including the solution behaviour of the n-paraffin molecules in the oil phase, the solid transition properties (normal melting point, enthalpy of melting, etc.) of each n-paraffin and the solution behaviour of the n-paraffin's in the wax phase. Accordingly, Coutinho used experimental data to conclude that the wax phase as a solid solution of mainly n-paraffins could be modelled by the equation below.

$$\frac{G^E}{RT} = - \sum_i n_i^W \ln \left(\sum_j x_j^W \exp(\lambda_{ji} - \lambda_{ii}) \right) \quad (7.1)$$

Where G^E is the excess Gibbs energy, R is the gas constant, n_i^W and x_i^W are the mole number and mole fraction of the component i in the wax phase and λ_{ji} and λ_{ii} are Wilson parameters defined by

$$\lambda_{ii} = -\frac{1}{3}(\Delta H_{sub,i} - RT) \quad (7.2)$$

$$\lambda_{ji} = \alpha_{ij} \min(\lambda_{ii}, \lambda_{jj}) \quad (7.3)$$

Where $\Delta H_{sub,i}$ the enthalpy of sublimation of component i , α_{ij} is a correction factor. Other correlation for the enthalpy of fusion ΔH_m , melting temperature for the n -paraffin below a carbon number 42 (but above 8) and the those equal or above 42 are well described in the study by Coutinho *et al.* (2001).

In this work, Figure 7-1 shows a typical single-phase waxy oil behaviour and the shapes of the wax precipitation curve clearly illustrates the effect of pressure and temperature on wax deposition from the Coutinho model. It is observed that as the temperature of the crude oil drops around the WAT (i.e. $\sim 32^\circ\text{C}$) wax crystals begin to precipitate and at this temperature, the amount of wax forming component that precipitated is small. The WAT predicted by Coutinho model in the Multiflash software proved the accuracy of this model and the value is within the acceptable experimental data.

The amounts of wax precipitated at temperatures below the WAT is significant, and the wax phase boundary predicted shows that at any given pressures and temperatures below the WAT the system is within the risk area of wax deposition. The same WAT value was observed as the pressure increased from 7.3 psi to 500 psi, which implies that the WAT of this crude oil sample is only affected by temperature change. This behaviour could be due to the highly waxy nature of the crude oil, and perhaps the amount of the dissolved gas presence is relatively small. However, in some cases, for instance, a study by Wang *et al.* (2019) have shown that the wax appearance temperature in a gas condensate was affected by both temperature and pressure. Which shows that pressure influences a system containing a gas component more than a single-phase system.

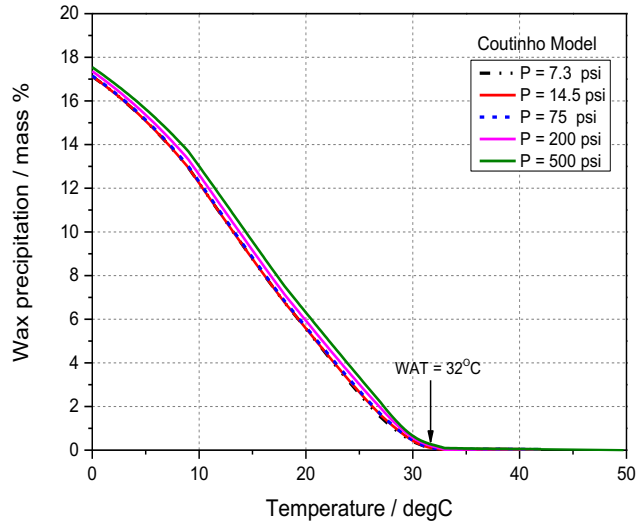


Figure 7-1: Wax precipitation curve from Coutinho thermodynamic model at different pressure and temperature

Similarly, it is seen that as the pressure increases from 7.3 to 14.5 and 75 psi, the same amount of wax that precipitated (i.e. 17.12 wax precipitation/mass%). Also, even at a higher pressure, for instance, from 200 to 500 psi, the increase in the wax precipitation is very limited, (from 17.35 to 17.5 wax precipitation/mass %). These behaviours proved that the pressure measured in this work, which ranges between 2 psi to 75 psi has little effects on the wax deposition. However, it is highly essential for monitoring and measurement of pressure drop. Since a reduction in the effective diameter of the pipe leads to additional pressure drop that can also cause back pressure to the production well and consequently decrease the production rate (Bai and Bai, 2005; Rittirong, 2014; Huang *et al.* 2015). Therefore, this study proved and concluded that wax deposition is highly thermal control process– drives by thermodynamic forces. The results show that the predicted WAT by Coutinho model matches the experiment.

7.2.2 Distribution of SCN and Phase Envelop of the Crude Oil

The single carbon number (SCN) distribution provides information regarding the total amount of hydrocarbon components in the crude oil, including both n-paraffins and non-n-paraffins. For a typical crude oil, only n-paraffins precipitate, whereas, the non-paraffins does not; due to their higher melting point than the n-paraffin component. *Figure 7-2* shows a comparison between the calculated single carbon number (SCN) distribution in the crude oil by Multiflash and the experimental results. The results show a good agreement between them with a little deviation.

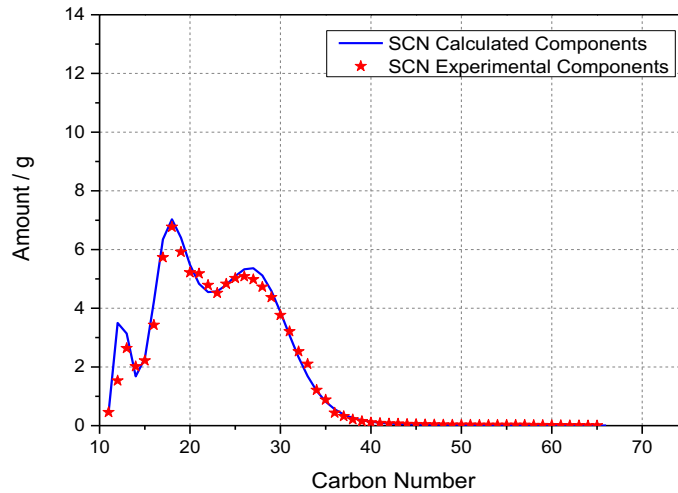


Figure 7-2: Single carbon number (SCN) distribution of the sample B crude oil predicted by Coutinho model matches the experimental data

On the other hand, a phase envelope was developed to understand the phase changes (gas/liquid/solid) in the system at different temperatures and pressures. *Figure 7-3* showed typical phase behaviour of the waxy crude oil sample. The analysis was carried out with conditions that include both the experimental and real field conditions. The phase envelop diagram showed that the fluid system is liquid phase dominant. However, below 32°C – the wax line (red line, point D), which correspond to WAT value of the oil sample; the system experiences solid wax deposition problem. A narrow two-phase (liquid and gas) region was observed, which skewed to the right between the bubble and dew point curve. The narrow area could be due to the nature and the properties of the oil sample. Similar fluid behaviour is reported by Wu *et al.* (2017). On the other hand, the gas-phase is present as a dissolved gas and breaks out at high-pressure and high-temperature. A critical point as observed is around 461.13°C and 222.39 psi.

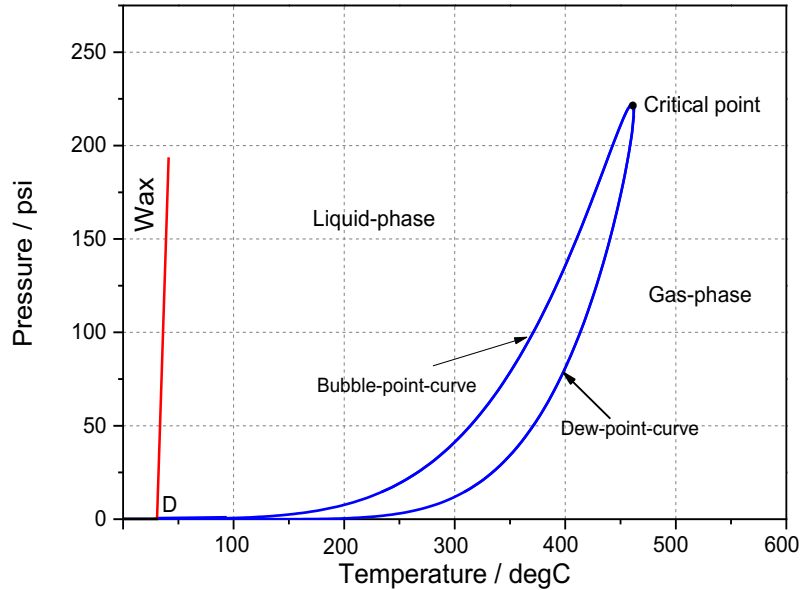


Figure 7-3: Phase envelope of sample B crude oil. The red line represents the wax extraction curve and the blue region represents are envelops for two-phase (oil-gas)

7.3 Wax Deposition Simulation using OLGA

In several years, a number predictive wax deposition software has been developed, and OLGA is one of the few and best known commercial transient multiphase simulator (Bendlken *et al.*, 1991; Seyfae *et al.*, 2012) for solving wax deposition problem. It incorporated modules that allow reproducing the wax deposition phenomenon, based on experiment or other field studies; these include the Rygg, Rydahl and Rønningsen (RRR), Matzain and Heat Analogy (Matzain, 1999).

In this section, an effort was made to mimic and simulate the experimental rig, which is quite challenging due to the complex system of the experimental setup. However, upon all the difficulties, the experimental results from the straight pipe test section were successfully simulated and compared. Whereas, the experimental results from the pipeline with 45° bend in horizontal flow and with elevation are compared. Initial, a base case simulation was developed with the straight pipeline through which sensitivity study of parameters such as wax porosity and selection of models type that would best match the experimental results are carried out.

7.3.1 Model Selection for Wax Simulation

Overall, the simulation study was carried out using the Matzain model. Analyses were carried out to decide the best model that could match the experimental thickness. *Figure 7-4* presents sample results comparing wax thickness predicted using the three models at a constant flow rate, simulation time and cooling temperature. The Matzain model, to some extent, allows reproducing the experimental deposit thickness compared to the other two models (RRR and Heat Analogy). Similar observations and conclusion were made by Giacchetta *et al.* (2019), Leporini *et al.* (2019), Noville and Naveira (2012) and Botne and Gudmundsson (2012). According to Giacchetta *et al.* (2019) and Leporini *et al.* (2019), the RRR model presented values (e.g. thickness) that are lower (Matzain *et al.*, 2002b) than the Matzain correlation. As shown in *Figure 6-4*, the predicted wax thickness by Matzain is 1.32 mm (i.e. the maximum point on the thickness line after specific simulation time), which is very close to 1.29 mm obtained from the experimental study after 2 hrs at $Q_{oil} = 5$ l/min and $T_{cooling} = 25^{\circ}\text{C}$. This is compared to the wax thickness of 1.19 and 0.92 mm for the RRR and the heat analogy mode respectively.

It is worth noting that although Matzain model is considered as a semi-empirical model; however, the model predicts wax thickness with acceptable accuracy (Pinho *et al.*, 2011). The model incorporates both molecular diffusion and shear dispersion alongside shear stripping mechanism to simulate wax deposition (Aiyejina *et al.*, 2011). Matzain model is primarily significant in this work due to the model's wax reducing mechanism (shear stripping) effect, which is crucial, especially under turbulent flow conditions (Aiyejina *et al.*, 2011). Similarly, the model is perhaps the only model that is suitable in curves pipes where the fluid experience separated flow and back mixing. In this model, shear dispersion is considered of minor importance unlike to the RRR model. This implies that the molecular diffusion is the predominant mechanism, however, at higher flowrate, the stripping effect may contribute to the removal of wax, and the small impact of share dispersion can be significant.

Matzain models used an empirical modification of Fick's law to calculate the rate of the wax build-up (Aiyejina *et al.*, 2011; Leporini *et al.*, 2019). The correlation (Eq.

7.4) incorporates parameters that account for the porosity effect on the rate of wax build-up and the deposition enhancement mechanism (Leporini *et al.*, 2019). This is perhaps another reason for a better agreement between the two results.

$$\frac{d\delta}{dt} = \frac{\Pi_1}{1 + \Pi_2} D_{wo} \left(\frac{dC_w}{dT} \frac{dT}{dr} \right) \quad (7.4)$$

Where Π_1 is the supplied empirical correlation accounting for the porosity effect and Π_2 account for the wax limiting effect of shear stripping defines as:

$$\Pi_1 = \frac{C_1}{1 - C_L/100}$$

$$\Pi_2 = 1 + C_2 N_{SR}^{C_3} \frac{C_1}{1 - C_L/100}$$

where $C_2=0.055$ and $C_3=1.4$. δ is the thickness of the wax layer deposited on the wall, D_{wo} is the diffusion coefficient calculated with the Wilke and Chang correlation, C_w the concentration of wax in solution, r is the pipe radial distance, T is the fluid temperature. C_L defines the amount of trapped oil in the wax layer.

$$C_L = 100 \left(1 - \frac{N_{Re}^{0.15}}{8} \right) \quad (7.5)$$

More details on the constant C_1 , flow regime dependent Reynolds number (N_{SR}) could be found in Leporini *et al.* (2019) study.

On the other hand, Leporini *et al.* (2019) described the Rygg, Rydahl and Rønningsen model (RRR) as a semi-stationary model, which predicts wax deposition build-up in wells and pipelines in a slower process than flow disturbances in a pipe (Rosvold, 2008). This factor may have contributed to the lower wax thickness prediction by this model since the experimental and simulation time is small. In this model, molecular diffusion and shear dispersion effect are considered the only mechanisms responsible for wax deposition.

Whereas, in the heat analogy model, according to Leporini *et al.* (2019), there is no sufficient data available in the literature to develop a better understanding as to what extent this model is better compared to the others. However, it was mentioned that “the model calculates the mass transfer rate of wax by employing the heat transfer analogy” (Leporini *et al.*, 2019; Singh *et al.*, 2000). It is worth noting that for OLGA with the Matzain wax deposition model; occasionally, the diffusion coefficient needs

to be tuned for the wax deposition simulation. Therefore, a multiplication factor of 5 for the diffusion coefficient was selected similar to BHR Group study reported by Pinho *et al.* (2011).

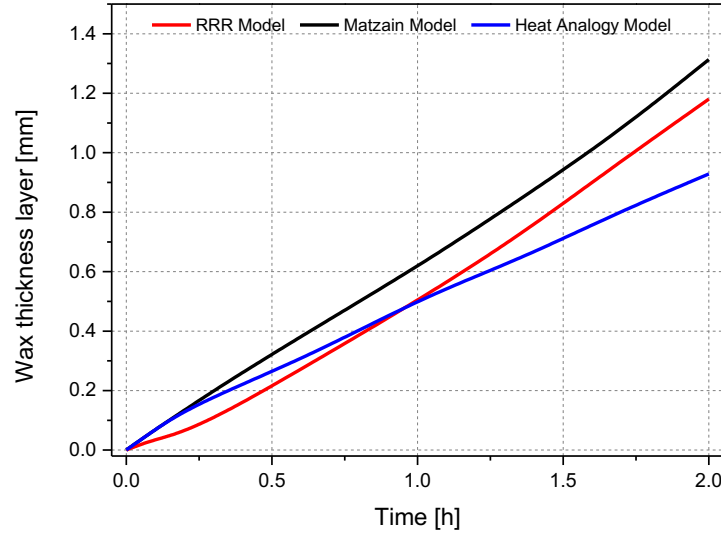


Figure 7-4: Trend plot comparison of wax thickness predicted using RRR, Matzain and Heat analogy models at a constant flow rate of 5 l/min, 80% wax porosity and cooling at 25°C.

7.3.2 Effect of Wax Porosity

Wax porosity significantly affects wax deposit thickness; in fact, the parameter represents the fractional amount of trapped oil in the deposit. It is important to note that the deposited wax is not 100% pure solid crystals, often contains some amount of trapped oils that are sometimes called wax porosity (Botne and Gudmundsson, 2012; Edmonds *et al.*, 2008). These studies have shown that “wax porosity has a significant effect on the simulation and the amount of wax deposit is sensitive to the assumed value of porosity”. Two porosities (60 and 80%) were studied by Edmonds *et al.* (2008), and the prediction shows a rapid wax build-up that reaches 2 mm at 80% porosity. According to Labes-Carrier *et al.* (2002) study, the value porosity to be used is mainly depended on the type of crude oil, flow regime and degree of turbulence. Literature has shown that the fraction of occluded oil or porosity usually varies between 60–90 mass % (Edmonds *et al.*, 2008), while others (such as Burger *et al.*, 1981; Labes-Carrier *et al.*, 2002) suggested that the range is between 50 – 90%. The solid wax deposit is divided into two based on the study reported by Botne

and Gudmundsson (2012); (i) Soft deposit – Where the fraction of occluded oil could be up to 90%. (ii) Hard deposit – could have the fraction of occluded oil between 50 – 72%. This means that the deposited layer with low porosity is delicate to pig-out of the system compared to the hard-soft deposit.

Therefore, in this study, three wax porosities (i.e. 0.6, 0.8 and 0.9) were used as tuning parameters in the OLGA to match experimental values. Figure 7-5 showed the comparative results of wax thickness simulation and the experimental data. It is seen that using 90% wax porosity the wax thickness is higher, which over predicts the deposition because of the increase in the amount of the trapped oil between wax structures in the deposited layer. In contrast, the wax deposition was under-predicted at low porosity (0.6). However, at 80% wax porosity produced a better match between the experimental and simulation results. Therefore, 0.8 wax porosity was used in this simulation study, as the wax thickness measured at this value is relatively close to the experiment.

It is worth noting that a wax content of about 20 wt% was obtained by acetone precipitation (described in Chapter 3), which implies that the occluded oil (or porosity) is expected to be around 80.3%. This value is approximately equal to the wax porosity (80%) chosen in the study. This result is in reasonable agreement when compared to a similar case study reported by Labes-Carrier *et al.* (2002). In Labes-Carrier *et al.* study, the oil has a wax content of about 45 wt.% (acetone precipitation), which measured oil content of about 55% is in reasonable agreement with the 60% wax porosity their study used in the OLGA simulations.

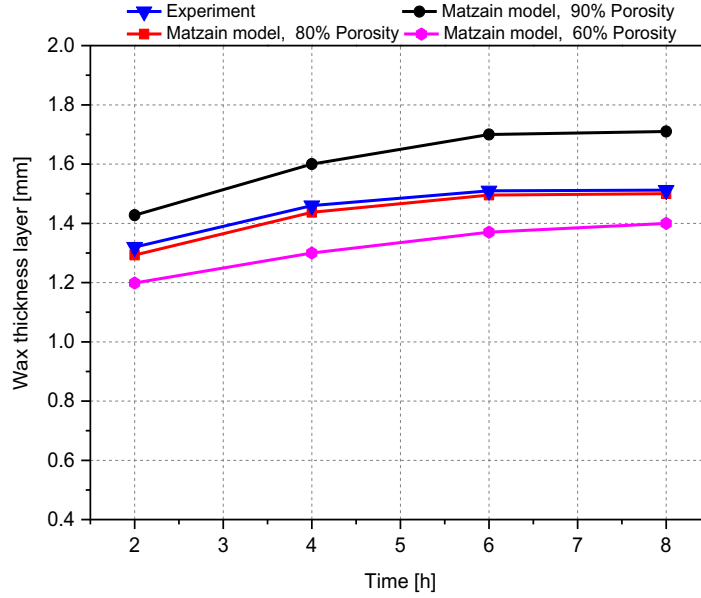


Figure 7-5: Effect of wax porosity on wax thickness predicted using Matzain model at a constant flow rate of 5 l/min and $T_{cooling} = 25^{\circ}\text{C}$.

7.3.3 Base Case: Simulation Study

Having selected the right model and the wax porosity value; it is essential to develop a good understanding of the wax deposition phenomena in terms of the change in the viscosity of the crude oil with temperature, decrease in the dissolved wax with an increase in the wax precipitation, pressure along the flowline. This study is necessary to ascertain the reliability of the results for comparative analysis.

Figure 7-6 and Figure 7-7 shows the behaviour of the variables mentioned above in a straight pipe section. As seen from the temperature profile in Figure 7-6, the oil temperature was kept at 45°C , i.e. above the wax appearance temperature at the inlet of the pipeline. This temperature drops gradually to around 23°C in the outlet section. This characteristic behaviour established was due to the influence of heat transfer between the inner pipe and the ambient conditions (annular space). Similarly, it is observed that at around 0.12 m (pipeline length), the wax crystals begin to precipitates; this is due to the oil temperature at this location drops to around WAT. Hence, with this observed behaviour, it is worth to states that in this study, the principle of wax deposition as a result of the temperature gradient between the bulk fluid and the ambient fluid conditioned is simulated.

Indeed *Figure 7-6* has shown that as the temperature drops continue below the WAT, a rapid increase in the growth of the amount of wax precipitation was observed. On the contrary, the pressure along the flow line drops as the wax deposit build-up. As a result of reduction in the hydraulic diameter of the pipe section, which increased frictional pressure drop over the entire pipeline section (Lashkarbolooki *et al.*, 2011). On the other hand, the viscosity of the crude oil increased linearly, due to the formation of the wax crystals. Which as a result, change the crude oil behaviour from Newtonian to a non-Newtonian fluid (Bai and Bai, 2005; Huang *et al.* 2015). It is seen that 1.43 mm deposit thickness was predicted at $Q_{oil} = 5$ l/min for a fixed simulation period of 4 hrs.

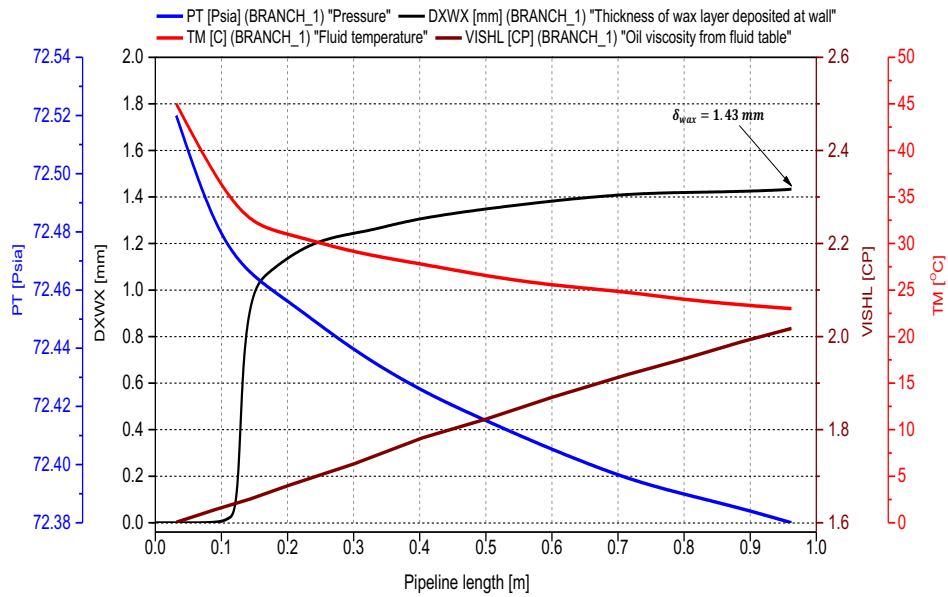


Figure 7-6: Wax deposition profile for the straight flow line section at a constant flow rate of 5 l/min, the cooling temperature at 25°C, and simulation period 4 hr.

Figure 7-7 shows a direct correlation between the total mass of the dissolved wax in crude oil and the total mass of wax particles precipitated out from the oil measured at a constant 5 l/min. According to a study by Huang *et al.* (2015), the amount of wax that remains soluble in the liquid phase should be equal to the total wax content minus the amount of wax that has precipitated. Therefore, Figure 7-7 (the red and the blue line) shows that the total mass of the wax dissolved in the crude oil decreases with a corresponding increase in the total mass of wax particles precipitated out of the crude oil.

This scenario is relatively depended on the effectiveness of the temperature gradient and the shearing effect in the pipeline. Crude oil is believed to exhibits a quasi-Newtonian rheological behaviour over an increasing shear rate (Kumar *et al.*, 2016). For instance, Figure 7-7 (b) shows a decrease of wax deposit thickness from 1.29 mm to 0.43 mm as the crude oil flow rate increases from 5 l/min (the criteria for lamina flow region) to 9 l/m (the criteria for turbulent flow region) at 2 hrs simulation period. Therefore, increasing the flow rate led to an increase in shear within the system, which reduces the thickness of wax deposition (Pham *et al.*, 2017). Therefore, it implies that the velocity of the fluid governs the shear stress and higher flow rate affects the heat loss along the pipe. The amount of heat loss along the pipeline is inversely proportional to the flowrate (Brown *et al.*, 1993; Creek *et al.*, 1999; Jennings and Weispfennig, 2005). In general, higher flow rate provides shorter residence time for the heat transfer to be effective, and to transports the precipitates along the pipe, which resulted in a small wax deposition.

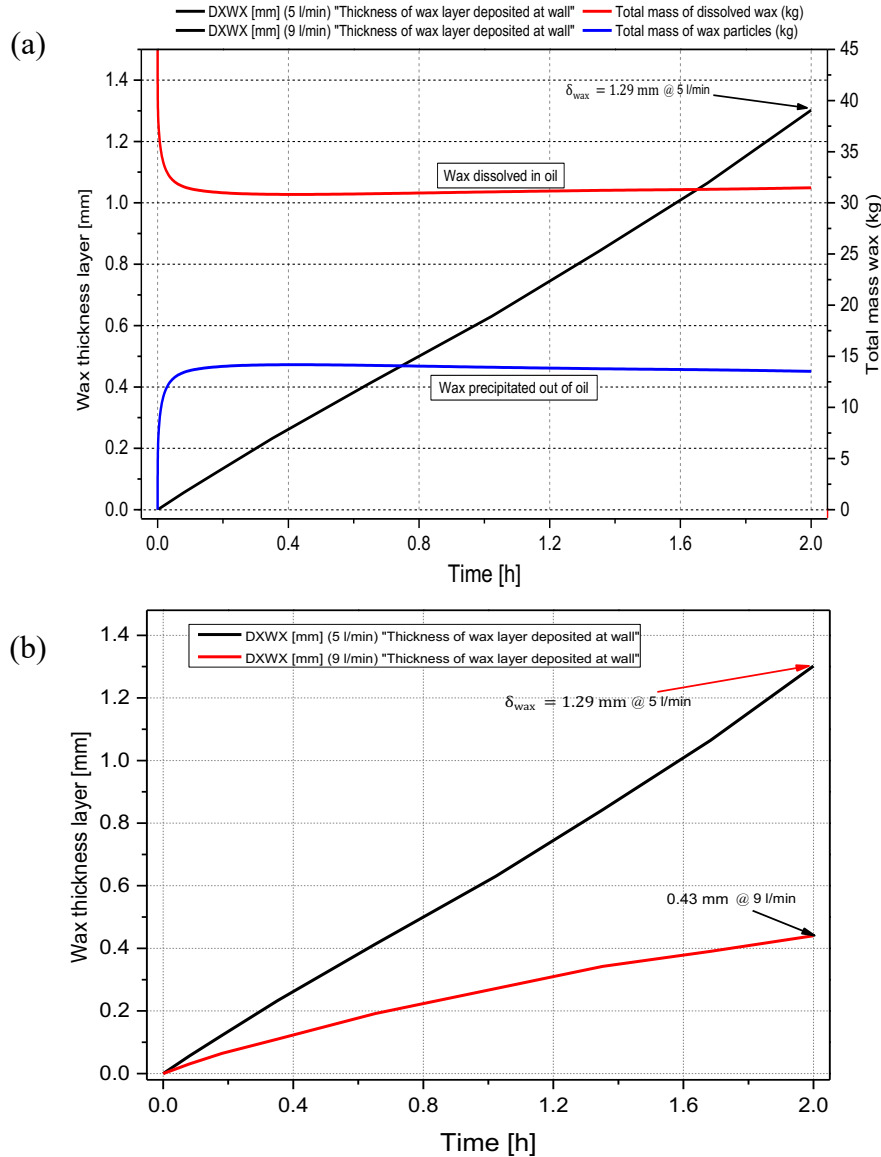


Figure 7-7: Trend plots for wax deposition in the straight flow line section at a constant cooling temperature of 25°C and 80% porosity. (a) Deposition at a constant flow rate of 5 l/hr for 2hrs simulation. (b) Deposition at two different flow rate of 5 and 9 l/min and

7.3.4 Comparison of Wax Simulations with Experiment: Straight Pipeline

Having established good understanding of the simulation in straight pipe, it is essential to study the influence of other parameters on wax deposition in the same pipeline and compare to experimental results. **Table 7-1** summarised some of the predicted results by the OLGAs and the experimental data. Figure 7-8 and 7-9 shows the comparisons over a different range of cooling temperature (15, 25 and 30°C), experimental time (2, 4, 6, and 8 hours) and two flow rates: $Q_{oil} = 5$ (i.e. at laminar

flow regime) and $Q_{oil} = 9$ l/min (i.e. at turbulent flow regime). The oil temperature was kept constant at 45 throughout the simulation.

Table 7-1: Experimental and simulation (with 80% porosity) results (deposit thickness) in a straight pipeline section at temperatures from $T_{oil} = WAT + 15^\circ C$ to T_h at 15, 25 and $30^\circ C$

Time (hr)	Cooling temperature 15°C		Cooling temperature 25°C		Cooling temperature 30°C	
	Experiment	Matzain Model	Experiment	Matzain Model	Experiment	Matzain Model
Flow rate: 5 l/min - Laminar flow regime						
2	1.90	1.84	1.32	1.29	0.36	0.35
4	2.06	2.02	1.46	1.43	0.41	0.40
6	2.15	2.12	1.50	1.49	0.43	0.42
8	2.15	2.12	1.51	1.50	0.44	0.44
Flow rate: 9 l/min - Turbulent flow regime						
2	1.45	1.43	0.45	0.43	0.00	0.00
4	1.53	1.51	0.49	0.48	0.00	0.00
6	1.55	1.53	0.50	0.49	0.00	0.00
8	1.55	1.54	0.50	0.49	0.00	0.00

All the deposit thickness (δ) are measured in mm

As outlined in the previous sections; the wax precipitation and the possible deposition commence as soon as the crude oil temperature is equal or less than WAT. However, this behaviour is influenced by the properties of circulating fluid and the transporting material such as flow rate and surface roughness. In most cases, at a low flow rate, the precipitated wax deposited to the inner surface of the pipe otherwise flows along with the bulk fluid at a higher flow rate.

Overall as shown in *Figure 7-8* and *Figure 7-9*, it could be concluded that the deposit thickness shows a linear trend to a large extent. Moreover, the simulation results, especially at a higher flow rate, are in agreement with experimental data. It is observed that the deposit thickness from the simulation is slightly lower than the experimental results. This behaviour is apparent at a low flow rate and low cooling temperature. For instance, in *Figure 7-8* at a cooling temperature of $15^\circ C$ (below the pour point) a wax thickness of 1.93 mm was seen from the experiment compared to 1.81 mm for the simulation study after 2 hours of production. However, this difference appears to decrease with an increase in temperature and flow rate.

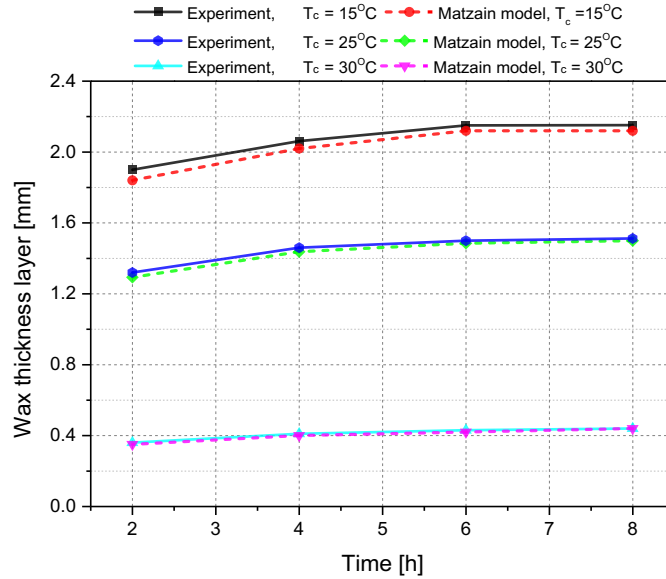


Figure 7-8: Comparison of deposit thickness as a function of different cooling temperature (15, 25, and 30°C) and 8 hrs testing between the experimental and simulation studies at constant $Q_{oil} = 5$ l/min, $T_{oil} = 45^\circ\text{C}$ and wax porosity (0.8) in a straight pipeline section.

As shown in *Figure 7-9*, increasing the coolant temperature from 15°C (below the pour point) to 25°C (at pour point) at flow rate 2 hrs simulation time; led to a decrease in the deposit thickness from 1.81 mm to 1.32 mm (experiment) and 1.41 mm to 0.43 mm (simulation). The deposit thickness reduces further as the coolant temperature increased to 30°C (T_c , at WAT). It reduces to zero, as shown in *Figure 7-9* (at 30°C), which means that when the $T_c = \text{WAT}$, there is not enough thermal driving force that could cause deposition at this flowrate. Similarly, at the higher flow rate (the turbulent flow regime) the wax particles move in random and rapid fluctuations of swirling currents that affect the deposition of the precipitated particles, unlike in the laminar flow condition.

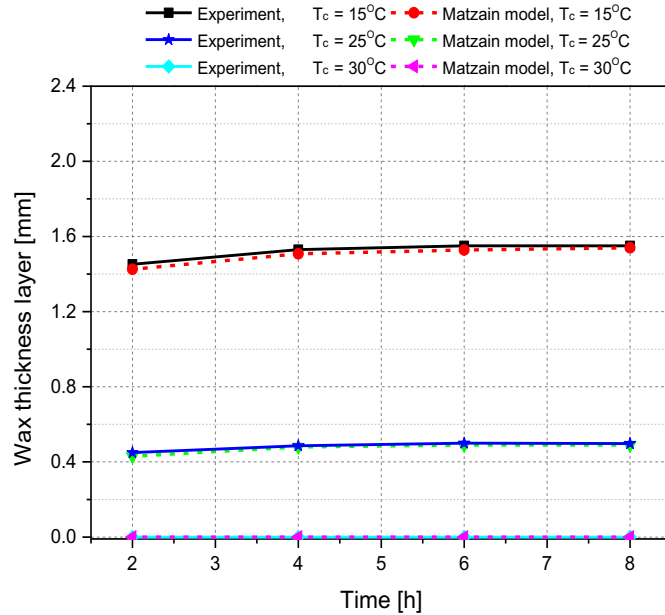


Figure 7-9: Comparison of deposit thickness as a function of different cooling temperature (T_c) and time between the experimental and simulation studies at constant $Q_{oil} = 9$ l/min, $T_{oil} = 45^\circ\text{C}$ and wax porosity (0.8) in a straight pipeline section.

Overall, it is comprehended that the used of 80% wax porosity and other assumed parameters (such roughness, a multiplication factor of 5 for the diffusion coefficient) improve the simulation and match with the experimental results for the straight pipe, however, with a slight difference between the two results (at a lower flow rate). The differences could be as a result of the assumed porosity value used in the simulation. As seen in *Figure 7-5*, the porosity did not completely match experimental data in some condition; however, it produces better results. Similarly, the wax roughness used in the simulation and the possible presence of the residual oil in the experiment could play a role for the divergence.

7.3.5 Simulation Study in the Straight Pipe with Elevation

In this section, the severity of wax deposition (in thickness) in the curved pipes was simulated and compared with the experimental data. It is worth to bear in mind that the base case simulation that was built using a straight pipeline was modified by incorporating an elevation as described in section 3.9.2 and highlighted in section 7.1. This modification allows the study of wax depositional behaviour in curved pipes and trying to validate the results with an experiment. Therefore, as aimed in this section, the simulation results are compared with the experimental flow rig

results built with a 45-degree bends pipe and elevation. Although, the studies (experimental and simulation) were made with pipe sections of equal length, diameter and material; however, their results are not expected to precisely match each other. Because in OLGA simulator, pipes are modelled either straight, vertical or incline with elevation. Thus, this is considered a significant limitation of this study, as there is no tools in OLGA to model bend. However, the simulation using curved pipes with bend provides different understanding of wax deposition behaviour.

Hence, the influence of parameters similar to those in section 7.3.4 was simulated and compared. *Figure 7-10* and *Figure 7-11* presented the deposit thickness under different flow rates; $Q_{oil} = 5$ (i.e. at laminar flow regime) and $Q_{oil} = 9$ l/min (i.e. at turbulent flow regime) over a different range of cooling temperature (15, 25 and 30°C), experimental time (2, 4, 6, and 8 hours). It is observed that in both studies, the deposit thickness increases with time and begins to reach a steady-state after 6 hrs of simulation. This is because the deposited layer creates an additional thermal resistance, which decreases the rate of heat transfer between the bulk fluid and the coolant. At this point, “the rate of thermal energy gained by the coolant is equal to the rate of heat transfer through four thermal resistances in series, namely the mixture (convection), deposit layer (conduction), tube wall (conduction), and coolant (convection)” (Ehsani *et al.*, 2019). *Figure 7-10* shows that the deposit thickness predicted by OLGA after 2 hr simulation reduces from 3.26 to 2.81 and 1.45 mm as coolant temperature drops from 15 to 25 and 30°C respectively. At the same conditions, the thickness decreases from 4.18 to 3.45 and 1.98 mm respectively.

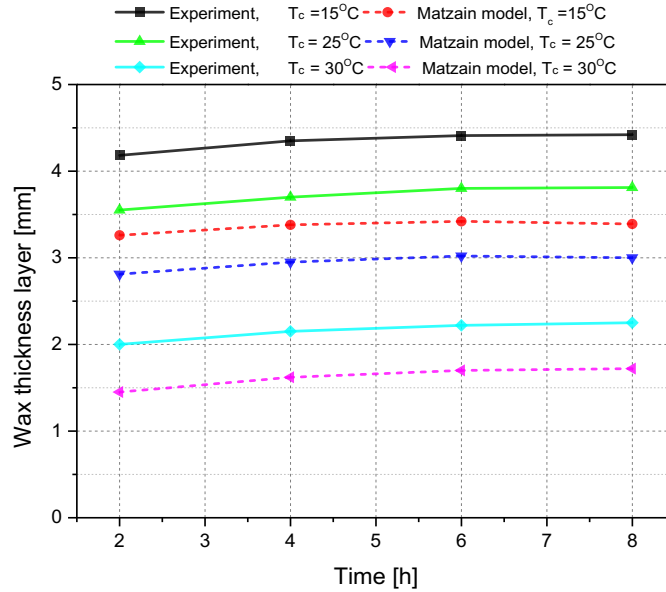


Figure 7-10: Deposit thickness as a function of different cooling temperature (T_c) and time between the experimental and simulation study at constant $Q_{oil} = 5$ l/min, $T_{oil} = 45^\circ\text{C}$ and wax porosity (0.8) in a pipeline section with elevation.

As shown in the Figure above, there is a massive difference between the deposit thickness from the simulation and experiment. Therefore, in this particular case, the predictions by the OLGA simulator do not in any conditions match the experimental results. It is observed that the severity of the wax deposition predicted by the simulator is lower compared to experiment. The disparity in the results could be due to the curvature replicated in the OLGA simulator lacks some parameters that could influence the deposition similar to the experiment; such as the equivalent radius of curvature and bend angle. As such, separated flow at the inner wall of the pipe bend requires particular curvature ratio determined from Babcock & Wilcox chart. Other issues that perhaps contribute to the wide gaps between the two results may be due to some of the uncertainty in both studies. For instance, during the experimental study with bend pipes, it is observed that no matter how much the pipe section is raised to drain the residual oil; some of the oil might stick to the surface, which potentially increased the thickness in the experiment.

Previously, it is shown that the deposit thickness decreases with an increase in the oil flow rate. Similarly, in this particular case, the results *Figure 7-10* (5 l/min) are compared *Figure 7-11* (9 l/min). These results are in agreement to the study in section 6.3.3.1 (for straight pipeline section) and those published by Creek *et al.* (1999), Zheng (2017), Giacchetta *et al.* (2019) and Mansourpoor *et al.* (2019).

Unlike in the straight pipeline section, a high wax deposit was measured in this study even as the cooling temperature equal to the WAT and under turbulent flow regime. This difference could be due to the relatively higher concentration of the wax crystals caused by the diffusion of wax particles and perhaps settling mechanism of the particles as a result of the gravitational effect.

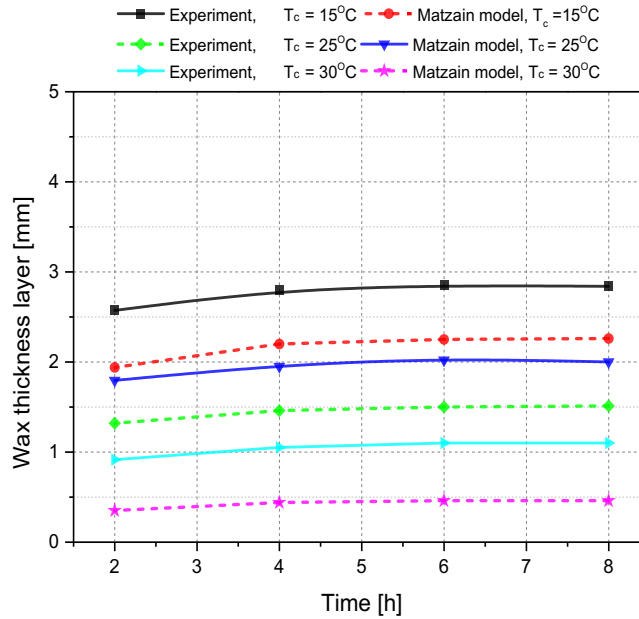


Figure 7-11: Deposit thickness as a function of different cooling temperature (T_c) and time between the experimental and simulation study at constant $Q_{oil} = 9$ l/min, $T_{oil} = 45^\circ\text{C}$ and wax porosity (0.8) in a pipeline section with elevation.

Although the predicted results through OLGA did not match the experimental data; however, still confirmed and proved that the severity of the deposition growth process increased. Notably, as the curvature of the pipes changes; from been straight to a curved pipe with or without elevation. Hence, it could be concluded that curvature in the pipe does affect the deposition of the suspended wax crystals in the flow line.

Chapter 8

Conclusions and Recommendation for Future work

8.1 Conclusions

In this thesis, the effect pipe curvatures on the behaviour of wax deposition were successfully investigated by experimental and numerical methods. The mitigation of wax deposition by the addition of chemical inhibitors was also explored. The key findings are summarised as follows:

- A pipeline flow rig was designed and built to simulate the deposition in flowlines. The flow rig incorporated three different test sections – a straight pipe, a pipe with a 45° bends and a pipe with 90° bends. All three test sections have an equal length.
- Three crude oil samples were characterised as highly paraffinic oils based on the analysis of their fundamental properties and the features such as the wax content, SARA fraction, n-Paraffin distribution, viscosity, macroscopic crystal morphology, CII, WAT, and pour point. The wax content in each sample is sufficient to entrap the liquid phase, which leads to an increase in oil viscosity or in some cases gels crude oil molecules on the cold surface. Consequently, this reduces the pipe diameter and impairs the effectiveness of oil recovery. In worst-case, this leads to the plugging of flowlines that usually causes very costly remediation or treatment. Similarly, the result of the morphology of wax crystals and other properties such as pour point and WAT revealed the complex nature of the oil samples, particularly the sample 'B' oil, which proved to be more problematic than the other sample even under the ambient conditions.
- The series of experiments carried out in the pipeline flow rig covered different crude oil flow rates from laminar to turbulent flow conditions at different ambient cooling temperatures between $T_{cool} \leq \text{pour point}$ and $T_{cool} \geq \text{WAT}$

alongside with different experimental durations. The thickness of wax deposition in the straight pipe test section was determined by four different methods to include: weight–balance, pressure drop, volume correlation and the heat transfer method. Parity plot was used to evaluate the uncertainty of these techniques. The results agreed well with those reported in the literature, i.e. weight–balance and pressure drop methods are the most reliable methods in single-phase study. More so, under the curved pipes experimental study, a new pressure drop model established showed the need for further studies in this area.

In a nutshell, the findings show that a large portion of wax is deposited at short times. Flow turbulence reverses the deposition of wax. Increasing the flow rate reduces wax deposition thickness. It was observed that the deposition thickness initially increases linearly at a faster rate after 2 hours and reached maximum with a slower rate after 6 hours. Wax deposition measured in the three curved pipes in horizontal flow showed that under the extreme case scenario (15°C and 5 l/min), 22% of the wax is deposited in straight pipe test section compared to 36% and 43.5% obtain in test sections with 45° bend and 90° bend. This implies at the same condition where the system experienced 0% wax deposition in the straight pipe it underwent 14% and 19% deposition, respectively, for the pipe with 45° and 90° bends. The severity of wax deposition in curved pipes simultaneous decreases with increasing coolant temperature and flow turbulence and vice versa. Contrary to the theory established in the literature that gravity settling mechanism can be neglected due to the possible re-dispersal of the particles by shear dispersion, in this study, however, it is observed that wax deposition increased as a result of switching the curved pipes section from horizontal to an inclined position. Hence, the study showed that apart from the molecular diffusion believed to be dominant mechanism, others such as shear dispersion and stripping, alongside with Brownian diffusion and gravity settling mechanism all contributed to the deposition process. The research demonstrates that more work is needed to fully understand these mechanisms so that a robust wax mitigation strategy is developed.

Similarly, the predictions of wax deposition from OLGA are to some extent, consistent with the experimental data when the wax shear removal mechanism is

considered. The model used incorporates both molecular diffusion and shear dispersion alongside shear stripping mechanism to simulate wax deposition. The disparities observed in the bend section results are related to the inability of OLGA to exactly replicate the bend pipe used in the experiment. However, the simulated results confirmed the higher deposition growth in the elevated pipeline than that in the straight pipe section.

- Four commercial wax inhibitors were analysed and screened through a comprehensive viscometric study and morphological characterisation using sample 'B' oil doped with inhibitors. All the wax inhibitors have effectively reduced the viscosity, pour point and WAT of the oil in the decreasing order of performance W2001>W2003>W2005>W2004. However, the new inhibitor (blend A) performed better than the original commercial samples. The macroscopic morphology results proved the inhibition performance of the new blended inhibitor, which transformed the needle-like or rod-like crystals of the oil samples into agglomerate and small particles dispersed in the oil matrix.
- Furthermore, during the flow rig study, the finding indicates that simultaneous usage of blend A wax inhibitor and flow turbulence reduced wax deposition significantly and in some cases, completely prevented the wax from deposition. The performance and the efficiency of the inhibitor slightly reduced at a lower concentration (e.g. 500-ppm) compared to a higher dosage (i.e. 1000, 1500, 1300, 1500, and 1800-ppm). This phenomenon is believed to be by the structural disorder introduced during the formation of wax crystals. The optimum concentration (i.e. 1500-ppm) produced the best inhibition performance. No improved behaviour was observed above this concentration. At this concentration when the oil was cooled down below the pour point (extreme temperature, 15°C) around 80% of wax deposit could be reduced under turbulent flow regime (9 and 11 l/min). At the same flow rate but at a relatively higher temperature of 25°C (i.e. pour point temperature), 100% wax prevention was reached even at a lower concentration (500-ppm). Whereas, in laminar flow regime (i.e. at 7 l/min), 100% wax deposition prevention could only be achieved at the higher concentrations of 1000 and 1500-ppm at 30°C (i.e. at WAT).

8.2 Recommendation for future works

One of the contributions of this work is that it sets the basis for understanding wax deposition from a different angle to those reported in the previous literature. The following recommendations are made for further work in the area.

- To investigate the effect of bends on wax deposition behaviour in larger diameter pipes. The diameter of the pipe has a significant effect on the secondary flow developed in the bend. Current work was carried out in a 15 mm pipe. Therefore, further work in a larger diameter pipe is recommended to establish the severity of the effect of bends on the wax deposition.
- To modify the test section to accommodate the sensors for wax film measurement, visual inspection and pressure drop monitoring. Currently, there is no sensor to measure the local wax thickness. The wax film is assumed symmetrically distributed in the pipe. This assumption may not be valid, particularly in a larger diameter pipe. Pressure drop is a sensitive parameter to the wax deposition. Therefore, multiple pressure sensors help to determine the wax distribution along the pipe and for better use of new model. Visualisation by high-speed camera gives direct observation to the flow phenomena in the pipe. The current rig has no transparent section for visualization.
- Current flow rig is designed for single-phase only. The presence of gas-phase causes different flow regimes and could significantly affect the general behaviour of wax deposition. The appropriate modification should be made for gas-liquid flow.
- The results of this study suggest that the gravity settling effect of wax particles plays a vital role in contributing to the wax build-up along the pipe bend - in an inclined flow. Perhaps ignoring this mechanism in the wax deposition models can result in under-prediction of the wax thickness, which might lead to unplanned additional wax treatment and frequent mechanical pigging. However, some models such as the Matzain model incorporated in OLGAs considered the effect of molecular diffusion, shear stripping and shear dispersion in the simulation of wax deposition; therefore, it is necessary to reconsider the

influence of gravity effect as suggested in this study.

- A software (3-D CFD) plugin or coupling with OLGA (1-D) is recommended to enhance the capability and applicability of OLGA for a full description of waxy oil behaviour in pipelines and around bends, particularly in two-phase (gas/liquid) system.

References

- Adeyanju, O. A. and Oyekunle, L. O. (2014) Influence of Long Chain Acrylate Ester Polymers as Wax Inhibitors in Crude Oil Pipelines, in: pp. 5–07.
- Adeyanju, O. and Oyekunle, L. (2013) Experimental Study of Wax Deposition in a Single Phase Sub-cooled Oil Pipelines, *Nigeria Annual International Conference and Exhibition*, 167515.
- Ahmed, T. (2007) *Equations of State and PVT Analysis. Applications for improved reservoir modeling*. Gulf Publishing Company Houston, Texas.
- Aiyejina, A., Chakrabarti, D. P., Pilgrim, A. and Sastry, M. K. S. S. (2011) Wax formation in oil pipelines: A critical review, *International Journal of Multiphase Flow*, 37 (7), pp. 671–694. DOI:10.1016/j.ijmultiphaseflow.2011.02.007.
- Ajayi, O. E. (2013) *Modelling of Controlled Wax Deposition and Loosening in Oil and Gas Production Systems*. MSc Thesis, Institutt for energi-og prosessteknikk.
- Akpabio, M. G. (2013) *Cold Flow In Long-Distance Subsea Pipelines*. Master's thesis, Norwegian University of Science and Technology.
- Al-Sabagh, A. M., Noor El-Din, M. R., Morsi, R. E. and Elsabee, M. Z. (2009) Styrene-maleic anhydride copolymer esters as flow improvers of waxy crude oil, *Journal of Petroleum Science and Engineering*, 65 (3–4), pp. 139–146. DOI:10.1016/J.PETROL.2008.12.022.
- Al-Safran, E. M. and Brill, J. P. (2017) *Applied multiphase flow in pipes and flow assurance oil and gas production*. Society of Petroleum Engineers (SPE).
- Al-yaari, M. (2011) Paraffin Wax Deposition : Mitigation & Removal Techniques, in: *Spe 155412*. pp. 14–16.
- Alcazar-Vara, L. A. and Buenrostro-Gonzalez, E. (2011) Characterization of the wax precipitation in Mexican crude oils, *Fuel Processing Technology*, 92 (12), pp. 2366–2374. DOI:10.1016/j.fuproc.2011.08.012.
- Alcazar-Vara, L. A., Garcia-Martinez, J. A. and Buenrostro-Gonzalez, E. (2012) Effect of asphaltenes on equilibrium and rheological properties of waxy model systems, *Fuel*, 93, pp. 200–212. DOI:10.1016/j.fuel.2011.10.038.
- Allen, O. T. and Roberts, P. A. (1978) *Production operations: well completions, workover, and stimulation. Volume 2*. 3rd ed. Oil & Gas Consultants International, Inc, Tulsa.
- American Petroleum Institute (2011) Robust Summary of Information on Crude Oil, *North*, (1997), pp. 1–130. Available from: <https://petroleumhvp.org/petroleum->

- [substances-and-categories/~media/89F496D8432545ABB06D85D0BD5D99D1.ashx](#) [Accessed 10 November 2019].
- Anosike, C. F. (2007) *Effect of Flow Patterns on Oil-Water Flow Paraffin Deposition in Horizontal Pipes*. University of Tulsa.
- Ansart, B., Marret, A., Rageot, O. and Parenteau, T. (2014) Technical and Economical Comparison of Subsea Active Heating Technologies, *Offshore Technology*.
- Anton Paar (2020) Rheological investigation of petrochemicals. Available from: <https://wiki.anton-paar.com/en/basics-of-rheology/rheological-investigation-of-petrochemicals/#c49283> [Accessed 15 July 2019].
- Apte, M. S., Matzain, A., Zhang, H.-Q., Volk, M., Brill, J. P. and Creek, J. L. (2001) Investigation of Paraffin Deposition During Multiphase Flow in Pipelines and Wellbores—Part 2: Modeling, *Journal of Energy Resources Technology*, 123 (2), pp. 150. DOI:10.1115/1.1369359.
- Ashoori, S., Sharifi, M., Masoumi, M. and Mohammad Salehi, M. (2017) The relationship between SARA fractions and crude oil stability, *Egyptian Journal of Petroleum*, 26 (1), pp. 209–213. DOI:10.1016/j.ejpe.2016.04.002.
- Asomaning, S. and Watkinson, A. P. (2000) Petroleum stability and heteroatom species effects in fouling of heat exchangers by asphaltenes, *Heat Transfer Engineering*, 21 (3), pp. 10–16. DOI:10.1080/014576300270852.
- Azevedo, L. F. A. and Teixeira, A. M. (2003) A critical review of the modeling of wax deposition mechanisms, in: *Petroleum Science and Technology*, 21, pp. 393–408.
- Baby, R. and Balaji, C. (2019) *Thermal Management of Electronics, Volume I: Phase Change Material-Based Composite Heat Sinks—An Experimental Approach*. Momentum Press.
- Bagdat, M. and Masoud, R. (2015) Control of Paraffin Deposition in Production Operation by Using Ethylene–TetraFluoroEthylene (ETFE), in: *Proceedings of the International Conference on Integrated Petroleum Engineering and Geosciences Icipeg 2014*. pp. 13–22.
- Bai, C. and Zhang, J. (2013) Thermal, macroscopic, and microscopic characteristics of wax deposits in field pipelines, *Energy and Fuels*, 27 (2), pp. 752–759. DOI:10.1021/ef3017877.
- Bai, Y. and Bai, Q. (2005) *Wax and Asphaltenes, Subsea Pipelines and Risers*. First edit. Great Britain: ELSEVIER. DOI:10.1016/B978-008044566-3.50023-3.
- Bello, O. O., Fasesan, S. O., Teodoriu, C. and Reinicke, K. M. (2006) An Evaluation of the Performance of Selected Wax Inhibitors on Paraffin Deposition of Nigerian Crude Oils, *Petroleum Science and Technology*, 24 (2), pp. 195–206.

DOI:10.1081/LFT-200044504.

- Bendlken, K. H., Maine, D., Moe, R. and Nuland, S. (1991) *The Dynamic Two-Fluid Model OLGA: Theory and Application*.
- Bern, P. A., Withers, V. R. and Cairns, R. J. R. (1980) Wax deposition in crude oil pipelines, in: *Society of Petroleum Engineers - European Offshore Technology Conference and Exhibition*. pp. 571–578.
- Birch, K. (2015) OTC2015 Solving Wax Deposition Issues - YouTube.
- Botne, K. K. and Gudmundsson, J. S. (2012) Modeling wax thickness in single-phase turbulent flow, *Petroleum Engineering and Applied Geophysics*, Master of (June), pp. 70.
- Bott, T. and Gudmundsson, J. (1977) Deposition of Paraffin Wax from Flowing Systems, *Institute of Petroleum Technical Paper, IP 77-007*.
- Brewer, P. G., Orr, F. M., Friederich, G., Kvenvolden, K. A. and Orange, D. L. (1998) Gas hydrate formation in the deep sea: In situ experiments with controlled release of methane, natural gas, and carbon dioxide, *Energy and Fuels*, 12 (1), pp. 183–188. DOI:10.1021/ef970172q.
- Brown, L. D. (2002) Flow Assurance: A π 3 Discipline, in: *Proceedings of the Annual Offshore Technology Conference*. pp. 183–189.
- Brown, T. S., Niesen, V. G. and Erickson, D. D. (1993) Measurement and prediction of the kinetics of paraffin deposition, in: *SPE Reprint Series*. Society of Petroleum Engineers, pp. 155–170.
- Buller, A., Funchs, S. and Klemp, S. (2002) Flow assurance, *Statoil's Research & Technology Memoir No. 1*.
- Buongiorno, J. (2006) Convective transport in nanofluids, *Journal of Heat Transfer*, 128 (3), pp. 240–250. DOI:10.1115/1.2150834.
- Burger, E. D., Perkins, T. K. and Striegler, J. H. (1981) Studies of Wax Deposition in the Trans Alaska Pipeline, *Journal of Petroleum Technology*, 33 (June), pp. 1075–1086. DOI:10.2118/8788-PA.
- Carbognani, L., Orea, M. and Fonseca, M. (1999) Complex nature of separated solid phases from crude oils, *Energy and Fuels*, 13 (2), pp. 351–358. DOI:10.1021/ef9801975.
- Cawkwell, M. G. and Charles, M. E. (1989) Characterization of Canadian arctic thixotropic gelled crude oils utilizing an eight-parameter model, *J. Pipelines*, 7, pp. pp.251-264.
- Cha, M., Shin, K., Kim, J., Chang, D., Seo, Y., Lee, H. and Kang, S. P. (2013) Thermodynamic and kinetic hydrate inhibition performance of aqueous ethylene glycol solutions for natural gas, *Chemical Engineering Science*, 99, pp. 184–190. DOI:10.1016/j.ces.2013.05.060.

- Chala, G. T., Sulaiman, S. A. and Japper-Jaafar, A. (2018) Flow start-up and transportation of waxy crude oil in pipelines-A review, *Journal of Non-Newtonian Fluid Mechanics*, 251 (February 2017), pp. 69–87. DOI:10.1016/j.jnnfm.2017.11.008.
- Chanda, D., Sarmah, A., Borthakur, A., Rao, K. V., Subrahmanyam, B. and Das, H. C. (1998) Combined effect of asphaltenes and flow improvers on the rheological behaviour of Indian waxy crude oil, *Fuel*, 77 (11), pp. 1163–1167. DOI:10.1016/S0016-2361(98)00029-5.
- Chen, X. T., Butler, T., Volk, M. and Brill, J. P. (1997) Techniques for Measuring Wax Thickness During Single and Multiphase Flow, *SPE Annual Technical Conference and Exhibition*. Society of Petroleum Engineers. DOI:10.2118/38773-MS.
- Chi, Y., Daraboina, N. and Sarica, C. (2016) Investigation of inhibitors efficacy in wax deposition mitigation using a laboratory scale flow loop, *AIChE Journal*, 62 (11), pp. 4131–4139. DOI:10.1002/aic.15307.
- Chi, Y., Daraboina, N. and Sarica, C. (2017) Effect of the Flow Field on the Wax Deposition and Performance of Wax Inhibitors: Cold Finger and Flow Loop Testing, *Energy and Fuels*, 31 (5), pp. 4915–4924. DOI:10.1021/acs.energyfuels.7b00253.
- Chrisman, E., Lima, V. and Menechini, P. (2012) Asphaltenes – Problems and Solutions in E&P of Brazilian Crude Oils, in: *Crude Oil Emulsions-Composition Stability and Characterization*.
- Cochran, S. (2003) Hydrate control and remediation best practices in deepwater oil developments, in: *Offshore Technology Conference*. pp. 179–192.
- Coto, B., Coutinho, J. A. P., Martos, C., Robustillo, M. D., Espada, J. J. and Peña, J. L. (2011) Assessment and improvement of n -paraffin distribution obtained by HTGC to predict accurately crude oil cold properties, *Energy and Fuels*, 25 (3), pp. 1153–1160. DOI:10.1021/ef101642g.
- Coto, B., Martos, C., Espada, J. J., Robustillo, M. D. and Peña, J. L. (2014) Experimental study of the effect of inhibitors in wax precipitation by different techniques, *Energy Science and Engineering*, 2 (4), pp. 196–203. DOI:10.1002/ese3.42.
- Coutinho, J. A. P., Edmonds, B., Moorwood, T., Szczepanski, R. and Zhang, X. (2006) Reliable wax predictions for flow assurance, *Energy and Fuels*, 20 (3), pp. 1081–1088. DOI:10.1021/ef050082i.
- Coutinho, J. A. P., Pauly, J. and Daridon, J. L. (2001) A thermodynamic model to predict wax formation in petroleum fluids, *Brazilian Journal of Chemical Engineering*, 18 (4), pp. 411–422. DOI:10.1590/S0104-66322001000400006.
- Couto, G. . (2004) *Investigation of Two-Phase Oil-Water Paraffin Deposition*. Doctoral dissertation, University of Tulsa.

- Creek, J. L., Lund, H. J., Brill, J. P. and Volk, M. (1999) Wax deposition in single phase flow, *Fluid Phase Equilibria*, 158–160, pp. 801–811. DOI:10.1016/s0378-3812(99)00106-5.
- Daraboina, N., Soedarmo, A. and Sarica, C. (2016) Microscopic study of wax inhibition mechanism, in: *Proceedings of the Annual Offshore Technology Conference*. Offshore Technology Conference, 2, pp. 1240–1249.
- Dean, W. R. (1927) XVI. *Note on the motion of fluid in a curved pipe*, *The London, Edinburgh, and Dublin Philosophical Magazine and Journal of Science*, 4 (20), pp. 208–223. DOI:10.1080/14786440708564324.
- de Oliveira, M., Vieira, L., Miranda, L., Miranda, D. and Marques, L. C. C. (2016) On the influence of micro-and macro-crystalline paraffins on the physical and rheological properties of crude oil and organic solvents, *Chemistry and Chemical Technology*, 10 (4), pp. 451–458. DOI:10.23939/chcht10.04.451.
- Del Carmen García, M., Carbognani, L., Orea, M. and Urbina, A. (2000) The influence of alkane class-types on crude oil wax crystallization and inhibitors efficiency, *Journal of Petroleum Science and Engineering*, 25 (3–4), pp. 99–105. DOI:10.1016/S0920-4105(99)00057-1.
- Deshannavar, U. B., Rafeen, M. S., Ramasamy, M. and Subbarao, D. (2010) Crude oil fouling: A review, *Journal of Applied Sciences*.
- Dickakian, G. and Seay, S. (1988) ASPHALTENE PRECIPITATION PRIMARY CRUDE EXCHANGER FOULING MECHANISM., *Oil and Gas Journal*, 86 (10), pp. 47–50.
- Dobbs, J. (1999) A Unique Method of Paraffin Control in Production Operations, in: *SPE Rocky Mountain Regional Meeting, 15-18 May, Gillette, Wyoming*. Society of Petroleum Engineers (SPE),.
- Duan, J., Liu, H., Jiang, J., Xue, S., Wu, J. and Gong, J. (2016) International Journal of Heat and Mass Transfer Numerical prediction of wax deposition in oil – gas stratified pipe flow, *International Journal of Heat and Mass Transfer*, 105, pp. 279–289. DOI:10.1016/j.ijheatmasstransfer.2016.09.082.
- Dutta, P., Saha, S. K., Nandi, N. and Pal, N. (2016) Numerical study on flow separation in 90° pipe bend under high Reynolds number by k-ε modelling, *Engineering Science and Technology, an International Journal*, 19 (2), pp. 904–910. DOI:10.1016/j.jestch.2015.12.005.
- Dutton, J. A. (2018) Phase Relations in Reservoir Engineering: The Hydrate Problem, *Pennsylvania State University, College of Earth and Mineral Sciences*. Available from: https://www.e-education.psu.edu/png520/m21_p3.html [Accessed 30 December 2019].
- Dwivedi, P. (2010) *An investigation of single-phase wax deposition characteristics of South Pelto oil under turbulent flow*. Doctoral dissertation, University of Tulsa.

- Edmonds, B., Moorwood, T., Szczepanski, R. and Zhang, X. (2008) Simulating wax deposition in pipelines for flow assurance, *Energy and Fuels*, 22 (2), pp. 729–741. DOI:10.1021/ef700434h.
- Ehsani, S., Haj-Shafiei, S. and Mehrotra, A. K. (2019) Experiments and modeling for investigating the effect of suspended wax crystals on deposition from ‘waxy’ mixtures under cold flow conditions, *Fuel*, pp. 610–621. DOI:10.1016/j.fuel.2019.01.089.
- Ekaputra, A. A., Sabil, K. M., Hosseinipo, A. and Saaid, I. Bin (2014) Impacts of Viscosity, Density and Pour Point to the Wax Deposition, *Journal of Applied Sciences*, 14 (23), pp. 3334–3338. DOI:10.3923/jas.2014.3334.3338.
- El-Dalatony, M., Jeon, B.-H., Salama, E.-S., Eraky, M., Kim, W., Wang, J. and Ahn, T. (2019) Occurrence and Characterization of Paraffin Wax Formed in Developing Wells and Pipelines, *Energies*, 12 (6), pp. 967. DOI:10.3390/en12060967.
- Erickson, D. D., Niesen, V. G. and Brown, T. S. (1993) Thermodynamic Measurement and Prediction of Paraffin Precipitation in Crude Oil, in: *SPE Annual Technical Conference and Exhibition*. Society of Petroleum Engineers,.
- Escobar-Remolina, J. C. M., Barrios-Ortiz, W. and Santoyo-Ramírez, G. (2009) Multi-solid model modified to predict paraffin precipitation in petroleum fluids at high temperatures and pressures, *CTyF - Ciencia, Tecnología Y Futuro*, 3 (5), pp. 35–52.
- Fagin, K. M. (1945) Automatic Scrapers Used in West Edmond Oil Wells, *Pet. Eng*, 105.
- Fairbank, J. A. and So, R. M. C. (1987) Upstream and downstream influence of pipe curvature on the flow through a bend, *International Journal of Heat and Fluid Flow*, 8 (3), pp. 211–217. DOI:10.1016/0142-727X(87)90030-0.
- Fan, T. and Buckley, J. S. (2002) Rapid and accurate SARA analysis of medium gravity crude oils, *Energy and Fuels*, 16 (6), pp. 1571–1575. DOI:10.1021/ef0201228.
- Fan, T., Wang, J. and Buckley, J. S. (2002) Evaluating Crude Oils by SARA Analysis, in: *SPE/DOE Improved Oil Recovery Symposium, 4 2002*. Society of Petroleum Engineers (SPE), pp. 883–889.
- Fan, Y. and Llave, F. M. (1996) Chemical Removal of Formation Damage From Paraffin Deposition Part I - Solubility and Dissolution Rate, in: *SPE Formation Damage Control Symposium, 4 1996*. Society of Petroleum Engineers,.
- Ford, P. ., Ells, J. . and Russell, R. . (1965) Pipelining high-pour-point crude. Pt. 3. Frequent pigging helps move waxy crude below its pour point., *Oil Gas J.:(United States)*, 63 (19).
- Fusi, L. (2003) On the stationary flow of a waxy crude oil with deposition

- mechanisms, *Nonlinear Analysis, Theory, Methods and Applications*, 53 (3–4), pp. 507–526. DOI:10.1016/S0362-546X(02)00315-2.
- Gao, C. (2003) *Investigation of Long Term Paraffin Deposition Behavior for South Pelto Oil*. Doctoral dissertation, University of Tulsa.
- Giacchetta, G., Marchetti, B., Leporini, M., Terenzi, A., Dall’Acqua, D., Capece, L. and Cocci Grifoni, R. (2019) Pipeline wax deposition modeling: A sensitivity study on two commercial software, *Petroleum*, 5 (2), pp. 206–213. DOI:10.1016/j.petlm.2017.12.007.
- Goia, F. and Boccaleri, E. (2016) Physical–chemical properties evolution and thermal properties reliability of a paraffin wax under solar radiation exposure in a real-scale PCM window system, *Energy and Buildings*, 119, pp. 41–50. DOI:10.1016/j.enbuild.2016.03.007.
- Golchha, A., Sarica, C. and Venkatesan, R. (2015) Settling of wax particles in near-gelling systems under quiescent conditions, in: *Proceedings of the Annual Offshore Technology Conference*. Offshore Technology Conference, 1, pp. 83–99.
- Goldman, Marcene S., and C. C. N. (1957) Prevention of paraffin deposition and plugging, *U.S. Patent*, No. 2 (817,635).
- Gong, J., Zhang, Y., Liao, L., Duan, J., Wang, P. and Zhou, J. (2011) Wax Deposition in the Oil/Gas Two-Phase Flow for a Horizontal Pipe, *Energy & Fuels*, 25 (4), pp. 1624–1632. DOI:10.1021/ef101682u.
- Groffe, D., Groffe, P., Takhar, S., Andersen, S. I., Stenby, E. H., Lindeloff, N. and Lundgren, M. (2001) A wax inhibition solution to problematic fields: A chemical remediation process, *Petroleum Science and Technology*, 19 (1–2), pp. 205–217. DOI:10.1081/LFT-100001235.
- Guan, H. (2016) Flow Assurance Risk Evaluation and Chemical Management in a Shale Gas Field, in: NACE International, Publications Division, 15835, pp. 1–14.
- Halim, N., Ali, S., Nadeem, M., Hamid, P. A. and Tan, I. M. (2011) *Synthesis of Wax Inhibitor and Assessment of Squeeze Technique Application for Malaysian Waxy Crude*. Available from: <http://eprints.utp.edu.my/8792/1/SPEnadhirah.pdf>
- Hammami, A. and Raines, M. A. (1999) Paraffin deposition from crude oils: Comparison of laboratory results with field data, *SPE Journal*, 4 (1), pp. 9–18. DOI:10.2118/54021-PA.
- Hammami, A., Ratulowski, J. and Coutinho, J. A. P. (2003) Petroleum Science and Technology Cloud Points: Can We Measure or Model Them? DOI:10.1081/LFT-120018524.
- Hammami, a and Ratulowski, J. (2007) Precipitation and Deposition of Asphaltenes

- in Production Systems: A Flow Assurance Overview, *Asphaltenes, Heavy Oils, and Petroleomics*, pp. 617–660. DOI:10.1007/0-387-68903-6_23.
- Hamouda, A. A. and Ravnøy, J. M. (1992) Prediction of wax deposition in pipelines and field experience on the influence of wax on drag-reducer performance, in: *Proceedings of the Annual Offshore Technology Conference*. Offshore Technology Conference, 1992–May, pp. 669–679.
- Hao, L. Z., Al-salim, H. S. and Ridzuan, N. (2019) A Review of the Mechanism and Role of Wax Inhibitors in the Wax Deposition and Precipitation, *Pertanika J. Sci. & Technol*, 27 (1), pp. 499–526.
- Hasbullah, N. B. (2011) *Investigation on the Removal of Paraffin Wax Deposition by Magnetic Field*. Universiti Teknologi Petronas. Available from : <http://utpedia.utp.edu.my/599/>
- Hasinger, M., Scherr, K. E., Lundaa, T., Bräuer, L., Zach, C. and Loibner, A. P. (2012) Changes in iso- and n-alkane distribution during biodegradation of crude oil under nitrate and sulphate reducing conditions, *Journal of Biotechnology*, 157 (4), pp. 490–498. DOI:10.1016/j.jbiotec.2011.09.027.
- Hayduk, W. and Minhas, B. S. (1982) Correlations for prediction of molecular diffusivities in liquids, *The Canadian Journal of Chemical Engineering*, 60 (2), pp. 295–299. DOI:10.1002/cjce.5450600213.
- Headen, T. F., Skipper, N. T., Boek, E. S. and Heenan, R. K. (2007) Asphaltene aggregation in the presence of laponite clay. Available from: <https://www.isis.stfc.ac.uk/Pages/Asphaltene-aggregation-in-the-presence-of-laponite-clay.aspx> [Accessed 7 January 2020].
- Hernandez, O. C. (2002) *Investigation of single-phase paraffin deposition characteristics*. Doctoral dissertation, Tulsa University.
- Hoffmann, R. and Amundsen, L. (2010) Single-phase wax deposition experiments, *Energy and Fuels*, 24 (2), pp. 1069–1080. DOI:10.1021/ef900920x.
- Hoffmann, R. and Amundsen, L. (2013) Influence of wax inhibitor on fluid and deposit properties, *Journal of Petroleum Science and Engineering*, 107, pp. 12–17. DOI:10.1016/j.petrol.2013.04.009.
- Holder, G. A. and Winkler, J. (1965) Crystal-Growth Poisoning of n-Paraffin Wax By Polymeric Additives and its Relevance to Polymer Crystallization Mechanisms, *Nature*, 207 (4998), pp. 719–721. DOI:10.1038/207719a0.
- Hsu, J. J. C. and Brubaker, J. P. (1995) Wax Deposition Measurement and Scale-Up Modeling for Waxy Live Crudes under Turbulent Flow Conditions, in: *International Meeting on Petroleum Engineering*. Society of Petroleum Engineers,.
- Huang, Z., Senra, M., Kapoor, R. and Fogler, H. S. (2011) Wax deposition modeling of oil/water stratified channel flow, *AIChE Journal*, 57 (4), pp. 841–851.

- DOI:10.1002/aic.12307.
- Huang, Z., Zheng, S. and Fogler, H. (2015) *Wax Deposition: Experimental Characterizations, Theoretical Modeling, and Field Practices*, CRC Press. DOI:10.1201/b18482.
- Idelchik, I. E. (1986) Handbook of hydraulic resistance (2nd revised and enlarged edition), *Washington, DC, Hemisphere Publishing Corp., 1986, 662 P. Translation*. Available from: <http://adsabs.harvard.edu/abs/1986wdch.book.....I> [Accessed 11 February 2019].
- IEA (2019) *World Energy Outlook 2019: IEA-Subsidies-2010-18*. Vol. 18. DOI:DOE/EIA-0383(2019) U.S.
- Irmann-Jacobsen, T. B. (2013) Flow Assurance – A System Perspective, in: *MEK4450 Offshore Technology Course*. universitet i Oslo, Matematisk Institutt.,.
- Jacobs, T. and Writer, J. P. T. T. (2015) The New Pathways of Multiphase Flow Modeling, (February), pp. 62–67.
- Jafari Behbahani, T., Beigi, A. A. M., Taheri, Z. and Ghanbari, B. (2015) Investigation of wax precipitation in crude oil: Experimental and modeling, *Petroleum*, 1 (3), pp. 223–230. DOI:10.1016/j.petlm.2015.07.007.
- Jamaluddin, A. K. M., Nighswander, J., Joshi, N. and Company, A. S. (2001) A Systematic Approach in Deepwater Flow Assurance Fluid Characterization, *Screening*.
- Jang, Y. H., Blanco, M., Creek, J., Tang, Y. and Goddard, W. A. (2007) Wax Inhibition by Comb-like Polymers: Support of the Incorporation–Perturbation Mechanism from Molecular Dynamics Simulations, *The Journal of Physical Chemistry B*, 111 (46), pp. 13173–13179. DOI:10.1021/jp072792q.
- Japper-Jaafar, A., Bhaskoro, P. T. and Mior, Z. S. (2016) A new perspective on the measurements of wax appearance temperature: Comparison between DSC, thermomicroscopy and rheometry and the cooling rate effects, *Journal of Petroleum Science and Engineering*, 147, pp. 672–681. DOI:10.1016/j.petrol.2016.09.041.
- Jennings, D. W. and Breitigam, J. (2010) Paraffin inhibitor formulations for different application environments: From heated injection in the desert to extreme cold arctic temperatures, in: *Energy and Fuels*. American Chemical Society, 24, pp. 2337–2349.
- Jennings, D. W. and Newberry, M. E. (2008) Paraffin inhibitor applications in deepwater offshore developments, in: *International Petroleum Technology Conference, IPTC 2008.2*, pp. 834–847.
- Jennings, D. W. and Weispfennig, K. (2005) Effects of shear and temperature on wax deposition: Coldfinger investigation with a Gulf of Mexico crude oil,

- Energy and Fuels*, 19 (4), pp. 1376–1386. DOI:10.1021/ef049784i.
- Jewell, D. M., Weber, J. H., Bunger, J. W., Plancher, H. and Latham, D. R. (1972) Ion-exchange, coordination, and adsorption chromatographic separation of heavy-end petroleum distillates, *Analytical Chemistry*, 44 (8), pp. 1391–1395. DOI:10.1021/ac60316a003.
- Jha, N. K., Jamal, M. S., Singh, D. and Prasad, U. S. (2014) Characterization of crude oil of upper assam field for flow assurance, in: *Society of Petroleum Engineers - SPE Saudi Arabia Section Technical Symposium and Exhibition*.
- Jing, G., Ye, P. and Zhang, Y. (2017) The action mechanism of wax inhibitors (WI) on pour point and viscosity of mixed waxy oil, *Petroleum Chemistry*, 57 (3), pp. 293–298. DOI:10.1134/s0965544117020153.
- Kalorazi, B. T., Ostergaard, K. K., Danesh, A., Todd, A. C. and Burgass, R. W. (1998) Gas hydrates: problem or source of energy.
- Kalpakli Vester, A., Sattarzadeh, S. S. and Örlü, R. (2016) Combined hot-wire and PIV measurements of a swirling turbulent flow at the exit of a 90° pipe bend, *Journal of Visualization*, 19 (2), pp. 261–273. DOI:10.1007/s12650-015-0310-1.
- Kang, P.-S., Lee, D.-G. and Lim, J.-S. (2014) Status of Wax Mitigation Technologies in Offshore Oil Production, *The Twenty-Fourth International Ocean and Polar Engineering Conference*, 3, pp. 31–38. Available from: www.isopec.org [Accessed 9 May 2019].
- Kang, P. S., Hwang, J. Y. and Lim, J. S. (2019) Flow Rate Effect on Wax Deposition Behavior in Single-Phase Laminar Flow, *Journal of Energy Resources Technology, Transactions of the ASME*, 141 (3). DOI:10.1115/1.4041525.
- Kasumu, A. S. (2014) *An investigation of Solids Deposition from Two-Phase Wax-Solvent-Water Mixtures*. Doctoral thesis, University of Calgary, Calgary, AB.
- Kasumu, A. S. and Mehrotra, A. K. (2013) Solids Deposition from Two-Phase Wax–Solvent–Water ‘Waxy’ Mixtures under Turbulent Flow, *Energy & Fuels*, 27 (4), pp. 1914–1925. DOI:10.1021/ef301897d.
- KAT Lab (2009) HTGC METHOD NOTES - T-SEP®. Kernow Instrument Technology. North Petherwin, Cornwall PL15 8TE. UK. Available from: <http://www.kat-lab.com/t-sep/tsep2.html> and <http://www.kat-lab.com/t-sep/index.html> [Accessed 13 March 2017].
- Keeper, G. (2013) Paraffin Wax : Formation , Mitigation Methods & Remediation Techniques, *Gibson Applied technology and Engineering, Inc*. Available from: <http://static1.squarespace.com/static/53556018e4b0fe1121e112e6/54b683d0e4b09b2abd348a7b/54b683e1e4b09b2abd348dbe/1421247457412/GAT2004-GKP-2013.04-Paraffin-Formation-Mitigation-and-Remediation-Techniques.pdf?format=original> [Accessed 9 May 2019].

- Kelland, M. A. (2009) *Production chemicals for the oil and gas industry, Production Chemicals for the Oil and Gas Industry*. CRC Press. DOI:10.1201/9781420092974.
- Kennedy, B. F. and Saint-Marcoux, J.-F. (2015) Functional Approach to Flow Assurance Applied to Deepwater Field Development, in: pp. 1–17.
- Kilincer, N. (2003) *Multiphase paraffin deposition behavior of a Garden Banks condensate*. Tulsa University, Tulsa, OK.
- Kok, M. V. and Saracoglu, O. (2000) Mathematical Modelling of Wax Deposition in Crude Oil Pipeline Systems, *Society of Petroleum Engineers*, pp. 7. DOI:10.1080/10916460008949895.
- Kumar, R., Banerjee, S., Mandal, A. and Naiya, T. K. (2016) Improvement in transportability of Indian heavy crude oil using novel surfactant, *Indian Journal of Chemical Technology*, 23 (4), pp. 262–270.
- Labes-Carrier, C., Rønningsen, H. P., Kolnes, J. and Leporcher, E. (2002) Wax Deposition in North Sea Gas Condensate and Oil Systems: Comparison between Operational Experience and Model Prediction, in: *Proceedings - SPE Annual Technical Conference and Exhibition*. Society of Petroleum Engineers, pp. 2083–2094.
- Lashkarbolooki, M., Esmailzadeh, F. and Mowla, D. (2011) Mitigation of Wax Deposition by Wax-Crystal Modifier for Kermanshah Crude Oil, *Journal of Dispersion Science and Technology*, 32 (7), pp. 975–985. DOI:10.1080/01932691.2010.488514.
- Lee, H. S. (2008) *Computational and Rheological Study of Wax Deposition and Gelation in Subsea Pipelines*. Doctoral dissertation, University of Michigan.
- Lee, H. S., Singh, P., Thomason, W. H. and Fogler, H. S. (2008) Waxy oil gel breaking mechanisms: Adhesive versus cohesive failure, *Energy and Fuels*, 22 (1), pp. 480–487. DOI:10.1021/ef700212v.
- Leporini, M., Terenzi, A., Marchetti, B., Giacchetta, G. and Corvaro, F. (2019) Experiences in numerical simulation of wax deposition in oil and multiphase pipelines: Theory versus reality, *Journal of Petroleum Science and Engineering*, 174 (December 2018), pp. 997–1008. DOI:10.1016/j.petrol.2018.11.087.
- Li, N., Mao, G. L., Shi, X. Z., Tian, S. W. and Liu, Y. (2018) Advances in the research of polymeric pour point depressant for waxy crude oil, *Journal of Dispersion Science and Technology*, 39 (8), pp. 1165–1171. DOI:10.1080/01932691.2017.1385484.
- Lim, Z. H., Al Salim, H. S., Ridzuan, N., Nguele, R. and Sasaki, K. (2018) Effect of surfactants and their blend with silica nanoparticles on wax deposition in a Malaysian crude oil, *Petroleum Science*, 15 (3), pp. 577–590. DOI:10.1007/s12182-018-0241-2.

- Lira-Galeana, C., Firoozabadi, A. and Prausnitz, J. M. (1996) Thermodynamics of Wax Precipitation in Petroleum Mixtures, *AIChE Journal*, 42 (1), pp. 239–248. DOI:10.1002/aic.690420120.
- Lira-Galeana, C. and Hammami, A. (2000) Chapter 21 Wax Precipitation from Petroleum Fluids: A Review, *Developments in Petroleum Science*, 40 (PART B), pp. 557–608. DOI:10.1016/S0376-7361(09)70292-4.
- Mahto, V. and Kumar, A. (2013) Effect of several parameters on wax deposition in the flow line due to Indian waxy crude oil, *International Journal of Applied Engineering Research and Development (IJAERD)*, 3 (4), pp. 1–10.
- Majeed, A., Bringedal, B. and Overa, S. (1990) Model calculates wax deposition for N. Sea Oils, *Oil and Gas Journal*, 88 (25), pp. 63–69.
- Makwashi, N., Sarkodie, K., Akubo, S., Zhao, D. and Diaz, P. (2019a) Investigation of the severity of wax deposition in bend pipes under subcooled pipelines conditions, in: *Society of Petroleum Engineers - SPE Europec Featured at 81st EAGE Conference and Exhibition 2019*. Society of Petroleum Engineers,.
- Makwashi, N., Soraia, D., Barros, D., Sarkodie, K., Zhao, D. and Diaz, P. A. (2019b) Depositional Behaviour of Highly Macro-Crystalline Waxy Crude Oil Blended with Polymer Inhibitors in a Pipe with a 45-Degree Bend, in: *Society of Petroleum Engineers SPE-195752-MS*.
- Mansoori, G. A. (2009) A unified perspective on the phase behaviour of petroleum fluids, *International Journal of Oil, Gas and Coal Technology*, 2 (2), pp. 141–167. DOI:10.1504/IJOGCT.2009.024884.
- Mansourpoor, M., Azin, R., Osfouri, S. and Izadpanah, A. A. (2019) Experimental investigation of wax deposition from waxy oil mixtures, *Applied Petrochemical Research*, 9 (2), pp. 77–90. DOI:10.1007/s13203-019-0228-y.
- Matzain, A. (1999) *Multiphase Flow Paraffin Deposition Modeling*. Ph.D. Dissertation, University of Tulsa. OK.
- Matzain, A., Apte, M. S., Zhang, H.-Q., Volk, M., Brill, J. P. and Creek, J. L. (2002a) Investigation of Paraffin Deposition During Multiphase Flow in Pipelines and Wellbores—Part 1: Experiments, *Journal of Energy Resources Technology*, 124 (3), pp. 180. DOI:10.1115/1.1484392.
- Matzain, A., Apte, M. S., Zhang, H.-Q., Volk, M., Brill, J. P., Creek, J. L., *et al.* (2002b) Investigation of Paraffin Deposition During Multiphase Flow in Pipelines and Wellbores—Part 2: Modeling, *Journal of Energy Resources Technology*, 124 (3), pp. 180. DOI:10.1115/1.1369359.
- Mehrotra, A. K. and Bidmus, H. O. (2004) Heat-Transfer Calculations for Predicting Solids Deposition in Pipeline Transportation of ‘Waxy’ Crude Oils, in: *Heat-Transfer Calculations. Chapter: 25*. McGraw-Hill Companies, pp. 1–18.
- Miao, Q. (2012) Numerical study on the effect of wax deposition on the restart

- process of a waxy crude oil pipeline, *Advances in Mechanical Engineering*, 2012. DOI:10.1155/2012/973652.
- Morrison, R. T. and Boyd, R. N. (1992) *Organic chemistry*. 6th ed. New Jersey: Prentice Hall.
- Mozes, G. E. (1982) Paraffin Products: Properties, Technologies, Applications, *Developments in Petroleum Science. Elsevier Science & Technology*.
- Murty, B. S. and Thandaveswara, B. S. (2014) Hydraulics, <http://nptel.ac.in/courses/105106114/>. Available from: <http://doer.col.org/handle/123456789/3973> [Accessed 11 February 2019].
- Nguyen, D. A. and Fogler, H. S. (2005) Facilitated diffusion in the dissolution of carboxylic polymers, *AIChE Journal*, 51 (2), pp. 415–425. DOI:10.1002/aic.10329.
- Nguyen, D. A., Scott Fogler, H. and Chavadej, S. (2001) Fused Chemical Reactions. 2. Encapsulation: Application to Remediation of Paraffin Plugged Pipelines †. DOI:10.1021/ie0009886.
- Noville, I. and Naveira, L. (2012) Comparison between real field data and the results of wax deposition simulation, in: *SPE Latin American and Caribbean Petroleum Engineering Conference Proceedings*.1, pp. 660–671.
- Pan, H., Abbas, F. and Fotland, P. (1997) Pressure and composition effect on wax precipitation: Experimental data and model results, *SPE Production and Facilities*, 12 (4), pp. 250–258. DOI:10.2118/36740-PA.
- Pan, S., Zhu, J., Zhang, D., Razouki, A., Talbot, M. and Wierchowski, S. (2009) Case studies on simulation of wax deposition in pipelines, in: *Society of Petroleum Engineers - International Petroleum Technology Conference 2009, IPTC 2009.2*, pp. 1168–1183.
- Panacharoensawad, E. (2012) *Wax deposition under two-phase oil-water flowing conditions*. PhD Thesis, University of Tulsa.
- Panacharoensawad, E. and Sarica, C. (2013) Experimental Study of Single-Phase and Two-Phase Water-in-Crude- Oil Dispersed Flow Wax Deposition in a Mini Pilot-Scale Flow Loop.
- Paso, K. G. (2014) Comprehensive Treatise on Shut-in and Restart of Waxy Oil Pipelines, *Journal of Dispersion Science and Technology*, 35 (8), pp. 1060–1085. DOI:10.1080/01932691.2013.833105.
- Paso, K. G., Krückert, K. K., Oschmann, H. J., Ali, H. and Sjöblom, J. (2014) PPD architecture development via polymer-crystal interaction assessment, *Journal of Petroleum Science and Engineering*, 115, pp. 38–49. DOI:10.1016/j.petrol.2014.02.002.
- Paso, K., Senra, M., Yi, Y., Sastry, A. M. and Fogler, H. S. (2005) Paraffin

- polydispersity facilitates mechanical gelation, *Industrial and Engineering Chemistry Research*, 44 (18), pp. 7242–7254. DOI:10.1021/ie050325u.
- Pedersen, K. S. (1995) Prediction of cloud point temperatures and amount of wax precipitation, *SPE Production and Facilities*, 10 (1), pp. 46–49. DOI:10.2118/27629-PA.
- Pedersen, K. S. and Rønningsen, H. P. (2003) Influence of wax inhibitors on wax appearance temperature, pour point, and viscosity of waxy crude oils, *Energy and Fuels*, 17 (2), pp. 321–328. DOI:10.1021/ef020142+.
- Perez, P., Boden, E., Chichak, K., Gurnon, A. K., Hu, L., Lee, J., *et al.* (2015) Evaluation of Paraffin Wax Inhibitors: An Experimental Comparison of Bench-Top Test Results and Small-Scale Deposition Rigs for Model Waxy Oils, *Offshore Technology Conference, Proceedings*, pp. 4–7. DOI:10.4043/25927-MS.
- Pham, S. T., Truong, M. H. and Pham, B. T. (2017) Flow Assurance in Subsea Pipeline Design for Transportation of Petroleum Products, *Open Journal of Civil Engineering*, 7 (2), pp. 311–323. DOI:10.4236/ojce.2017.72021.
- Pinho, S. P. G., Montesanti, J. R. T., Shang, W. and Sarica, C. (2011) A case study of scale-up of wax deposition model predictions using flow loop wax deposition data for pipeline design, *BHR Group*, pp. 35–50.
- Prajapati, D. B., Sahu, A. K. and Student, M. E. (2015) *Design of Prototype Internal 20k Helium Gas Purification System for Helium Plant & Test Facility*, *IJSTE-International Journal of Science Technology & Engineering* |. Vol. 1. Available from: www.ijste.org
- Quintella, C. M., Lima, A. M. V. and Silva, E. B. (2006) Selective inhibition of paraffin deposition under high flow rate as a function of the crude oil paraffin type and content by fluorescence depolarization: Polypropylene and high-density polyethylene, *Journal of Physical Chemistry B*, 110 (14), pp. 7587–7591. DOI:10.1021/jp055934u.
- Ramirez-Jaramillo, E., Lira-Galeana, C. and Manero, O. (2004) Modeling wax deposition in pipelines, *Petroleum Science and Technology*, 22 (7–8), pp. 821–861. DOI:10.1081/LFT-120038726.
- Ramírez-Jaramillo, E., Lira-Galeana, C. and Manero, O. (2001) Numerical simulation of wax deposition in oil pipeline systems, *Petroleum Science and Technology*, 19 (1–2), pp. 143–156. DOI:10.1081/LFT-100001231.
- Rashidi, M., Mombekov, B. and Marhamati, M. (2016) A Study of a Novel Inter Pipe Coating Material for Paraffin Wax Deposition Control and Comparison of the Results with Current Mitigation Technique in Oil and Gas Industry, *OTC-26695-MS*.
- Rehan, M., Nizami, A. S., Taylan, O., Al-Sasi, B. O. and Demirbas, A. (2016) Determination of wax content in crude oil, *Petroleum Science and Technology*,

- 34 (9), pp. 799–804. DOI:10.1080/10916466.2016.1169287.
- Rittirong, A. (2014) *Paraffin deposition under two-phase gas-oil slug flow in horizontal pipes*. PhD thesis, University of Tulsa.
- Rittirong, A., Panacharoensawad, E. and Sarica, C. (2015) An Experimental Study of Paraffin Deposition under Two-Phase Gas-Oil Slug Flow in Horizontal Pipes, in: *Offshore Technology Conference*.32, pp. 99–117.
- Rittirong, A., Panacharoensawad, E. and Sarica, C. (2016) Experimental Study of Paraffin Deposition Under Two-Phase Gas / Oil Slug Flow in Horizontal Pipes, (August 2015), pp. 4–7.
- Rittirong, A., Panacharoensawad, E. and Sarica, C. (2017) Experimental study of paraffin deposition under two-phase gas/oil slug flow in horizontal pipes, in: *SPE Production and Operations*.32, pp. 99–117.
- Roenningsen, H. P., Bjoerndal, B., Baltzer Hansen, A. and Batsberg Pedersen, W. (1991) Wax precipitation from North Sea crude oils: 1. Crystallization and dissolution temperatures, and Newtonian and non-Newtonian flow properties, *Energy & Fuels*, 5 (6), pp. 895–908. DOI:10.1021/ef00030a019.
- Ruwoldt, J., Kurniawan, M. and Oschmann, H.-J. J. (2018) Non-linear dependency of wax appearance temperature on cooling rate, *Journal of Petroleum Science and Engineering*, 165, pp. 114–126. DOI:10.1016/j.petrol.2018.02.011.
- Sarica, C. and Panacharoensawad, E. (2012) Review of paraffin deposition research under multiphase flow conditions, *Energy and Fuels*, 26 (7), pp. 3968–3978. DOI:10.1021/ef300164q.
- Sarica, C. and Volk, M. (2004) *Tulsa University Paraffin Deposition Projects*. Technical Report, The University of Tulsa (US). DOI:10.2172/834175.
- Serintel, S. (2017) *Subsea Technology and Equipments*. Available from: <http://www.oil-gasportal.com/subsea-technology-and-equipments/>
- Seyfaee, A., Lashkarbolooki, M., Esmaeilzadeh, F. and Mowla, D. (2012) Investigation of the Effect of Insulation on Wax Deposition in an Iranian Crude Oil Pipeline with OLGA Simulator, *Journal of Dispersion Science and Technology*, 33 (8), pp. 1218–1224. DOI:10.1080/01932691.2011.605649.
- Shuard, A. M., Mahmud, H. B. and King, A. J. (2017) An optimization approach to reduce the risk of hydrate plugging during gas-dominated restart operations, *Journal of Petroleum Science and Engineering*, 156 (April 2016), pp. 220–234. DOI:10.1016/j.petrol.2017.05.024.
- Sifferman, T. R. (1979) FLOW PROPERTIES OF DIFFICULT-TO-HANDLE WAXY CRUDE OILS., *JPT, Journal of Petroleum Technology*, 31 (8), pp. 1042–1050. DOI:10.2118/7409-PA.
- Siljuberg, M. K. (2012) *Modelling of paraffin wax in oil pipelines*. Norwegian

- University of Science and Technology. Available from :
<https://ntnuopen.ntnu.no/ntnu-xmlui/handle/11250/239864>
- Singh, A., Lee, H.S., Singh, P. and Sarica, C. (2011) SS: Flow Assurance: Validation of Wax Deposition Models Using Field Data from a Subsea Pipeline, in: *Offshore Technology Conference*. pp. 2–5.
- Singh, A., Lee, H. S., Singh, P. and Sarica, C. (2011) Flow Assurance: Validation of Wax Deposition Models Using Field Data from a Subsea Pipeline, in: *Offshore Technology Conference*.
- Singh, P. and Fogler, H. S. (1998) Fused chemical reactions: The use of dispersion to delay reaction time in tubular reactors, *Industrial and Engineering Chemistry Research*, 37 (6), pp. 2203–2207. DOI:10.1021/ie9706020.
- Singh, P., Fogler, H. S. and Nagarajan, N. (1999) Prediction of the wax content of the incipient wax-oil gel in a pipeline: An application of the controlled-stress rheometer, *Journal of Rheology*, 43 (6), pp. 1437–1459. DOI:10.1122/1.551054.
- Singh, P., Venkatesan, R., Fogler, H. S. and Nagarajan, N. (2000) Formation and aging of incipient thin film wax-oil gels, *AIChE Journal*, 46 (5), pp. 1059–1074. DOI:10.1002/aic.690460517.
- Singh, P., Walker, J., Lee, H. S., Gharfeh, S., Thomason, B. and Blumer, D. (2007) An application of Vacuum-Insulated Tubing (VIT) for wax control in an arctic environment, in: *Offshore Technology Conference, 1–4 May.22*, pp. 127–136.
- Singhal, H. K., Sahai, G. C., Pundeer, G. S. and Chandra, K. (1991) Designing and selecting wax crystal modifier for optimum field performance based on crude oil composition, in: *Proceedings - SPE Annual Technical Conference and Exhibition*.Pi, pp. 251–262.
- Sloan, E. D. and Koh, C. A. (2007) *Clathrate hydrates of natural gases*, CRC press, Third Edition.
- Soedarmo, A. A., Daraboina, N. and Sarica, C. (2017) Validation of wax deposition models with recent laboratory scale flow loop experimental data, *Journal of Petroleum Science and Engineering*, 149. DOI:10.1016/j.petrol.2016.10.017.
- Song, Y., Han, S. and Ren, T. (2010) Impact of alkyl methacrylate-maleic anhydride copolymers as pour point depressant on crystallization behavior of simulated diesel fuel, *Petroleum Science and Technology*, 28 (8), pp. 860–867. DOI:10.1080/10916460903058210.
- Sousa, A. L., Matos, H. A. and Guerreiro, L. P. (2019) Preventing and removing wax deposition inside vertical wells: a review, *Journal of Petroleum Exploration and Production Technology*,
- Sousa, A. M., Matos, H. A. and Guerreiro, L. (2019b) Wax deposition mechanisms and the effect of emulsions and carbon dioxide injection on wax deposition:

- Critical review, *Petroleum*. KeAi Communications Co.
DOI:10.1016/j.petlm.2019.09.004.
- SPT Group (2015) Dynamic Multiphase Flow Simulator. Available from:
<http://www.sptgroup.com/upload/documents/Brochures/Transient-Well-Flow-Simulations.pdf> [Accessed
- Sreenivas, J. (2011) Bends, Flow and Pressure Drop In;, *A-to-Z Guide to Thermodynamics, Heat and Mass Transfer, and Fluids Engineering*. Thermopedia. DOI:10.1615/AtoZ.b.bends_flow_and_pressure_drop_in.
- Sulaiman, A. D. I., Ajiienka, A. J. and Sunday, I. S. (2011) Application of piezoelectric energy generated from quartz plus semiprecious metals on wax deposition control, *Journal of Petroleum and Gas Engineering*, 2 (May), pp. 93–98.
- Sulaiman, S. A., Biga, B. K. and Chala, G. T. (2017) Injection of non-reacting gas into production pipelines to ease restart pumping of waxy crude oil, *Journal of Petroleum Science and Engineering*, 152, pp. 549–554. DOI:10.1016/j.petrol.2017.01.046.
- Sum, A. K. (2013) Prevention, management, and remediation approaches for gas hydrates in the flow assurance of oil/gas flowlines, in: *Proceedings of the Annual Offshore Technology Conference.2*, pp. 1011–1016.
- Svendsen, J. A. (1993) Mathematical modeling of wax deposition in oil pipeline systems, *AIChE Journal*, 39 (8), pp. 1377–1388. DOI:10.1002/aic.690390815.
- Swartz, K. I. (2015) Setting the Standard, *Vertical Magazine*, 21 (15), pp. 32. Available from:
<https://web.archive.org/web/20150418013604/http://www.verticalmag.com/news/article/31306>
- Teo, M. (2016) Flow assurance for offshore production, *World Pumps*, 2016 (3), pp. 20–22. DOI:10.1016/S0262-1762(16)70024-1.
- Theyab, M. A. (2017) *Study of Fluid Flow Assurance in Hydrocarbon Production – Investigation Wax Mechanisms*. PhD Thesis, London South Bank University.
- Theyab, M. A. (2018) Experimental Methodology Followed to Evaluate Wax Deposition Process, *Journal of Petroleum & Environmental Biotechnology*, 9 (1). DOI:10.4172/2157-7463.1000357.
- Theyab, M. A. and Diaz, P. (2016a) Experimental study of wax deposition in pipeline – effect of inhibitor and spiral flow, *International Journal of Smart Grid and Clean Energy*, pp. 174–181. DOI:10.12720/sgce.5.3.174-181.
- Theyab, M. and Diaz, P. (2016b) Experimental Study on the Effect of Inhibitors on Wax Deposition, *Journal of Petroleum & Environmental Biotechnology*, 7 (6). DOI:10.4172/2157-7463.1000310.

- Thota, S. T. and Onyeanuna, C. C. (2016) Mitigation of wax in oil pipelines, *International Journal of Engineering Research and Reviews*, 4 (4), pp. 39–47.
- Time, R. W. (2011) Flow Assurance and Multiphase Flow (Part II). The University of Stavanger, Department of Petroleum Engineering, - *Seminar Presented at Aker Solutions, Stavanger*.
- Towler, B. F., Jaripatke, O. and Mokhatab, S. (2011) Experimental investigations of the mitigation of paraffin wax deposition in crude oil using chemical additives, *Petroleum Science and Technology*, 29 (5), pp. 468–483. DOI:10.1080/10916460903394029.
- Towler, B. F. and Rebbapragada, S. (2004) Mitigation of paraffin wax deposition in cretaceous crude oils of Wyoming, *Journal of Petroleum Science and Engineering*, 45 (1–2), pp. 11–19. DOI:10.1016/J.PETROL.2004.05.006.
- Trejo, F., Ancheyta, J., Morgan, T. J., Herod, A. A. and Kandiyoti, R. (2007) Characterization of asphaltenes from hydrotreated products by SEC, LDMS, LAMDI, NMR, and XRD, *Energy and Fuels*, 21 (4), pp. 2121–2128. DOI:10.1021/ef060621z.
- Turner, D., Boxall, J., Yang, D., Kleehamer, C., Koh, C., Miller, K., *et al.* (2005) Development of a Hydrate Kinetic Model and Its Incorporation Into the OLGA2000® Transient Multi-Phase Flow Simulator, in: *Proceedings of the 5th International Conference on Gas Hydrates*.
- Turner, W. (1971) Normal alkanes, *Ind Eng Chem Prod Res Develop*, 10 (3), pp. 238–260. DOI:10.1021/i360039a003.
- UIO (2004) Flow In Pipe, in: *FLUID MECHANICS*. pp. 321–343.
- Valinejad, R. and Nazar, A. R. S. (2013) An experimental design approach for investigating the effects of operating factors on the wax deposition in pipelines, *Fuel*, 106, pp. 843–850. DOI:10.1016/j.fuel.2012.11.080.
- Van Der Geest, C., Guersoni, V. C. B. and Bannwart, A. C. (2019) Experimental study of the time to restart the flow of a gelled waxy crude in rheometer and pipeline, *Journal of Petroleum Science and Engineering*, 181, pp. 106247. DOI:10.1016/J.PETROL.2019.106247.
- Venkatesan, R. (2004) *The Deposition and Rheology of Organic Gels*. Doctoral dissertation, University of Michigan.
- Vester, K. A., Sattarzadeh, S. S. and Örlü, R. (2016) Turbulent flows in curved pipes: Recent advances in experiments and simulations, *Applied Mechanics Reviews*, 68 (5). DOI:10.1115/1.4034135.
- Visintin, R. F. G., Lapasin, R., Vignati, E., D'antona, P. and Lockhart, T. P. (2005) Rheological Behavior and Structural Interpretation of Waxy Crude Oil Gels. DOI:10.1021/la050705k.

- Volk, M., Michael Volk, M. and Cem Sarica, C. (2003) Tulsa University Paraffin Deposition Projects. DOI:10.2172/825598.
- Wang, C.-C., Youn Chen, I., Yang, Y.-W. and Hu, R. (2004) Influence of horizontal return bend on the two-phase flow pattern in small diameter tubes, *Experimental Thermal and Fluid Science*, 28 (2–3), pp. 145–152. DOI:10.1016/S0894-1777(03)00033-5.
- Wang, J. and Buckley, J. (2002) Standard Procedure for Separating Asphaltenes from Crude Oils, *New Mexico Tech, PRRC*, pp. 02–02.
- Wang, J., Zhou, F., Zhang, L., Huang, Y., Yao, E., Zhang, L., Wang, F. and Fan, F. (2019) Experimental study of wax deposition pattern concerning deep condensate gas in Bozi block of Tarim Oilfield and its application, *Thermochimica Acta*, 671 (June 2018), pp. 1–9. DOI:10.1016/j.tca.2018.10.024.
- Wang, K. S., Wu, C. H., Creek, J. L., Shuler, P. J. and Tang, Y. (2003) Evaluation of effects of selected wax inhibitors on paraffin deposition, in: *Petroleum Science and Technology*.21, pp. 369–379.
- Wang, Q., Sarica, C. and Volk, M. (2008) An experimental study on wax removal in pipes with oil flow, *Journal of Energy Resources Technology, Transactions of the ASME*, 130 (4), pp. 0430011–0430015. DOI:10.1115/1.3000136.
- Wang, W. and Huang, Q. (2014) Prediction for wax deposition in oil pipelines validated by field pigging, *Journal of the Energy Institute*, 87 (3), pp. 196–207. DOI:10.1016/j.joei.2014.03.013.
- Wang, W., Huang, Q., Wang, C., Li, S., Qu, W., Zhao, J. and He, M. (2015) Effect of operating conditions on wax deposition in a laboratory flow loop characterized with DSC technique, *Journal of Thermal Analysis and Calorimetry*, 119 (1), pp. 471–485. DOI:10.1007/s10973-014-3976-z.
- Wang, Y., Yang, Z., Li, H., Zhou, X., Zhang, Q., Wang, J. and Liu, Y. (2014) A novel cocrystal explosive of HNIW with good comprehensive properties, *Propellants, Explosives, Pyrotechnics*, 39 (4), pp. 590–596. DOI:10.1002/prop.201300146.
- Wardhaugh, L. T., Boger, D. V and Tonner, S. P. (1988) Rheology of Waxy Crude Oils, in: *International Meeting on Petroleum Engineering, 1-4 November, Tianjin, China*. Society of Petroleum Engineers (SPE),.
- Wasden, F. K. (2003) Flow assurance in deepwater flowlines and pipelines - Challenges met, challenges remaining, in: *Proceedings of the Annual Offshore Technology Conference*.2003–May, pp. 1139–1141.
- Watson, M. J., Pickering, P. F. and Hawkes, N. J. (2003) The flow assurance dilemma: Risks vs. costs, *Hart's E and P*, 76 (5). Available from: http://www.engr.mun.ca/~spkenny/Courses/Undergraduate/ENGI8673/Reading_List/2003_Watson_Flow_Assurance.pdf [Accessed 10 February 2019].

- Wayne, C. and Sue, D. (2015) Agilent collaborates with university to solve significant problem for oil refineries, *Agilent*. Available from: <https://www.agilent.com/en-us/newsletters/accessagilent/2015/jul/sara?cid=11649> [Accessed 17 July 2019].
- Wei, B. (2015) Recent advances on mitigating wax problem using polymeric wax crystal modifier, *Journal of Petroleum Exploration and Production Technology*, 5 (4), pp. 391–401. DOI:10.1007/s13202-014-0146-6.
- Wilke, C. R. and Chang, P. (1955) Correlation of diffusion coefficients in dilute solutions, *AIChE Journal*, 1 (2), pp. 264–270. DOI:10.1002/aic.690010222.
- Won, K. W. (1989) Thermodynamic calculation of cloud point temperatures and wax phase compositions of refined hydrocarbon mixtures, *Fluid Phase Equilibria*, 53 (C), pp. 377–396. DOI:10.1016/0378-3812(89)80104-9.
- Woo, G. T., Garbis, S. J. and Gray, T. C. (1984) Long-term control of Paraffin deposition, in: *Proceedings - SPE Annual Technical Conference and Exhibition*. Society of Petroleum Engineers (SPE),.
- Wu, X., Li, C., He, Y. and Jia, W. (2017) Dynamic modeling of the two-phase leakage process of natural gas liquid storage tanks, *Energies*, 10 (9), pp. 1399. DOI:10.3390/en10091399.
- Wu, Y., Ni, G., Yang, F., Li, C. and Dong, G. (2012) Modified Maleic Anhydride Co-polymers as Pour-Point Depressants and Their Effects on Waxy Crude Oil Rheology, *Energy & Fuels*, 26 (2), pp. 995–1001. DOI:10.1021/ef201444b.
- Xing, L., Yeung, H., Shen, J. and Cao, Y. (2013) Experimental study on severe slugging mitigation by applying wavy pipes, *Chemical Engineering Research and Design*, 91 (1), pp. 18–28. DOI:10.1016/j.cherd.2012.06.020.
- Yang, F., Zhao, Y., Sjöblom, J., Li, C. and Paso, K. G. (2015) Polymeric Wax Inhibitors and Pour Point Depressants for Waxy Crude Oils: A Critical Review, *Journal of Dispersion Science and Technology*, 36 (2), pp. 213–225. DOI:10.1080/01932691.2014.901917.
- Yadav, M. S. *et al.* (2014) ‘Experiments on geometric effects of 90-degree vertical-upward elbow in air water two-phase flow’, *International Journal of Multiphase Flow*. Pergamon, 65, pp. 98–107. doi: 10.1016/J.IJMULTIPHASEFLOW.2014.05.014.
- Yen, A., Yin, Y. R. and Asomaning, S. (2001) Evaluating Asphaltene Inhibitors: Laboratory Tests and Field Studies, *SPE International Symposium on Oilfield Chemistry*, (Cii). DOI:10.2118/65376-MS.
- Zeng, H., Zou, F., Lehne, E., Zuo, J. Y. and Zhang, D. (2012) Advanced Gas Chromatography - Progress in Agricultural, Biomedical and Industrial Applications. DOI:10.5772/2518.
- Zhang, F. and Chen, G. Q. (2007) Viscoelastic properties of waxy crude oil, *Journal*

- of Central South University of Technology (English Edition)*, 14 (1 SUPPL.), pp. 445–448. DOI:10.1007/s11771-007-0303-x.
- Zhang, G. and Liu, G. (2010) Study on the wax deposition of waxy crude in pipelines and its application, *Journal of Petroleum Science and Engineering*, 70 (1–2), pp. 1–9. DOI:10.1016/j.petrol.2008.11.003.
- Zhang, X., Queimada, A., Szczepanski, R. and Moorwood, T. (2014) Modeling the shearing effect of flowing fluid and wax ageing on wax deposition in pipelines, *Proceedings of the Annual Offshore Technology Conference*, 2, pp. 1089–1110. DOI:10.4043/24797-ms.
- Zhang, Y., Gong, J. and Wu, H. (2010) An experimental study on wax deposition of water in waxy crude oil emulsions, *Petroleum Science and Technology*, 28 (16), pp. 1653–1664. DOI:10.1080/10916460903096822.
- Zhao, D., Omar, R., Abdulkadir, M., Abdulkareem, L. A., Azzi, A., Saidj, F., Hernandez Perez, V., Hewakandamby, B. N. and Azzopardi, B. J. (2017) The control and maintenance of desired flow patterns in bends of different orientations, *Flow Measurement and Instrumentation*, 53, pp. 230–242. DOI:10.1016/j.flowmeasinst.2016.09.003.
- Zhao, L. (2012) *Particles in wall turbulence*. PhD Thesis, Norwegian University of Science and Technology.
- Zheng, S. (2017) *Wax Deposition from Single-Phase Oil Flows and Water-Oil Two-Phase Flows in Oil Transportation Pipelines*. PhD Thesis Chemical Engineering, The University of Michigan.
- Zheng, S., Saidoun, M., Mateen, K., Palermo, T., Ren, Y. and Fogler, H. S. (2016) Wax Deposition Modeling with Considerations of Non-Newtonian Fluid Characteristics, *Offshore Technology Conference*, (January), pp. 0–20. DOI:10.4043/26914-MS.
- Zheng, S., Saidoun, M., Palermo, T., Mateen, K. and Fogler, H. S. (2017) Wax Deposition Modeling with Considerations of Non-Newtonian Characteristics: Application on Field-Scale Pipeline, *Energy and Fuels*, 31 (5), pp. 5011–5023. DOI:10.1021/acs.energyfuels.7b00504.
- Zheng, S., Zhang, F., Huang, Z. and Fogler, H. S. (2013) Effects of operating conditions on wax deposit carbon number distribution: Theory and experiment, *Energy and Fuels*, 27 (12), pp. 7379–7388. DOI:10.1021/ef402051n.
- Zhu, T., Walker, J. a, Liang, J. and Laboratory, P. D. (2008) *Evaluation of Wax Deposition and Its Control During Production of Alaska North Slope Oils*. DOI:10.2172/963363.

Appendices

Appendix A:

Table A1 Table A2 show the wide range of n-paraffin distribution of crude oil sample A (C₁₅ to C₇₄) and B (C₁₅ to C₆₇) obtained through the HTGC analysis.

Table A1: HTGC Process Data for the Crude Oil Sample ‘A’

Carbon Number	Sensitivity (pA*s/ng)	WHOLE OIL			TOPPED OIL			MERGED DATA		
		RT (mins)	Area (pA*s)	Mass (ng)	RT (mins)	Area (pA*s)	Mass (ng)	Adj. Mass (ng)	Mass (ng)	n-Paraffin Wt %
10	16.47	3	240.79	14.62				0	14.62	0.585
11	16.89	4.07	278.21	16.47				0	16.47	0.659
12	17.32	5.28	302.88	17.49				0	17.49	0.699
13	17.75	6.53	372.5	20.99				0	20.99	0.839
14	18.18	7.74	441.54	24.29	7.77	0.34	0.02	0.01	24.29	0.972
15	18.6	8.91	388.16	20.86	8.91	3.02	0.16	0.05	20.86	0.835
16	19.03	10.02	357.64	18.79	10.01	11.46	0.6	0.19	18.79	0.752
17	19.46	11.09	751.88	38.64	11.07	55.72	2.86	0.91	38.64	1.546
18	19.89	12.09	297.81	14.98	12.08	97.97	4.93	1.57	14.98	0.599
19	20.31	13.05	298.56	14.7	13.05	289.68	14.26	4.55	14.7	0.588
20	20.74	13.97	297.38	14.34	13.99	533.82	25.74	8.21	14.34	0.574
21	20.95	14.85	332.47	15.87	14.88	815.39	38.93	12.41	15.87	0.635
22	21.15	15.7	308.14	14.57	15.73	894.07	42.27	13.48	14.57	0.583
23	21.36	16.52	348.61	16.32	16.55	1093.23	51.19	16.32	16.32	0.653
24	21.56	17.3	290.21	13.46	17.33	919.8	42.66	13.6	13.6	0.544
25	21.77	18.05	307.19	14.11	18.09	1009.03	46.36	14.78	14.78	0.591
26	21.97	18.78	269.08	12.25	18.81	921.33	41.93	13.37	13.37	0.535
27	22.18	19.48	295.57	13.33	19.52	1011.54	45.61	14.54	14.54	0.582
28	22.38	20.15	252.1	11.26	20.19	886.9	39.63	12.64	12.64	0.505
29	22.59	20.81	258.27	11.43	20.84	897.6	39.74	12.67	12.67	0.507
30	22.79	21.44	218.09	9.57	21.47	689.06	30.23	9.64	9.64	0.386
31	22.68	22.05	176.04	7.76	22.08	626.74	27.64	8.81	8.81	0.353
32	22.57	22.64	133.97	5.94	22.67	425.27	18.85	6.01	6.01	0.24
33	22.45	23.22	95.18	4.24	23.24	321.9	14.34	4.57	4.57	0.183
34	22.34	23.78	64.04	2.87	23.79	210.07	9.4	3	3	0.12
35	22.22	24.32	41.56	1.87	24.34	158.67	7.14	2.28	2.28	0.091
36	22.11	24.85	28.33	1.28	24.86	109.28	4.94	1.58	1.58	0.063
37	22	25.36	33.27	1.51	25.38	90.04	4.09	1.31	1.51	0.06
38	21.88	25.87	16.57	0.76	25.88	55.13	2.52	0.8	0.8	0.032
39	21.77	26.36	23.01	1.06	26.37	58.24	2.68	0.85	1.06	0.042
40	21.66	26.84	12.24	0.57	26.85	47.81	2.21	0.7	0.7	0.028
41	21.64	27.3	11.21	0.52	27.31	46.11	2.13	0.68	0.68	0.027
42	21.62	27.76	11.24	0.52	27.77	42.13	1.95	0.62	0.62	0.025
43	21.59	28.2	11.26	0.52	28.21	42.26	1.96	0.62	0.62	0.025
44	21.57	28.63	9.87	0.46	28.64	37.68	1.75	0.56	0.56	0.022
45	21.55	29.05	10.53	0.49	29.07	39.01	1.81	0.58	0.58	0.023
46	21.53	29.47	8.51	0.4	29.48	33.14	1.54	0.49	0.49	0.02
47	21.51	29.87	10.08	0.47	29.89	39.39	1.83	0.58	0.58	0.023
48	21.49	30.27	7.71	0.36	30.28	30.98	1.44	0.46	0.46	0.018

49	21.47	30.66	7.87	0.37	30.67	29.58	1.38	0.44	0.44	0.018
50	21.45	31.04	7.19	0.34	31.05	27.77	1.29	0.41	0.41	0.017
51	21.04	31.41	7.74	0.37	31.42	26.95	1.28	0.41	0.41	0.016
52	20.63	31.77	6.7	0.32	31.79	24.93	1.21	0.39	0.39	0.015
53	20.22	32.13	6.74	0.33	32.14	25.7	1.27	0.41	0.41	0.016
54	19.81	32.48	5.95	0.3	32.49	23.73	1.2	0.38	0.38	0.015
55	19.4	32.82	6.08	0.31	32.84	26.98	1.39	0.44	0.44	0.018
56	18.99	33.16	6.44	0.34	33.17	22.57	1.19	0.38	0.38	0.015
57	18.58	33.49	6.31	0.34	33.5	24.48	1.32	0.42	0.42	0.017
58	18.17	33.81	4.96	0.27	33.82	20.51	1.13	0.36	0.36	0.014
59	17.76	34.13	4.43	0.25	34.14	20.56	1.16	0.37	0.37	0.015
60	17.34	34.44	3.34	0.19	34.46	15.62	0.9	0.29	0.29	0.011
61	17.34	34.75	2.87	0.17	34.76	13.65	0.79	0.25	0.25	0.01
62	17.34	35.05	2.42	0.14	35.06	9.97	0.57	0.18	0.18	0.007
63	17.34	35.34	2	0.12	35.36	9.45	0.55	0.17	0.17	0.007
64	17.34	35.64	1.21	0.07	35.65	7.74	0.45	0.14	0.14	0.006
65	17.34	35.92	1.26	0.07	35.94	6.44	0.37	0.12	0.12	0.005
66	17.34	36.22	1.09	0.06	36.22	5.3	0.31	0.1	0.1	0.004
67	17.34				36.5	4.36	0.25	0.08	0.08	0.003
68	17.34				36.76	6.8	0.39	0.13	0.13	0.005
69	17.34				37.03	4.12	0.24	0.08	0.08	0.003
70	17.34				37.3	3.98	0.23	0.07	0.07	0.003
71	17.34				37.57	2.25	0.13	0.04	0.04	0.002
72	17.34				37.86	3.42	0.2	0.06	0.06	0.003
73	17.34				38.09	2.11	0.12	0.04	0.04	0.002
74	17.34				38.36	1.7	0.1	0.03	0.03	0.001
Wax content										12.05

Table A2: HTGC Process Data for the Crude Oil Sample 'B'

Carbon Number	Sensitivity (pA*s/ng)	WHOLE OIL			TOPPED OIL			MERGED DATA		
		RT (mins)	Area (pA*s)	Mass (ng)	RT (mins)	Area (pA*s)	Mass (ng)	Adj. Mass (ng)	Mass (ng)	n-Paraffin Wt %
10	16.47									
11	16.89	4.26	43.1	2.55					2.6	0.102
12	18.38	5.08	340.3	18.52					18.5	0.786
13	18.56	6.18	289	15.57					15.6	0.651
14	18.74	7.93	219.5	11.71					11.7	0.483
15	18.92	8.92	185.3	9.79	8.97	0.1	0.01	0	9.8	0.398
16	19.11	10.03	257.3	13.46	10.05	0.7	0.04	0.01	13.5	0.541
17	19.29	11.14	1269.5	65.81	11.12	5.8	0.3	0.05	65.8	2.310
18	19.47	12.11	495	25.42	12.11	16.6	0.85	0.15	25.4	0.996
19	19.66	13.07	555.5	28.26	13.08	117.7	5.99	1.03	28.3	1.094
20	19.84	14	601.9	30.34	14.02	512.7	25.84	4.45	30.3	1.161
21	20.4	14.88	603.9	29.61	14.92	1254.2	61.49	10.58	29.6	1.153
22	20.48	15.73	614.8	30.01	15.79	2092.6	102.16	17.58	30	1.163
23	20.53	16.54	615.1	29.97	16.62	2703.2	131.7	22.66	30	1.152
24	20.57	17.32	621.7	30.23	17.41	3066.5	149.1	25.65	30.2	1.153
25	20.61	18.08	608.4	29.52	18.17	3247.4	157.57	27.11	29.5	1.118
26	20.65	18.8	592.5	28.69	18.9	3305.4	160.06	27.54	28.7	1.115
27	20.69	19.5	589.8	28.5	19.61	3361.6	162.45	27.95	28.5	1.079

28	20.74	20.18	552.7	26.66	20.28	3173.2	153.03	26.33	26.7	1.064
29	20.78	20.83	538.6	25.92	20.94	3130.5	150.67	25.92	25.9	0.973
30	20.82	21.46	456.2	21.91	21.56	2654.7	127.51	21.94	21.9	0.817
31	23.86	22.07	414.2	17.36	22.17	2525	105.82	18.21	18.2	0.781
32	23.84	22.66	306.5	12.86	22.75	1808.4	75.86	13.05	13.1	0.562
33	23.85	23.24	263.6	11.05	23.33	1644.9	68.96	11.87	11.9	0.514
34	23.86	23.79	140.1	5.87	23.86	859.6	36.02	6.2	6.2	0.270
35	23.88	24.33	101.4	4.25	24.39	619.4	25.94	4.46	4.5	0.196
36	23.89	24.86	50.3	2.11	24.9	306.8	12.84	2.21	2.2	0.097
37	23.9	25.37	37.2	1.56	25.41	223.2	9.34	1.61	1.6	0.071
38	23.92	25.87	23.6	0.99	25.91	147.9	6.18	1.06	1.1	0.047
39	23.93	26.36	16.1	0.67	26.4	101.5	4.24	0.73	0.7	0.033
40	23.94	26.84	11.9	0.5	26.87	70.9	2.96	0.51	0.5	0.023
41	22.07	27.3	9.1	0.41	27.33	59.3	2.69	0.46	0.5	0.019
42	22.07	27.76	7.6	0.34	27.79	47.4	2.15	0.37	0.4	0.015
43	22.07	28.2	6.2	0.28	28.23	42.8	1.94	0.33	0.3	0.014
44	22.07	28.64	5.7	0.26	28.66	36	1.63	0.28	0.3	0.012
45	22.07	29.06	4.4	0.2	29.09	33.5	1.52	0.26	0.3	0.011
46	22.07	29.47	3.4	0.15	29.5	26.8	1.22	0.21	0.2	0.009
47	22.07	29.88	3.1	0.14	29.9	24.1	1.09	0.19	0.2	0.008
48	22.07	30.27	2.7	0.12	30.3	20.9	0.95	0.16	0.2	0.007
49	22.08	30.66	2.9	0.13	30.69	19	0.86	0.15	0.1	0.006
50	22.08	31.04	2.2	0.1	31.07	18.2	0.82	0.14	0.1	0.006
51	33.99	31.42	2.2	0.06	31.44	17	0.5	0.09	0.1	0.006
52	34	31.78	2	0.06	31.8	14.9	0.44	0.08	0.1	0.005
53	34.17	32.14	1.8	0.05	32.16	15.3	0.45	0.08	0.1	0.005
54	34.33	32.49	1.5	0.04	32.51	13.9	0.4	0.07	0.1	0.005
55	34.5	32.83	1.5	0.04	32.86	14	0.41	0.07	0.1	0.005
56	34.67	33.17	1.3	0.04	33.19	12.8	0.37	0.06	0.1	0.005
57	34.84	33.5	1.3	0.04	33.52	13.5	0.39	0.07	0.1	0.005
58	35.01	33.82	0.7	0.02	33.85	11.2	0.32	0.06	0.1	0.004
59	35.18	34.14	0.8	0.02	34.16	11.3	0.32	0.06	0.1	0.005
60	35.35	34.45	0.6	0.02	34.48	8.4	0.24	0.04	0	0.003
61	17.34	34.77	0.3	0.02	34.78	8.5	0.49	0.08	0.1	0.003
62	17.34	35.08	0.6	0.04	35.09	4.8	0.28	0.05	0	0.002
63	17.34	35.37	0.3	0.02	35.38	5.3	0.3	0.05	0.1	0.002
64	17.34	35.7	0.4	0.03	35.67	2.6	0.15	0.03	0	0.001
65	17.34	35.98	0.3	0.02	35.96	2.2	0.12	0.02	0	0.001
66	17.34				36.25	0.7	0.04	0.01	0	0.000
67	17.34				36.53	0.7	0.04	0.01	0	0.000
Wax Content										20.05



Figure A1: Photo of the four commercial wax inhibitors supplied by Roemex oil company

Figure 1, 2 and 3 are chromatographs description of n-C17 and pristane

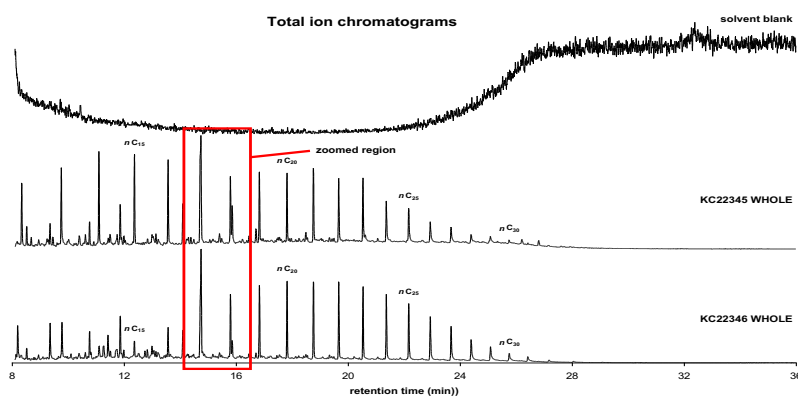


Figure A 2: Total ion chromatograms of solvent blank (top) and WHOLE oil samples A (middle) and sample B (bottom).

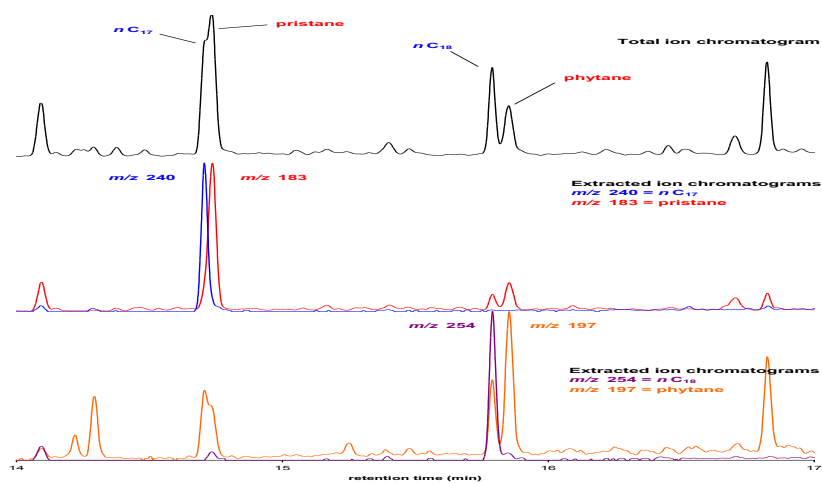


Figure A 3: Zoomed region total ion chromatogram of sample 'A' WHOLE oil (top) and extracted ion chromatograms for (middle) nC17 (m/z 240) and pristane (m/z 183), and (bottom) nC18 (m/z 254) and phytane (m/z 197).

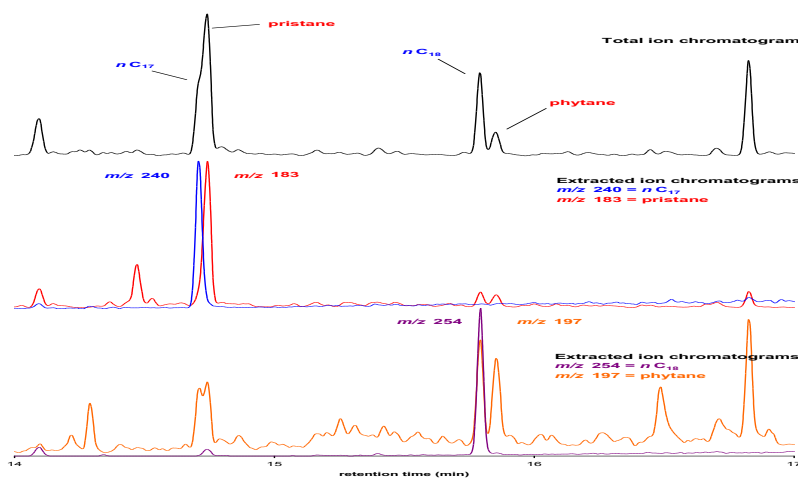


Figure A 4: Zoomed region total ion chromatogram of sample 'B' WHOLE oil (top) and extracted ion chromatograms for (middle) nC17 (m/z 240) and pristane (m/z 183), and (bottom) nC18 (m/z 254) and phytane (m/z 197).

Appendix B:

Sample properties of the oil and wax generated through Multiflash for simulation in OLGA and the geometry of the pipe.

Some of the simulation steps implemented in the OLGA

Step 1: Input – Preparation of the input boundary and initial conditions, fluid data and pipe and process data.

- Add and define the pipeline materials and pipe.
- Add network component, i.e. nodes and flow path.
- Define the properties for flow path; connect the flow path to the nodes.
- Create flow path geometry for the pipeline using case study information.
- Add boundary and initial conditions for pipeline length.
- Remove water in the Flash mode (the only hydrocarbon are preset)
- Select the model to calculate wax deposition (RRR model, HEATANALOGY model, MATZAIN model).

Step 2: Output – variables are defined in the output file and are viewed using trends and profile plot for viewing after the simulation has been run. The trend variables are– PT (pressure), TM (temperature), QLT (liquid flow rate), QG (gas flow rate), USG (superficial gas velocity), USLT (superficial liquid velocity), ACCLIQ (accumulated liquid flow), SURGELIQ (surge volume). While the profile variables considered are– DXWX (thickness of wax layer deposited at wall), MWXWALL (specific wax mass at the wall), MWXDIS (mass of wax dissolved in oil), HOL (liquid holdup fraction), PT, TM, VISHLTAB (oil viscosity from fluid tables) and ID (flow regime identification).

Step 3: Process – calculations of variables along the pipeline.

- the start and end time of the simulation are Specified.
- Simulation case is verified for possible error before running.

Table B1: Wax table before flash at fixed P and T

T (degC) =	40	P (psi) =	500
NO. PHASES =	2	CONVERGED	STABLE
COMPONENT	OVERALL	PHASE1	PHASE2
	fractions	LIQUID1	WAX
	fractions	fractions	fractions
I11-24	1.90E-01	1.90E-01	0
I24	5.73E-02	5.73E-02	0
I25-27	4.02E-02	4.02E-02	0
I27	3.13E-02	3.13E-02	0
I28	2.49E-02	2.49E-02	0
I28A	1.91E-02	1.91E-02	0
I29	1.49E-02	1.49E-02	0
I29-31	2.87E-02	2.87E-02	0
I31	1.19E-02	1.19E-02	0
I32	8.85E-03	8.85E-03	0
R32-36	2.38E-02	2.38E-02	0
R36-38	5.21E-03	5.21E-03	0
R38-42	2.14E-03	2.14E-03	0
R42+	5.56E-04	5.56E-04	0.00E+00
ASPHALTENE	1.66E-03	1.66E-03	0.00E+00
C11-14	1.23E-01	1.23E-01	0.00E+00
C14-17	1.23E-01	1.23E-01	0.00E+00
C17-20	1.23E-01	1.23E-01	0.00E+00
C20-23	8.50E-02	8.50E-02	8.41E-04
C23-25	2.68E-02	2.68E-02	6.19E-04
C25	1.72E-02	1.72E-02	7.37E-04
C26-28	1.23E-02	1.23E-02	9.13E-04
C28	9.09E-03	9.09E-03	1.23E-03
C29	6.84E-03	6.84E-03	1.57E-03
C30	5.13E-03	5.13E-03	2.00E-03
C31-33	3.78E-03	3.78E-03	2.80E-03
C33-35	2.68E-03	2.68E-03	3.74E-03
C35-37	1.76E-03	1.75E-03	6.57E-03
C37-43	9.67E-04	9.63E-04	2.13E-02
C43+	2.85E-04	8.81E-05	0.957716
Total(mole)	0.337454	0.337385	6.93E-05
Z (Fug. Model)	0.473865	0.473762	0.97383
Av.Mol.Wt.	296.275	296.197	672.68
Den/V(kg/m3)	827.837	827.8	914.598
Visc. (Pas)		1.14E-02	
Th.C.(W/m/K)		0.13105	

Table B 2: Screenshot of wax properties table compatible with OLGA software

The screenshot shows a Notepad window titled 'OL-WAX-2tab - Notepad' containing a table of wax properties. The table has 15 columns and 100 rows of data. The columns are: T (degC), wax concs(mol/mol), Dens_wax(kg/m3), Gas Mw, Liq Mw, Wax Mw, Visc(J/kg), Cp(kJ/kgC), Therm Cond(w/m K). The data rows show values for various temperatures and wax concentrations, with some values in scientific notation.

Table B 3: Screenshot of PVT table compatible with OLGA software

The screenshot shows a Notepad window titled 'OL-WAX-2tab - Notepad' containing a PVT table. The table has 15 columns and 100 rows of data. The columns are: P (Pa), T (degC), DROGDP, DROHLD, RS, VISC, VISHL, CPG, CPHL, HG, HHL, TCG, TCHL, SIGGHL, SEG, SEHL. The data rows show values for various pressures and temperatures, with some values in scientific notation.

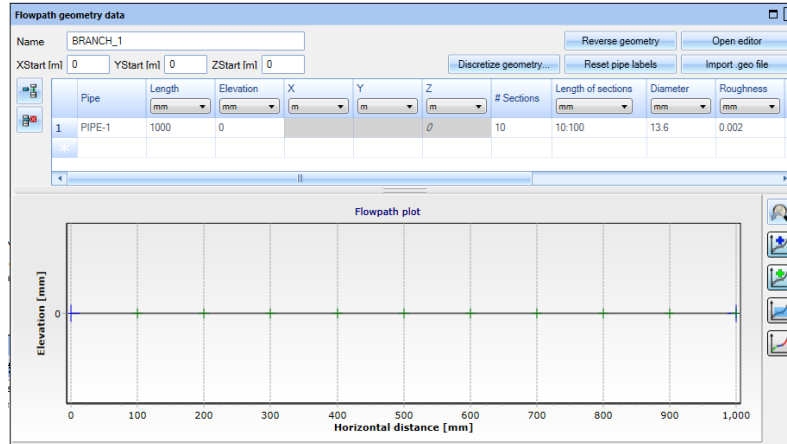


Figure B1: Screenshot of the flow path geometry data view for a straight horizontal pipeline.

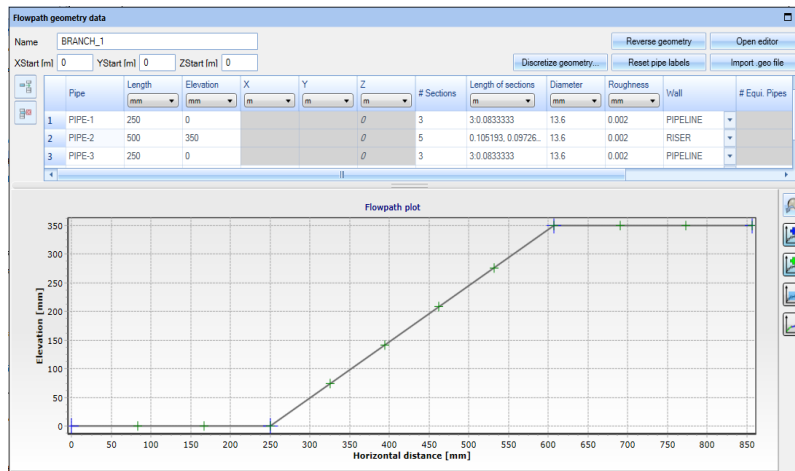


Figure B2: Screenshot of the flow path geometry data for the pipeline with a 45-degree bend.

Appendix C: Babcock & Wilcox chart

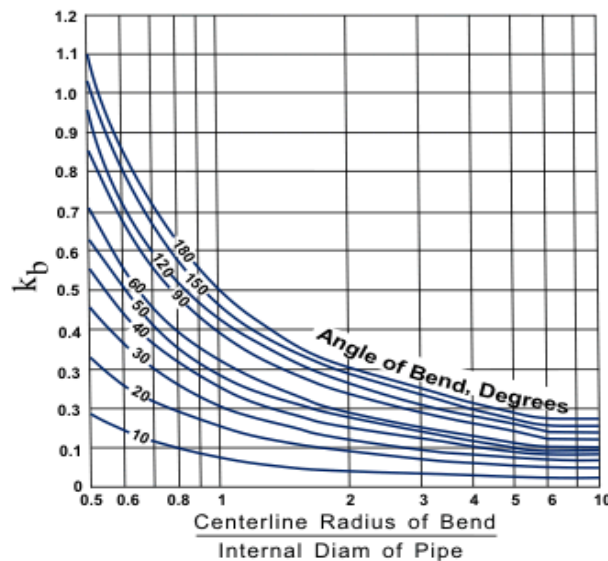


Figure C 1: Bend loss coefficients for a pipe proposed by Babcock & Wilcox Co. (1978) (Sreenivas, 2011).

Appendix D:

Tables below showed sample computation of wax deposition results. The deposit thickness, mass and volume reported are presented in **Figure 5-3** and **Figure 5-4** (Section 5.3.2).

Table D1: Measured and computed wax deposition results at constant oil temperature (45°C), constant coolant temperature (15°C), Viscosity (0.0056 Pa Density (915 kg/m³))

Parameters										Average Deposit Thickness							
Flow Rate		Reynolds Number	Volume of Wax		Weight of Wax		Pressure Drop	Radius, R (D _{in} =13.6)	R ²	Weight Correlation		Volume Correlation		Pressure Drop Method		Heat Transfer Method	
l/min	m ³ /s		ml	m ³	g	kg	(Pas)	m		m	mm	m	mm	m	mm	m	mm
2	3.3E-05	5.1E+02	16.8	1.68E-05	77.04	0.077	1265	0.0068	4.62E-05	2.39E-03	2.39	2.31E-03	2.31	2.40E-03	2.40	2.45E-03	2.45
3	5.0E-05	7.6E+02	15.4	1.54E-05	74.3	0.0743	1800	0.0068	4.62E-05	2.28E-03	2.28	2.21E-03	2.21	2.34E-03	2.34	2.37E-03	2.37
4	6.7E-05	1.0E+03	13.05	1.31E-05	69.8	0.0698	2040	0.0068	4.62E-05	2.11E-03	2.11	2.04E-03	2.04	2.15E-03	2.15	2.20E-03	2.20
5	8.3E-05	1.3E+03	10.5	1.05E-05	64	0.064	2050	0.0068	4.62E-05	1.90E-03	1.90	1.83E-03	1.83	1.89E-03	1.89	2.01E-03	2.01
7	1.2E-04	1.8E+03	7.2	7.20E-06	54.8	0.0548	3400	0.0068	4.62E-05	1.59E-03	1.59	1.51E-03	1.51	1.65E-03	1.65	1.65E-03	1.65
9	1.5E-04	2.3E+03	6	6.00E-06	50.6	0.0506	4500	0.0068	4.62E-05	1.45E-03	1.45	1.38E-03	1.38	1.47E-03	1.47	1.50E-03	1.50
11	1.8E-04	2.8E+03	4.5	4.50E-06	45	0.045	5500	0.0068	4.62E-05	1.27E-03	1.27	1.20E-03	1.20	1.28E-03	1.28	1.30E-03	1.30

Table D 2: Measured and computed wax deposition results at constant oil temperature (45°C), constant coolant temperature (30°C), Viscosity (0.0056 Pa) Density (915 kg/m³)

Parameters										Average Deposit Thickness							
Flow Rate		Reynolds Number	Volume of Wax		Weight of Wax		Pressure Drop	Radius, R (D _{in} =13.6)	R ²	Weight Correlation		Volume Correlation		Pressure Drop Method		Heat Transfer Method	
l/min	m ³ /s		ml	m ³	g	kg	(Pas)	m		m	mm	m	mm	m	mm	m	mm
2	3.3E-05	5.1E+02	2	2.00E-06	30.3	0.0303	400	0.0068	4.62E-05	8.25E-04	0.83	7.98E-04	0.80	9.29E-04	0.93	8.70E-04	0.87
3	5.0E-05	7.6E+02	1.5	1.50E-06	25	0.025	505	0.0068	4.62E-05	6.73E-04	0.67	6.91E-04	0.69	6.70E-04	0.67	7.05E-04	0.71
4	6.7E-05	1.0E+03	1.1	1.10E-06	20	0.02	610	0.0068	4.62E-05	5.32E-04	0.53	5.92E-04	0.59	5.17E-04	0.52	5.60E-04	0.56
5	8.3E-05	1.3E+03	0.4	4.00E-07	14	0.014	700	0.0068	4.62E-05	3.68E-04	0.37	3.57E-04	0.36	3.81E-04	0.38	3.90E-04	0.39
7	1.2E-04	1.8E+03	0.3	3.00E-07	9.5	0.0095	1050	0.0068	4.62E-05	2.47E-04	0.25	3.09E-04	0.31	2.26E-04	0.23	2.60E-04	0.26
9	1.5E-04	2.3E+03	0	0.00E+00	0	0	1405	0.0068	4.62E-05	0.00E+00	0.00	0.00E+00	0.00	1.30E-06	0.00	0.00E+00	0.00
11	1.8E-04	2.8E+03	0	0.00E+00	0	0	2015	0.0068	4.62E-05	0.00E+00	0.00	0.00E+00	0.00	4.13E-07	0.00	0.00E+00	0.00

Table D3: Some sample calculation for Reynolds number – laminar/transition/turbulent flow

Flow Rate		Density	Pipe Diameter	Viscosity	Reynolds Number
l/min	m ³ /s	kg/m ³	m	Pa	
2	3.3333E-05	915	0.136	0.0056	509.832578
3	5E-05	915	0.136	0.0056	764.748867
4	6.6667E-05	915	0.136	0.0056	1019.665156
5	8.3334E-05	915	0.136	0.0056	1274.581445
7	0.00011667	915	0.136	0.0056	1784.414023
9	0.00015	915	0.136	0.0056	2294.246601
11	0.00018333	915	0.136	0.0056	2804.079179